



# University of HUDDERSFIELD

## University of Huddersfield Repository

Sahboun, Salahaddin

V-Band Joint Torsional Load Capacity

### Original Citation

Sahboun, Salahaddin (2015) V-Band Joint Torsional Load Capacity. Doctoral thesis, University of Huddersfield.

This version is available at <http://eprints.hud.ac.uk/id/eprint/28321/>

The University Repository is a digital collection of the research output of the University, available on Open Access. Copyright and Moral Rights for the items on this site are retained by the individual author and/or other copyright owners. Users may access full items free of charge; copies of full text items generally can be reproduced, displayed or performed and given to third parties in any format or medium for personal research or study, educational or not-for-profit purposes without prior permission or charge, provided:

- The authors, title and full bibliographic details is credited in any copy;
- A hyperlink and/or URL is included for the original metadata page; and
- The content is not changed in any way.

For more information, including our policy and submission procedure, please contact the Repository Team at: [E.mailbox@hud.ac.uk](mailto:E.mailbox@hud.ac.uk).

<http://eprints.hud.ac.uk/>

# **V-BAND JOINT TORSIONAL LOAD CAPACITY**

**Salahaddin Musbah Sahboun**

**PhD Thesis**

**2015**

# V-Band Joint Torsional Load Capacity

A thesis submitted to the University of Huddersfield in  
Partial fulfilment of the requirement for the Degree of  
Doctor of Philosophy

Salahaddin Musbah Sahboun

Main Supervisor: Doctor Simon Mark Barrans

Co-Supervision: Professor Liam Blunt

School of Computing and Engineering  
University of Huddersfield

2015

## Abstract

This research thesis presents an analysis of the torsional loads on V-band clamps. In some applications, the relative rotational movement of the flanges connected by V-band clamps can result in catastrophic system failure. The ability to understand the factors impacting on torsional load capacity is therefore essential. In this research project, a theoretical model of a V-band joint subjected to torsional loads was developed. This model is used to identify those parameters that will impact on the joint's reliability. An experimental investigation was conducted to validate a theoretical model using a newly developed test rig. The development and features of this test rig are presented in this report. This experimental investigation also allowed the impact of those parameters that are difficult to control, to be determined. A total of three V-bands were used with different diameters but nominally identical cross sections were studied. In the research results, the initial slip point between flanges and the V-band clamp was identified by experimentation within this research project. Different sizes of V-bands were used under boundary conditions and loads. From the simulation results it was determined that the friction effect on the V-band depends on the size of the V-band. For the largest size of V-band, there was moderate correlation of the experimental and theoretical results. For the smallest size, the results suggest that with band tightening, flange contact is localised, rather than being throughout the band's entire circumference. The research demonstrated the significant relevance of the band and flanges' contact points and the coefficient of friction, especially that between the flanges, on the V-band clamp's theoretical torsional load capacity.

*Key words: V-bands clamps, Finite Element Model, Coefficient of Friction*

## Acknowledgement

I would like to gratefully acknowledge the enthusiastic supervision of Doctor Simon Barrans, and Professor Liam Blunt. For the guidance and constant supervision as well as for providing me the necessary information regarding the project and also supporting in completing the project. Special thanks go to my major advisor, Doctor Adelle Waterworth.

I would like to express my special gratitude and thanks to Technicians Mr Dennis Town, Mr Richard Bailey, Mr Steven Goldstein, and Mr Philip Holdsworth for advising and manufacturing the Test Rig, and giving me such attention and time. My thanks and appreciations also go to my colleague in developing the project and people who have willingly helped me out with their abilities.

Many thanks go to Mr Peter Gavigan for assisting and advising me, particularly in regards to my written English, during my research journey at the University of Huddersfield.

Thanks also to Deborah Birch and the Engineering Research School Office at the University for their advice and support, as well as to my colleagues in Tripoli for their assistance before I started my PhD. Last, but by no means least, I wish to express my special thanks to my parents and family for their ongoing support, love and help during this long and challenging project.

---

# Chapter One

## Research Project Undertaken

### 1.1 Introduction to V-band Retainer Clamps

This introductory overview is intended to offer a fundamental understanding of V-band functional objectives, prior to the more detailed description that follows. A V-band, as shown in Figure 1 - 1, is circular in shape. V-band clamps are employed to connect circular flanges, often using a single bolt. Figure 1 - 1 illustrates the application of V-band clamps for engine turbochargers (Couplings, 2015).

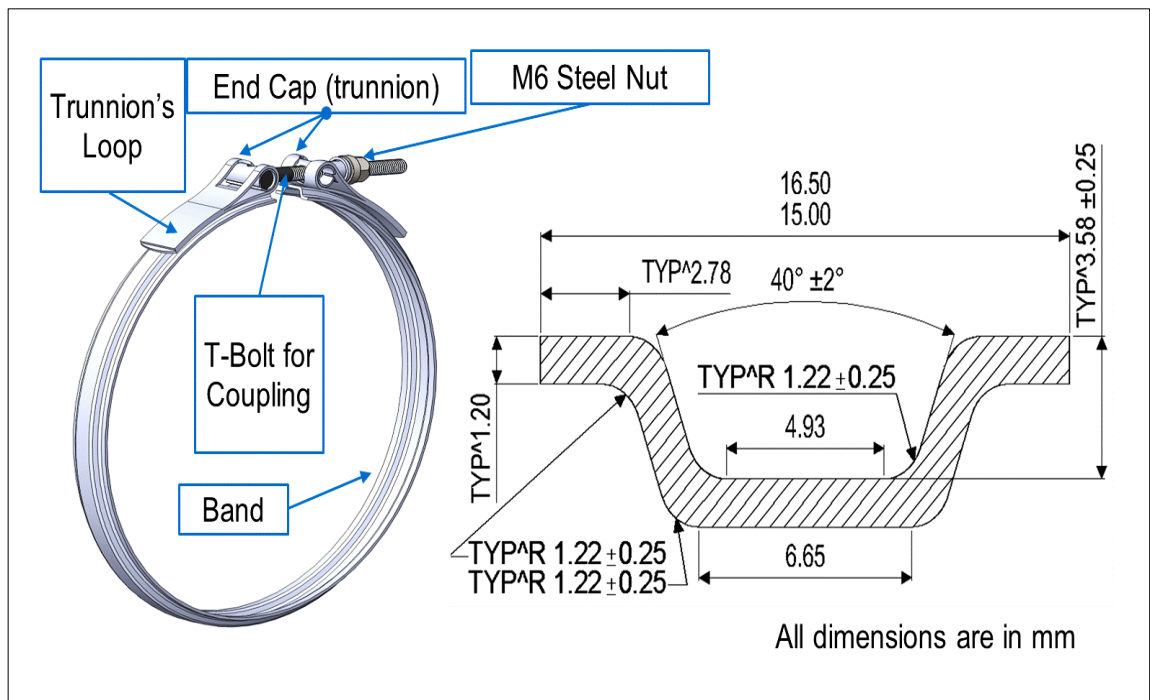


Figure 1 - 1: 181mm V-band Clamp in Solid Model

V-band clamps are expected to be usable under testing conditions relating to temperature variation, vibration and stress and to perform reliably and safely. They are therefore employed in a wide variety of settings and applications such

---

---

as Material Handling, Ducting or Air Conditioning Systems, Vehicles and Space Exploration. They can be made of North American Stainless Steel 304/L/H (Shoghi, 2005) and Austenetic stainless steel (Teconnex, 2013). Manufacturers offer different closure mechanisms. Teconnex offer over 50 for a range of applications. Common closure mechanisms include lever operated, t-bolt and quick coupler. See appendix A for more details.

## 1.2 Marman Ring / Marman Clamp and V-band Clamps

A Marman clamp is an example of a heavy-duty circular clamp, involving two flat cylindrical surfaces to be clamped together using a band clamp. This can sometimes be called a 'Marman ring' (see Figure 1 - 2).

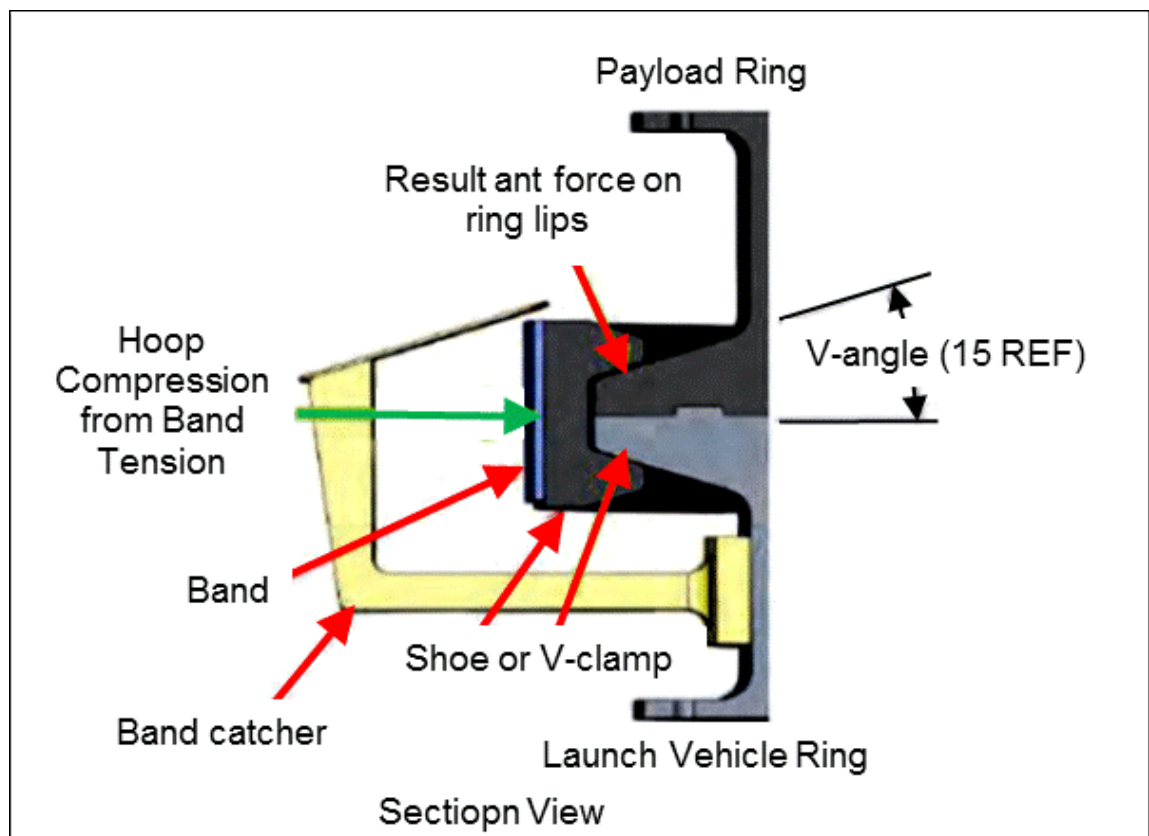


Figure 1 - 2: Marman Clamp System Section

---

---

A Marman clamp, or as (Lazansky, 2012) refers to them, a Marman Clamp Separation System, is an example of a heavy-duty circular clamp, involving two flat cylindrical surfaces to be clamped together using a band clamp. This is a generic ring clamp employed for fastening two cylinders butted together end to end. The name comes from the company that produced the first of this type of clamp, 'Marman Products', in the 1930s. These clamps were first used during the Second World War after their conception by the Marmon Corporation.

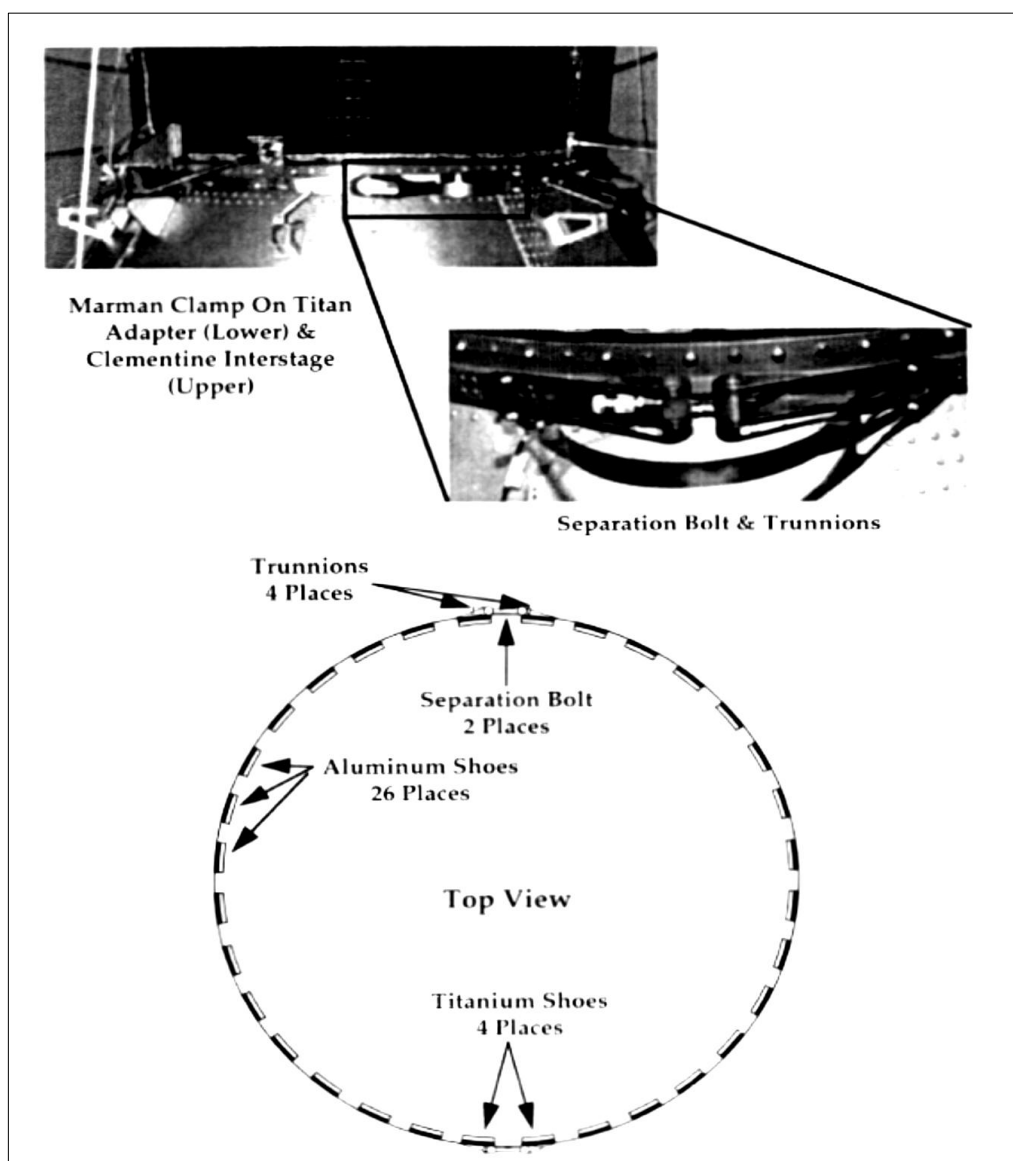


Figure 1 - 3: Marman Clamp System (William 1995)

---

---

The clamps were a rational choice in the 1960s for use in spacecraft separation. Their advantage was that they reduced the number of bolts to be cut for separation and thereby improved reliability. They have therefore been used successfully on many space programmes. They can sometimes also be called a "Marman clamp" (see Figure 1 - 3).

Engineering applications in the automotive and aerospace industries have benefited immensely from the V-band clamp since their invention. Currently V-band clamps are commonly employed in the joining together of the housing of diesel engine turbochargers. Furthermore, these clamps are also used for connecting satellites to their launching mechanisms. (K. Shoghi, S. Barrans, & H. Rao, 2004)

Over time, and as their role in engineering applications has become more pronounced, research studies have been conducted with the intention of finding ways of improving the distribution of load. This can be done by creating overlaps at the ends of the band and introducing inserts into the area beneath the T-bolt. The above suggestions are discussed by Shoghi et al (2004), who observed that there was no likelihood of achieving an even distribution of load. This observation was based on the frictional effects inherent in the elastic behaviour of the clamps.

There are different types of V-band clamps: differences include the method of closure used, the number of t-bolts used and the materials used in their manufacture. These factors will be relevant to different applications such as medical engineering and aerospace.

---

---

### **1.3 Differences between V-Band Clamps and Marman Rings**

From an overview it can be seen that both these devices are widely used in a range of applications. The V-band clamps and Marman rings can be seen to have similar work loading functions. However, applications will differ depending upon specific usage, materials used in manufacture and manufacturing design.

The main difference between Marman clamps and V-bands is that Marman clamps are made of relatively stiff, machined V segments, which are forced circumferentially against the flanges by a separate band. V-bands are formed from a pressed or rolled part without an external band. In addition, Marman clamps have a separation between the band and the V-section which is not the case with V-band clamps.

### **1.4 V-Band Clamp; the Working Forces**

From Figure 1 - 4 of the V-band clamp, the working force torsional loads attempting to rotate one flange relative to another and the bending loads attempting to separate the flanges in a non-uniform manner, are illustrated.

These loads can be generated by the movement, expansion or contraction of other engine system components attached to the turbocharger and also as a thrust generated by the gas flow. By tightening the V-band, the Radial Force (see Figure 1 – 4) is generated in two contact areas between the V-band area and the turbocharger flanges. The axial load capacity is found in the axis of the V-band. A further load is the banding load capacity which affects the V-band. In addition there is the vibration force which impacts on the loading on the joint

---

---

V-band Clamps, Couplings (2015). Figure 1 – 4 demonstrates Newton's 2nd Law; "For every action, there is an equal and opposite reaction."

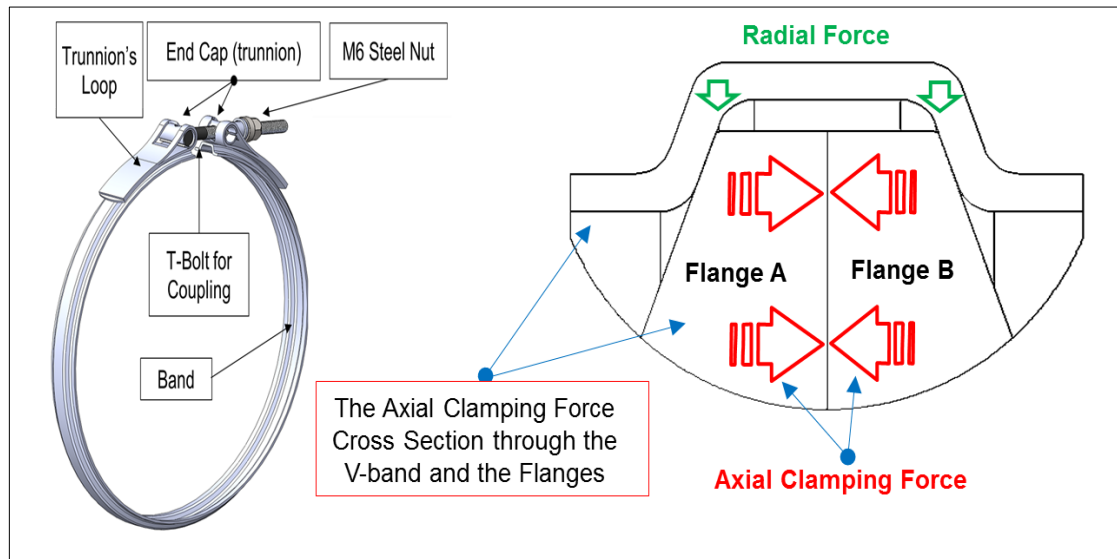


Figure 1 - 4: V-band Clamp Working Forces

### 1.5 Uses of V-bands

Besides the previous V-band applications noted, there are other applications such as in the oil industry, where the V-band used must be opened from time to time. In such applications the V-band can be a quick-release stainless steel V-band clamp. This makes it easy to take apart and reassemble. To summarise then, the benefits of the V-clamp are as follows:

- Rapid and simple assembly and removal
  - Strong axial force to seal against gas or fluid pressure
  - Low initial cost for standard sections
  - Reduction in weight compared with bolted joints
  - Low maintenance costs.
-

These advantages are a major factor in favour of V-band clamps. There is every reason to believe that, with such advantages, the V-band clamp will continue to be more widely used.

Currently, this project deals with automotive engineering and the application of V-bands within turbochargers (see Figure 1 - 6). Within a modern turbocharger, V-bands are often used to form the mechanical connections between the compressor and turbine housing and the bearings housing, as can be seen in Figure 1 – 5.

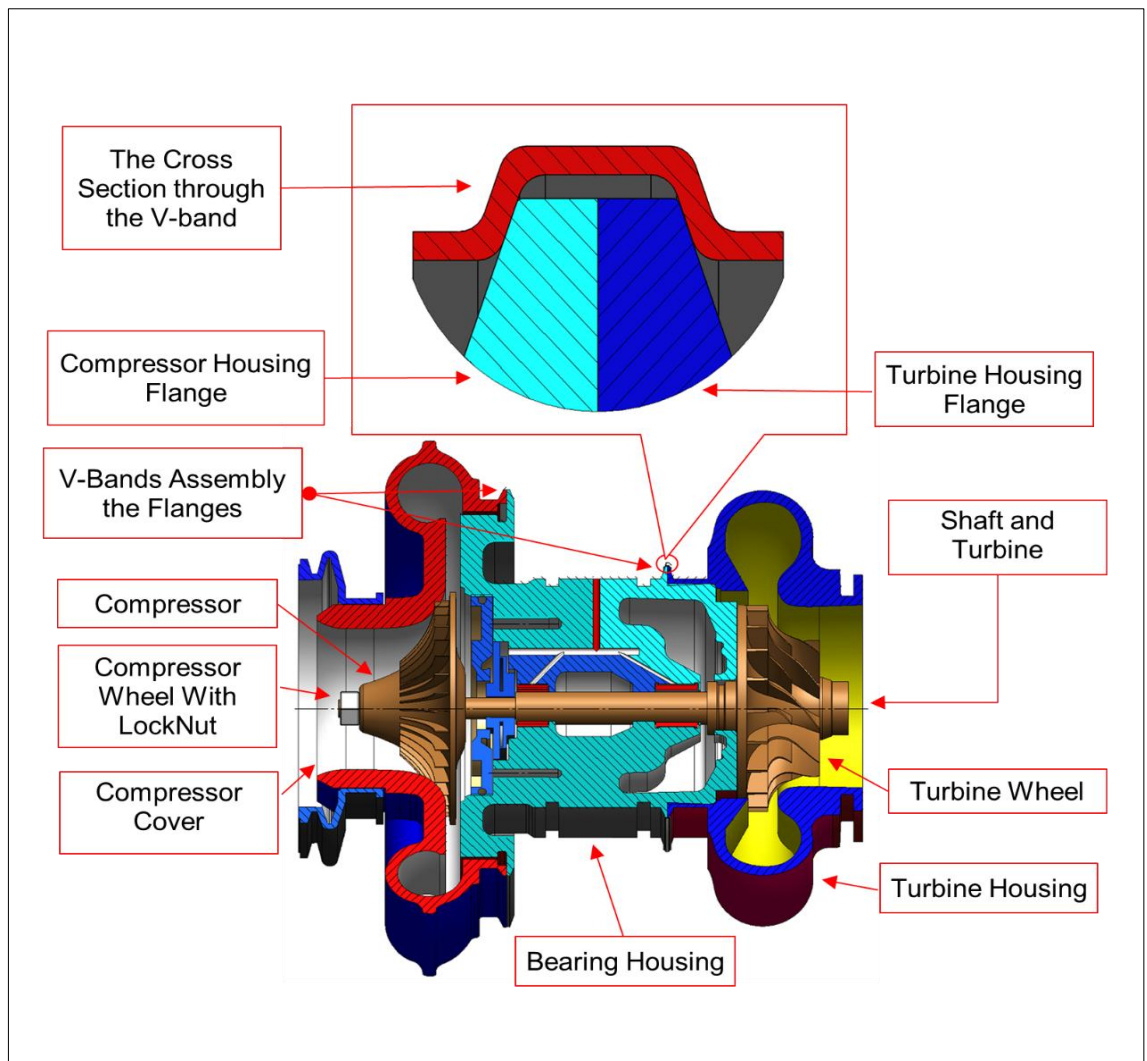


Figure 1 - 5: Automobile Engine Turbocharger in Solid Model

---

## 1.6 Torsional Problems that Effect a Turbocharger

When a turbocharger is activated the resulting vibrations lead to torsional loading as well as banding load capacity.

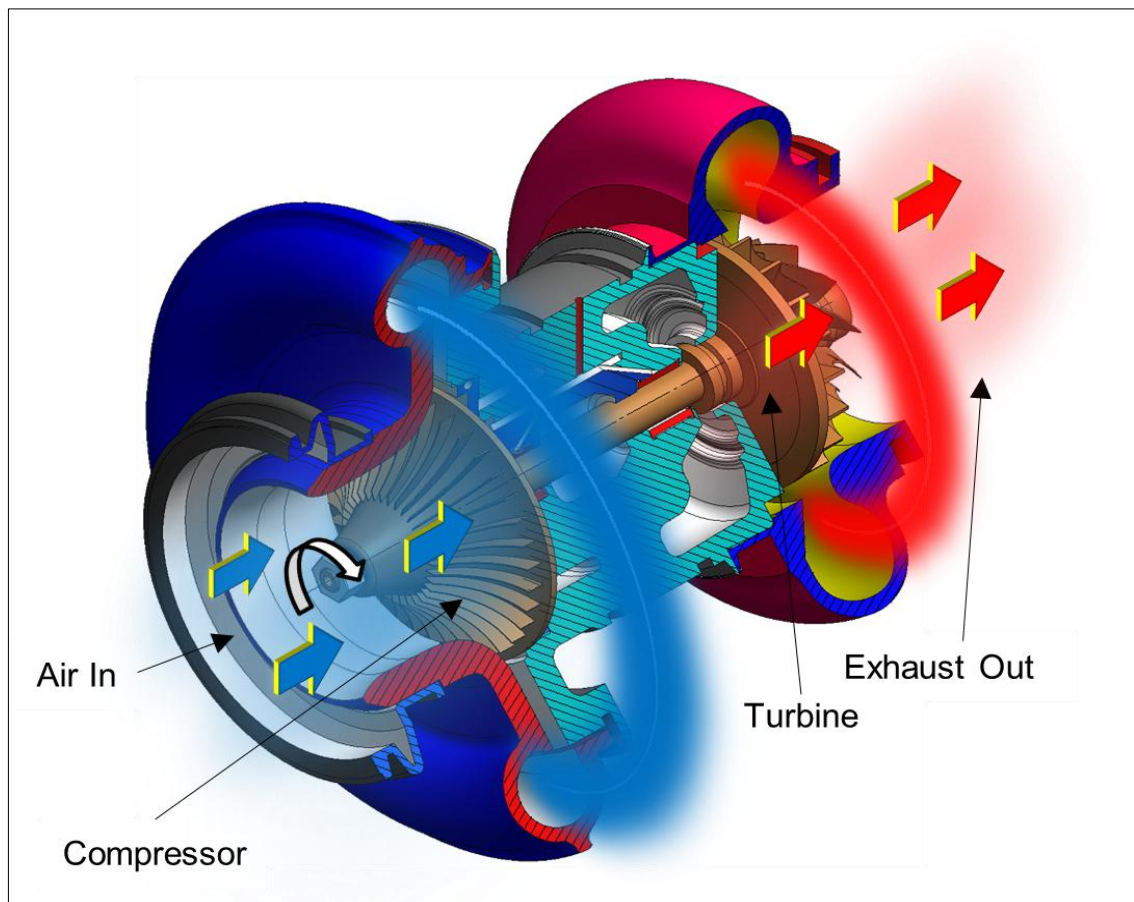


Figure 1 - 6: Engine Turbocharger Under Loading

During operation, gas pressure, Barrans, et al. (2014) inertia forces and thermal expansion can all result in torsional loads being applied to the V-band joints.

---

From Figure 1 - 7 can be seen the forces generated by the torque loading acting on the V-band. This is the torsional load capacity that will be measured during this research project.

During the working of a turbocharger (see Figure 1 - 6), temperatures can reach 700 °C at the turbine housing and the exhaust outlet. The temperature changes will cause thermal expansion in the air intake, exhaust outlet and compressed air pipes supplying the turbocharger.

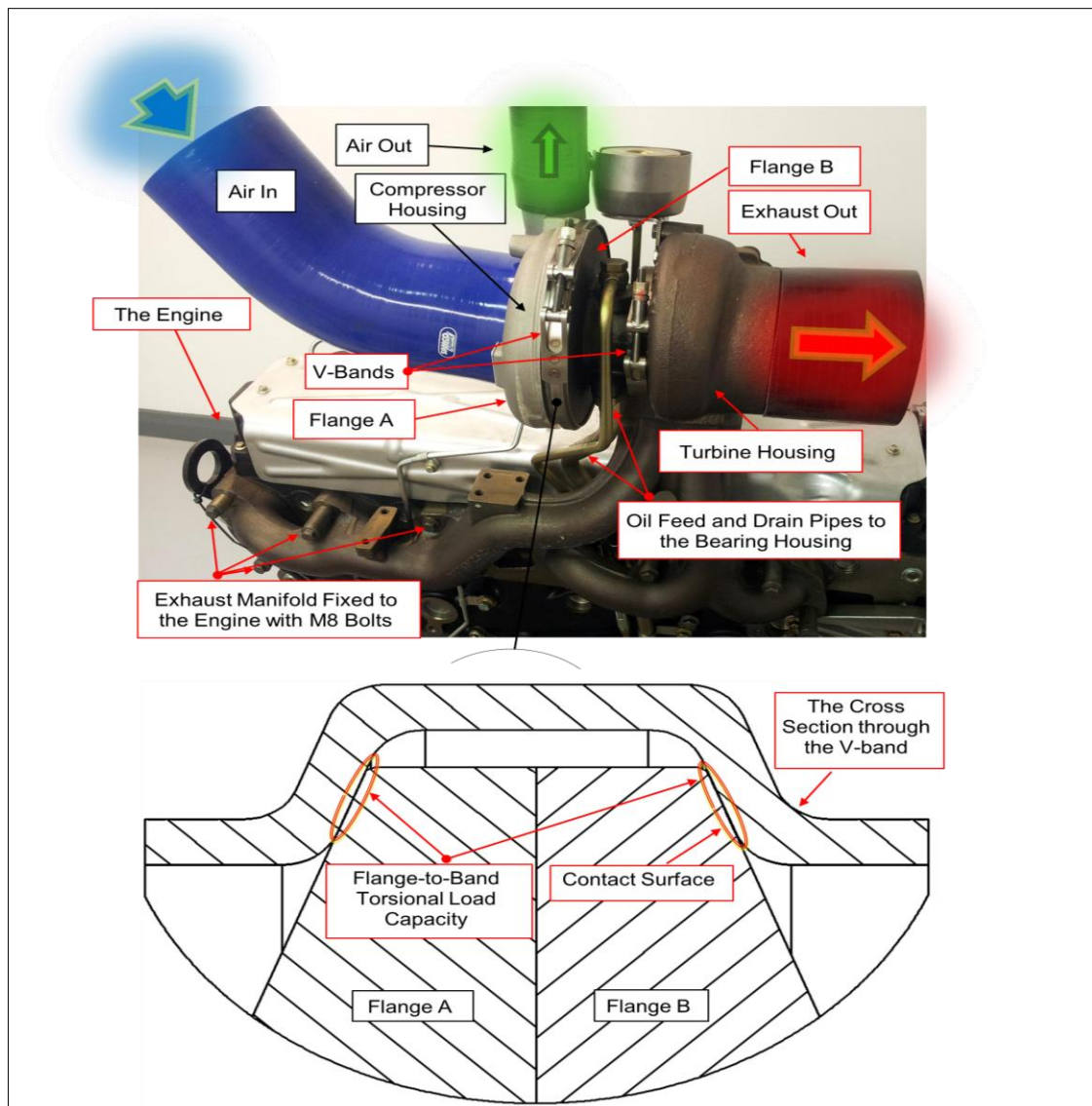


Figure 1 - 7: Sources of Torque Loading on V-bands in a Turbocharger

---

At the compressor end of the turbocharger, temperatures are in the range 100-200°C. In Figure 1 – 8, the turbocharger installed in the engine, using 8 lock nuts, converts the initial loading from the engine into torsional loading acting on the V-bands clamps. The vibration from the engine is transferred to the turbocharger, creating the torsional load capacity acting on the V-band clamps (see Figure 1 – 8).

### **1.7 Aim of the Research Project**

From the overview of the previous sections the research aim is to provide a robust method of predicting the torsional load capacity of a V-band clamp and validate the theory developed by this research project. This work is intended to extend the current theory to encompass torsional loading. The computer simulation used when is involved the development of the theoretical model has limitation identified and addressed. The FE models were employed to simulate the maximum Torsional Load Capacity. In addition the computer simulation will be used to help quantify the impact and address the limitations of the theoretical model. A theoretical model will be validated through the experimental work investigation. The Theoretical model produces the quicker results, where the Finite Element model results takes longer, with the experimental investigation results taking even longer to produce.

### **1.8 Objectives of the Research Project**

- Determine through the literature review, research and approaches that have been undertaken and which are relevant to the research project being done.
-

- 
- Develop a detailed understanding of the V-band clamp design and function.
  - Build and run 3D Finite Element models of the V-band clamps and validate the model against experimental data.
  - Be able to predict by using 3D Finite Element models of a V-band clamp, the impact of model variables on the V-band's performance.
  - Develop features of the V-band torsional test rig. Using technical calculations, validate the test rig development design and produce data and handling characteristics. In relation to the test rig, work through the concept selection, with subsequent robustness exercises and verification.
  - Identify the point of initial slip between flanges and the V-band.
  - Theoretical analyses of the V-band clamps results involving the Theoretical Model approach and Finite Element Analysis approach, which will be used with the experimental results, to validate the experimental investigation approach.

## **1.9 Research Methodology**

A flow chart illustrating the analysis methodology is given in Figure 1 – 9. The research project will involved three different stages:

- The first stage involved the development of the Theoretical model
  - The second stage involved the development of FE models.
  - The last stage involved the Experimental investigation.
-

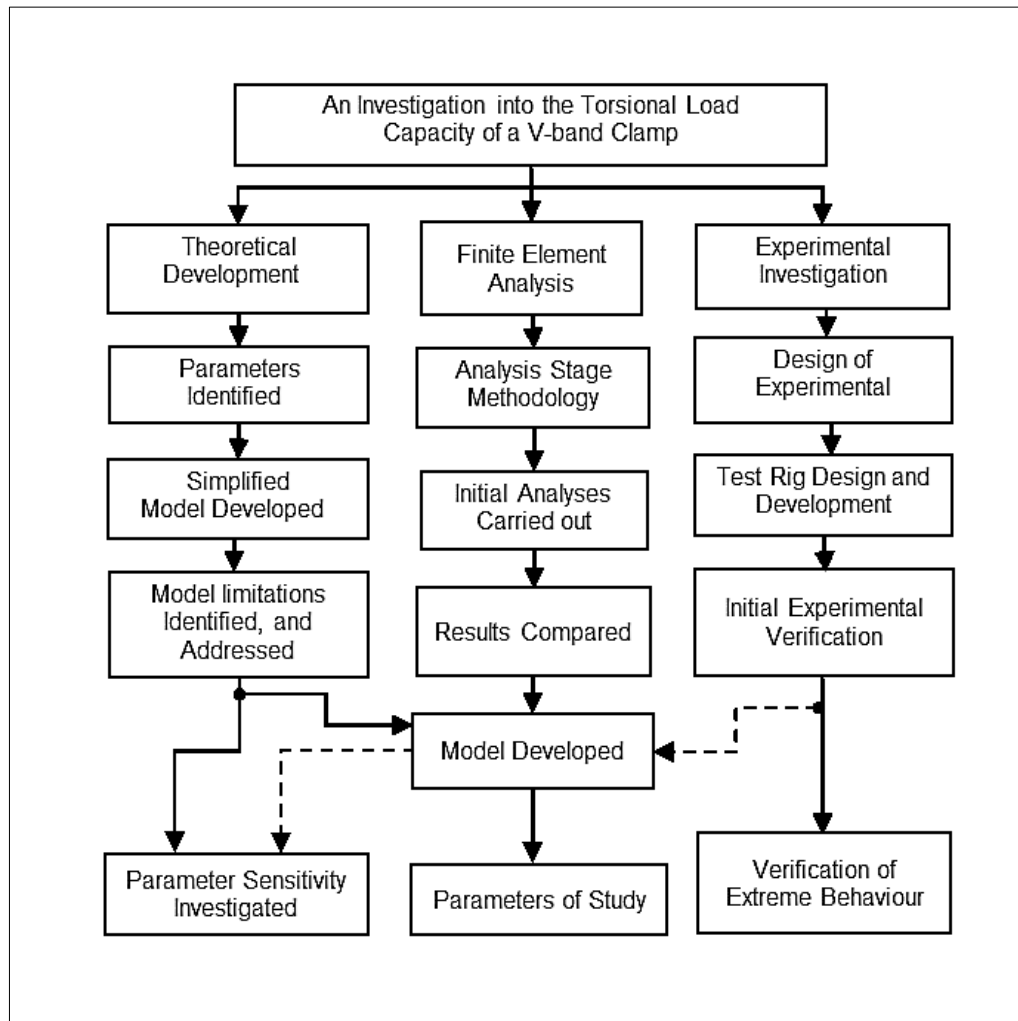


Figure 1 - 8: Elements of the Project Structure

- The first stage will develop the full torsional load capacity model. This will consist of two parts; the torque at the flange-to-band and the torque at the flange-to-flange interface (Barrans et al, 2014). The torque at the flange-to-flange interface will be determined using single plate clutch theory, assuming a uniform pressure (see Hannah & Stephens, 1984). This aspect of the Theoretical model's development is linked to the work of Guo et al (2010).
- The second stage will use half of full 3D finite element models of half the V-band joint for three different sizes of V-bands. The computer simula-

---

tion will be used to help quantify to impact of and address limitations of the theoretical model. For example, the theoretical model will be linear and will therefore not account for changes in the V-band cross section as it is tightened onto the flanges. The finite element model will not be restricted in this way. A finite element model will be preferable to an experimental test at this stage as the experimental method will introduce a number of uncon-trolled parameters (for example the coefficients of friction at the interfaces)

- The last stage will provide experimental data to validate the theoretical model results and the FE results, and will quantify the impact of those parameters which cannot be controlled. The experimental work will be carried out on a specially developed torsional test rig, which was designed and built at the University of Huddersfield (Barrans et al, 2014).

### **1.10 Research Risk Assessment**

Experimental work undertaken in this research will be performed in the University of Huddersfield's Laboratory. All the laboratory equipment is subjected to the Health and Safety requirements of the University of Huddersfield's policy (2010 - 2014). The health and safety procedure has been reviewed for the project's experimental work. See appendix B for more details.

### **1.11 Conference and Journal Publications**

As a part of this research, the results have been published in research articles and presented to conferences. See appendix C for more details.

---

---

## 1.12 Outline of the Thesis

**Chapter 1:** Gives an introduction to the research and an overview of the V-band clamps' problems regarding torsional loading capacity. The Aims and Objectives and Research Methodology are also presented.

**Chapter 2:** Literature survey: this chapter details the literature relating to V-band clamps that is relevant to this PhD thesis. Analysis of the torsional load capacity of V-band clamps is the most important thing discussed. It will be shown clearly how this occurs and what the effect is on the system as a whole.

**Chapter 3:** Theoretical Analysis - this chapter shows how the Theoretical Model was developed.

**Chapter 4:** Test rig - this chapter discusses and shows the development of the test rig.

**Chapter 5:** FE Model – this chapter details how the FE model works and how it was developed.

**Chapter 6:** Experimental Investigation stage, this chapter details the validation of the results from the Theoretical Model (Chapter 3) and the FE model (Chapter 5).

**Chapter 7:** Comparison of the results from the three different stages.

**Chapter 8:** Discussion and Conclusion - this is the final chapter that summarises the research project findings and the main conclusions of the research.

The research project will also include the development of an experimental test rig to provide the data required to validate the theory. The research is intended to find the point of initial slippage between flange and V-band clamp as identified in the research project

---

---

# Chapter Two

## Literature Survey

### 2.1 Introduction

This chapter gives the results of the literature survey that was carried out on the application of V-bands in turbochargers. From the literature survey, an understanding can be gained regarding the history and development of the V-band and Marman clamps and the functional requirements of V-bands.

### 2.2 Historical Background

#### 2.2.1 Flat Band Clamps

In 1921, the London Patent Office (LPO) granted the first patent for the Jubilee Clip device to Lumley Robinson. The Jubilee Clip was designed to hold a soft, circular pipe. Many variations were subsequently developed and now there are many other clips with a similar design.

Between the 1920s and 1940s, the analysis and design of bolted clamps was further refined in the United States, United Kingdom and Germany. These refinements led to design rules for clamp joints being introduced by the American Society of Mechanical Engineers (ASME) in the 1940s. The method of design has not changed radically since then, as the basic design has proved to be successful across a wide variety of applications.

#### 2.2.2 Marman Clamps

Hagen, et al (1948), and Christopherscn et al (1951) successfully applied for a US Patent for the Marman clamp. The initial design of the clamp has been

---

---

very successful and has been further developed across a wide range of applications. The design of bolted clamps has also been further refined in other countries including the United States.

Lazansky (2012) has noted that “Marman Products” was the name of the company which first produced this type of clamp in the 1930s. Lazansky (2012), has stated that the “Marman clamp” or “Marman ring” is a generic ring clamp used to join two cylinders butted together at each end. The first Marman clamps were flexible straps or bands around a series of circumferential V-wedges over the angled flanges of mated cylinders.

A description of Marman clamps has been provided in Chapter One (Section 1.3). According to research undertaken by NASA (NASA, 2000), for Marman clamps it is desirable to have low friction. However, friction control is more important with regard to repeatability and predictability. The required clamping strap preload is reduced by friction at the V-segment-to-ring interface.

NASA uses V-segments to clamp the flanges in an assembly method similar to that used in the current research. In addition, the assembly method also generates a similar ring radial loading to that of the current research. However, the NASA Marman clamps involve two t-bolts on opposite sides, whereas the clamps used in this research involve only a single t-bolt. This could have implications for the effects of loading to be analysed within current research.

Variations have been developed subsequently and there are now many other Marman clamps with similar designs used under testing conditions to do with mechanical problems such as torsion, banding and stress. Under these exact-

---

---

ing conditions the clamps perform reliably and safely. They have therefore been employed in a wide variety of settings and applications such as material handling, ducting or air conditioning systems and space exploration.

Di Tolla et al (Dorf & Kusiak, 1994), used experimental tests to demonstrate that the gap capability (when the flanges separate) of a Marman Clamp joint is independent of the application of load cycles. They further investigated the joint using axisymmetric finite element simulations.

The Detroit Flex Defense (2015), company offers many different types of closure mechanism such as the Marman Quick Latch Coupling, to meet different application requirements. There are some common core variants that are lever operated such as t-bolt and quick coupler with different closure mechanisms. These can be fabricated from type 321 Stainless Steel, Detroit Flex Defense, (2015).

### **2.2.3 V-band Clamps**

Mountford (1980), developed guidelines for the use of V-band clamps and formulated equations that allowed for the appropriate band to be chosen for a particular application. However, Shoghi (2003), questioned the empirical basis of Mountford's (1980), equations and therefore they should only be viewed as design guidelines. Specifically, Mountford did not account for the V-section's angle's effect, or for the friction effect between retainer and flange surfaces. However, it should be noted that Fritskey (2012), takes the same empirical approach as Mountford (1980).

---

---

For the eighty years that band clamps have been in use, attempts have been made to ensure that the radial load is evenly distributed. This has been achieved by overlapping the ends of the band and including inserts in the area under the t-bolt. Recently however, Shoghi et al (2004), has described the elastic behaviour of such clamps and demonstrated that, owing to frictional effects, it is unlikely that the radial load will actually be evenly distributed.

Within the aerospace industry, V-band retainers are widely used to connect satellites to their delivery systems, both during launch and ascent. When used in this way they are often referred to as Marman clamps. (Stavrinidis, Stavrinidis, Klein, Brunner, & Newerla, 1996), has done work on placing two parts of the V-band clamp, such as flanges, together. This is relevant to the current research.

Another dynamic analysis was carried out by Lin and Cole (1997), who showed that the stiffness of the clamp segments is a key variable. They claimed that the stiffness values given by the manufacturers were inaccurate.

Ungar's (1964), cited in Ibrahim & Pettit (2003), research into joints, flanges and surface finish effects on energy dissipation found that for each system, the energy dissipation rate was non-linearly dependent on the applied force's amplitude. Ungar (1964), found that bolt tension showed an overall decrease over time, dependent on the induced tensile stress in the bolt, joint geometry and surface properties.

### **2.3 Clamp Stresses**

On this subject, work has previously been published by Shoghi et al (2004), in the article 'Stress in V-section band clamps' and within the thesis by Shoghi

---

---

(2003). Through experimentation as well as FEA results, these authors have developed a theory that accounts for friction working between the flange and the V-band in the circumferential direction. This allows for a more rational method of analysis and helps with the design of V-band clamps.

Shoghi et al (2005), set out to develop a method of predicting the axial clamping load, which is the load necessary to overcome the preload of the clamped joint. This finding is a development from the research previously conducted by the same researchers, Shoghi et al (2004).

Shoghi et al (2005) were looking to analyse the deformation of V-bands in turbocharger applications that use a single t-bolt. Shoghi et al's (2005), research is relevant here as the current research also uses a single t-bolt in a turbocharger application.

Qin et al (2010), found that their presented joint model's validity was verified in their research. Simulations undertaken for the clamp band joint system within its proposed dynamic model showed that the joint diminished the system stiffness and brought nonlinearity to it.

In Qin et al's (2010), research, their model viewed the flange as deformable and the V-band segment as rigid. However, the current research views the flange as a rigid body and the V-band as deformable. The current research is designed to discover the circumferential contact area with the flanges.

Qin et al (2010), found that: "variation of the preload had no obvious effect on the system response as the excitation stayed within the allowable clamp design load" (p.4500). Qin et al's (2011a), simulation results also showed that there

---

---

was a lessening of the clamp band joint interface's local stiffness, which resulted in changes to the system resonance frequencies and response amplitudes.

The effect became more pronounced and therefore could not be ignored when "considering relatively higher mode" (Qin et al, 2011a, p. 2172). However, Qin et al (2011a), also found that when the LV/SC (launch vehicle and spacecraft), system was subjected to longitudinal impact excitation, the joint interface stiffness altered along with the impact amplitude, and thus affected the response of the spacecraft nonlinearly: "Due to the application of the spline configuration at the joint surface between the interface ring and the payload adapter, the clamp band joint has little effect on the lateral impact response of the LV/SC system" (Qin et al, 2011a, p.2172).

## **2.4 Clamp Joint**

Research done by Shoghi et al (2004), found a method for predicting the axial load generated in a V-section band clamp joint, which takes into account both transverse and circumferential friction.

The validity of the theoretical model they used was found through practical testing of V-band clamps with extreme diameters. However, the practical results' agreement with the theoretical model fell "within the error band due to uncertainty regarding the coefficient of friction within the joint" (p.12). Shoghi et al (2004), also found that in some cases the V-band's axial load effect on other turbocharger components can be significant.

Shoghi et al (2004), recommend further work to extend the current theory around prediction of the V-band's ultimate failure. The theory does however

---

---

predict failure around the internal corners of the V-band. To further develop the theory they advise that section bending and the effect of residual stresses due to the forming process would have to be included.

The experimental method they used still has two potentially significant error sources. One is the misalignment of flanges and the other is the application of undesirable torsional load to the t-bolt load cell.

Shoghi et al (2004), advise a solution to the former “by running the two flanges on the same ground shaft within a purpose built test rig” (p.12). For the latter, they were reviewing alternative methods for the application of the t-bolt’s tensile loading.

Barrans & Müller (2009), state that the ultimate axial strength of V-band clamps is presently only ascertainable through physical testing and that this testing points to the strength being determined by “two different types of structural deformation” (p.2): plastic and elastic deformation modes.

In the paper by Guo et al (2010), they present an analytical methodology for the prediction of the axial clamping force (from Shoghi et al, 2004), and anti-rotating torque. They found that this methodology provides knowledge for both designing and using the V-band joint. However, they acknowledge certain limitations of the analytical methodology, including; not considering the duty cycle effect, only predicting anti-rotating torque and the axial clamping force at room temperature and being only applicable for V-bands with one t-bolt and for larger size V-bands. In addition, there are assumptions in the paper including; constant contact pressure between the two housings and no radial direction friction,

---

---

that lead to prediction errors, Guo et al (2010). Consequently, Guo et al (2010), recommend that further work should focus on “reducing the error sources, and including temperature effects and cycle-to-cycle variation” (p.9).

Ibrahim and Pettit (2003), state that many factors affect bolted joints, including hardness, finish, friction and the relative dimensions of all the parts involved. Due to usage or manufacturing tolerances, each factor varies from joint to joint and bolt to bolt and this allows parametric uncertainty for all jointed structures and joints.

(Richardson & Hershberger, 2012)), researched joints, the components of a gas turbine including a turbine section, bleed air collector box, compressor section and V-band clamp. They noted that before the turbine section is the compressor section, which includes the compressor case that in turn encloses the compressor part. Attaching the compressor case to the bleed air collector box is the V-band clamp.

Ignaczak and Chen (2012), state that when the V-band is fastened to a pair of tubular body end flanges, it involves the clamp extending around the circumference from a first to a second end, with a latch assembly positioned at both of these band ends and a number of V-inserts positioned radially beneath the band. The latch assembly comprises a fastener used to fasten the V-band clamp and a number of V-insert segments that include both first and second V-insert segments. These tighten the V-band on to the pair of end flanges so that the V-band tracks circumferentially and is independent relative to the 2<sup>nd</sup> V-insert segment, Ignaczak and Chen (2012).

---

---

Johnson and Friedrich (2013), successfully applied for a US Patent band clamp that clamps together first and second pipe sections. These each have outward projecting flanges with flange faces opposing that projection about the circumference. Johnson and Friedrich (2013), explained that the clamp includes a conforming material placed between the outward projecting flanges and the band clamp and arranged to link with the outward projecting flanges. This produces an inward directed radial force at the time the band clamp is tightened and to “radially pilot the outer surfaces and the first and second pipe sections relative to each other and the corresponding centerlines”, Johnson and Friedrich (2013, p. 1).

Simons et al (2014), found a number of different brackets and shoes. A tensioning device and a band clamp are among the techniques for detachably fastening a 1<sup>st</sup> and 2<sup>nd</sup> component. The band clamp’s configuration enables the number of different shoes to engage with both the 1<sup>st</sup> and 2<sup>nd</sup> components’ abutting cylindrical flanges and provide enough clamping pressure to join these two components. Each of the different brackets attaches to one of the two components. The adequate clamping pressure derives from redundant, independently inspectable sources, with the band clamp’s circumferential tension being a primary redundant source. Tightening the tensioning device delivers a 1<sup>st</sup> radial restraining force on the shoes, the second radial restraining force being a secondary redundant source given the number of different brackets on the band clamp, (Simons, Wittmer, & Bray, 2014).

Friedrich and Gary (2011), stated that the V-band clamp is comprised of the inner and outer surfaces of a curved band and 1<sup>st</sup> and 2<sup>nd</sup> ends. Characteristic of the band is a substantial V-shaped cross-section in the band’s radial plane.

---

---

The band's inner surface defines the V-shaped cross-section's inside contour. The clamp's fastener is configured to bring together both ends so that the band can be tightened around adjacent flanges of objects to be held together. Its inner surface is designed so as to push the flanges together and fasten the objects. The V-band has a reinforcement designed to stiffen the substantial V-shaped cross-section and lessen its yielding when clamping the objects, Friedrich and Gary (2011).

Murphy et al's (2015), patent application concerns a clamp for the internal coupling and decoupling of two parts. This can include a base that fits within the interior of one or both parts to be joined together. It can also include an engagement member which is movably supported on the base. This member can interface with and connect with interior sections of both parts when they are joined together and be separated from the interior sections of the two parts when decoupled. The clamp can include a wedge that is movably supported about the base and which aids the movement of the engagement member between its coupled and decoupled positions. Additionally, the clamp can have a secure and release mechanism. This connects with the wedge and the base to alternately fasten the wedge in maintaining the engagement member in its coupled position and releasing the wedge to aid the engagement member's movement to the decoupled position.

#### **2.4.1 Development of the V-band Clamp**

Bhosale et al (2012), did their research on a multistage satellite launch vehicle due to the fundamental importance of stage separations. Separation of spacecraft and satellite parts during flight, when they are no longer required, must

---

---

happen with clean separation and at the appropriate times during the flight. Bhosale et al (2012), stated that during separation there should be no shock loads, no contact between separating parts and no harmful debris. Otherwise, these could lead to damage to structure and critical equipment, attitude errors and could cause mission failure. In Bhosale et al's (2012), research on a Band Release System, an extended motion analysis study was conducted. They used ADAMS (Automatic Dynamic Analysis of Mechanical System), and in addition motion analysis of the entire system was undertaken with a view to evaluating the reliability of the system with regard to clean separation. Research was conducted on band and wedge blocks' velocity and displacement and acceleration after the use of the pyro-thruster using motion analysis of the system. With the intention of determining how reliable the system is in performing clean separation, motion analysis of the entire system was undertaken, Bhosale et al (2012). Additionally, release failure owing to the snagging of the wedge block was indicated. This was shown by the maximum displacement values found from the simulation results as compared with the minimum displacement necessary for clean release.

Barrans et al (2014), state that the apparently simple V-band clamp component is widely used in modern turbochargers to connect the three housings. Therefore the clamps are an important part of the same load path as the bearing housing for containment and burst loads as well as external loads. This can be demonstrated by the V-band clamp's failure during a burst and containment test. V-band clamps, as well as guarding against containment failure, must also precisely locate the housings so as to maintain the very small clearances be-

---

---

tween the housings and the rotor wheels. If the clearance between these components increases, there is a significant decrease in turbocharger efficiency.

With regard to the V-band as a structural component, as noted before, V-bands are critical parts in terms of both external loads and also for containment purposes. They are also an integral part of the load path between the turbocharger housings. Barrans et al (2014), citing Shoghi (2003), pointed to the near absence of any theoretical understanding of V-band behaviour. Subsequently, progress has occurred with Shoghi et al (2004), developing a theory for both the stresses produced in a clamp when it is connected onto flanges and the axial clamping load produced by a clamp.

Recently, a theory for predicting the axial stiffness of this type of connector has been developed by Barrans et al (2014), and although this agrees significantly with FEA simulations, it needs experimental validation. Additional work is also needed for determining how this clamp type interacts with flanges that are separated by a flexible gasket. Analysis of the torsional capacity of a joint formed using this type of connector has also been undertaken by Barrans et al (2014), although refining the theoretical model is still required for low aspect ratio bands.

The ANSI Std (2014), research project used a V-band clamp to fasten securely in position a flexible, flat seal that butts up to the plenum lip seen in Figure 2 - 1. To tighten the clamp after installation requires access to the seal.

---

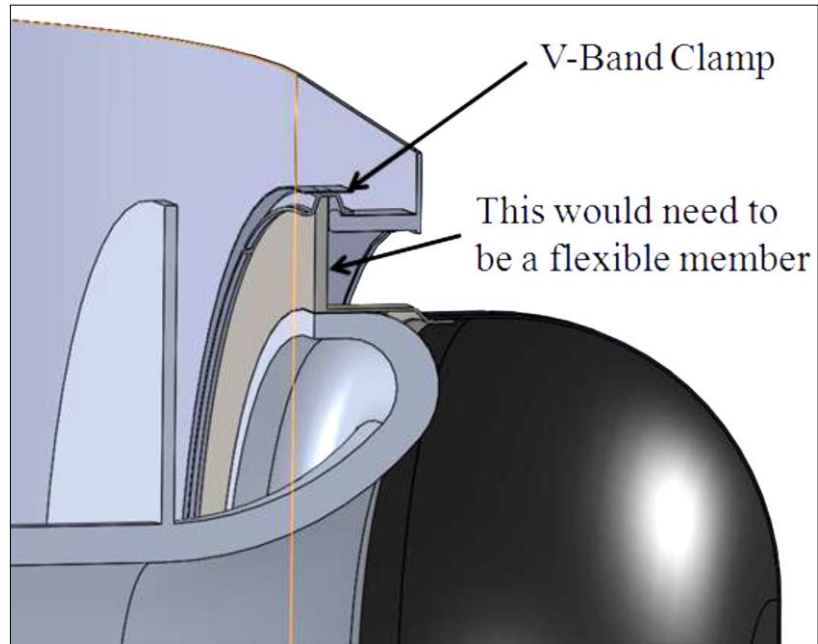


Figure 2 - 1: V-band Clamp Seal Concept, ANSI Std, (2014)

The cartridge clamp works in a similar fashion to the V-band clamp, as can be seen in Figure 2 - 2. The top half of the clamp would be fastened to the plenum and the lower half accompanies the turbine and mates up with the top side and is then fastened in place.

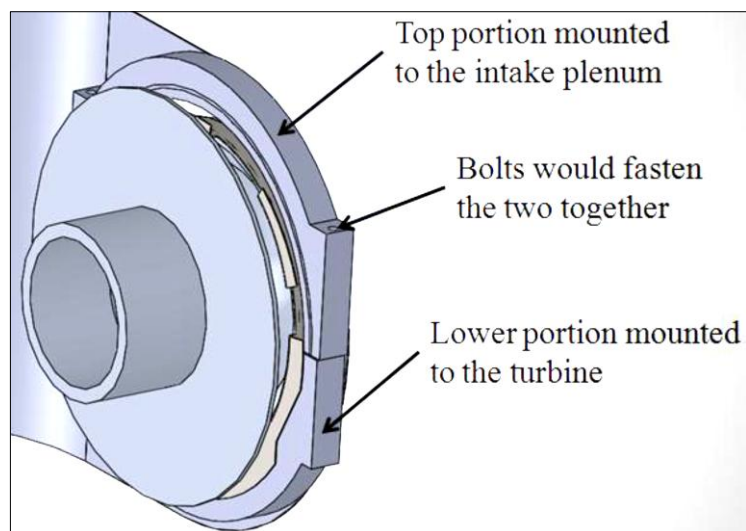


Figure 2 - 2: Cartridge Clamp Seal Concept (ANSI Std, 2014)

The standards governing the grooved clamp coupling and flanges that join the intermediate pressure and temperature ducting in the pneumatic systems of aircraft can be found in AS4751, SAE International (2013). The SAE Aerospace Information Report AIR869B, notes that V-Couplings will work as intended only if installation is correct and gives further information regarding both application and installation, SAE International (2014).

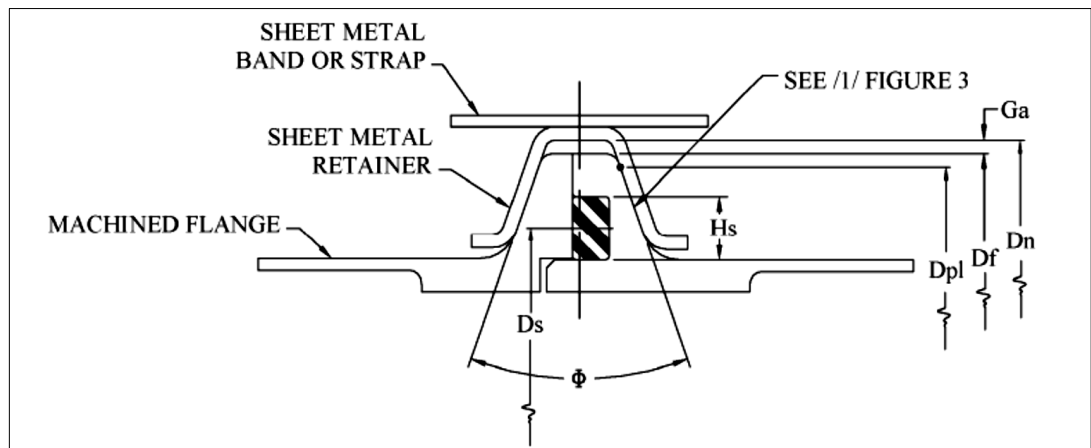


Figure 2 - 3: V-band Coupling Joint and Machined Flanges, SAE (2014)

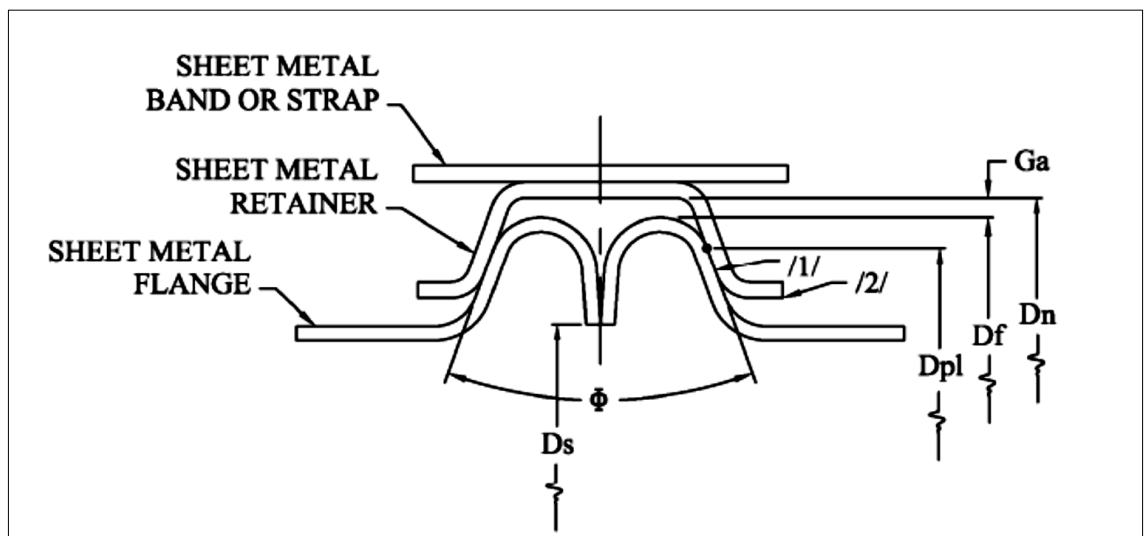


Figure 2 – 4: V-band Coupling Joint and Sheet Metal Flanges SAE (2014)

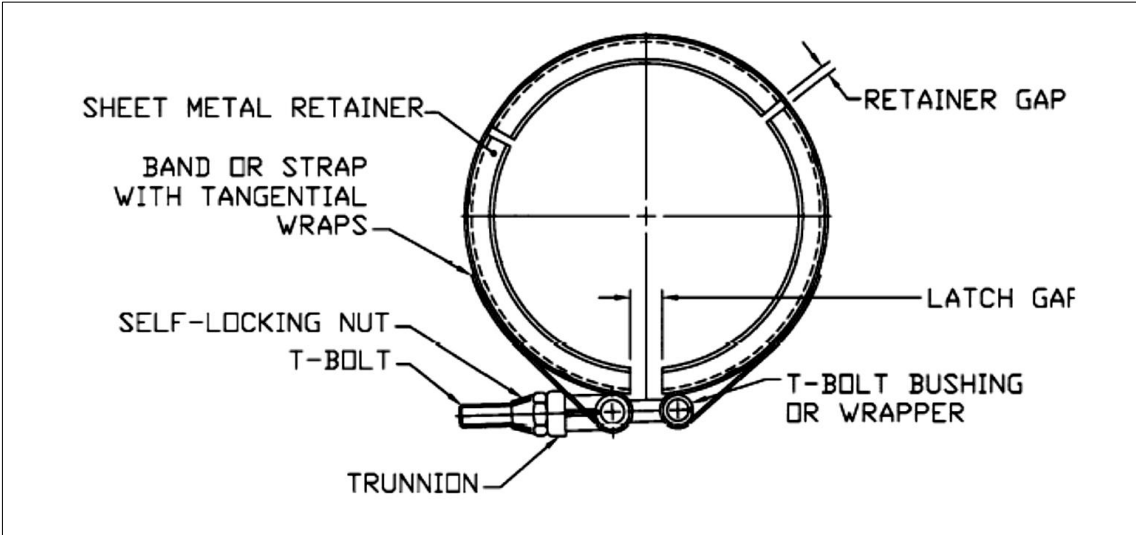


Figure 2 - 4: V-band Coupling, SAE (2014)

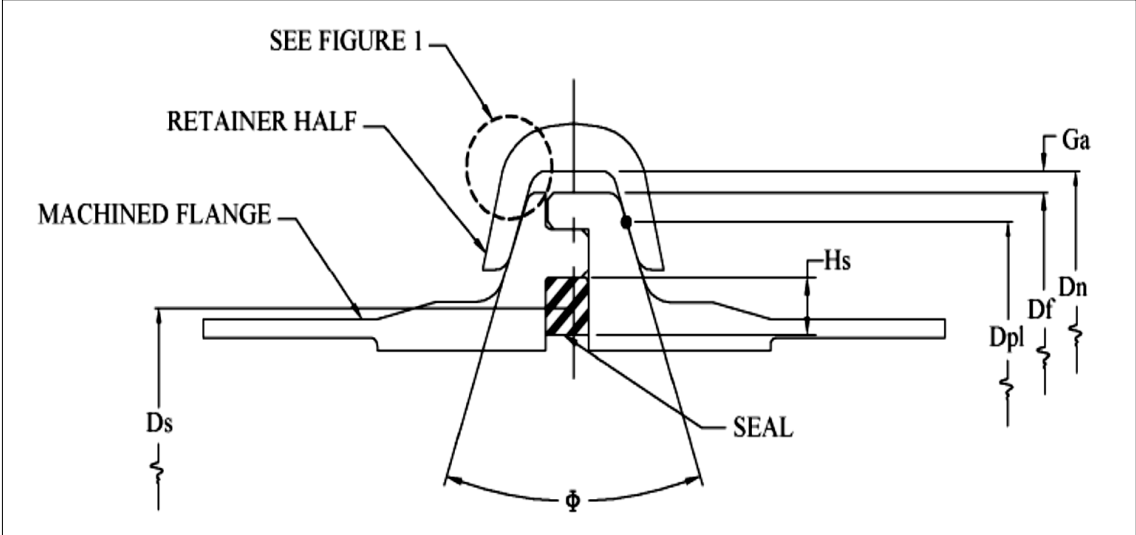


Figure 2 - 5: V-band Coupling Joint and Sheet Metal Flanges, SAE (2014)

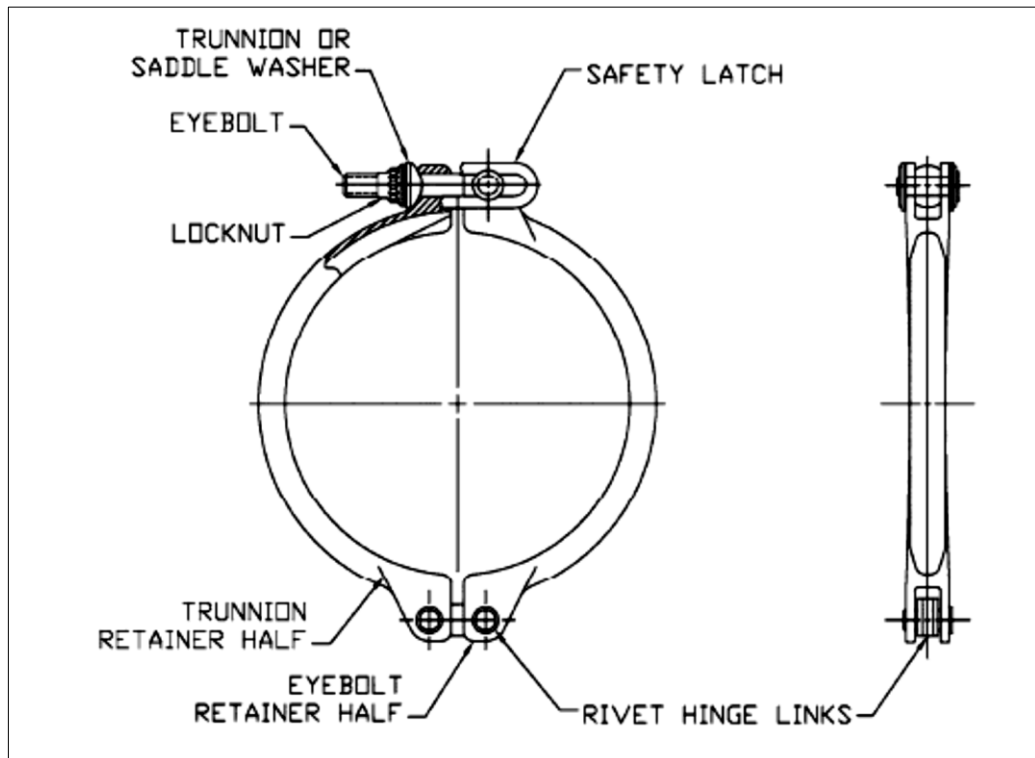


Figure 2 - 6: V-Retainer Coupling, SAE (2014)

A V-Coupling joint is composed of two flanges joined by a V-Coupling. A V-Coupling is composed of V-band couplings as well as V-retainer couplings. The V-Band Coupling design can be seen in (Figure 2 -3, Figure 2-4 & Figure 2-5), and the V-Retainer Coupling design is illustrated in (Figure 2-6& Figure 2-7).

#### 2.4.2 Flexible Interface Rings

A satellite separation system's typical clamp band joint, as often used in LM-3B launch vehicles, is used as an example for performing the separation dynamics contrastive analysis between the new rigid-flexible coupling simulation and the rigid models.

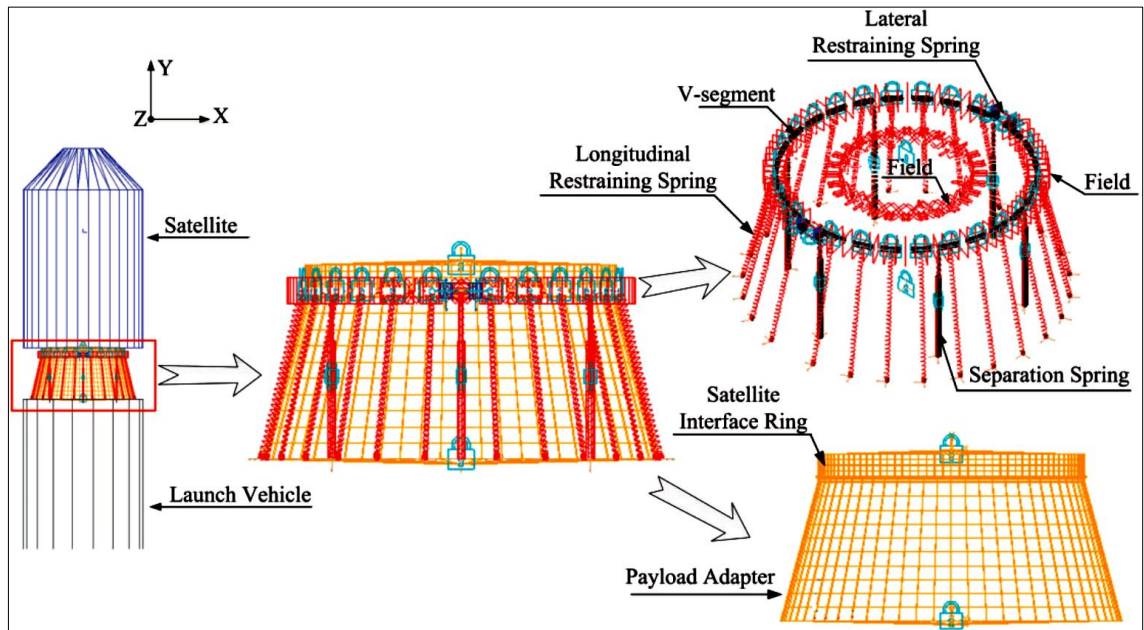


Figure 2 - 7: The Simulation Model in ADAMS, Cui et al, (2014)

Figure 2 - 8, shows the newly proposed simulation model's configuration, where the last rocket stage, clamp band joint and flexible interface rings of the satellite are illustrated.

Cui et al (2014), research purpose was to investigate the position effects in relation to the separation plane, the friction coefficient and the explosive bolts' pyroshock on separation shock responses and clamp band preload. Cui et al's (2014), paper gives a reference for the starting engineering design of the satellite separation system's clamp band joint.

#### 2.4.3 Torque Applied to the T-bolt and the Clamping Load Generated

Yoon & Hwang (2013), examined the V-insert clamp's sealing performance across various applied torques when used in automobile exhaust pipes. They used a specially designed pneumatic testing system for this purpose. The V-insert clamp's axial clamping forces were assessed by a clamping performance test.

---

This test showed that increasing the torque brought a gradual increase in the axial clamping force with all the gaps that were considered between exhaust pipes, and with a slight increase in the torque resulting in a relatively high axial clamping force.

Yoon & Hwang (2013), found that when pipes were joined together using the V-insert clamp, an applied torque of at least 4 N/m was required for the V-insert clamp to function effectively. They also concluded from their research that the V-insert clamp demonstrated “sufficient sealing performance to support the applied pressure of up to 100 kPa within the exhaustion system when relatively high torque was applied”, Yoon & Hwang (2013, p.1).

Yoon & Hwang (2013), were duplicating Shoghi et al's (2004), research on the axial load capacity of V-section band clamp joints and their work confirmed the results found by Shoghi et al (2004). However, in the research done by Yoon & Hwang (2013), they used a clamp with a different cross section and with differing conditional loads applied to the V-section band clamp joints. The current research has been guided by both research elements noted above.

Qin et al (2010), use a free-body diagram of the upper portion of a V-segment and a radial section of the interface ring (see Qin et al, 2010, p.4488), to show where the interface ring is partitioned into a cylindrical shell and a flange. They note that flange deformation involves outer edge torsion and radial compression during both preload and axial loading.

---

---

In Cui et al's (2014), study, the SRS curves for different pyroshock amplitudes of explosive bolts help determine if the pyrotechnic shock of the explosive bolt is one of the satellite separation shock's dominant components.

Notably, the separation shock is not "in proportion nor in inverse proportion" (p.14) regarding the explosive bolts' pyroshock amplitudes for the entire frequency range, but is almost constant. This suggests that the pyrotechnic shock is not the primary separation shock component at the study's measurement point of 30mm above the explosive bolt. Cui et al's (2014), analysis results agree significantly with Han et al's (2007), experimental findings. The current research investigates the effect of torque applied to the t-bolt and the clamping load generated in order to predict the V-band clamps' torsional load capacity.

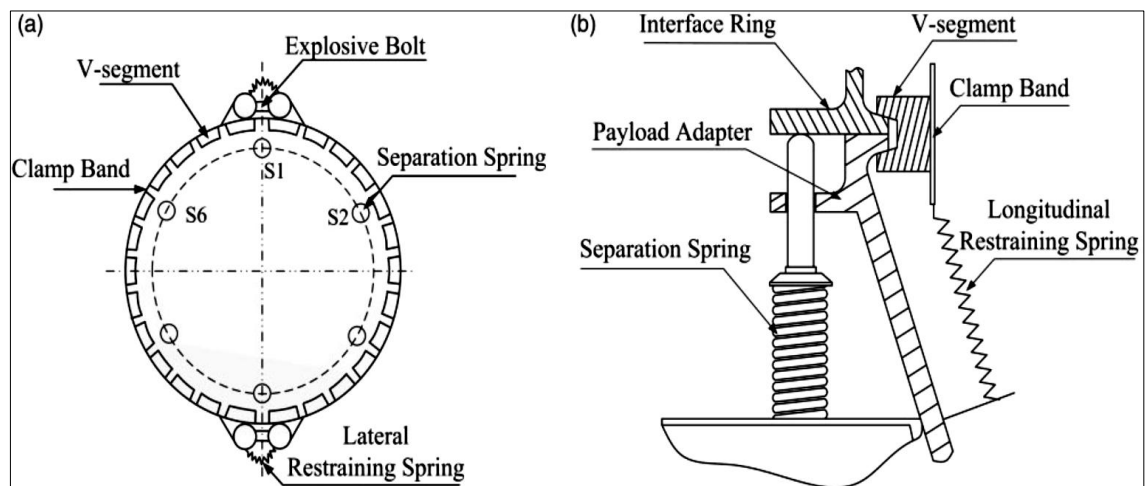


Figure 2 - 8: Lock and Release Mechanism, Cui et al (2014)

## 2.5 Ultimate Axial Load Capacity

In their research, Müller & Barrans (2009), developed a finite element model for predicting the ultimate axial load capacity (UALC), of V-band clamps. Physical testing indicated that ultimate axial strength is determined by both elastic and plastic deformation modes.

---

---

Müller & Barrans (2009), note that from initial use of the finite element model, “analysis of this class of problem is not straightforward”( p.1). However, they present a refined version of the finite element model able to predict both the UALC of V-band clamps and the high strain concentrations, particularly regarding plastic strain at the edge of the V-band’s flat section. Muller & Barrans (2010), work showed that UALC depends mainly on the flange / V-band diameter, due to “the complex plastic-elastic failure mode” (p.16).

Müller (2011), research involved the ultimate axial load capacity of V-band retainers. FEA and theoretical models were used for prediction and validated by using experimental testing. Using V-bands with a single t-bolt and of different diameters, he discovered a new method for the prediction of the Ultimate Axial Load Capacity (UALC) of joints that are formed using V-band clamps. Müller (2011), found that his research led to several unanswered questions and his methodology uses three different approaches. In addition, the FEA addresses the limitations of the theoretical model. The V-band materials that Müller used were in three sizes and the current research repeats this approach.

Barrans & Müller (2009) generated a model able to predict both structural deformation of V-band clamps and the ultimate axial load capacity, by using finite element analysis. However, the accuracy of results was dependent on both; “the element size and amount of elements along the sliding contact surface” (Barrans & Müller, 2009, p.9). Besides which, they were also dependent on the type of mesh.

---

---

Barrans & Müller (2009), suggested further work to develop the model, so as to improve the prediction of “the interplay of elastic and plastic deformation mode” (p.9), whilst taking the influence of several V-band diameters into account.

## **2.6 FEA Methods used to Analyse Marman and V-band Clamps**

Cui et al (2014), propose a modelling and simulation method for fully predicting satellite separation dynamics and involving the interface rings' flexibility. They undertook contrastive analysis of separation dynamics to determine the flexible interface rings' effects on the dynamic characteristics of satellite separation, followed by parametric studies of satellite separation dynamics. Cui et al (2014), researched the flexibility effect on satellite separation dynamic characteristics using a contrastive analysis. Subsequently, parametric studies were done evaluating various structural parameters, including the dynamic envelope of the clamp band, the attitude of the separating satellite and the separation shock. Cui et al's (2014) analysis revealed that the interface rings' flexibility has important effects on the separation shocks and the satellite's attitudes. In particular, the calculated resultant angular velocity within the dynamic model that considered the flexibility of interface rings and within the same boundary condition, is 24.2% higher than for the rigid model. In addition, the maximum shock response achieved a value almost 260 times as much as those taken from the rigid model, thus pointing to Cui et al's (2014), newly proposed simulation model as being realistic and appropriate to reveal the dynamic characteristics during satellite separation “ (p. 14).

The parametric studies showed that increasing the explosive bolts' impulse and decreasing the lateral restraining springs' stiffness could significantly enlarge

---

---

the clamp band's dynamic envelope radii. The studies also showed that the separation shock responses were significantly influenced by the preload of the clamp band and by the circumferential and longitudinal locations relative to the separation plane. In addition, the friction coefficient between interface rings and V-segments only marginally affects the axial shock responses for the high-frequency region, whilst the explosive bolts' pyroshock was not the primary separation shock element.

Cui et al's (2014), proposed modelling and simulation method is suggested as "a reference for the initial engineering design of the clamp band joint of satellite separation system" (p. 15).

Qin et al (2011), used the FEA ANSYS software for their analysis of V-segment bands and the current research uses the FEA ABAQUS software for the same purpose.

Notably, according to Qin et al (2011), "the existing 3D FE models should be extended to analyse V-band joints with larger band diameters, include a finer mesh and should then be compared to the axisymmetric analyses" (p.180).

Barrans & Müller's (2009), research used initial finite element analysis rather than the physical testing used in previous research. It was found that the analysis of structural deformation is not straightforward. There were difficulties simulating the specific component interaction when contact pressures are large and contact is very localised. Barrans & Muller (2009), used an asymmetric model in their simulations because the 3D FE model was too big to be covered in their research project.

---

---

Rome et al's (2009), research looked at two computational techniques in regards to assessing the structural capability of clamp band usage and both techniques used three-dimensional finite element models (3D FEM). researcher found that the analytical predictions for the full 3D model showed significant agreement with test data. However, the cyclic symmetry model was poor in its estimation of hardware capability in withstanding applied loads. Test metrics used to find when gapping occurs were also evaluated analytically. However, they were unable to clearly identify when gapping occurs. Rome et al's (2009), analysis showed that a robust safety factor was required.

Zhang et al (2014), researched contact stress analysis using V-band clamps and piping systems. They used FEA, the new software package COMSOL multi-physicals, theoretical modelling and experimental validations. They found that, because of the spatial non-uniformities of the moment of inertia and the clamp's section area, the bending moment effect was observed in their simulation results. In addition, this effect led to some vertical displacement of the clamp's trunnion when high contact pressure was applied. In conclusion, they recommended that a pre-bent t-bolt design is employed to counteract the offset effect.

In another research article in 2014, Zhang et al (2014a), used FEA to find the initial contact areas between V-band clamps and piping systems. The focus was on the mechanism and effects of mallet tapping on the equalization of contact pressure distribution between these components. They employed a piezoelectric sensor to measure the contact pressures in the initial stage before and after mallet tapping, and used the new software package COMSOL multi-

---

---

physicals for their analysis. Their results pointed to non-uniform contact pressure and this was verified by the FEA simulation. In addition, their results, “reasonably explained the working principle of applying mallet tapping during the entire clamp instalment procedure” (Zhang et al, 2014, p. 59).

Qin et al’s (2011), research modelled the clamp band joint using the FEA analysis software ANSYS and validated the joint model through a number of static experiments. The paper presented the general behaviour and mechanical characteristics of the joint when subjected to preload and axial load. The analysis found two frictional slip stages between the V-segments and the interface rings. These are the micro and macro slip stages.

### **2.6.1 Modelling Techniques and Contact Formulations**

Kitamura et al (2012), constructed two FE models that were created to investigate vibrations produced in the central cylinder (see Figure 2 - 5):

- 1) the central cylinder model
- 2) an assembly built from web panels and a central cylinder. This develops the central cylinder’s rigidity and that of the anti-earth panel on the satellite body’s base surface, (as illustrated in Figure 2 – 6).

The cylinder model (1) enables verification of the computational accuracy when it is modelled solely in a cylindrical shell. The assembly model (2) accounts for the central cylinder and coupling panels’ effects and the structure’s asymmetric properties.

Kitamura et al (2012), stated that, in future, the researchers intend to investigate ways of differentiating the shock response of the central cylinder from that of the

---

---

equipment set on the satellite body, with the aim of designing the whole satellite body with regard to shocks.

Shoghi's PhD thesis (2003, p.139), notes that finite element methods could be employed to assess specific clamps' stress conditions, for a given load condition, while admitting that these methods are usually expensive and time-consuming.

Barrans et al (2014), researched the distribution of interface contact between the flange and V-band when the coupling is in place. They found it "essential information" (p.1), to find the joint's pressure distribution and contact area since it determines the coupling's integrity. A 3D FE modelling technique was used and the results revealed that around the V-band's circumference, contact pressure is non-uniform and the t-bolt area has the maximum contact pressure. This is in line with the theory in the subject area. Barrans et al (2014), also found that the interface pressure distribution curve's form was noticeably influenced by the magnitude and presence of friction and that the band's diameter has a relationship with the effects of friction.

Barrans et al (2014), conclude that especially when the coefficient of friction is large, there occurs important variation around the V-band joint in contact pressure distribution. This can only be revealed in an FE analysis that employs a 3D model. The research also concludes that if the friction in the circumferential direction is dealt with, then the effect of transverse friction will be taken away and that this is important for larger V-bands.

---

---

Zhang et al (2014), built a V-band clamp model to research the contact pressures generated between certain piping systems, specifically the manifold and bellows. In their analysis they included FEA employing COMSOL multi-physicals, theoretical modelling and experimental validations. Owing to the spatial non-uniformities of the section area of the clamp and moment of inertia, the bending moment effect due to the offset of centroid lines between the trunnion and clamp was noted in the simulation results. This effect led to high contact pressure beneath the trunnion and a slight vertical displacement.

The modelling of engineering problems has relied on “ordinary and partial differential equations” (Junker and Wallace,1984), often being non-linear in nature. The finite element method, developed over the last 50 years, has become a powerful tool to solve these differential equations and therefore is to be used within this research. Contact modelling uses two families of formulation for the contact surface with friction. The first is the Penalty Method, and the second is the Lagrange Multiplier Method. These methods are in the normal and in the tangential direction of contact surface for contact modelling and are used as follows:

### **2.6.2 Penalty Method**

To use Finite Element Analysis (FEA), certain conditions need to be considered and met. These include identifying with confidence the optimal design and predicting the design’s performance and behaviour. The latter involves calculating the safety margin and identifying design weaknesses accurately. In addition, the physical behaviours of complex objects must be understood. An FEA appli-

---

---

cation concerns stress analysis which is a primary concern of this research. The stress analysis in this research involves static and nonlinear elements. According to Pisan et al (2010), Penalty Function involves a displacement-based solution. Konter (2000), notes that Penalty Function involves penetration and contact stiffness and controls contact by the addition of springs to a model at each Gauss point element. Surface-to-surface contact, as in a V-band, transmits contact pressure among Gauss points, not forces among nodes, with contact stiffness measured in units of force / length. In reality, penetration never happens between two bodies in contact and because of this, Pisan et al (2010, page 4), describes this as ‘a mathematical “avatar”. It only exists to make sure that the contact force is not zero. However, even if very tiny, it affects the solution and in order to find a converged contact stress, it has to be as small as possible. Penetration can be derived by raising contact stiffness as much as is feasible, although if contact stiffness is too high it will create “an ill-conditioned system matrix, with very high ratio in rigidity terms of the system matrix”, Pisan et al (2010, page 4). However, it does create problems for direct solvers.

### **2.6.3 Lagrange Multipliers Method**

Müller’s PhD thesis (2011, page 42), cites Konter (2000), as discussing the Lagrange Multiplier Technique’s disadvantages, but sees it as being more precise than the Penalty Method since the Lagrange Multiplier Technique includes an extra variable. However, Müller’s PhD thesis (2011, page 42), cites Wriggers (2006), as pointing to the Penalty Method as more robust and more likely to lead to a converged solution, since the energy system comprises the single displacement variable.

---

---

Piscan et al (2010, page 5), states that for Lagrange Multipliers, contact forces are included as a separate DOF. The software calculates directly for pressure or contact forces. Therefore, Lagrange Multipliers add equations to model and bring a higher computational cost.

Additionally, it involves zero diagonal terms in the system matrix leading to a limited solver selection (direct solvers only). For small models, direct solvers are more efficient. However, occasionally they require additional computer resources to handle larger models. An advantage of Lagrange Multipliers is that they do not involve contact stiffness Piscan et al (2010). Penetration still exists, but it is basically dependent on mesh size, as a finer mesh corresponds to a higher number of contact detection points.

For Piscan et al (2010, page 6), when simulating the actions of machine-tools, defining joints is amongst the most difficult aspects since many variables can affect the joint's properties. From finite element analysis programs, the machine tool's dynamic characteristics, static stiffness and machine tool components can be calculated. Piscan et al (2010 , page 10), notes that by knowing a bolted joint's behaviour, the stiffness of machine tools can be improved. Therefore, the bolted joint's stiffness can be increased by knowing the optimal contact stiffness and the optimum preload. This work marked a beginning with regard to joints contact deformations analysis.

Song et al (2014), considered the friction in high pressure torsion as an important technique that creates pronounced plastic deformation during production of bulk materials with ultrafine or nano grained microstructures. Song et al (2014), researched the effective strain distribution at contact surfaces in the

---

---

HPT samples using different CoFs. Similarly, the current research employed two significant CoFs and considered friction in the rigid contact surfaces / areas between flanges and V-bands.

Guo & Wang (2010), using FE analysis, simulated the behaviours of V-bands and the results validating the research methodology. The FE model is required to include all interactions between the housings and the V-band and therefore involves a significant amount of contact. This required non-linear analysis which can be time consuming. In addition, special techniques should be employed and measures adopted to lessen computing time and deal with the issue of numerical convergence. This can be done by eliminating small holes and other small features, modelling the V-band and t-bolt together and removing the sizeable clearance and penetration between contact pairs. As this can be time consuming it is therefore not practical to employ FE analysis for routine product design with V-bands, as would be the case for turbochargers.

Barrans et al (2014), noted that the V-band joint's contact pressure distribution showed significant variation especially when the CoF is large. It was also concluded that this can only be demonstrated with the use of a 3D FE model. Additionally, if friction in the circumferential direction is overcome, then the transverse friction effect will be taken away and that for larger V-bands this effect is significant.

Qin et al (2015), stated that a 2D FE model was employed because of its greater efficiency when used to research a clamp band joint's structure and its dynamics when "subjected to longitudinal base excitations" (p.1). The 3D FE

---

---

model was described as computationally expensive and not efficient when performing transient analyses that involves contact nonlinearity. There was agreement that the FE method is a powerful tool for analysing structures put together with joints. For the current research, the researcher had access to high performance computers for simulations and therefore found the 3D FE model to be appropriate.

Used in a wide range of mechanical components, interference fitted assemblies are important due to their high rigidity and compactness. Lanoue et al (2009), calculated the nominal contact pressure from the theoretical calculations they used based on Lamé's theory. The focus was on "two compound cylinders of infinite lengths and same material with interference" (p.1588). Evidence from several experimental observations shows that the fatigue life of mechanical parts is significantly lessened by fretting. Surface damage is due mainly to three independent factors: friction coefficient, slip amplitude and contact pressure.

Lanoue et al (2009), stated that important FEA considerations were the following: convergence, contact formulations and meshing. Research focused on submodeling, mesh convergence and contact options, so as to achieve accurate stress and displacement results. Lanoue et al (2009), used a FEA model based on Nishioka's work but, since rotation was not included, replication is not exact. The main concluding point was that particular attention must be given to contact algorithm options. All four algorithms employed can give accurate results. Penetration, contact stiffness and allowable elastic slip are all parameters

---

---

to control. Therefore, calculation time is the primary criterion in the choice of method employed.

#### **2.6.4 FE Analysis of the Effect of the CoF Level**

Patil & Eriten (2015), used a 3D FE model and surface-to-surface contact formulation with the Penalty Method in their research into the "Effects of Interfacial Strength and Roughness on the Static Friction Coefficient." A rigid flat contact surface was used on a deformable sphere, whilst the current research focuses on the surface-to-surface contact of the rounded surfaces of V-bands. Patil & Eriten (2015), found that using higher CoF's than in the present research, at 0.6 and above, resulted in contact weakening due to the interplay between interfacial slip and plasticity. This eventually leads to a lowering of the global CoF to less than the assigned value.

Song et al (2014), considered the friction in high pressure torsion as an important technique that creates pronounced plastic deformation during production of bulk materials with ultrafine or nano grained microstructures. Song et al (2014), researched the effective strain distribution at contact surfaces in the HPT samples using different CoF's. Similarly, the current research employed two significant CoF's and considered friction at the rigid contact surfaces / areas between flanges and V-bands.

Pop et al (2011), researched 3D static contact surface issues with dry friction and also adopted the Penalty Method alongside FE analysis. This approach has been replicated in the current research project.

---

---

Barrans et al (2014), found that for a small band with a radius of 57 mm and a lower CoF, there was a good match between the FEA and both theories. However, when including transverse friction there was more dissimilarity between the two theories. This is because the friction produces more variation in the V-band's circumferential contact pressure. However, with a greater CoF and in contrast to the larger V-band result, they found that the FEA model shows a greater agreement with the transverse friction theory.

Barrans et al (2014), found that another important difference between the two bands was that the larger bands contact pressure was significantly less than that of the smaller bands. This finding suggests that the circumferential force in the larger band is enough to overcome friction in the circumferential direction. Thus, in the transverse direction, friction generates no resistance. However, in the smaller band, the greater contact pressure ensures that the circumferential force is not enough to supersede friction in the circumferential direction and therefore the transverse friction effect continues.

Qin et al (2011b), states that the contact surface friction coefficient between the V-segment and the interface ring and the wedge angle affects the bending stiffness, and that "the values of those parameters should be chosen carefully to meet the requirement of both the connection and the separation" (p.13).

Ibrahim and Pettit (2003), point to the importance of knowing the relationship between the axial bolt force and the changes in the contact stress distribution at the time an external force is applied to a joint (p.46).

---

---

## 2.7 Experimental Methods

Barrans & Müller (2009), note that by 2009, despite the wide use of V-band clamps, their behaviour is still not fully understood and ultimate axial strength is currently only available through physical testing.

Zhang et al's (2014), experimental work involved verifying the theoretical analysis of the contact pressure of the V-band clamp and the circumferential stress. Ten polymer polyvinylidene fluoride (PVF) piezoelectric sensors were used, evenly placed on one side of the band to measure the circumferential strains. Apart from peak stress at the 7th sensor location, the remaining data presented the changing tendency of the circumferential strain and their experimental results showed the circumferential strain, or force, experiencing a faster decline.

Zhang et al (2014), found that the higher the stress, the smaller the displacements near the clamp ends and that this was important in terms of the V-band clamp sealing. V-band clamp deformation was also noted. It was found that stress distribution tended to match the exponential distribution of the contact pressure and that high local clamping force decreased the clamp curvature beneath the trunnion. There was also an increase in the clamp curvature proximally leading to a weak sealing in the piping system.

Zhang et al (2014), concluded that by using FEA analysis, theoretical modelling and experimental testing, a thorough analysis of an interference fit model between the V-band clamp and the piping systems was achieved. FEA simulation corresponded with experimental testing for contact pressures under low load and for the finding of the initial contact points. In order to explain the contact pressure deviation from the classical theory, contact mechanics and point load

---

---

were employed. The offset between the direction of tension force and centroid line of clamp caused bending stress and contributed to the unusual stress distribution. Zhang et al (2014), suggested a pre-bent t-bolt design for counteracting the effect of the offset.

Zhang et al (2014), investigated the mallet tapping mechanism on contact pressure distribution equalisation between the piping system and V-band clamp. For collecting quasi-static measurements of the contact pressure during loading, a sensor platform with charge mode amplifier was constructed. Piezoelectric sensor tests were used for measuring contact pressures in the initial stage before and after mallet tapping. FEA was employed to ascertain the initial contact areas. Controlled measurement enabled verification of mallet tapping viability regarding contact pressure redistribution.

Kitamura et al (2012), present a method for the analysis of separation shock response on satellites, as the satellite body structure is subject to large shocks during separation. Based on information regarding satellite design, an FE model was constructed. Static analysis of the V-band clamping was used to calculate the force loaded onto the satellite part which separates from the rocket body. Then an input parameter for the released force was used in order to predict the shock response experienced by the satellite body. Transient response analysis incorporating the mode superimposition method was employed. Comparing the calculation with the result of the shock test, it was found that the proposed method was effective. This involved evaluation of the panels tied to the cylinder as this was the satellite component involved in the separation.

---

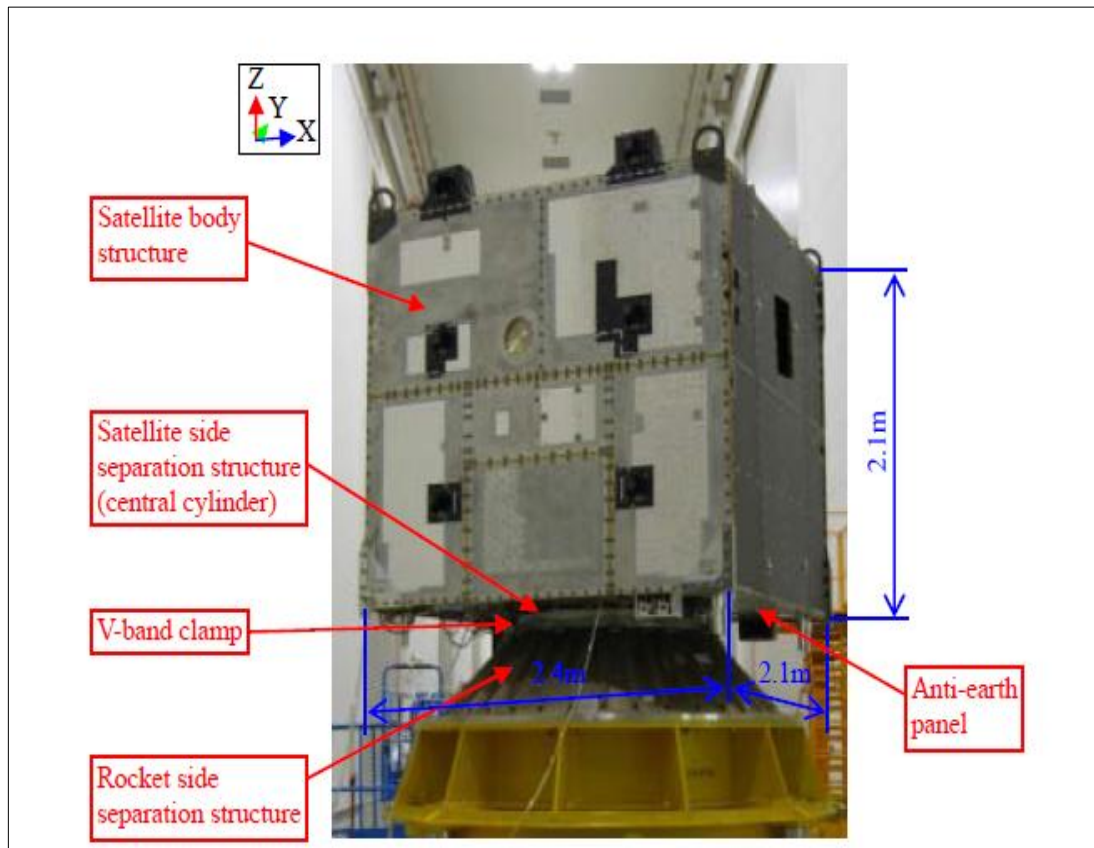


Figure 2 - 9: Overview of Test Specimen, Kitamura et al, (2012)

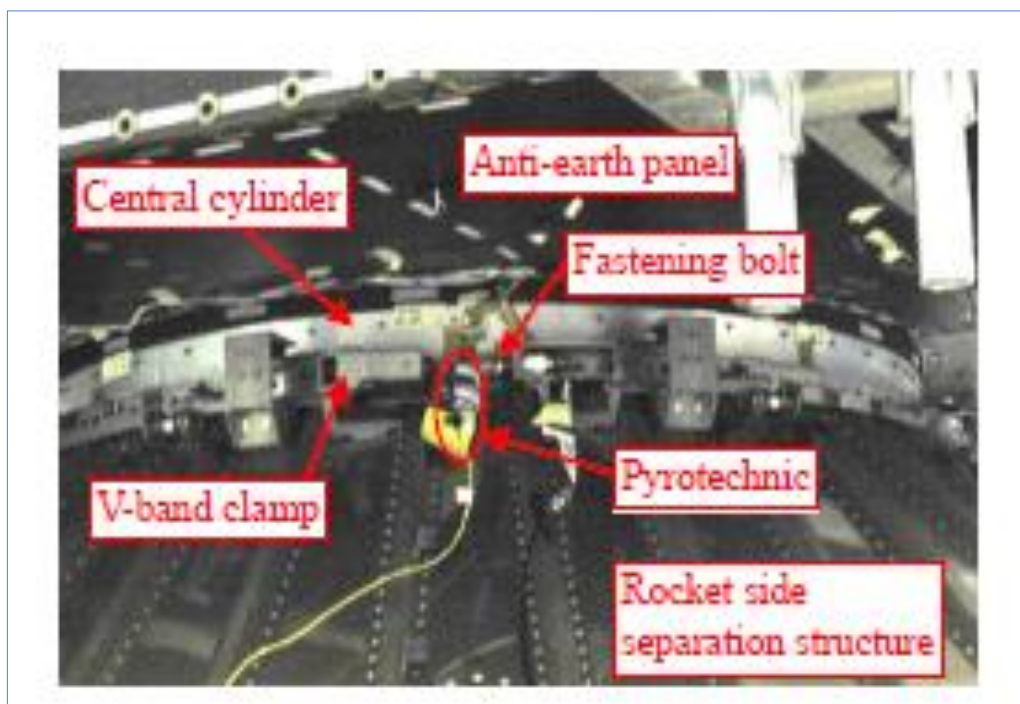


Figure 2 - 10: Area Around the V-band Clamp, Kitamura et al, (2012)

---

Shoghi's thesis (2003, p.138), states that the investigation into the relationship between displacement and stress in V-section bands provided valuable information. This is despite the theory not accounting for radial penetration of the V-section band and the consequent results not correlating well with the finite element models. It is concluded that the experimental outcomes came; "well within the range of predicted results" (p.138). This is despite the apparent high susceptibility of the circumferential stresses produced during the initial and contact stages in the V-section band clamp, to both manufacturing tolerances and the effects of operating conditions, such as the coefficient of friction.

Müller (2011), recommends further areas for research and further questions for research, as well as recommendations regarding how this research should be conducted. These include: measuring precisely the cross section of the flange pair before all future tests are undertaken, with these measurements focused on determining the precise V-band cross section of all bands, so as to ascertain the degree of irreversible deformations during failure.

This would enable a determination regarding the impact of certain V-band and flange geometric parameters on the UALC. Measurements could include the surface roughness and form of the inner V-band surface as well as any circumference differences. This would then prove the non-uniformity of the contact pressure distribution around the circumference.

Further tests were recommended by Müller (2011), on a larger range of band diameters, particularly band sizes beyond 40mm. Therefore, larger V-band retainers and flanges would need to be manufactured and more measurement

---

---

points used for the development of hardness throughout the roll forming process. This would enable validation of the finite element simulation of this process.

Such investigations should also include the development and growth of cracks, ascertaining their precise starting point and measuring the hardness in that area. This would hopefully enable a better understanding of how these cracks in the bent area are preventable, through the introduction of changes and improvements within the manufacturing process.

## **2.8 Clutch**

Abdullah et al (2013), describe the main function of the clutch as the transmission of power and consequently motion from one part or component to the next. Clutches are well known in automotive vehicles, where they are used to link the engine with the gearbox. However, they are also used widely in many types of production machinery. Within this area, research shows that wear between two rubbing surfaces is dependent on the speed at which they rub and the pressure between them. In addition, two theories focus on the torque needed to create slip between the clutch surfaces. One of them assumes that there is even pressure over the contact surface, but predicts higher wear on the outside owing to greater rubbing velocity.

In the case of a friction clutch, when it engages, slippage occurs between the contact surfaces such as the clutch disc, pressure plate and flywheel. Due to this slippage, heat energy is generated at the friction surfaces interface. An essential factor in the performance of the friction clutch, is the pressure distribution

---

---

due to the heat generated between the contact surfaces during the slippage period.

Hannah (1984), notes that clutches are mechanical devices which allow the operator to control power transmission by connecting or disconnecting the source of power from other areas. Hannah (1984), states that there are two main types of clutch: positive and friction. As the friction clutch is relevant to this research, it will now be discussed.

Friction clutches are based on frictional forces that are created by two or more surfaces which are in contact. The slippage within friction clutches is useful during engagement when a driver wishes to accelerate a load with minimum shock. This is relevant to current lab research as the test rig employs a pair of flanges and clamps them together using a V-band. This involves friction and slippage.

Any wear between the two surfaces is dependent upon the pressure between those surfaces and the speed of rubbing. There is a theory concerning the required torque for producing slippage between flange edges. This theory assumes that pressure is even and the wear is uniform at the flange edges.

## **2.9 Effect of Friction**

Cui et al (2014), conducted simulations employing various friction coefficients to study the effect of the friction coefficient between the interface rings and V-segments. The analysis noted axial shock responses “slightly increasing with the friction coefficient in the high-frequency region” (p. 13). Noticeably, for the same pyroshock and preload amplitude, increasing the friction coefficient can

---

---

increase the frictional force. This could possibly raise the separation shock magnitude due to the high-speed relative motion between the interface rings and V-segments under separation. However, both operating distance of the frictional force and the action time during satellite separation are very short and do not involve significant effects.

Shoghi et al (2006), noted that increasing the friction coefficient between the band and the flanges decreases the load applied. This circumferential frictional load also affects the theoretical torque resistance between the band and flanges. Therefore, an increase in the coefficient of friction increases the torque resistance even accounting for the decrease in applied axial load.

According to the NASA Marman clamp research project, it is desirable to have low friction. However, friction control is more relevant as this results in repeatability and predictability. The required clamping strap preload is reduced by friction at the V-segment-to-ring interface.

### **2.9.1 Micro Slip**

Ouyang et al (2006), define micro slip as a relatively small tangential displacement in the contact area interface, with the remaining contact area interface not being relatively displaced tangentially. Ouyang et al (2006), also point out that the dissipation of frictional energy is an extremely nonlinear event occurring at a joint interface and is difficult for a researcher to present as an analytical expression. This is related to current research because the processes of micro slip and the dissipation of frictional energy occur within this research. Macro slip is the same slippage effect but on a bigger scale and also occurs within current research.

---

---

Furthermore, Qin et al (2011a), found that in the micro slip stage the axial joint stiffness was approximately linear, whereas the joint displayed nonlinear behaviour in the macro slip stage where the hysteresis loop was formed. Between the interface rings and the V-segments there are slips due to friction, which lead to energy dissipation. Qin et al (2012), present the general mechanical behaviour of the clamp band joint when subjected to axial loads. It was found that two frictional slip stages occur – micro and macro - between the interface rings and the V-segments.

The parametric studies of Qin et al (2012), indicate that improved axial load capability could be obtained by decreasing the wedge angle and increasing the number and central angle of the V-segment, the friction coefficient and the preload. Additionally, it was found that axial joint stiffness increased as the friction coefficient decreased and the accompanying “increment of the V-segment number and the central angle subtended by the V-segment”(Qin, Yan, & Chu, 2012). Yet varying the wedge angle and the preload had no noticeable effects on the stiffness of the axial joint. Axial joint stiffness is the rigidity of the joint and its resistance to deformation when force is applied.

Qin et al's (2011b), proposed analytical model estimated the bending behaviour of the clamp band joint, as well as estimating the effects of the structural parameters on the bending stiffness of the joint and of the preload.

The parametric studies of Qin et al (2011a), demonstrated that the amount of preload had a small influence on the clamp band joint. The simulation results revealed that the magnitudes of the joint bending stiffness differed owing to the

---

---

unilateral constraint at the joint interface. Additionally, a clamp band joint with a large radius allowed increased bending stiffness.

## **2.10 Conclusion**

Within this chapter the evolution of the V-band has been considered as well as issues which have arisen through application to a variety of uses within differing environments. From the Literature Survey, it was seen that there was a small research study involving testing done on the torsional load capacities of V-band clamps. However, there is still a sizeable gap in research work, which will form a unique and exciting part of this research project. In the Literature Survey a large number of publications are referenced. These detail previous examples of attempts to address mechanical issues relating to the V-band joint clamp. The FEA modelling techniques of the V-band joint clamp and Marman clamp were investigated through numerical techniques analysis which captured the significant effects of differing levels of the coefficient of friction. The FEA method is widely used by researchers as a tool for understanding issues relating to the V-band joint clamp.

FEA modelling includes both the Penalty Method and the Lagrange Multipliers Method. The Penalty Method has greater applicability for this research due to the differing V-band sizes and different levels of friction examined. Previous research has not fully explored issues to do with the t-bolt and trunnion loop in generating tightening load. This has been largely due to the number of contact areas involved. Instead, the torque applied to the t-bolt has been the focus of enquiry. From the review carried out in this chapter, a key area of FEA modelling analysis has been identified for further investigation in this PhD thesis. One

---

---

key area is concerned with the design and diagnostics of the torsional load capacity of a V-band clamp. Therefore, a software engineering modelling technique is required to analyse the V-band clamp, which can take into account transient aspects such as torsional load capacity effects.

In addition, the Literature Survey detailed different experimental methods relating to mechanical issues to do with the V-band joint clamp. Muller (2011), established an experimental method using tensile testing and hardness measurements. It was recommended that measurement should be precise regarding the cross section of the flange pair. Measurement should also include the inner contact surface of the V-band.

The Literature Survey also details the development of a theoretical model which demonstrates a good relationship with the simulation results. The theoretical approach involves transforming theory into mathematical equations or formulas, so as to test and prove validity. Facts and useful information can then be extracted from the theory to enable accurate practical work.

This Literature Survey showed the existence of a significant knowledge gap in the field of V-band clamp applications and therefore directed attention to research areas detailed in the following chapters.

---

---

---

---

# Chapter Three

## Theoretical Development

### 3.1 Introduction

The purpose of this chapter is to provide background information regarding the theoretical development of the V-band. A fundamental theoretical understanding of the torsional load capacity of the V-band clamp will then be developed. This analysis is based on previous work by Shoghi (2004) regarding the stress generated in V-band clamps due to clamping. In addition, within this chapter, the current research investigates the effects of joint parameters on joint performance.

### 3.2 Development of the Theory

Torque at the flange-to-band interface and torque at the flange-to-flange interface make up the two parts of the full torsional load capacity of the joint:

$$T_t = T_b + T_f$$

3 - 1

Where:

$T_t$  = Total torque capacity

$T_b$  = Torque capacity at the band-to-flange interface

$T_f$  = Torque capacity at the flange-to-flange interface

---

The first part  $T_b$  is determined by employing single plate clutch theory and assumes a uniform pressure (Hannah & Stephens, 1984). This theoretical development accords with that stated by Guo et al (2010).

With reference to Figure 3 – 1 and ignoring second order terms, the elemental ring's area  $A$ , with width  $dr$  and radii  $r$  is given by:

$$A = 2\pi r dr \quad 3 - 2$$

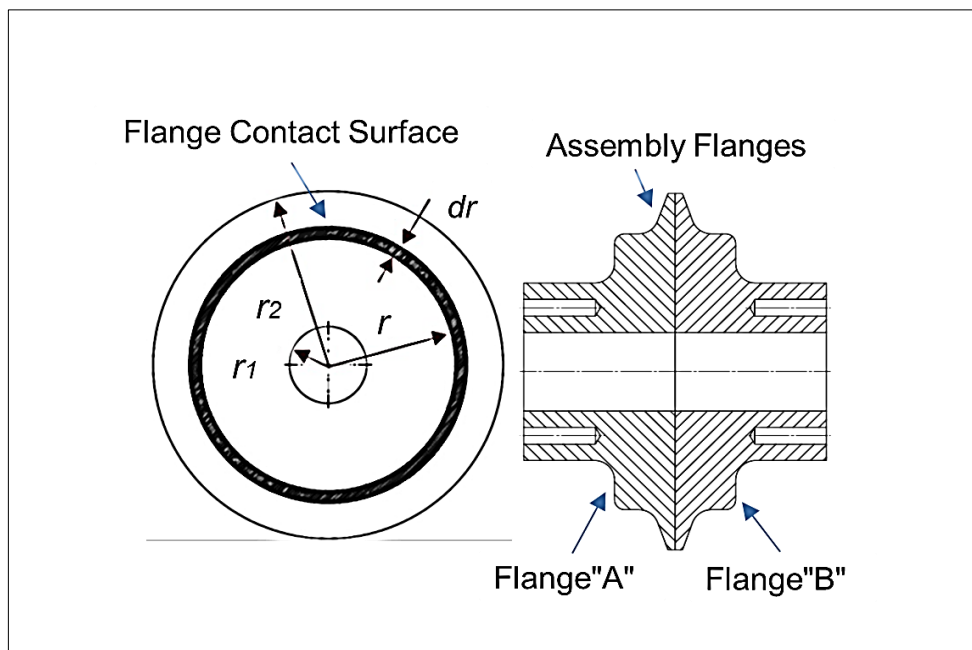


Figure 3 - 1: Area of an Elemental Ring with Flat Surfaces in Contact

The force resulting from friction  $F_f$  on the elemental ring is:

$$F_f = \mu_f P \times A \quad 3 - 3$$

Where  $\mu_f$  is the coefficient of friction between the two flange contact surfaces.

$P$  = uniform contact pressure, this force's moment about the axis is:

---

$$dT_f = \mu_f P \times 2\pi r^2 dr \quad 3 - 4$$

Contact between the flange surfaces takes place over the ring shaped area between the inner radius,  $r_1$ , and outer radius,  $r_2$ . Hence, torque generated between the flanges  $T_f$  is given by:

$$T_f = 2\pi \int_{r_1}^{r_2} \mu_f P r^2 dr \quad 3 - 5$$

With the assumption that the CoF and contact pressure are uniform in the contact area:

$$T_f = \frac{2\pi}{3} \mu_f P (r_2^3 - r_1^3) \quad 3 - 6$$

In addition, as the pressure is assumed to be uniform in the contact area, it can be related to the applied axial force,  $F_a$ , as:

$$P = \frac{F_a}{\pi(r_2^2 - r_1^2)} \quad 3 - 7$$

Thus, the transmitted torque force equation can be written as:

$$T_f = \frac{2}{3} \mu_f F_a \frac{(r_2^3 - r_1^3)}{(r_2^2 - r_1^2)} \quad 3 - 8$$

---

---

For a V-band joint the axial clamping load  $F_a$ , has been defined by Shoghi et al (2005) as:

$$F_a = \frac{(1 - \mu_b \tan \phi) F_\beta (\sin \phi + \mu_b \cos \phi)}{\mu_b (\tan \phi + \mu_b)} \left[ 1 - \exp\left(\frac{-\mu_b \beta}{(\mu_b \cos \phi + \sin \phi)}\right) \right] \quad 3 - 9$$

The term  $\phi$  is defined in Figure 3 – 2 and  $\beta$  is defined in Figure 3 – 3. Hence, when combining equation 3 – 9 and 3 – 8, the total torque transmitted by the flange-to-flange interface  $F_f$ , in terms of t-bolt force  $F_\beta$ , can be written as:

$$T_f = \frac{2}{3} \mu_f \left( \frac{r_2^3 - r_1^3}{r_2^2 - r_1^2} \right) \frac{(1 - \mu_b \tan \phi) F_\beta (\sin \phi + \mu_b \cos \phi)}{\mu_b (\tan \phi + \mu_b)} \left[ 1 - \exp\left(\frac{-\mu_b \beta}{(\mu_b \cos \phi + \sin \phi)}\right) \right] \quad 3 - 10$$


---

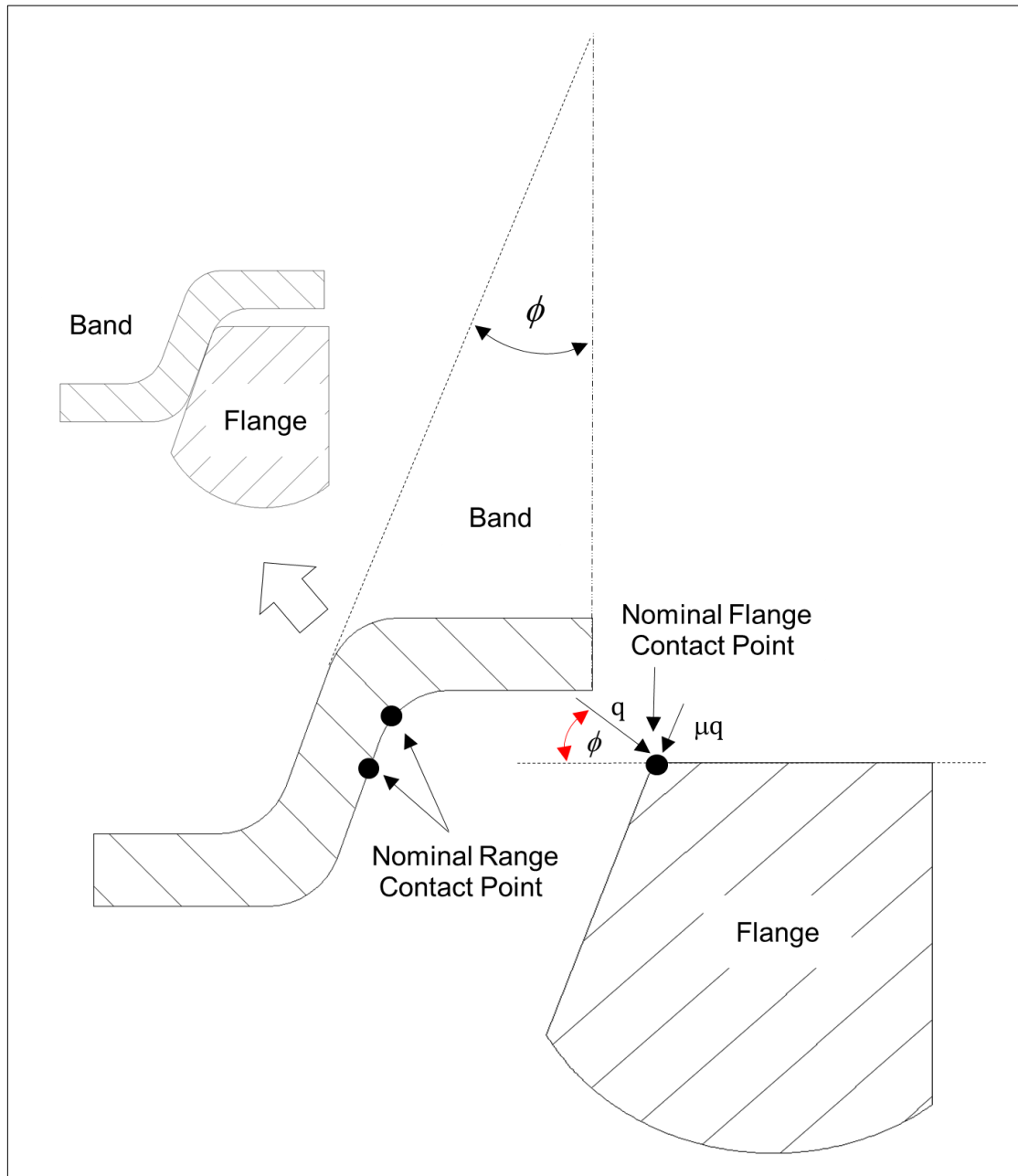


Figure 3 - 2: Definition of  $\phi$

To find the torque capacity,  $T_b$ , of the interface between flange and band, Shoghi et al's (2006) theory was developed. Tightening the t-bolt within the V-band joint will generate a normal force per unit length  $q$  between flange and V-band,

as given in Figure 3 – 3. In addition, the normal force per unit length  $q$  is connected to the radial force per unit length,  $f_r$ , as:

$$\frac{f_r}{2} = q (\sin \phi + \mu_b \cos \phi) \quad 3 - 11$$

Where  $\mu_b$  is the static CoF between the band and the flange, as shown in Figure 3 – 2.

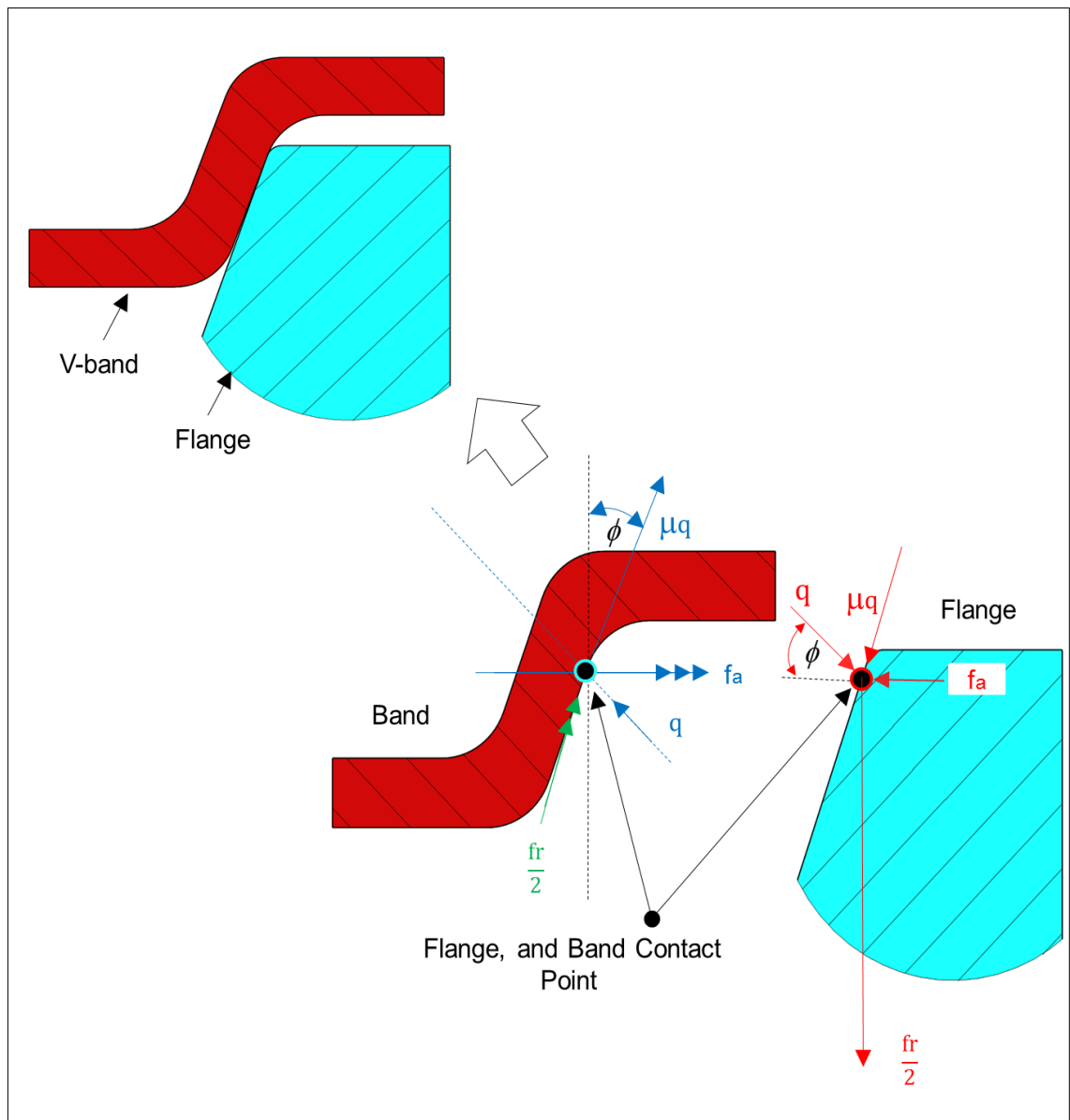


Figure 3 - 3: Forces at the Contact Point On A Flange With Band

---

As with Shoghi et al's (2006) previous work,  $q$  is connected to the circumferential force  $F_\alpha$ , produced in the band through the tightening of the t-bolt. (Force components per unit length  $q$  between the band and the flange are shown in Figure 3 – 4).

$$f_r R_c d\alpha - 2F_\alpha \sin \frac{d\alpha}{2} = 0 \quad 3 - 12$$

Then  $F_\alpha = f_r R_c$

So

$$q = \frac{F_\alpha}{2(\sin \phi + \mu_b \cos \phi)R_c} \quad 3 - 13$$

Taking into account the minute annular segment  $d\alpha$  of the band, as shown in Figure 3 - 3, the torque reaction between one flange,  $dT_b$  and the band is shown by the following equation:

$$dT_b = q \times \mu_b \times R_c \times d\alpha \times R_c \quad 3 - 14$$

when  $R_c d\alpha$  is the unit length over which the load  $q$  is acting and  $R_c$  is the torque radius.

---

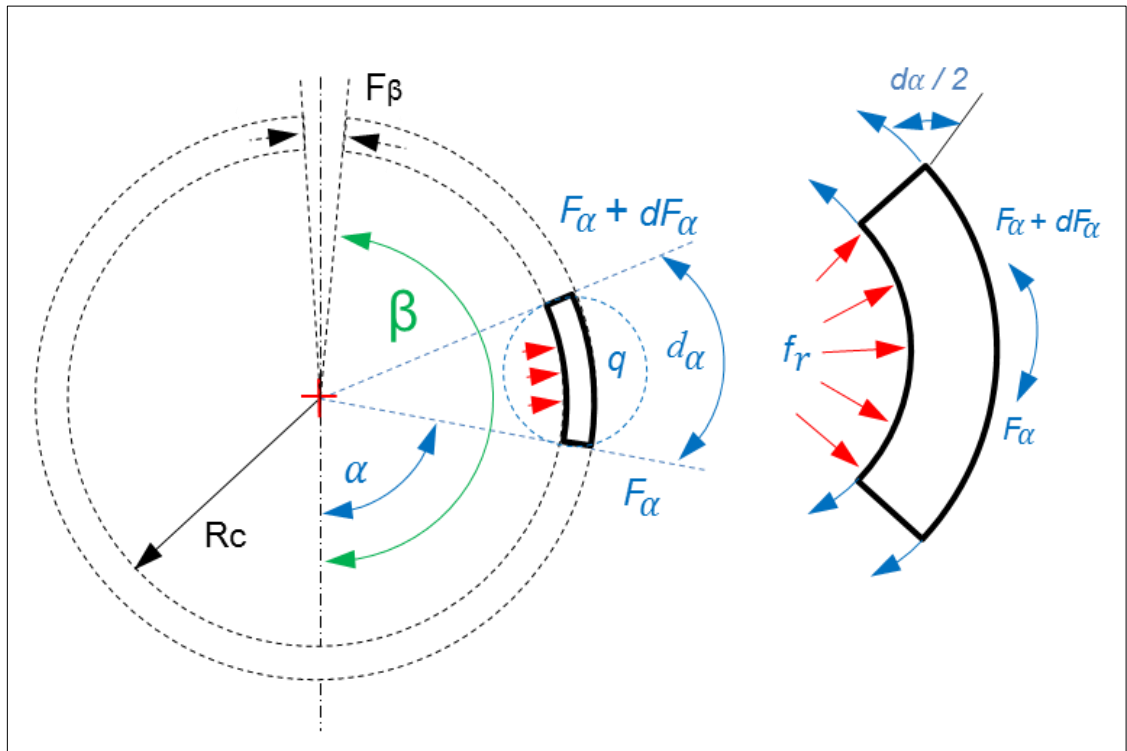


Figure 3 - 4: V-band Definition of  $F_\alpha$ ,  $q$ , and  $F_\beta$

By involving the previous definition of  $q$ :

$$dT_b = \frac{F_\alpha \mu_b R_c d\alpha}{2(\sin \phi + \mu_b \cos \phi)} \quad 3 - 15$$

In reference to Shoghi et al (2006),  $F_\alpha$  is connected to the t-bolt load  $F_\beta$  as:

$$F_\alpha = F_\beta e^{\left[ \frac{\mu_b (\alpha - \beta)}{\mu_b \cos \phi + \sin \phi} \right]} \quad 3 - 16$$

Then

---


$$dT_b = \frac{\mu_b R_c F_\beta}{2(\sin \phi + \mu_b \cos \phi)} e^{\left[\frac{\mu_b(\alpha-\beta)}{\mu_b \cos \phi + \sin \phi}\right]} d\alpha \quad 3 - 17$$

The complete torque reaction between one flange and the band  $T_b$  is thus:

$$T_b = 2 \int_0^\beta dT_b$$

3 - 18

$$= 2 \frac{\mu_b R_c F_\beta}{2(\sin \phi + \mu_b \cos \phi)} \int_0^\beta e^{\left[\frac{\mu_b(\alpha-\beta)}{\mu_b \cos \phi + \sin \phi}\right]} d\alpha$$

Giving:

$$T_b = R_c F_\beta \left[ 1 - e^{\left(\frac{-\mu_b \beta}{\mu_b \cos \phi + \sin \phi}\right)} \right] \quad 3 - 19$$

Therefore, from equations, 3 - 1, 3 - 12 and 3 - 19:

$$T_{\text{total}} = \left[ \left( \frac{2}{3} \mu_f \left( \frac{r_2^3 - r_1^3}{r_2^2 - r_1^2} \right) \frac{(1 - \mu_b \tan \phi)(\sin \phi + \mu_b \cos \phi)}{\mu_b (\tan \phi + \mu_b)} \right) + R_c \right] F_\beta \left( 1 - \exp\left(\frac{-\mu_b \beta}{\mu_b \cos \phi + \sin \phi}\right) \right)$$

3 - 20

---

---

### **3.3 Conclusion**

This chapter has presented the development of the theoretical model's mathematical aspects of the torsional load capacity of V-band clamps when assembled onto rigid flanges. The theoretical model developed has been shown to have predictive value with regard to the experimental results. The coefficient of friction, particularly that between band and flanges, has a substantial impact on the theoretical torsional load capacity of the V band clamp. The contact point between band and flange has an effect on the theoretical torsional load capacity. Therefore the ability to understand the factors impacting on torsional load capacity is essential for undertaking the current research.

In this current research project, a theoretical model of a V-band joint subjected to torsional loads has been employed. This model has been used to identify those parameters which will impact on the reliability of the joint.

---

---

# Chapter Four

## Development of the V-Band Torsional Test Rig

### 4.1 Introduction

This chapter will present and discuss the development of the torsional test rig detailing use in previous research and its use, mechanisms and components in current research.

### 4.2 Initial Design of the Test Rig

#### 4.2.1 Mechanical Design

Recently, experimental investigation has been designed primarily to determine the maximum torsional loading capacity of a V-band clamp and to identify the point of initial slip between flanges assembled on a V-band. Investigation has been through the use of a torsion test rig, as seen in Figure 4 - 1. A total of twelve single beams were used to build the test rig frame. The test rig consists of welded joints at the end of each single beam, see Beardmore, R. (2013), with another attached beam to complete the assembly test rig frame. This will enable a maximum applied load of 80kN which will be sufficient for the theoretical development of the V-band. The method of assembly for the test rig will meet all relevant safety requirements.

---

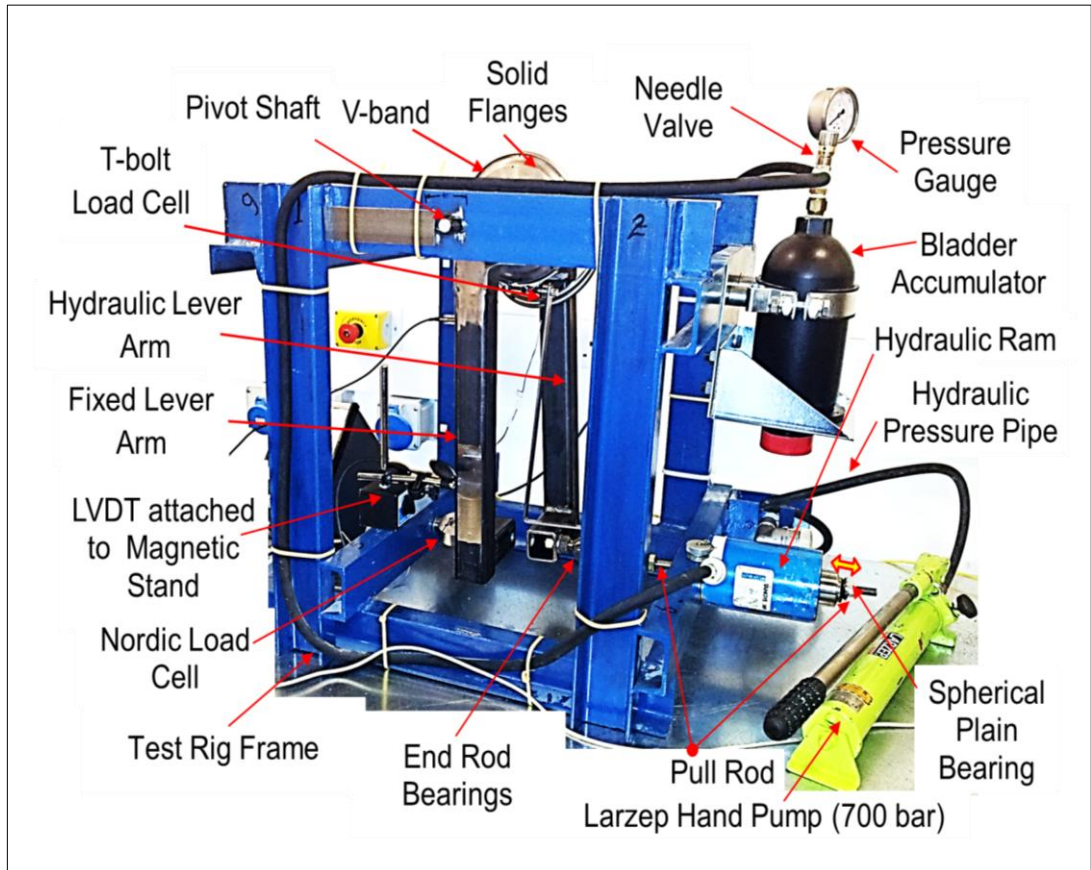


Figure 4 - 1: Mechanical Test Rig Components

The torsional test rig has two main parts: the first part is the assembly frame and the second part is the illustration system assembly (see Section 4.4, Test Rig Development). The latter consists of the following mechanical test rig components:

- Pivot Shaft: a 40mm diameter ground, solid steel bar provided by SKF UK Ltd, SKF (2012). The pivot shaft is used to attach different size flanges and is positioned by a horizontal slot at right angles to the horizontal beam of the test rig. The t-bolts holding the pivot arm in position have been replaced by headless t-bolts which are threaded into each end of the pivot shaft, see Figure 4-1.

- 
- Solid Flanges: Five flanges with dimensions: 114mm, 154mm, 181mm, 204mm and 235mm, compatible with the pivot shaft. Threaded holes allow for the attachment of the test rig lever arm, and spacers fit within an indented base to allow for the testing of different sized areas of friction between the flange contact surfaces. A V-band is mounted across both flanges and pressure applied to the lever arm until the slip point is reached. This is why a pair of flanges are used.
  - Spherical Plain Bearing, provided by Huddersfield Bearings (2012): A 12mm bearing is located at the end of the pull rod and allows the pull rod to pivot when activating the lever arm.
  - Tangye XR Hydraulic Ram, Tangye XR (2012): Pressure is applied to the pull rod through a 20t load capacity hydraulic ram and is provided by a hand pump.
  - Fixed Lever Arm (400mm in length), with Nordic Load Cell and Hydraulic Lever Arm, both designed and manufactured at the University of Huddersfield workshop. The Fixed Lever Arm is attached to one of the flanges and any movement during testing is measured by the Nordic Load Cell. Pressure is applied by the Hydraulic Ram to the Hydraulic Lever Arm which is attached to the other flange.
  - Bladder Accumulator, provided by MP FILTRI UK Ltd: The 1.5 litre Bladder Accumulator is pressurised by the hand pump and pressure is released to the Hydraulic Ram through a Needle Valve.
  - V-band: Circular in shape, the V-band is mounted across both flanges and tightened using a single T-bolt. (see section 1.1)
-

---

## 4.2.2 Instrumentation

### 4.2.2.1 LVDT Sensor

The following is a list of diagrams and figures which illustrate the instruments used in the test rig and the processes involved in the use of the LVDT Sensor, (Figure 4 – 2), TESA, (2012). The oscilloscope also collected data from two LVDT probes. These were positioned at the beginning of each test to be in compressive contact with the two arms, (the arms moved away from the LVDT probes as the test was carried out).



Figure 4 - 2: LVDT Sensor, TESA (2012)

### 4.2.2.2 Connections to the LVDT Sensor

The LVDT sensor connects to the Tesatronic TTA20, the PicoScope 2024 – 4C, Pico Technology (2012), and then to the PC, (see the Figure 4 - 3).

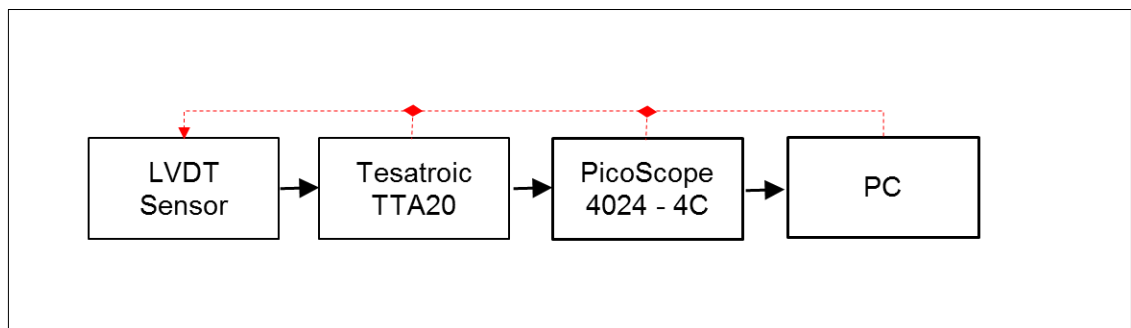


Figure 4 - 3: Diagram of the LVDT Sensor Connection Path

---

---

#### 4.2.2.3 Nordic Load Cell (Transducer)

The Nordic Load Cell is attached on both sides by an M12 bolt, (Transducer, 2012). One side is attached to the lever arm and the other side attached to the test rig. (see the Figure 4 - 4)



Figure 4 - 4: Nordic Load Cell, Transducer (2012)

#### 4.2.2.4 Connections to the Nordic Load Cell

The Nordic Load Cell connects with the Nordic Load Cell Amplifier, the Pico-Scope 2024 – 4024, and then to the PC, (see the Figure 4 -5).

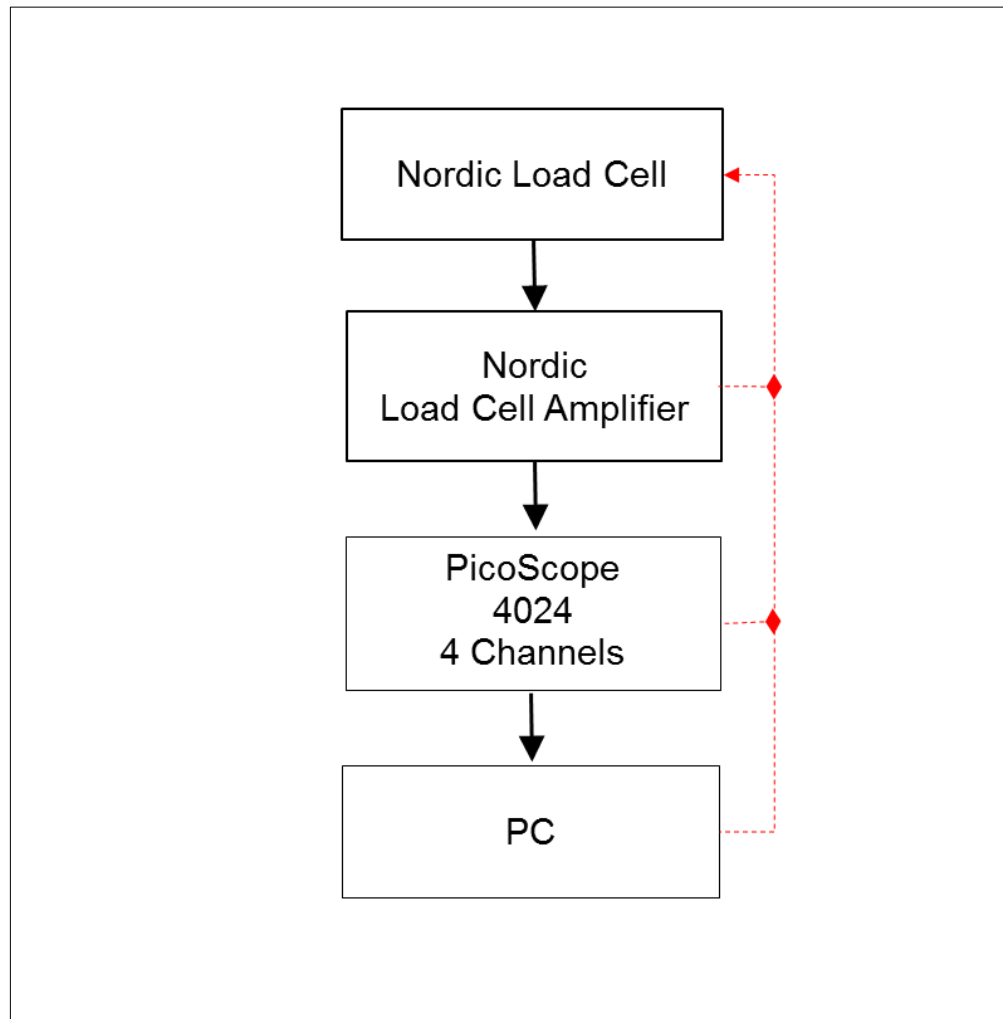


Figure 4 - 5: Connections to the Nordic Load Cell

#### 4.2.2.5 Omega Load Cell

The Omega Load Cell (OLC), (Omega; UK Limited, 2012), is attached to the V-bands t-bolt, (see in Figure 4 – 7). For accurate results during the V-band’s torsional test, the Omega Load Cell (OLC), should not interfere with the V-band. This can be achieved by use of the Omega Load Cell Solid Part, (see in Figure 4 -7), (Omega; UK Limited, 2012). This experimental procedure should then be used for all subsequent V-band torsional tests.

---

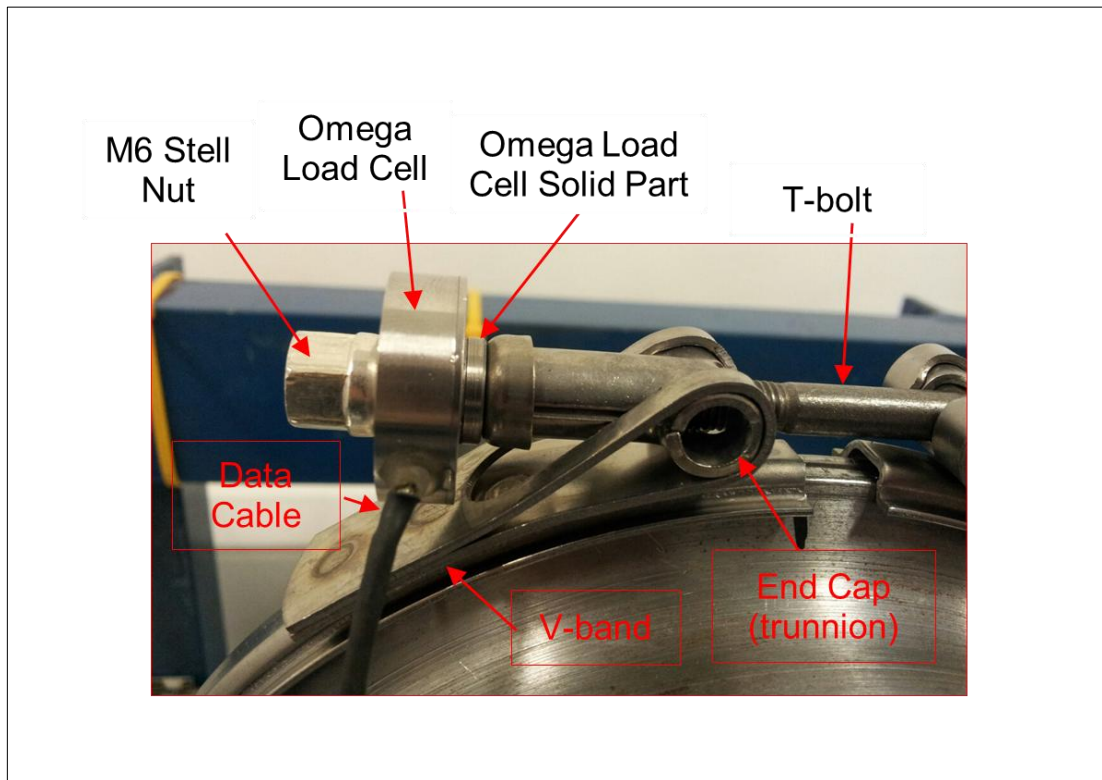


Figure 4 - 6: Omega Load Cell

#### 4.2.2.6 Connection to the Omega Load Cell

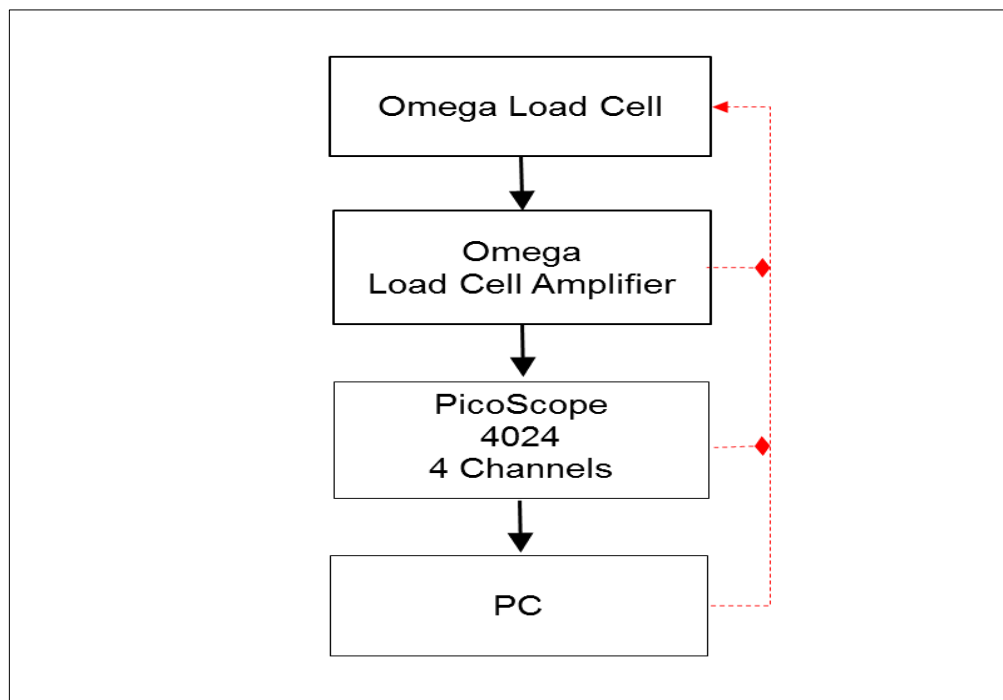


Figure 4 - 7: Connections to the Omega Load Cell

---

### 4.2.3 Experimental Procedure

Figure 4 – 1 shows the initial experimental test rig in its test configuration. The following components can be noted: Larzep Hand Pump (700 bar), Hydraulic Pressure Pipe (quarter inch, 500 bar), Needle Valve, Bleeder Valve, Pressure Gauge, Magnetic Stands 1 & 2, Nordic Load Cell, LVDT1, LVDT2, Conditioning Signal Box 1, Conditioning Signal Box 2 and a PicoScope 4024, Pico Technology (2012). Further detail regarding these components will now be provided.

- Larzep Hand Pump (700 bar), which pumps a range of pressures into the hydraulic ram through the hydraulic pressure pipe.
  - Hydraulic pressure pipe (quarter inch, 500 bar), that is 120cms in length and connects the hand pump to the hydraulic ram via the triangular thread adaptor.
  - Needle valve, that has a small port and needle-shaped plunger. The purpose is to precisely control the flow of hydraulic fluid during the experimental work.
  - Bleeder valve, that in this research test rig is used to release air from the system.
  - Pressure gauge (up to 18.2 bars), is an instrument used to measure pressure in the Bladder Accumulator.
  - Magnetic stands are used for attaching the LVDTs to the test rigs lever arms by means of a moveable permanent magnet, Mitutoyo UK Ltd (2012). Stand 1 is connected to leg 1 of the test rig, which is attached to LVDT 1 and used to measure the movement from lever arm A.
-

---

Stand 2 is connected to leg 4 of the test rig, which is attached to LVDT 2, and used to measure the movement from lever arm B.

- PicoScope 4024, is a high quality oscilloscope with 4 channels for viewing wavelengths during this experiment. It has a 1100 volt input range and 80 MS/s sampling, Pico Technology Limited, (2012). The Picoscope 4024 is a software package that allows a PC to show voltage waveforms.

### **4.3 Initial Design Evaluation**

The initial design was effective although some areas required improvement particularly around aspects to do with the loading geometry. Issues around the initial design are noted in the following:

- Firstly, the friction level was too high when using spherical plain bearings which resulted in a tightening of the lever arm.
- Secondly, the beam hole did not give sufficient flexibility to the test rig system and so it was subsequently enlarged. In addition, there was concern with regard to the smaller set of flanges, as it appeared that the load was being transferred from the flanges to the pivot shaft. The pivot shaft was attached to the test rig by a t-bolt.
- Lastly, the hand pump did not allow for the progressive and smooth application of pressure.

### **4.4 Test Rig Development**

The test rig was initially designed and partially constructed in 2008 by a project student working under the direction of Dr Barrans. Due to time limitations,

---

---

comissioning of the rig was not completed at that time. In order to address the problems identified in the previous section, the following modifications were made to the initial test rig and experimental procedure.

To deal with the problems resulting from the use of spherical plain bearings, they were replaced by end rods, Huddersfield Bearings (2012). Size M16 male and female end rods have been added to the test rig as shown in Figure 4 – 4. The purpose of the end rods is to allow for a curving upward movement of the lever arm when pressure is applied by the hydraulic system.

---

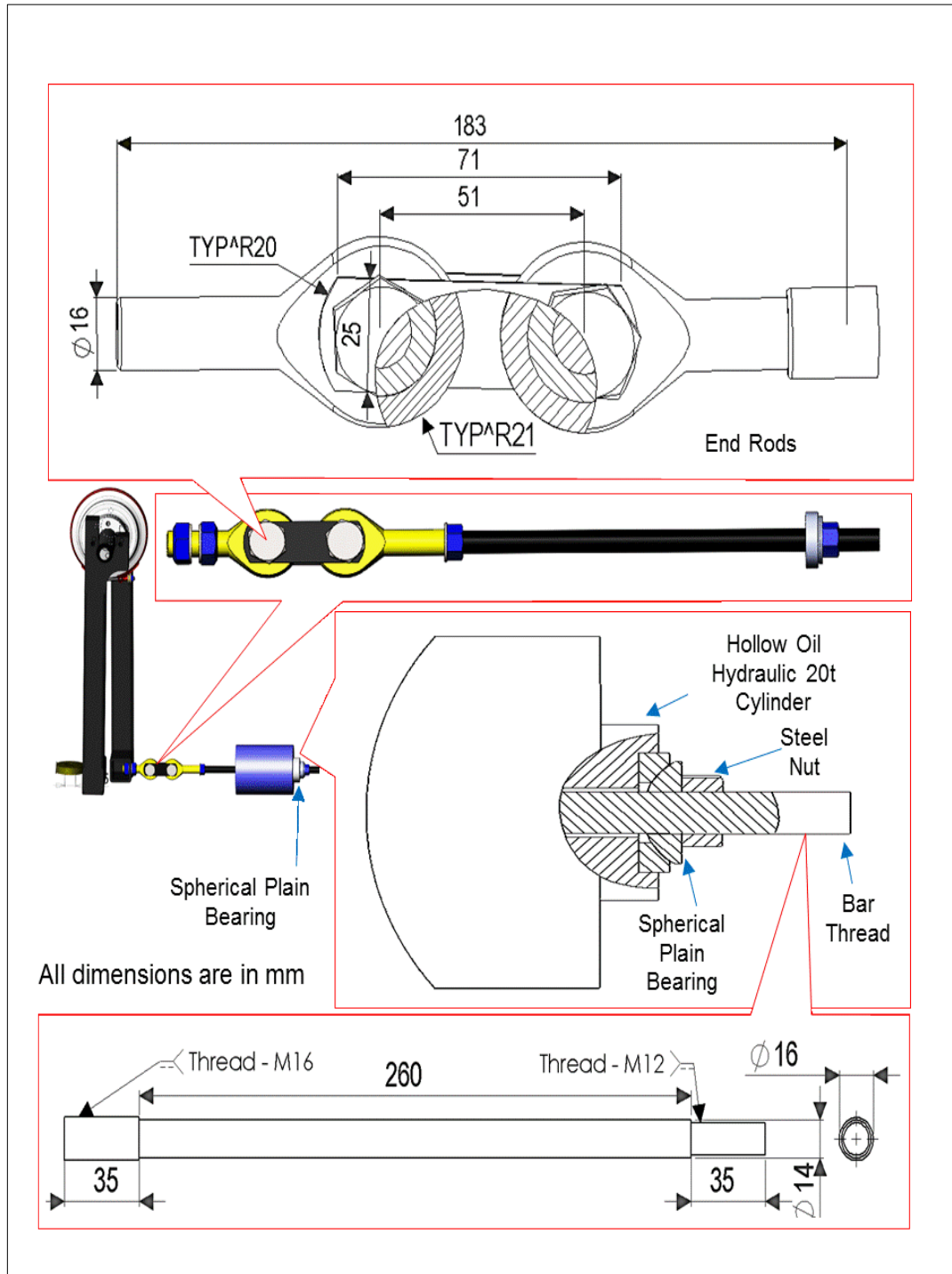


Figure 4 - 8: Revised Pull-Rod Assembly

A spherical plain bearing was added to the design of the test rig (see Figure 4 - 4) and was placed within a newly designed seat (see Figure 4 - 5). This combi-

nation is locked by a 14mm steel nut with steel washer and allows greater freedom of movement for the 14mm hydraulic bar.

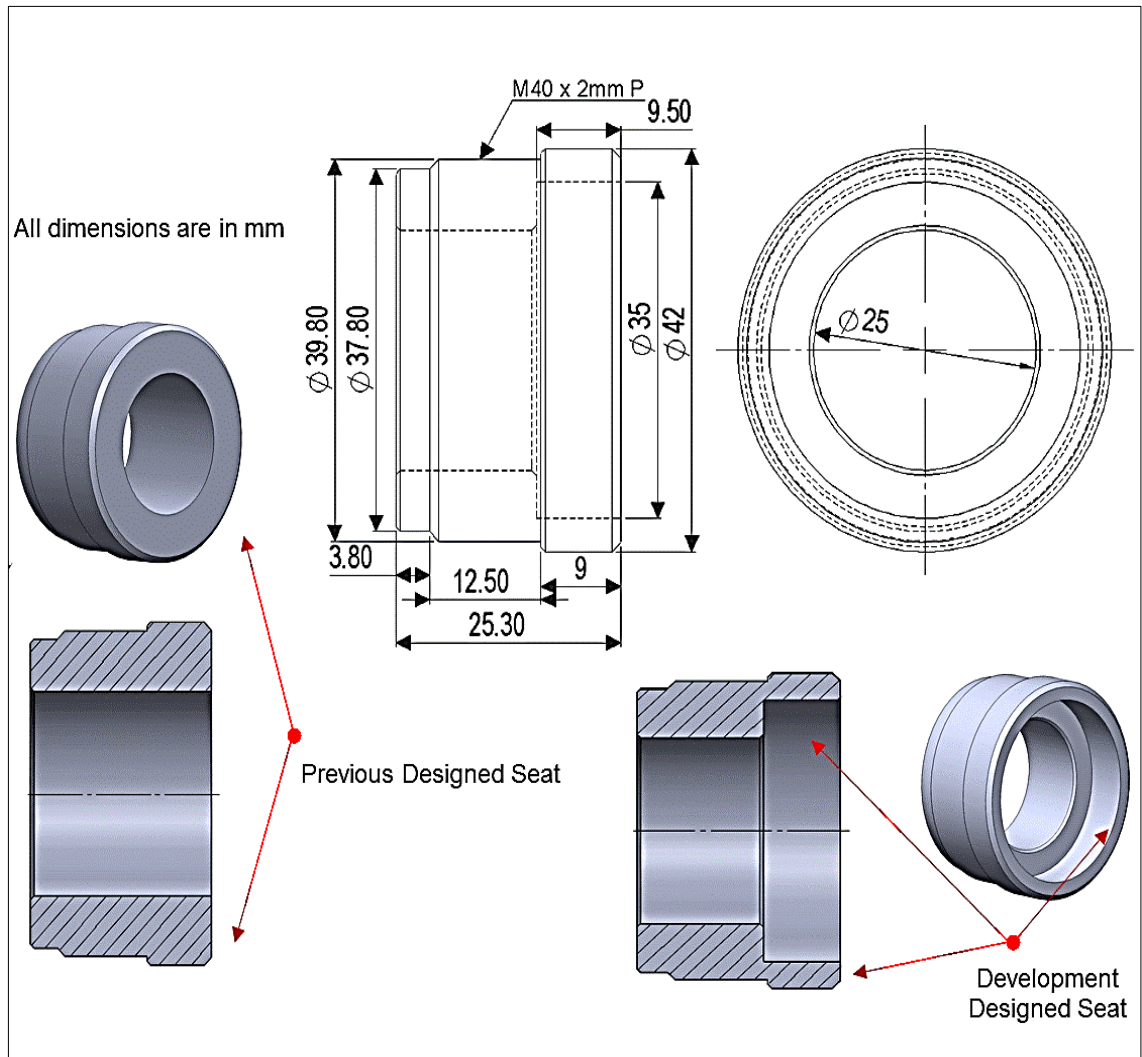


Figure 4 - 9: Designed Seat

Previously, spherical plain bearings were used (see Figure 4 – 9), but high friction in the bearings did not allow the required upward curved movement of the lever arm when it was activated during testing.

With the addition of the end rods, a spherical plain bearing was also added to the head of the hydraulic arm. This allows for the vertical movement of the end

---

rods and gives enough freedom to allow the previously noted curved upward movement of the lever arm (see Figure 4 - 9).

In the initial test rig design, lever arm 'B' was fixed by two nuts, one internal to lever arm 'B' and one external. Both connected to spherical plain bearings which were in turn connected to the hydraulic ram and closed off by a steel washer and nut. The hollow hydraulic ram is fixed to the test rig frame by two M12 steel screws.

Lever arm 'A' (see Figure 4 - 1), is attached to the test rig's 'C' channel by M12 steel screws. A 40mm diameter pivot arm is used to attach different sizes of flanges and positioned by a horizontal slot in the horizontal beam of the initial test rig. The existing t-bolt holding the pivot arm in position has been replaced by a headless t-bolt (See Figure 4 - 10).

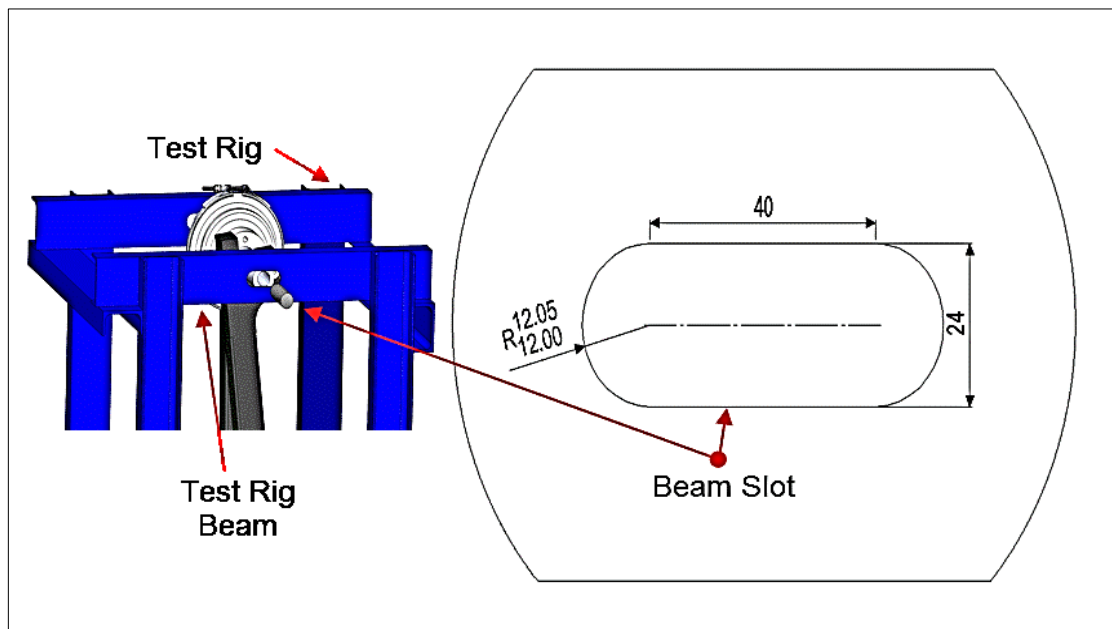


Figure 4 - 10: Beam Slot

---

---

Flange 'A' is attached to lever arm 'A', which in turn is attached to the Nordic Load Cell. Flange 'B' is attached to lever arm 'B', which in turn is attached to the rod ends and the M14 hydraulic ram. Quarter inch tubing is used to connect to the hand pump.

The previous test rig assembly using spherical plain bearings is illustrated in Figure 4-12.

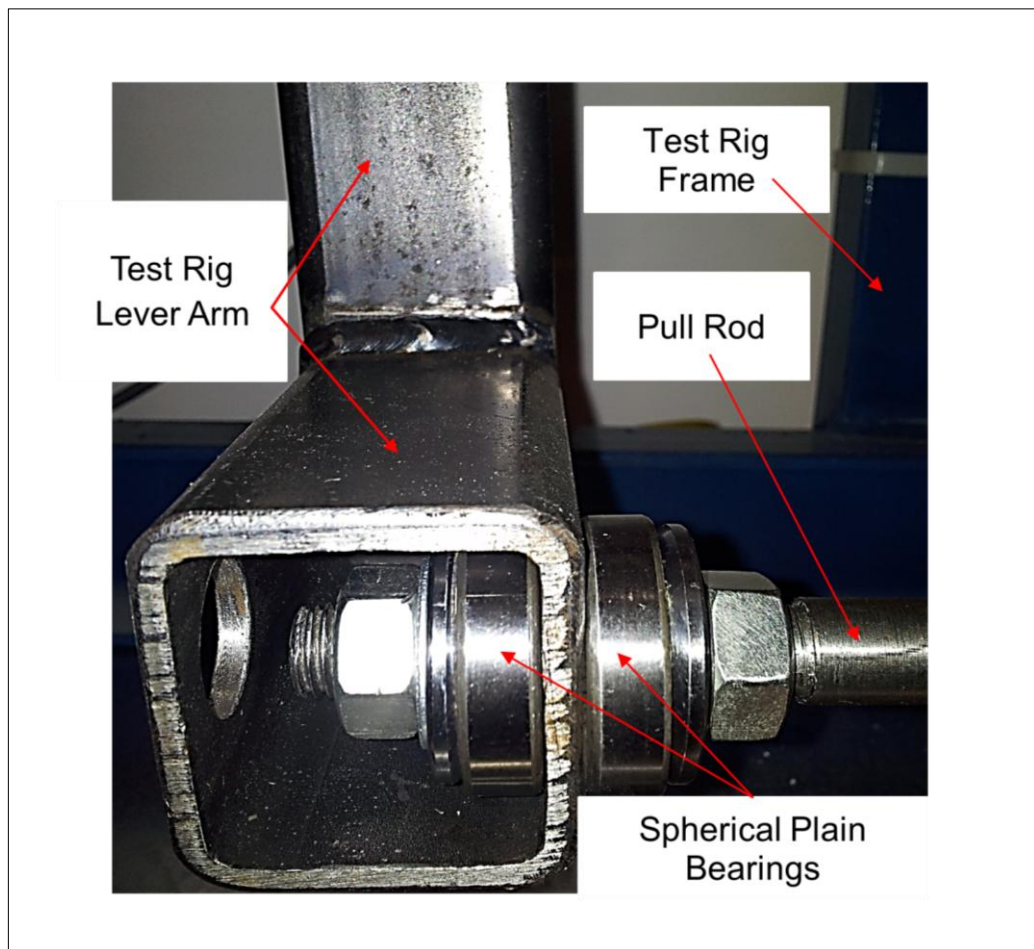


Figure 4 - 11: Spherical Plain Bearings

The use of spherical plain bearings effects the torsional load capacity results. Where the spherical plain bearings contact the 14mm bar, the test rig lever arm allowed a small movement in a horizontal direction, and friction loads are affected. There was an issue with the dynamic mechanism system of the torsion-

---

---

al test rig and this problem affects the most recent torsional load capacity results.

The current system output has an oscillation slip curve (see Figure 4-13), between the specified values, with an undesirable slip when load pressure is applied into the system using a hand pump.

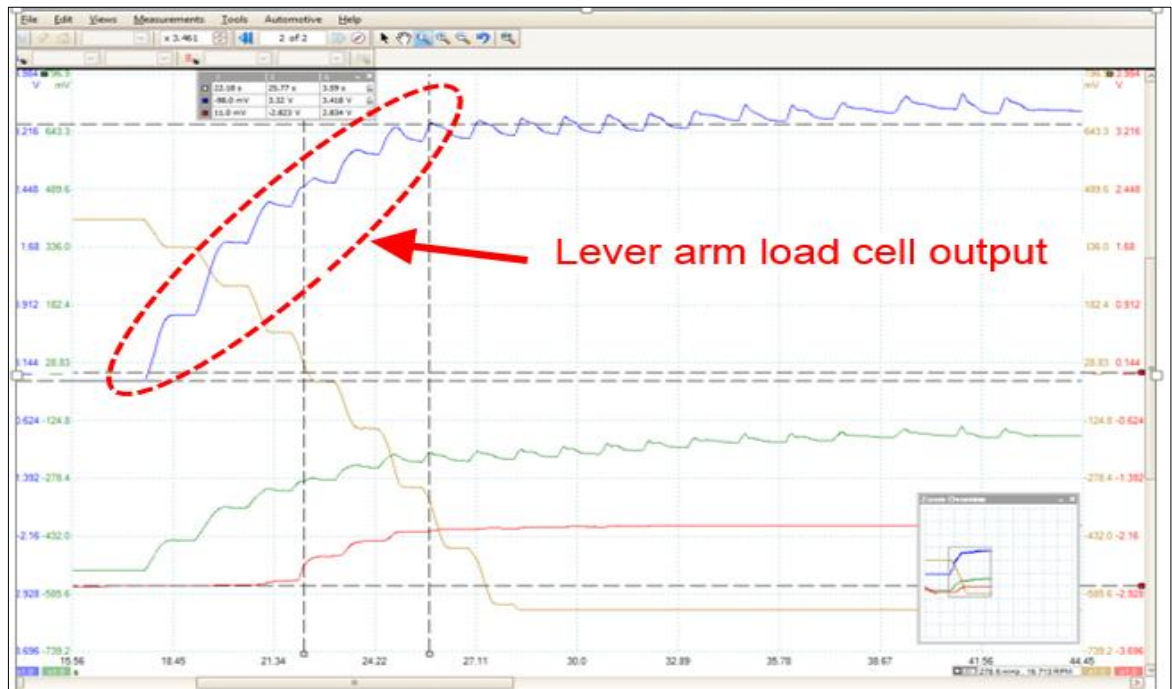


Figure 4 - 12: PicoScope Graph of Data: Test 2 - 114mm at 7kN

To achieve a smoother application of pressure, an air pressure system was considered, but this was eventually thought to be too expensive for research purposes. Based on calculations a 1.5 litre bladder accumulator was used as an alternative. Calculations indicated that around a 1.2 litre capacity was required with the nearest available capacity being 1.5 litre.

Although not yet tested, it is anticipated that the accumulator will supply a continuous and progressive pressure required for the testing of V-bands. Initial tests would appear to confirm this view. The results are shown in Figure 4-15.

---

---

The PicoScope graph of the data shows the first experimental results when using a 114mm V-band, and a tightening of 7kN into the M6 T-bolt. The hydraulic hand pump generated non-continuous pressure volume with around a 5 second gap for each stroke.

To reduce the oscillation slip curve between the specified values, several types of “power assist” systems were introduced. However, the mechanical connection is a major drawback as far as the systems functional features are concerned. Elimination of the hydraulic hand pump and mechanical joint connections would be beneficial. In this case, the overall development dynamic mechanism system of the torsional test rig and test rig development, convenience and functionality would significantly improve the oscillation slip curve between the specified values.

In addition, the friction between the mechanical joint connections will reduce, which leads to effective power pressure generated by use of the hydraulic hand pump.

#### **4.5 Development of the Flanges**

In previous research by (K. Shoghi, S. M. Barrans, & H. Rao, 2004), on the Axial Load Capacity of V-Section Band Clamp Joints, 235mm and 181mm flange sizes were used. Subsequent research has replicated this method. Current research uses 235mm, 181mm and 114mm flange sizes.

Qin et al (2010), has also done experimental work but relating to the large diameter Marman clamps used in the aerospace industry. These clamps have relatively rigid, discrete V-segments and a very flexible outer band.

---

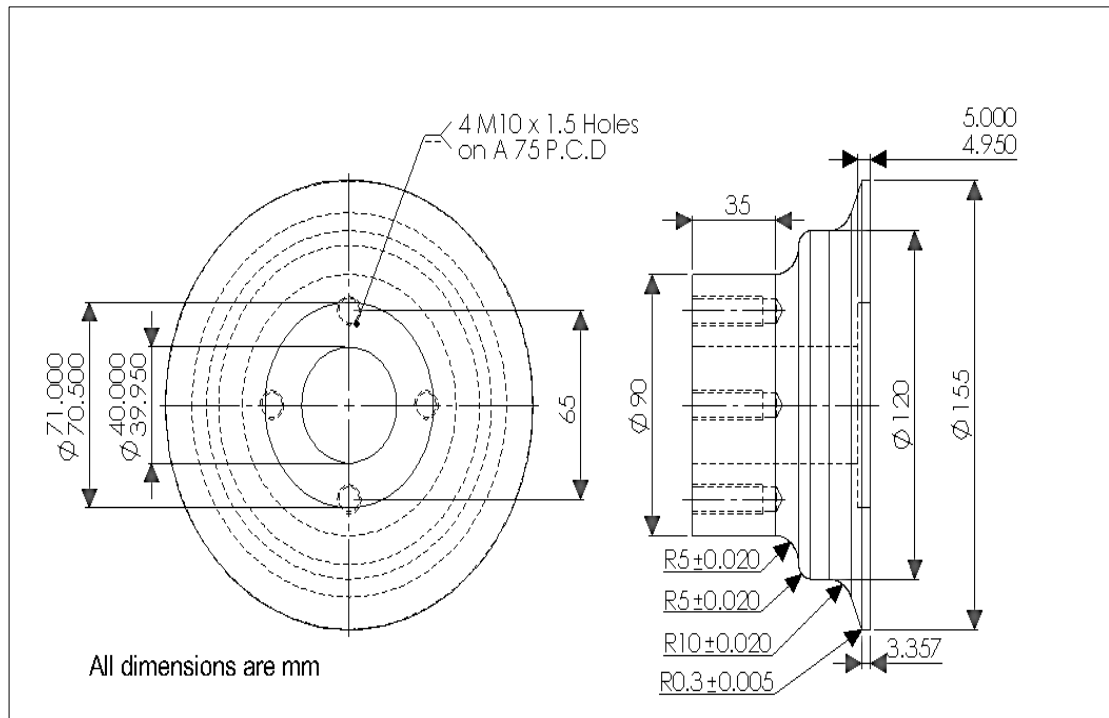


Figure 4 - 13: Flanges Development (155mm Flange)

These were not the only changes regarding flange development within this research. In the central part of the flange a well was bored to hold a spacer for reducing dry friction and the coefficient of friction during testing. The spacers used were 5mm and 10mm wide, with 0.05mm+ tolerances (Figure 4 – 14). This tolerance can affect the contact point between flange faces, which in turn affects the contact point between the flange edges and the V-bands legs. The initial tests undertaken using the 5mm spacer indicated some beneficial results. These benefits included reducing dry friction and the coefficient of friction between flange faces. The width of the spacers affects the contact point between flange and band, but no further testing was carried out and this is an area that is recommended for further research.

For the new flange sizes used in this research, the angle at the lip of the flange was changed from 18 to 20 degrees. The distance between the face of the flange and the central corner of the flange is a maximum of 3.56mm. This length is different to that used in Shoghi's (2004) research, which was 4mm with a +0.10mm tolerance. There is also a difference in length between the flange face and the back end of the flange. In this research the difference is 75mm, with +0.0020 tolerances whereas Shoghi's (2004) research used 50.80mm.

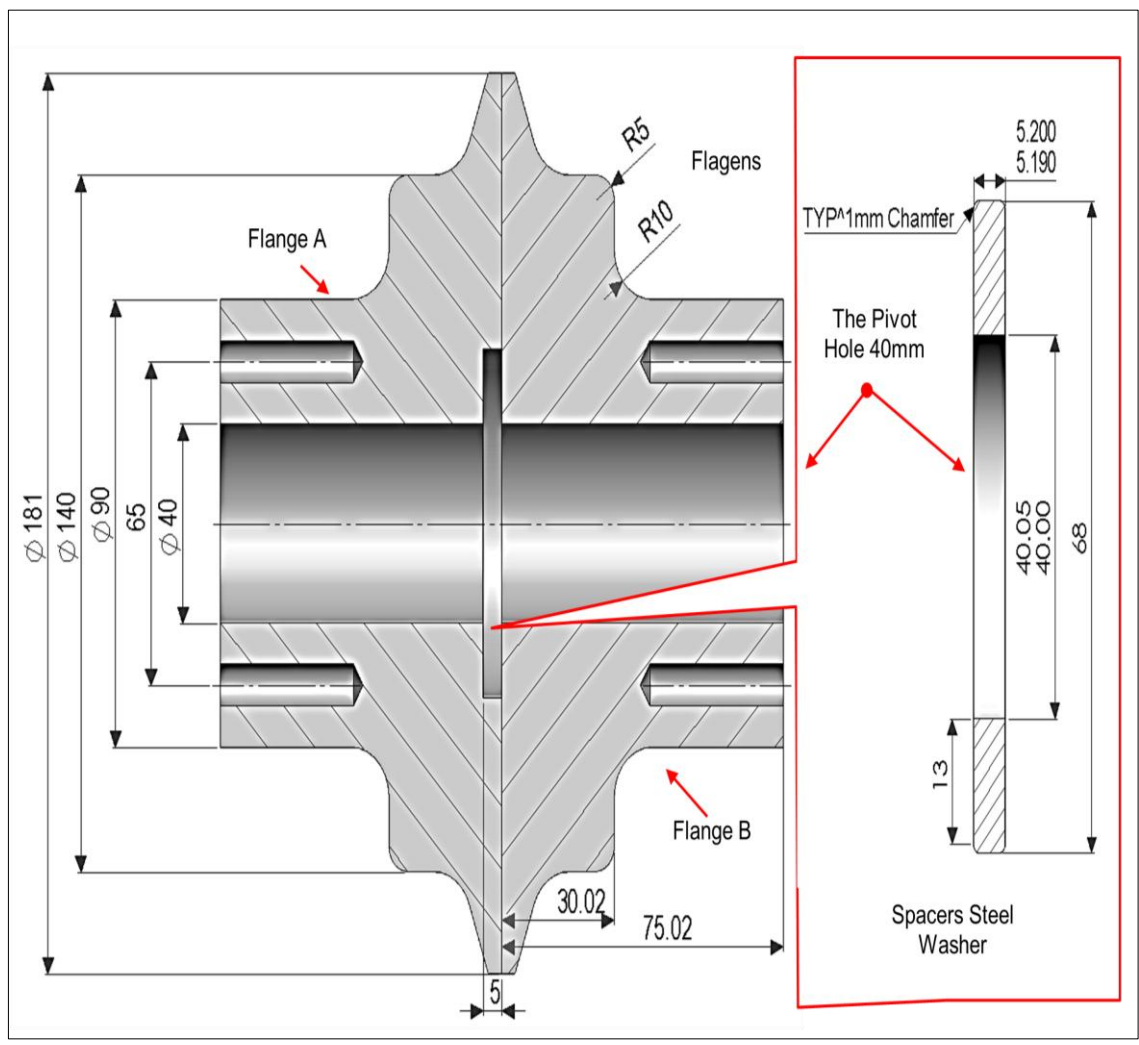
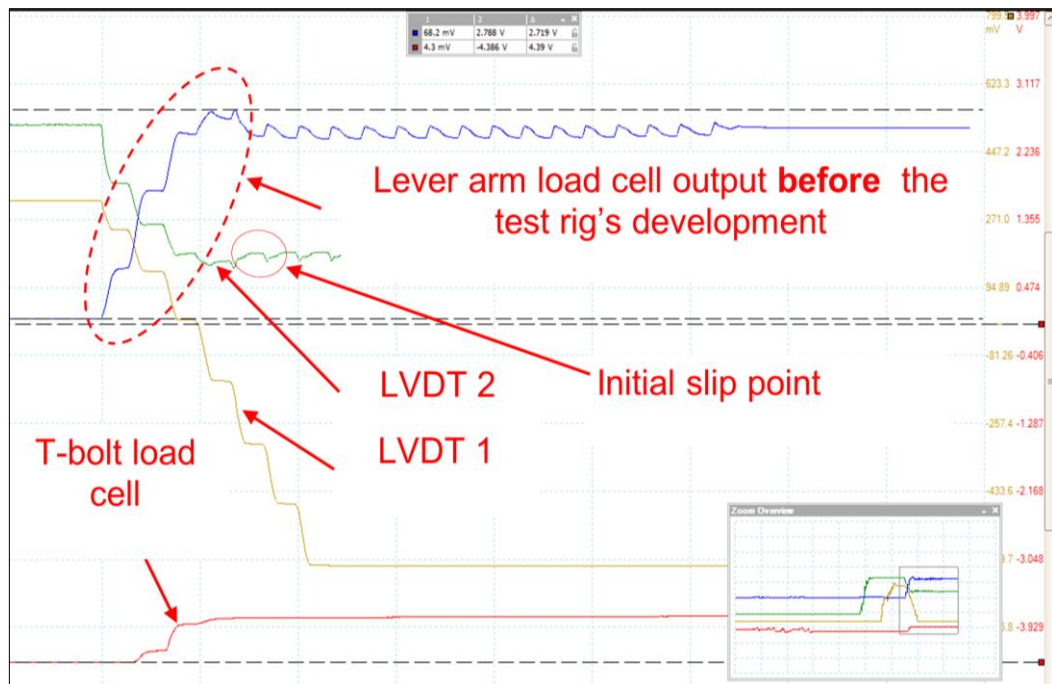


Figure 4 - 14: Development of the Flanges (181mm Flanges)

In this research flanges and spacers were constructed using EN24 T steel. The flanges were produced in the University of Huddersfield workshops. The flanges and spacers are essential components in the test rig and in the testing of the torsional load capacity of the V-band clamps. This is because it is through the flanges that the torsional load is passed on to the V-bands during testing.

#### 4.6 Evaluation of the Revised Rig

Figure 4-13 shows the output of the PicoScope graph which was obtained through the initial tests. As will be noted, the lever arm load cell output is now smoother without the interference previously indicated.



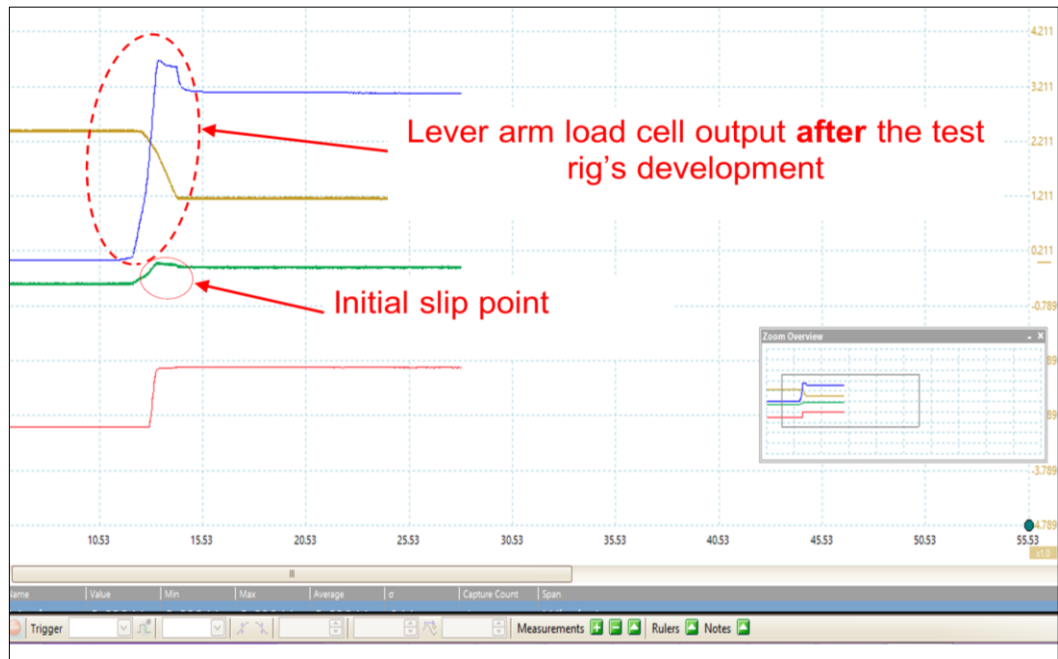


Figure 4 - 15: Graph Plots of PicoScope Graphs of Data Obtained

Figure 4-15 shows the advantage of accumulator systems and the proliferation of mechanical joint connections in the test rig.

With regard to the outstanding issues detailed in this chapter the following solutions are suggested:

To develop the dynamic mechanism system of the torsional test rig, non-skidding spherical plain bearings should be replaced by end rod bearings. This will also reduce friction and allow the test rig lever arm to move more freely. For the application of continuous pressure the bladder accumulator system should be used.

#### 4.7 Conclusion

Problems found with the initial test rig design included:

- Friction levels were too high when using spherical plain bearings

- 
- Insufficient locational flexibility was provided by the the beam hole when postioning the pivot shaft
  - A concern that for the smaller set of flanges it seemed that load was being transferred to the pivot shaft from these flanges
  - The hand pump did not allow the progressive and smooth application of pressure

New parts for the test rig were added to improve the operation of the specialised torsional test rig. These new parts were: end rods, pivot shaft support slot, spherical plain bearings and a bladder accumulator.

- End rods, male and female, to allow more flexibility in the lever arm's rotation (See section 4 - 4).
- Pivot shaft support slot, employed to allow horizontal movement of the pivot and avoid loading of the slot
- Spherical plain bearings, that are low friction and maintenance free and suitable for uni-directional axial loads or combined radial and axial loads
- Bladder accumulator, which allows for a smooth transfer of pressurised fluid to the hydraulic ram and hence torsional load to the V-band joint

For the performance of the new test rig, see Figure 4 – 15, which shows the outputs of the PicoScope graph obtained from initial tests. As can be seen in the Figure 4 – 15, the lever arm load cell now shows a smoother output without the interference previously indicated.

The test rig is capable of a maximum applied load of 80kN as seen in the theoretical development results

---

---

# Chapter Five

## Finite Element Model Analysis of the Torsional Load Capacity of the V-band Clamp Joint

### 5.1 Introduction to FEA

Within the Literature Survey, Finite Element Analysis (FEA) was introduced and described. The present chapter expands on this to both describe the general uses of an FE model and its specific use in the analysis of the data generated by the Torsional Load Capacity of the V-band clamp joint.

The FE method came about mostly because of the physical observations of engineers and not due to mathematicians developing abstract methods, Cook (1994). A description of the FE method lacking sophistication considers it as involving the dismantling of a structure into several parts, pieces or elements and seeing each element's behaviour in a separate way. The elements are then reconfigured as 'nodes' as though they were droplets of glue which held the elements together. This process led to a group of simultaneous algebraic equations. For the purposes of stress analysis, these are equilibrium equations of the nodes and may result in many thousands of such equations, therefore requiring high performance computers, Cook (1994). Rome et al (2009), research looked at two computational techniques with regard to assessing the structural capability of clamp band usage. Both techniques used three-dimensional finite element models (3D FEM).

---

---

Barrans & Muller (2009), used an asymmetric model in their simulations because the 3D FE model was too big to be covered in their research project. Significantly, according to Qin et al (2011), “the existing 3D FE models should be extended to analyse V-band joints with larger band diameters, include a finer mesh and should then be compared to the asymmetric analyses” (p.180). Under simulation options, Lanoue et al (2009), stipulated boundary conditions and loading. A static structural analysis was used but the rotational velocity was ignored as its effect on contact pressure is less than 1 MPa.

Since rotation was not included, the simulation does not replicate exactly that of Nishioka’s experiment. Using a 20-node solid element with total integration, meshing was achieved. Qin et al (2011), used the FEA ANSYS software for analysis of V-segment bands, whilst the current research used the FEA ABAQUS software. In the research results, the initial slip point between flanges and the V-band clamp was identified through experimentation. Different sizes of V-bands were used under boundary conditions and loads.

For this research project, several types of simulation technique methods were employed by the researcher. These were the Frictional Constraint Enforcement Method, otherwise known as the Penalty Technique Method, and the Lagrange Multiplier’s Technique Method. The problem that this research investigates is the maximal torsional load capacity of the V-band. In addition, the analysis will determine the maximum stress around the internal circumference of the V-band. This is the area in contact with the flanges under different loading conditions.

---

---

As in Qin et al research (2011), this study is concerned with the analysis of wedge angle, coefficient of friction and preload regarding different sizes of Teconnex V-band clamps. However, Qin et al (2011), used ANSYS software for Finite Element Analysis, but in this research ABAQUS 6.13 was employed, within the Finite Element Model (FEM). A three dimensional model was employed for the FEM simulation.

## **5.2 Contact Modelling**

For contact modelling, the Penalty Method and Lagrange Multiplier Method are used as follows:

### **5.2.1 Penalty Technique Method**

According to Laursen (2002, p.85), the problem of constrained minimisation follows from the linear elastic case and means the contact problem should be treated by a range of techniques. The Penalty Technique Method has the specific advantage of taking away the explicit limitations from the variational formulation, allowing the issue to be understood as one of unconstrained optimisation.

The Penalty Technique Method is used because the Lagrange Multiplier's Technique Method is not appropriate with larger sizes of V-bands and with high amounts of friction. The Penalty Technique Method works with both larger sizes of V-band clamps and high and low levels of friction, as shown in the simulation results.

---

---

### **5.2.2 Lagrange Multiplier Method**

The Lagrange Multiplier Method has to deal with the problem of frictionless contact, which is found by using a particular form for the contact distribution (Laursen, 2002, p.85). The Lagrange Multiplier's Technique is used in this research to enable reduction of the constrained minimisation issue. It can give solutions to complex non-linear engineering problems, and can be employed for functions of multiple variables. With large V-band sizes and low levels of friction, the Lagrange Multiplier's Technique can be used. The Lagrange Multiplier's Technique has the advantage of not dealing with contact stiffness, as well as being more accurate than the Penalty Method discussed by Piskan et al (2010). The simulation results of the Lagrange Technique Method were very close to the results of the Penalty Technique Method when using an elastic slip of volume 0.001. This finding is also close to the theoretical calculations.

### **5.2.3 Comparison between the Penalty and Lagrange Methods**

The torque band, when using the Penalty Method, shows a good correlation at 0.001 volume level of significance, which accords with the FEA theory. In addition, the Penalty Method uses 0.2 and 0.4 Coefficients of Friction (CoF) levels. (see Chapter Six Measurement of Friction section). However, both the Penalty and Lagrange Methods use Standard analysis rather than Implex or Simplex analysis.

In addition, the Penalty Method gives complete computer simulation analysis for all three sizes of V-band clamps with different levels of significance for the CoF. However, the Lagrange Method of analysis works successfully for the three sizes only with a lesser amount of significance for CoF. Due to the error in the ini-

---

---

tial contact step, the Lagrange Method does not allow a complete analysis with higher levels of friction.

### **5.3 V-band Torsional Load Capacity Model**

In this research project three FE V-band model simulations will be used and are intended to replicate real life. The model will include two parts, the V-band and flange. The following table (Table 5 – 2), will describe the elements type. This model includes both Young's modulus and Poisson's ratio. The initial steps for construction of the model are, back contact, side contact, tightening and torsional (see Figure 5 – 3). The model starts with the back contact. This step applies to the opposite area of the V-band gap, which is also opposite the area of the t-bolt load and was based on theoretical results from the research. The side contact step spins around the circle of the V-band. However, it does not spin around the back contact site, because the back contact site applies load towards the centre of the V-band.

The modulation of the contact surface frictional behaviour was derived from the Penalty Friction formulation. This involved isotropic material properties and a CoF of 0.4, and 0.2, with an elastic slip of 0.01mm (see Chapter Six Measurement of Friction section). Both master and slave surfaces were used with contact. In the model the master surfaces were defined by the band and the rigid surface because, according to Abaqus documentation (2014), the master surfaces should be selected to be the more rigid body. The arbitrary rotation of the surfaces, and the separation and sliding of finite amplitude were formulated by finite sliding. No adjustment for overclosure was required.

---

---

Since the vertical displacement involved was discovered to be less than the tolerance specified, hard contact was selected with a user defined formulation. There is a possibility to set friction dependent field variables, temperature and slip rate. A number of properties can be noted with a friction model, Abaqus documentation (2014). This section is entirely taken from the author's own publication, Sahboun & Barrans (2015).

### 5.3.1 Model Geometry

Shown in Figure 5 – 1 is a 3D geometrical diagram of a V-band. All dimensions are in millimetres and the material type is solid deformable. In this research, deformation involves an object changing its size or shape due to an applied force. The forces are twisting and pushing (compressive), Barrans, Waterworth & Sahboun, (2014).

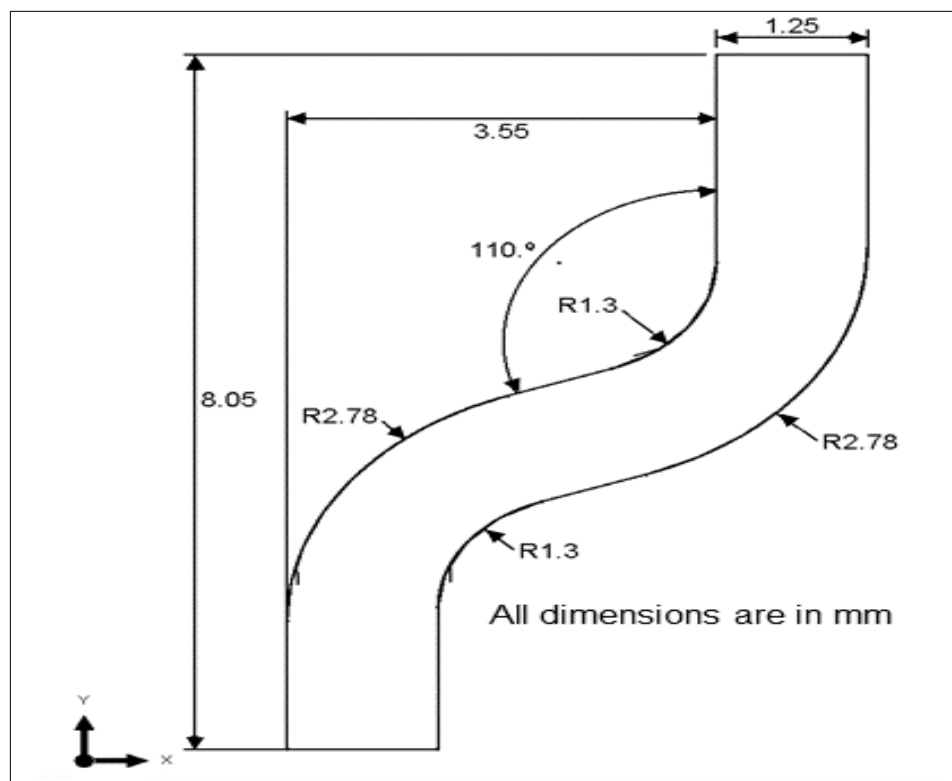


Figure 5 - 1: 181mm V-band in 3D

---



---

end A and end B of the V-band. The load magnitudes were equal (see Figure 5 - 3). The torsion step involves the rotation of the FE V-band model (Global Co-ordination System). This step applies to the circumference of the symmetrical V-band (see Figure 5 - 3).

The tightening step includes a load magnitude of -82.42 N/m (2kN), applied to each end of the V-band. The torsion step applies rotation to the FE V-band model, which is a CSYS (Global Co-ordination System), with radius of .001mm. This step applies to the circumference of the symmetrical V-band.

The steps required are an initial contact step, a t-bolt load tightening step and finally a rotation step. The initial contact step involves contact between the external surface of the flange and the internal surface of the V-band. The t-bolt load tightening step involves simply tightening the T-bolt, which in turn brings the two ends of the V-band clamp closer together. In the rotation step, the flange is rotated and during this rotation a torsional load capacity is generated on the V-band contact surface. The contact area of the flange is defined as the master surface. The V-band contact area is defined as the slave surface, with 0.2 and 0.4 CoF used for this step (see Chapter Six Measurement of Friction). The same materials as used in Shoghi et al's (2004) research.

### **5.3.3 Load Application - Justification of FE Idealisation**

The reasoning behind using half of the 3D FE model was that using the full 3D model would be too large to simulate and take too longer for the computer simulation. For the FE analysis, the Penalty Function method and the Lagrange Multiplier method are employed and both of these methods can be used to enforce both the tangential stick/slip condition and the normal contact between the

---

---

surfaces. However, FE analysis of V-band clamps requires complicated multi-step model definition and considerable computer simulation timings.

Figure 5 - 3 shows an overview of the FE model. It involves half the band portion of the clamp, formed as a mesh of hexahedral elements circling around the central axis. The quantity of elements produced during the sweep was in proportion to the band circumference. Therefore, the element aspect ratio was close to all of the models. As an analytical rigid body, a flange was included in the model, Abaqus documentation (2014).

Before the tightening step, the band can experience rigid body motion in the plane of symmetry. Summarised in Table 5 - 1, a loading and constraining regime was set to avoid the analysis becoming unstable. Within the initial analysis step, band symmetry was restricted by preventing axial displacement on the symmetry plane. With 6 degrees of freedom at reference point A, the flange was also constrained. Furthest from the t-bolt, added constraint in the circumferential direction was applied to the band on a line on the section's outside.

---

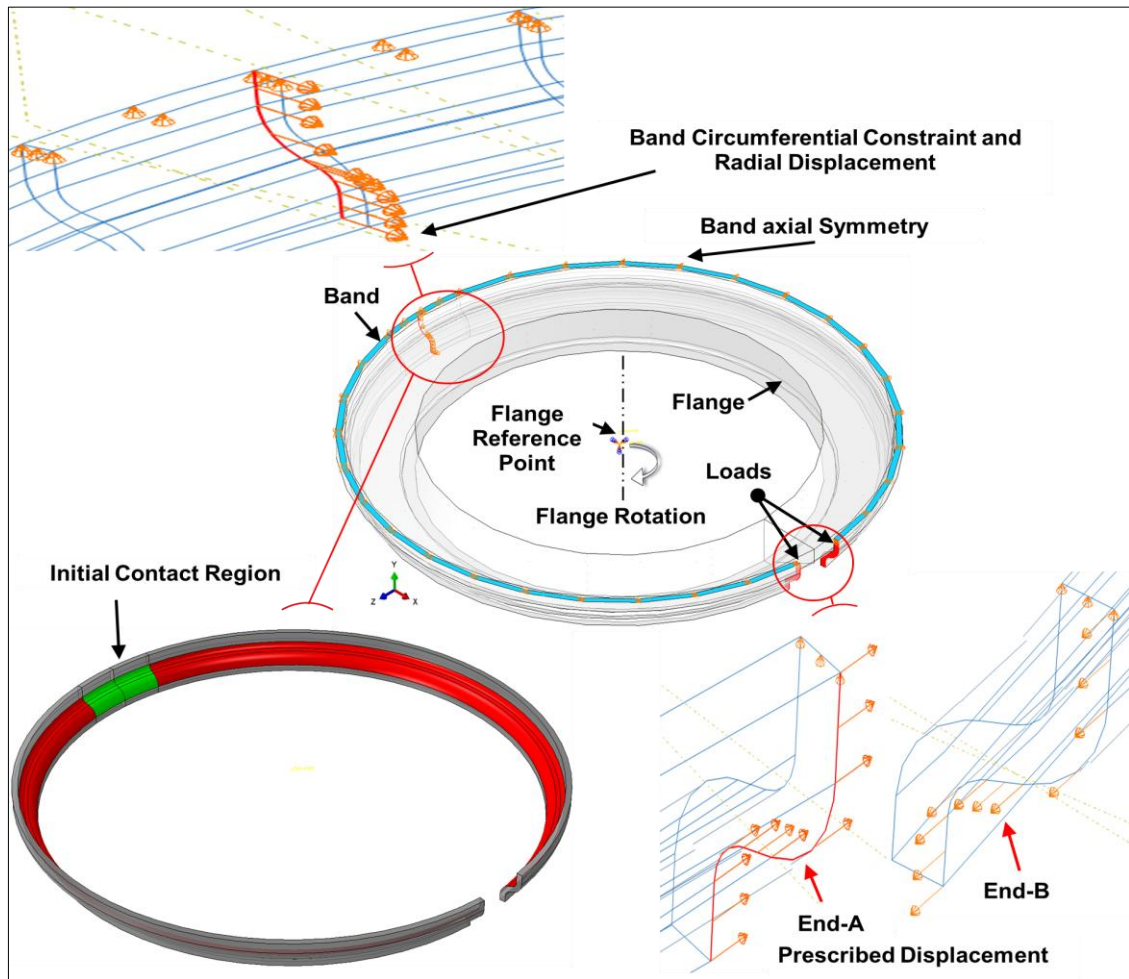


Figure 5 - 3: Summary of finite element model

Table 5 - 1: Boundary Condition Implementation within Analysis Steps

Boundary Condition	Step (time/s)				
	Initial (0)	Back-contact (1)	Side-contact (2)	Tighten (3)	Torsion (8)
Band circumferential constraint	Created	Propogated	Propogated	Propogated	Inactive
Band axial symmetry	Created	Propogated	Propogated	Propogated	Propogated
Flange reference point constraint	Created	Propogated	Propogated	Propogated	Modified
Initial contact region		Created	Propogated	Propogated	Propogated
Band radial displacement		Created	Propogated	Inactive	Inactive
Major contact region			Created	Propogated	Propogated
End A circumferential displacement			Created	Inactive	Inactive
End B circumferential displacement			Created	Inactive	Inactive
End A circumferential traction				Created	Propogated
End B circumferential traction				Created	Propogated
Band circumferential symmetry					Created
Flange rotation					Created

Table: 5 - 1 (Source: Sahboun, S. & Barrans. S., 2015)

---

The first loading step involved displacing the band in the radial direction to force it into contact with the flange. Either side of the back of the band, this initial contact region extended  $\pm 10^\circ$ . The purpose of this small contact area was to improve the stability of the analysis.

For the second load step, the contact region was extended circumferentially, running completely around the band. The band and flange were brought into contact by employing a circumferential displacement to the band's ends. The size of this displacement was adapted to make sure that contact was made around the full circumference. However, the stresses produced were not large.

For the third load step, both the circumferential and radial displacements defined in the 'side-contact' and 'back-contact' steps were discontinued and substituted by circumferential tractions applied to the band's ends. The amount of this traction was such that when multiplied by the band's cross sectional area, it produced a specific t-bolt load. Notably, the circumferential constraint on the band's back was still evident in this load step. This negated any potential rigid body motion owing to numerical imbalance between the circumferential traction loads.

In the fourth and final load step, the circumferential constraint on the band's back was substituted with a circumferential constraint on the symmetry plane. This constraint simulated the anti-symmetry effect deriving from the band's other half, interacting with the second flange under torsion. Additionally, in this load step, the limit on rotation around the axis of the flange reference point was substituted with a prescribed rotation about the axis to simulate flange rotation.

---

---

The loads at end 'A' and end 'B' (as shown in Figure 5 – 3), must be acting in the circumferential direction and defined using the global coordinate system.

The boundary conditions have been activated in the tighten step, or else they will cause interference with the applied loads. The applied displacement on the ends is deactivated. The loads were applied to the outer edges of the end of the band because the displacement and load can not be applied on the same surface. Prescribed displacement involves the two open ends of the V-band moving towards each other or closing, Table 1 -5, (Sahboun & Barrans, 2015).

Additionally, the magnitude of the boundary condition should not have been too high in the initial running of the computer simulations. The load at both ends 'A' and 'B', began at 1kN, equivalent to 41.355N/mm<sup>2</sup>, and then evaluations were made. This was done for each increased loading up to a maximum of 10kN, equivalent to 413.55N/mm<sup>2</sup>. It was applied for each and every V-band size in the computer simulations. 10kN was the highest load applied in the simulations.

As can be seen from Figure 5 – 3, the flange reference point has been created in a central axle. The flange was created as a rigid shell as previously noted. This flange reference point will apply at the next step which is the rotation step. The rotation step is applied to reference point RP and is allowed to rotate the flange in an anti-clockwise direction.

It is necessary for designers to determine if the symmetry FE modeling approach normally applied in practice, produces conservative or accurate results. Parametric analysis provides data relative to 3D effects (See Rome at al 2009, page 2). A 3D cyclic symmetry model, which could not accommodate non-

---

---

axisymmetric loading, was developed by modelling one full block and applying cyclic boundary conditions. A 3D cyclic symmetry model, not accommodating non-axisymmetric loading, was created.

Rome et al (2009), noted significant problems to do with contact modelling which became apparent during initial analysis of the clamp band system. These issues were around rigid body motions, chattering of surfaces and poor numerical convergence. Different Abaque commands were therefore employed in relation to these issues.

#### **5.3.4 Two Levels of Coefficient of Friction for the FE Analysis**

Sahboun & Barrans (2015), found that from the FE analysis they undertook, “increasing the coefficient of friction increases the torsional load capacity of the joint.” (p.5). Yet Sahboun & Barrans (2015), also found that, “a doubling of the coefficient of friction does not lead to a doubling of the load capacity as may be expected.” (p.5). The research gave the main reason for this being that, though “the increased coefficient of friction provides greater resistance to movement in the circumferential direction during torsion, it also provides increased resistance to movement in this direction during tightening of the band.” (p.5). The two CoF levels used in the current research were due to the CoF measures between steel and cast iron being 0.2 and 0.4.

Once the V-band has been tightened around the flange, the CoF effects the displacement. This occurs at the ends of the V-band due to the tightening of the t-bolt and also effects mesh densities. When the CoF is high, as in the two CoF measures used in the current research, Barrans et al (2014), found that, “There is significant variation in the contact pressure distribution around the V-

---

---

band joint” (p.6). Equally, Barrans et al (2014), found that using low CoF levels showed a good linkage between FEA and their use of the two theories dealing with the use and non-use of transverse friction. As the current research used higher CoF levels than in Barrans et al (2014), research, their findings have possible implications both for current and future research.

### **5.3.5 Differences in FEA Theory**

The main difference between the two FEA theories is that one considers the transverse friction component and the other ignores it, (see Sahboun & Barrans, 2015). Additionally, in contrast to prior assumptions when developing half of 3D FE models, Barrans et al (2014), 3D FEA results demonstrated that the contact pressure is non-uniform along the V-band’s internal circumference and showed maximum contact pressure at the t-bolt.

Another difference is that the experimental results involve flange-to-flange friction and the theoretical method only considers band-to-flange friction in the contact area. Another difference between the experimental results and the theoretical results is that there are controllable variables (e.g. testing force, size of V-band), and uncontrollable variables (e.g. tolerances of V-bands, friction between V-band and flanges) in the experimental results. These do not occur in the theoretical results. Using the 0.2 and 0.4 CoF measures means that there are gaps regarding these measures which could be dealt with in future research.

FE models were developed for three different V-band sizes, with diameters of 114, 181 and 235mm. For each band size the model was run 10 times so as to produce results for 10 different t-bolt loads. The analysis was repeated for CoF measures of 0.2 and 0.4. (See Figure 5 - 4 for the results of this analysis).

---

---

Within these graphs, the theoretical results' average is given by equation 5 - 1 and equation 5 - 2 and shown as solid lines with error bars that indicate the results from the two theories. The lower finding is as a result of accounting for transverse friction.

For the lower CoF level, the FE results are slightly bigger than the theoretical result that accounts for transverse friction. For the higher CoF, the theory that ignores transverse friction gives a better match regarding the FE results. It is notable that this result was consistent across a range of V-band diameters. This suggests that the difference in the results is not owing to the band's relative flexibility, as had previously been suggested by Barrans et al (2014).

In relation to both theories, and as confirmed by the FE analysis, increasing the CoF increases the torsional load capacity of the joint. However, a doubling of the CoF does not deliver a doubling of the load capacity as might be expected. The main reason for this is that whilst the increased CoF delivers larger resistance to movement in the circumferential direction during torsion, it also delivers increased resistance to movement in this direction during the band's tightening. Therefore, the normal force between the flange and band is lessened, as forecast in Shoghi et al (2006).

Additionally, increases in the torsional resistance for a given t-bolt load come with increasing the band diameter. Though Shoghi et al (2006), demonstrated that the axial clamping load of the V-band joint is not dependent on band diameter, this reaction between the flange and band is transmitted at a larger diame-

---

---

ter. Therefore, the torque arm is bigger. In this way, doubling the band diameter leads to a doubling of the torsional resistance.

#### **5.4 The Mesh Structure of the V-band FE Model**

Mottram & Shaw (1996), note that structures deform when exposed to external restraining forces that are in equilibrium. These forces are imposed through the body and the level of force explains the effect on the structure involved. A definition of these quantities can be found by using the engineering concepts of stress and strain. Stress analysis is basically a branch of statics, which considers in detail how the intensity of force or stress, at a place in the structure varies. Mottram & Shaw (1996), state that, with the exception of fracturing, variations in stress and strain within a structure are continuous and can be described by functions with single values. Such functions are not found readily, unless in cases where both loading and geometries are basic.

Fish & Belytschko (2007, p.181), state that hexahedral and tetrahedral elements are the two basic categories of three-dimensional elements. Hexahedrals are generalisations of quadrilateral elements, whilst tetrahedrals are generalisations of triangular elements. By collapsing the nodes of a hexahedral element, wedge-shaped elements can be made, as in the case of a triangle made from a quadrilateral. For each category, in addition to various high order flat-face or curved-face elements, there is also the simplest lower order element.

In the current research, the elements were improved by using 16 elements in a range around the circumference contact area of the flange. This is in order to generate more accurate results (Figure 5 – 4).

---

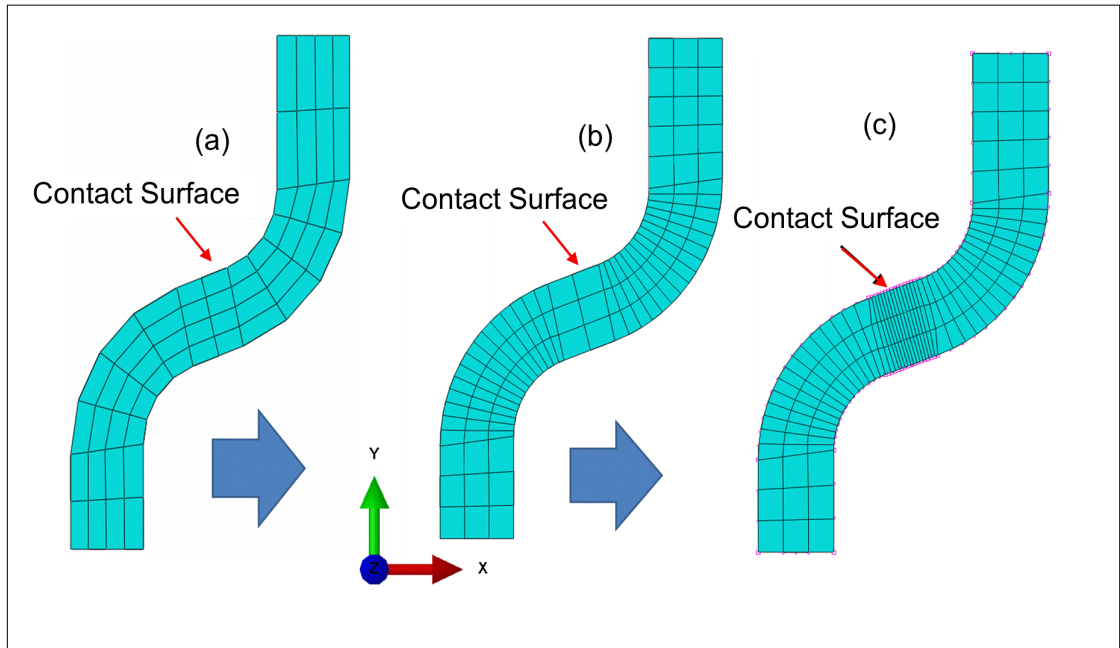


Figure 5 - 4: Cross Section of V-band Mesh Structures

Table 5 - 2: Element Size and Mesh Type of V-bands

Structural Part	Element Size	Mesh Type
114 mm Band	109026	C3D8R - Fine
181 mm Band	175122	C3D8R - Fine
235 mm Band	228582	C3D8R - Fine

### 5.5 Torque Band $T_b$ Required to Slip the V-band Against the Flange

The total band torque,  $T_b$ , required to slip the band against the flange can be estimated by the FEA and validated by experimental investigation between the band and one flange. The total torque reaction  $T_b$  is therefore:

$$T_b = RF_\beta \left[ 1 - e^{\left( \frac{-\mu_b \beta}{\mu_B \cos \phi + \sin \phi} \right)} \right] \quad 5 - 1$$

When:

---

$\mu$	coefficient of friction
$\beta$	band half angle (rad)
$\phi$	section angle (rad)
$p$	pressure on ends (N/mm <sup>2</sup> )
$R$	contact point radius
$F_{\beta}$	force applied by t-bolt
$T_b$	torque capacity at the band-to-flange interface

Therefore, the total torque is comprised of both flange torque and band torque, (Equation 5 – 1). The flange torque transmitted,  $T_F$ , in terms of t-bolt load,  $F_{\beta}$ , combined with Equation 5 – 2, gives the total torque capacity acting on a V-band.

As an example, theoretical calculations of the 114mm V-band used at 0.2 and 0.4 CoF measures are given in Table 5 – 3. As can be seen in Table 5 – 4, at a t-bolt loading of 1kN with a band area of 12.09 mm<sup>2</sup>, the resulting  $T_b$  is 38.20Nm. A different approach to the axial clamping load ignores the transverse friction component. A similar approach for predicting the limiting torque gives the Equation 5 – 2 :

$$T_b = RF_{\beta} \left[ 1 - e^{-\frac{\mu_b}{\sin\phi}} \right] \quad 5 - 2$$

---

## 5.6 Result Plots using the Penalty Technique Method

From Figure 5 – 5, the plot of the reaction banding moment (RM2), is shown for the maximum value in the Y direction. How the V-band works is shown in Figure 1 – 5. The V-band is pressed on to the flange along its circumference and the reaction banding moment is the result.

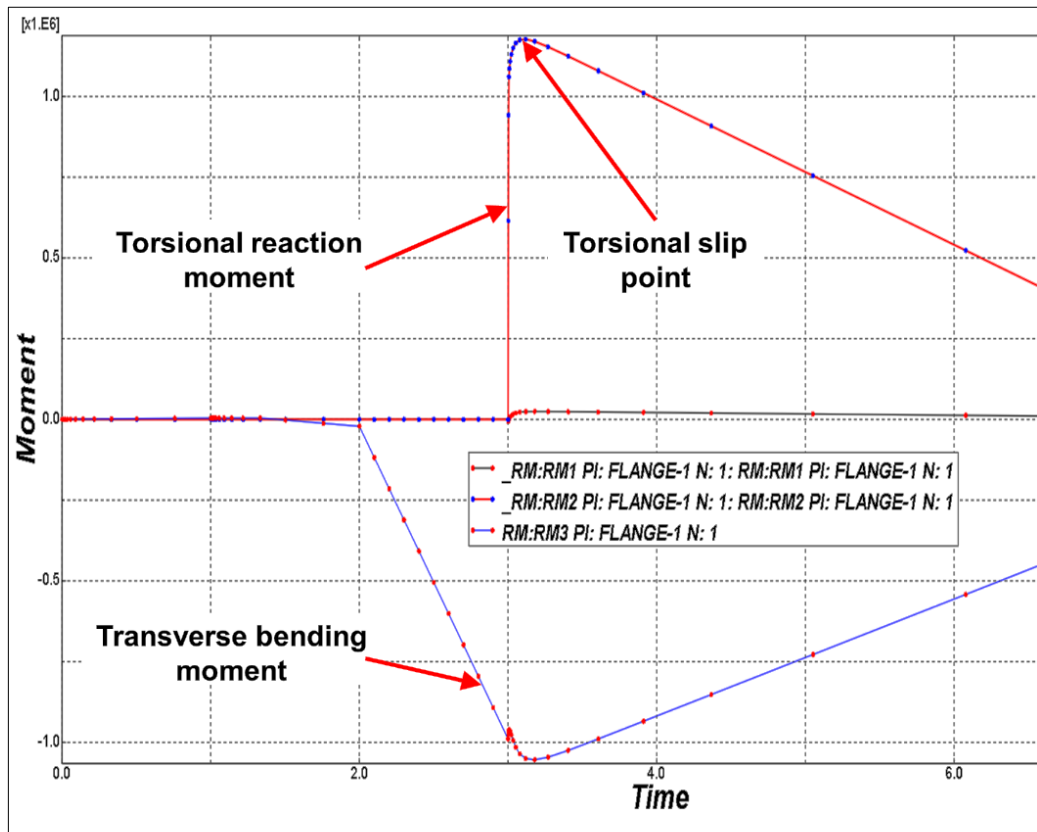


Figure 5 - 5: Plot of the RM2 at 0.2 CoF Level

Table 5 – 3, shows that the elastic slip torque for the band sizes 0.01 and 0.001, at the reaction banding moment with 0.2 and 0.4 CoF, was the most significant at RM2. For the colour scheme of Table 5 – 3 to 5 - 8, the darker the colour the more significant the result, and the most significant results are in bright red. The table shows the results of the Penalty Computer Simulation method. The CoF and the size of the V-band affect the simulation results. Examples of this are

---

the results and plotted graph lines for the V-band sizes 114mm, 181mm and 235mm. As shown in Table 5 - 3, the values were calculated in Microsoft Office Excel. Figure 5 - 5, defines the reaction banding moment (RM2), at the minimum and maximum point as well as at RF2 points 1, 2, and 3.

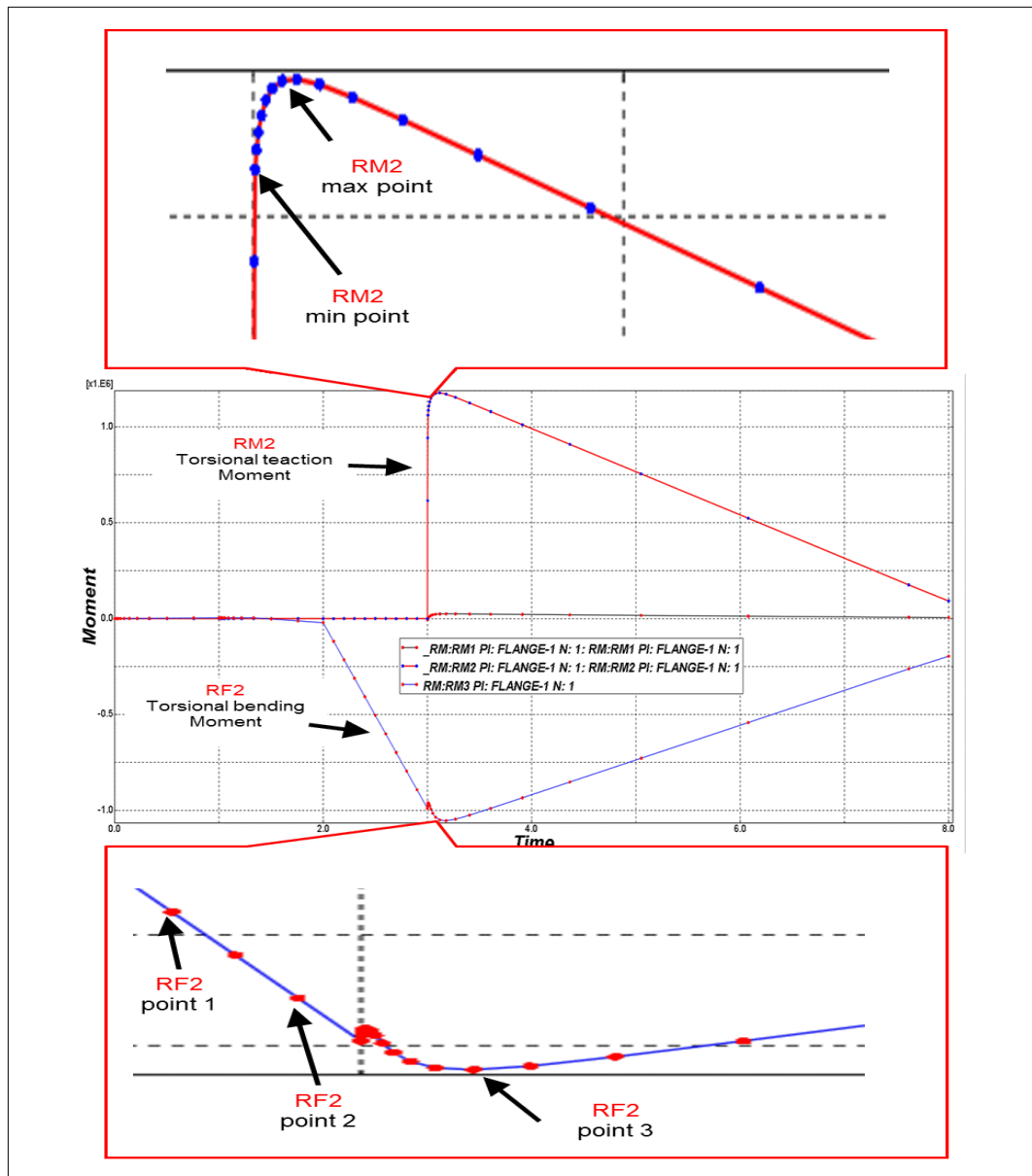


Figure 5 - 6: Definition of the RM2 and RF2 Points

Table 5 - 3: Elastic Slip 114mm Band Reaction Moment (RM2) at 0.2 CoF

						114		0.2 CoF			
		RM:RM2				RF:RF2					
		Min Point		Max Point		Point 1	Point 1	Point 2	Point 2	Point 3	Point 3
T-bolt (kN)	(Nmm)	(Nm)	(Nmm)	(Nm)	(Nmm)	(Nm)	(Nmm)	(Nm)	(Nmm)	(Nm)	
1	38744	38.74	38809.20	38.81	2719.92	2.72	29478.50	29.48	2962.59	2.96	
2	77306	77.31	77790.30	77.79	5464.29	5.46	58874.10	58.87	5947.32	5.95	
3	111651	111.65	117191.00	117.19	8234.57	8.23	85699.60	85.70	8972.04	8.97	
4	147565	147.57	156298.00	156.30	11025.90	11.03	113925.00	113.93	11976.20	11.98	
5	182684	182.68	196093.00	196.09	13841.50	13.84	145448.00	145.45	15081.70	15.08	
6	216132	216.13	235609.00	235.61	16674.20	16.67	178923.00	178.92	18153.70	18.15	
7	248406	248.41	275375.00	275.38	19556.40	19.56	203690.00	203.69	21252.20	21.25	
8	279285	279.29	315107.00	315.11	22452.40	22.45	232611.00	232.61	24360.70	24.36	
9	307335	307.34	356125.00	356.13	25387.50	25.39	262527.00	262.53	27656.20	27.66	
10	371781	371.78	396852.00	396.85	28351.90	28.35	292514.00	292.51	30884.40	30.88	

Table 5 - 4: Elastic Slip 114mm Band Reaction Moment (RM2) at 0.4 CoF

						114		0.4 CoF			
		RM:RM2				RF:RF2					
		Min Point		Max Point		Point 1	Point 1	Point 2	Point 2	Point 3	Point 3
T-bolt (kN)	(Nmm)	(Nm)	(Nmm)	(Nm)	(Nmm)	(Nm)	(Nmm)	(Nm)	(Nmm)	(Nm)	
1	50266	50.27	53937	53.94	1732	1.73	1991	1.99	2056	2.06	
2	100710	100.71	107578	107.58	3472	3.47	3963	3.96	4108	4.11	
3	146793	146.79	161303	161.30	5211	5.21	5701	5.70	6144	6.14	
4	200680	200.68	215040	215.04	6958	6.96	7895	7.89	8215	8.22	
5	230691	230.69	268477	268.48	8716	8.72	9419	9.42	10267	10.27	
6	299506	299.51	321925	321.93	10478	10.48	11606	11.61	12310	12.31	
7	344341	344.34	375156	375.16	12255	12.25	13482	13.48	14352	14.35	
8	387463	387.46	429143	429.14	14035	14.04	14852	14.85	16501	16.50	
9	429969	429.97	482842	482.84	15827	15.83	16666	16.67	18583	18.58	
10	469569	469.57	533720	533.72	17639	17.64	18474	18.47	20440	20.44	

Table 5 - 5: Elastic Slip 181mm Band Reaction Moment (RM2) at 0.2 CoF

						181		0.2 CoF			
		RM:RM2				RF:RF2					
		Min Point		Max Point		Point 1	Point 1	Point 2	Point 2	Point 3	Point 3
T-bolt (kN)	(Nmm)	(Nm)	(Nmm)	(Nm)	(Nmm)	(Nm)	(Nmm)	(Nm)	(Nmm)	(Nm)	
1	61858	61.86	61683	61.68	2783	2.78	2948	2.95	2943	2.94	
2	122765	122.77	124358	124.36	5584	5.58	5839	5.84	5939	5.94	
3	183593	183.59	186783	186.78	8402	8.40	8800	8.80	8728	8.73	
4	244120	244.12	249320	249.32	11238	11.24	11642	11.64	11949	11.95	
5	304368	304.37	312263	312.26	14084	14.08	14333	14.33	14976	14.98	
6	364817	364.82	375535	375.54	16962	16.96	17464	17.46	18031	18.03	
7	424860	424.86	438678	438.68	19842	19.84	20381	20.38	21086	21.09	
8	485112	485.11	502172	502.17	22752	22.75	23706	23.71	24165	24.17	
9	545285	545.29	565763	565.76	25678	25.68	26274	26.27	27320	27.32	
10	605625	605.63	630576	630.58	28632	28.63	29713	29.71	30470	30.47	

Table 5 - 6: Elastic Slip 181mm Band Reaction Moment (RM2) at 0.4 CoF

	181 0.4 CoF									
	RM:RM2				RF:RF2					
	Min Point		Max Point		Point 1	Point 1	Point 2	Point 2	Point 3	Point 3
T-bolt (kN)	(Nmm)	(Nm)	(Nmm)	(Nm)	(Nmm)	(Nm)	(Nmm)	(Nm)	(Nmm)	(Nm)
1	82362	82.36	84643	84.64	1791	1.791	1937	1.94	2013	2.01
2	161999	162.00	169099	169.10	3584	3.584	3887	3.89	4024	4.02
3	240372	240.37	253632	253.63	5383	5.383	5763	5.76	6045	6.04
4	314472	314.47	339737	339.74	7188	7.188	7622	7.62	8054	8.05
5	402983	402.98	422658	422.66	8998	8.998	9657	9.66	10095	10.10
6	480764	480.76	507240	507.24	10815	10.815	11533	11.53	12121	12.12
7	555109	555.11	591682	591.68	12636	12.636	13648	13.65	14167	14.17
8	626714	626.71	676007	676.01	14463	14.463	15549	15.55	16215	16.22
9	695282	695.28	760205	760.21	16297	16.297	17447	17.45	18266	18.27
10	804327	804.33	836551	836.55	18136	18.136	19344	19.34	20319	20.32

Table 5 - 7: Elastic Slip 235mm Band Reaction Moment (RM2) at 0.2 CoF

	235 0.2 CoF									
	RM:RM2				RF:RF2					
	Min Point		Max Point		Point 1	Point 1	Point 2	Point 2	Point 3	Point 3
T-bolt (kN)	(Nmm)	(Nm)	(Nmm)	(Nm)	(Nmm)	(Nm)	(Nmm)	(Nm)	(Nmm)	(Nm)
1	80278	80.28	80278	80.28	2820	2.82	2940	2.94	2940	2.94
2	160282	160.28	161164	161.16	5653	5.65	5863	5.86	5907	5.91
3	240005	240.01	241949	241.95	8494	8.49	8784	8.78	8882	8.88
4	319701	319.70	323034	323.03	11353	11.35	11710	11.71	11870	11.87
5	399258	399.26	404215	404.22	14222	14.22	14637	14.64	14866	14.87
6	478831	478.83	485590	485.59	17107	17.11	17572	17.57	17880	17.88
7	558345	558.35	567099	567.10	20003	20.00	20512	20.51	20890	20.89
8	637701	637.70	648452	648.45	22907	22.91	23454	23.45	23954	23.95
9	717207	717.21	731010	731.01	25829	25.83	26410	26.41	27013	27.01
10	796865	796.87	813425	813.43	28769	28.77	29380	29.38	30088	30.09

Table 5 - 8: Elastic Slip 235mm Band Reaction Moment (RM2) at 0.4 CoF

	235 0.4 CoF									
	RM:RM2				RF:RF2					
	Min Point		Max Point		Point 1	Point 1	Point 2	Point 2	Point 3	Point 3
T-bolt (kN)	(Nmm)	(Nm)	(Nmm)	(Nm)	(Nmm)	(Nm)	(Nmm)	(Nm)	(Nmm)	(Nm)
1	105437	105.44	108542	108.54	1824	1.82	1907	1.91	1985	1.99
2	211089	211.09	217075	217.08	3649	3.65	3822	3.82	3971	3.97
3	316148	316.15	325387	325.39	5476	5.48	5726	5.73	5955	5.95
4	419300	419.30	433729	433.73	7308	7.31	7717	7.72	7947	7.95
5	521785	521.79	542165	542.17	9143	9.14	9452	9.45	9101	9.10
6	621580	621.58	650500	650.50	10983	10.98	11307	11.31	11930	11.93
7	716827	716.83	758675	758.68	12826	12.83	13160	13.16	13845	13.84
8	838773	838.77	867378	867.38	14673	14.67	15806	15.81	15908	15.91
9	941300	941.30	976020	976.02	16524	16.52	17107	17.11	17894	17.89
10	1043220	1043.22	1084650	1084.65	18379	18.38	19499	19.50	19962	19.96

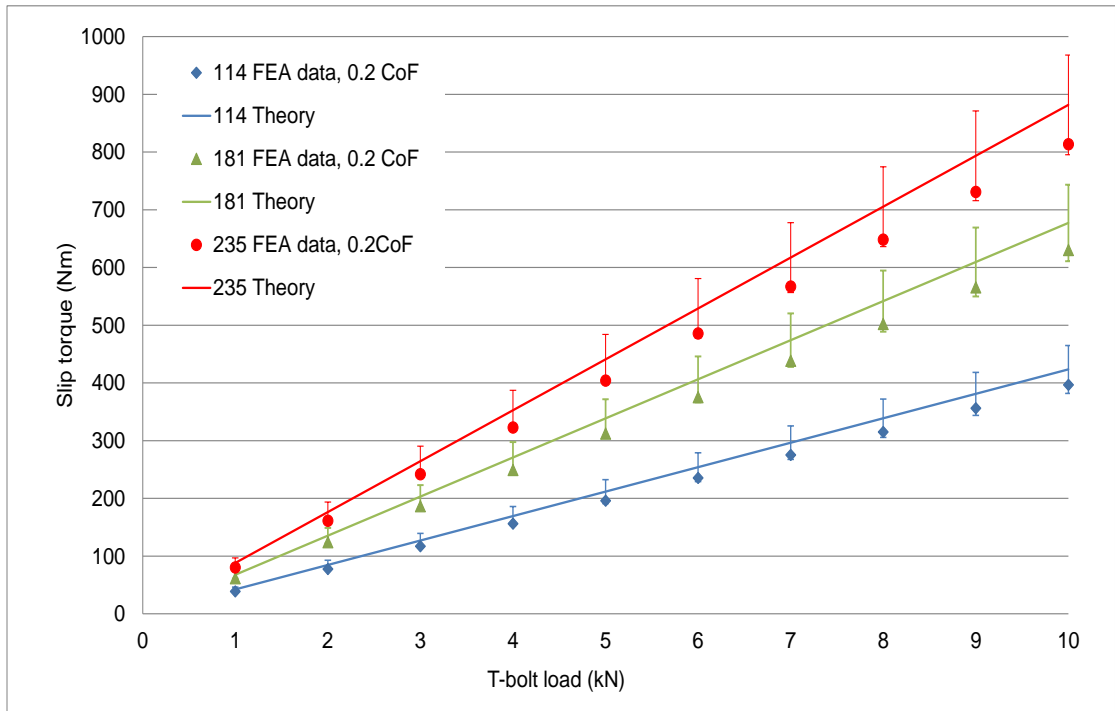


Figure 5 - 7: Comparison of FE and Theoretical Results With 0.2 CoF

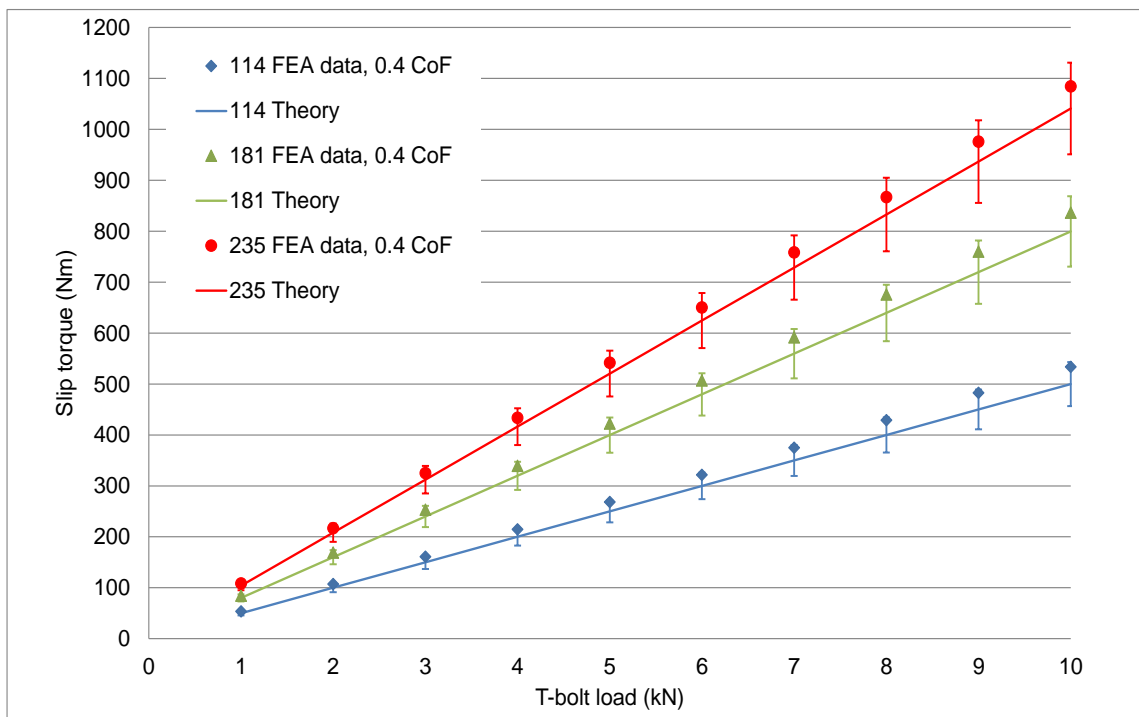


Figure 5 - 8: Comparison of FE and Theoretical Results With 0.4 CoF

---

From Figure 5 – 6, it can be seen that the elastic slip at the significant factor of 1 (results in red), is significant for all band sizes. In addition to Figure 5 – 6, Table 5 – 3 shows the  $T_b$  results for a CoF of 0.2. This shows a steeper and more significant increase than those for a CoF of 0.4.

### 5.7 Results - Stress Distribution

From the computer simulation results, it can be seen that the area of highest stress is where the V-band contacts the flange with a maximum tightening load of 10kN (Figure 5 – 9 & Figure 5 - 10). Directly opposite the point of the T-bolt closure is the area of lowest stress in the V-band's circumference.

From different views of the V-band's contact with the flange, additional results show that the stress distribution is around the circumference of the V-band.

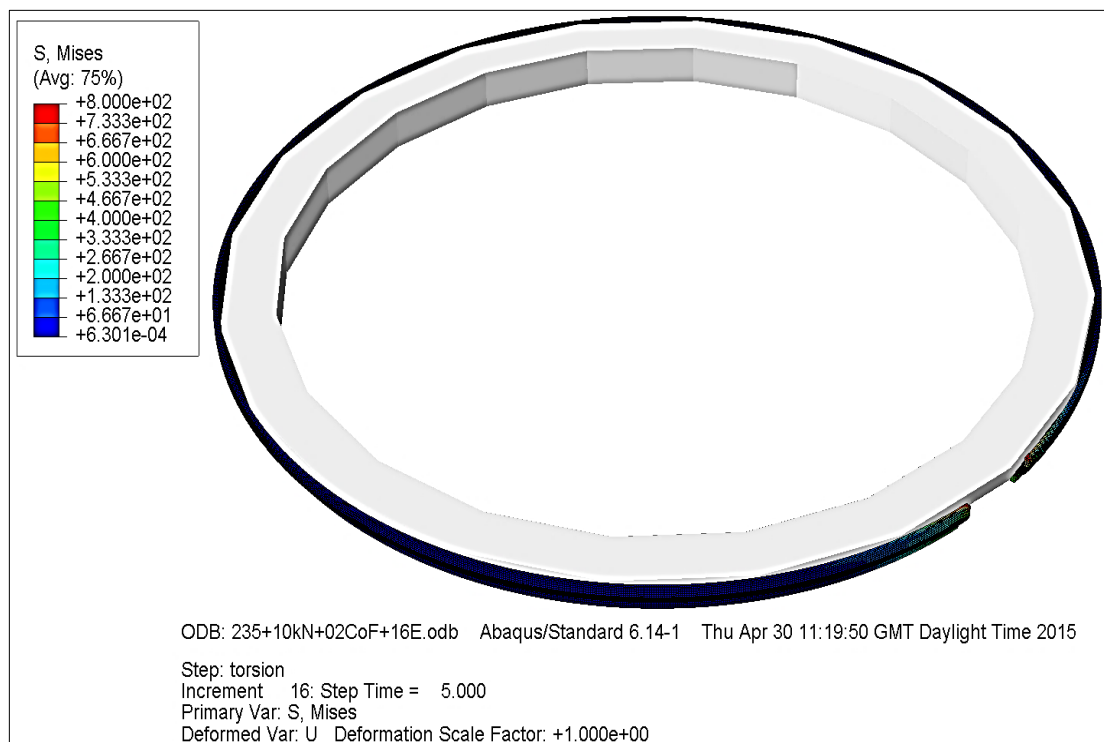


Figure 5 - 9: V-band Stress Distribution Results

---

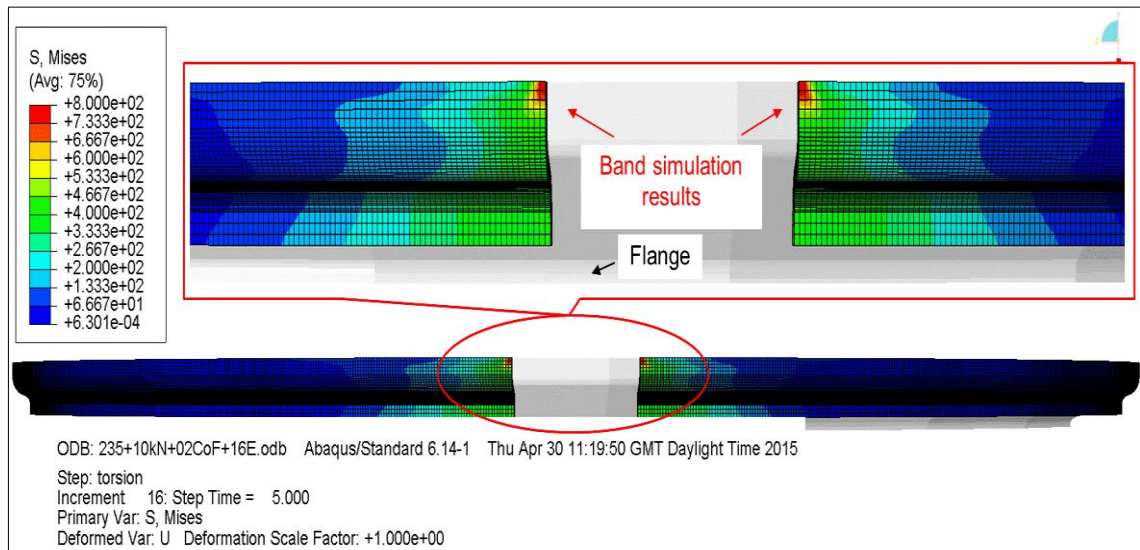


Figure 5 - 10: End of V-band Stress Distribution Results

## 5.8 Conclusion

The purpose of this chapter on Finite Element Model Analysis has been to explain the creation and use for simulation of the FE model. This was done successfully employing different software technique steps such as: Material Properties, Mesh Density, Boundary Conditioning, Loads, Displacement and Interaction Properties. The results of the Penalty Method Technique at 0.2 and 0.4 CoF levels and within the t-bolt load range 1kN - 10kN, correlated closely with the theoretical calculations. A discussion of the results will be covered in Chapter Seven.

In the future this model should be used to create a full band and two flanges. One of the flanges should be fixed as it is now. The other flange should be fixed for the contact and tighten steps. A third load step should then be added where this flange is rotated. This will then simulate what has happened in the research.

---

Theoretical Development results were compared to the Finite Element Analysis simulation results. These used 0.2 and 0.4 CoF levels and differing V-band sizes. The results were produced using a hand pump to apply hydraulic pressure within the test rig. The Theoretical Development and Finite Element Analysis results detailed in this chapter were presented in Rome, Italy in July 2015.

---

---

# Chapter Six

## Experimental Work

### 6.1 Introduction

As noted in Chapter 4, the University of Huddersfield engineering workshop produced a test rig, which was used as a prototype for testing the torsional load capacity of V-band clamps. The dynamics and functionality of the test rig were developed for the purpose of determining the torsional load capacity of different sizes of V-band clamps used in turbochargers. These bands help the joint connection between the compressor housing and the bearing housing and between the bearing housing and the turbine housing of a turbocharger. Some manufacturers use the same size of bands for both of these joint connections within the turbocharger. Other manufacturers use different sizes of V-bands for the same turbocharger. The testing in current research used and tested one size of V-band clamp at a time.

### 6.2 Experimental Setup

Figure 6 -1, details the equipment connections and the test rig configuration used in the research. The system has two inductive axial movement gauge heads (LVDTs). Each one is connected to a conditioning signal box (Tesatronic TTA20), which in turn is connected to the PicoScope (4024 – 4 channels). The lever arm load cell is a nautical load cell (see lever arm load cell), and is connected to the load cell amplifier, which in turn is connected to the PicoScope (4024 – 4 Channels). The t-bolt load cell is connected in the same way.

---

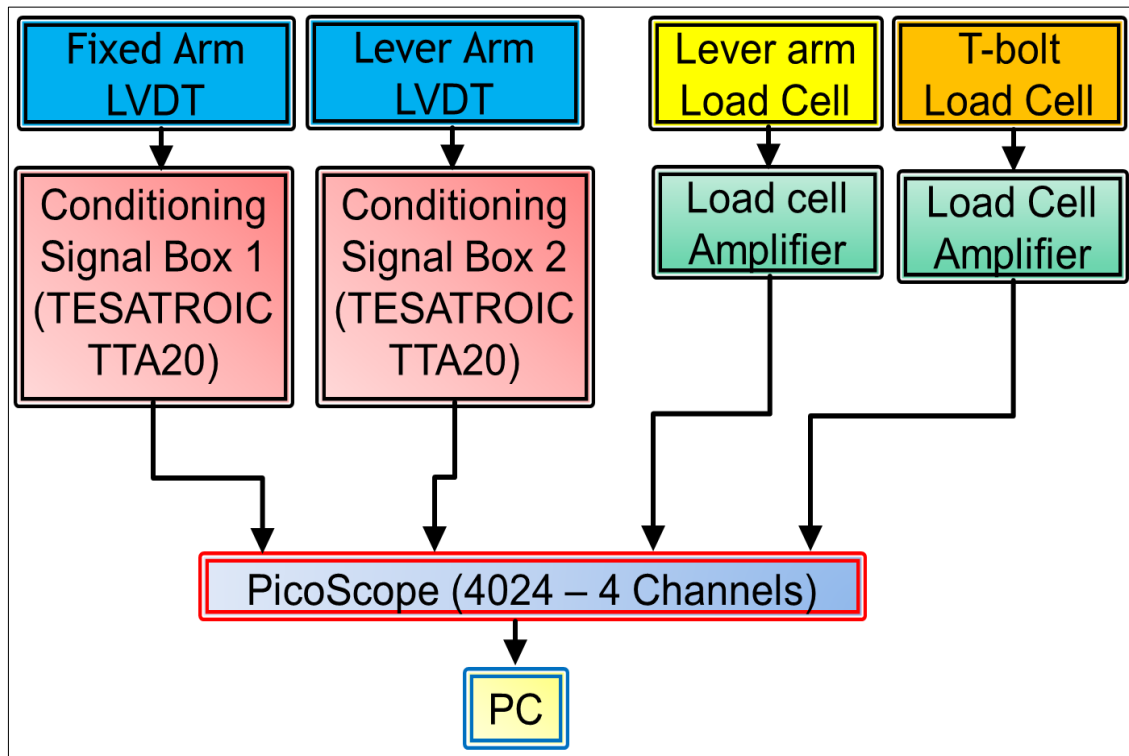


Figure 6 - 1: Connections in Test Configuration

### 6.3 Experimental Method

In much of the previous research work, t-bolt tension has not been measured directly. Instead, the torque applied to the T-bolt was recorded. The objective was to measure the axial load as it was being generated, rather than measuring the pre-load effect due to the axial load.

Previous research used a total of three Teconnex V-bands with different diameters: 235mm, 181mm, and 141mm, with all the V-bands using a single M6 T-bolt. For each V-band, T-bolt tension was increased from 1kN to 10kN in 1kN increments. The load was applied by hydraulic ram (working in a horizontal direction) until V-band slippage occurs. To release the loading for each test, the

---

V-band T-bolt was released and the hydraulic hand pump valve was loosened prior to the start of the next loading test.

For the present experimental work, three Teconnex V-bands diameter sizes were used: 114mm, 181mm and 235mm. All V-bands used the same T-bolt and steel nut size.

In addition, the hand pump provided an uneven application of pressure as can be noted by the blue line in Figure 6.2. Therefore, a bladder accumulator was employed in the current research, with the aim of supplying a more even oil pressure.

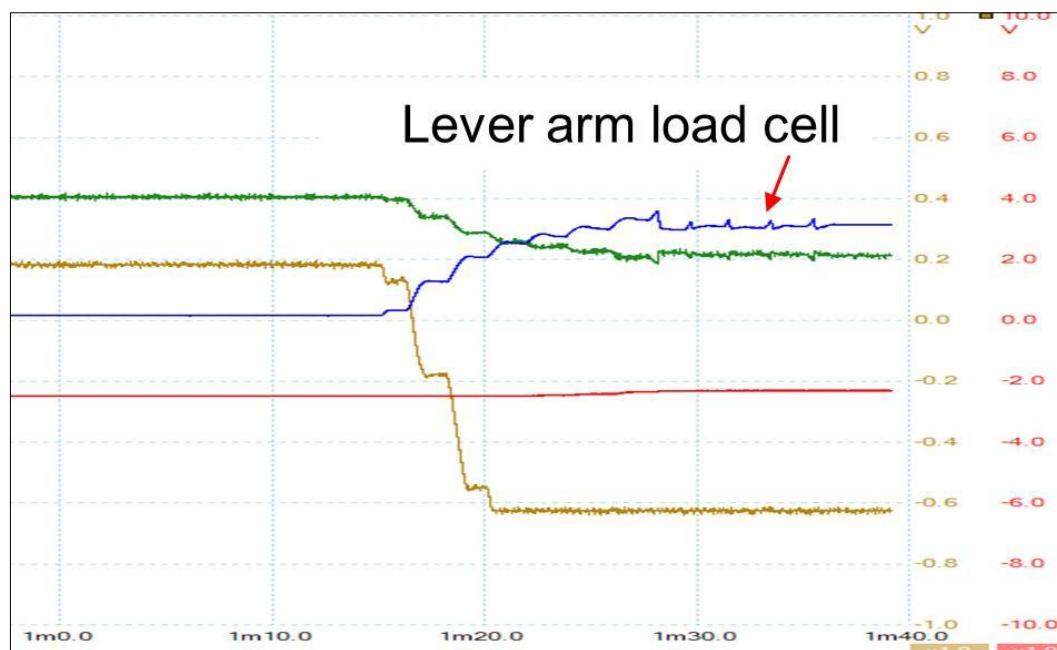


Figure 6 - 2: Data Obtained at Test 6kN Using a 235mm V-band

The current test rig still uses a hand pump. However, with the addition of a pressure gauge connected to the bladder accumulator, the tester can see the pressure bars being built up with the use of the hand pump. The system is designed to move the lever arm connected to the flange at a pressure of 18.2 bar,

---

---

when using the biggest flange of 235mm, with its accompanying V-band of the same size. Additionally, a bleeder valve is part of the new system, and is used to lessen the pressure within the system. Once the maximum desired pressure of 18.2 bar is reached, the needle valve is used to allow pressure into the hydraulic ram.

For new testing with the current setup, new LVDT (GT 21) inductive axial movement gauge heads were used. This is because the previous LVDT, attaching to lever arm B, was out of range. However, the previous configuration using an LVDT attached to lever arm A continued in the same position, 80mm above the Nordic load cell.

#### **6.4 Replicates of Flange and V-band Contact Surfaces**

The purpose of this stage was to find out the shapes of the initial contact points between the V-bands and the flange edges. This is because the V-bands can be unsymmetrical in design, shaping and manufacture, which can then effect experimental results. This issue is also noted by Shoghi et al (2004).

The software package 'SolidWorks 2013', was used to partition the geometry of the V-bands and to make prints of the model for the V-band sizes: 114mm (A4 landscape), 181mm and 235mm (A3 landscape). A3 printing was used because the larger V-band clamps would not fit on A4 size paper (see Figure 6 - 3).

---

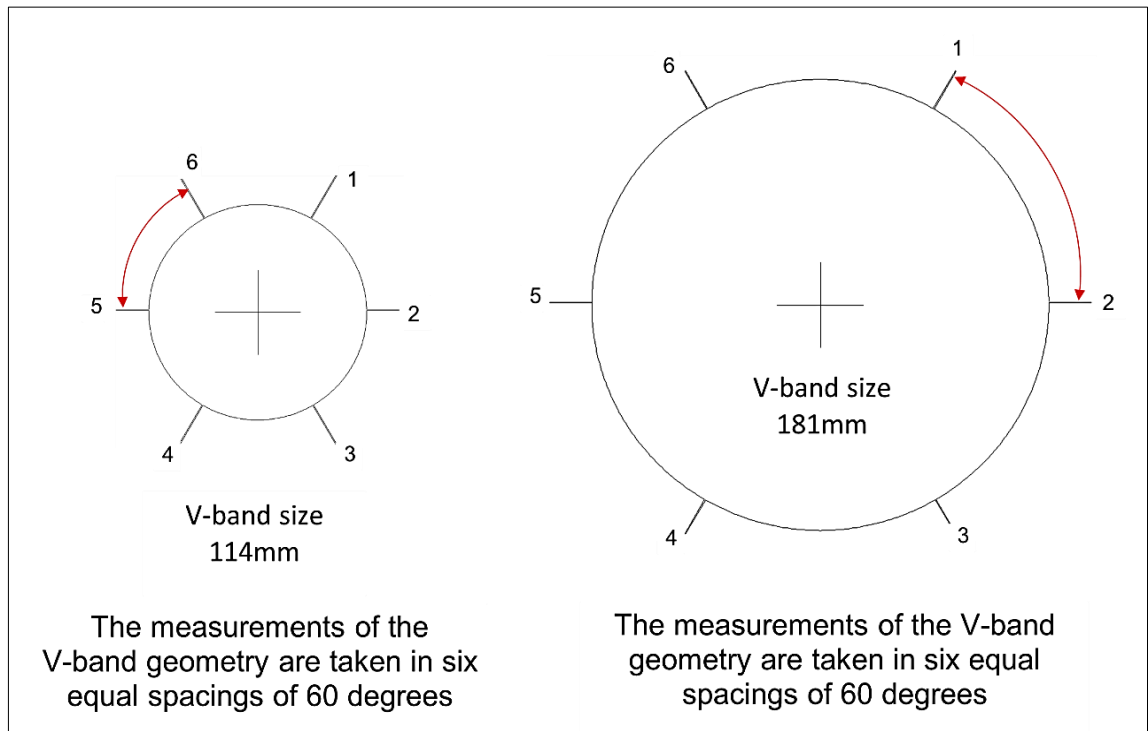


Figure 6 - 3: Partition of the Geometry of the V-bands

To ascertain the exact shape of the initial contact points between the V-bands and the flange edges, mouldings were taken of all three V-band sizes and all three flange sizes used in the experimental work. Mouldings were also made for each 60 degree section of both the V-band and flange 360 degree circumferences. This reflects the 'SolidWorks 2013' geometrical partitioning of both V-band and flange. The mould length was 30mm, with a width of 20mm and with depths of 20mm and 10mm from the edges.

For the mouldings, a two-part silicone compound was used. This produces a high resolution 3D replica of the flange and V-band contact surfaces. Plasticine was used to construct a wall around the surfaces to be moulded and a Microset dispensing gun of 50ml (Figure 6 – 4), was used to put the two-part silicone compound into the walled area.

---

The 3D mouldings for both flange and V-band were scanned by a shadowgraph at NBL laboratories and the shadowgraph was used to construct draught engineering diagrams. These diagrams show the actual contact points between V-band and flange used in the research.

## **6.5 Calibration of Load Cells**

### **6.5.1 Calibration of the Omega Load Cell**

The data derived from calibrating an Omega Load Cell with an INSTRON Testing System, INSTRON (2012), is given in Table 6 - 1 and plotted in Figure 6 - 8. The load cell was calibrated for tension and compressive load, (see Appendix K).

Table 6- 1: Omega Load Cell Calibration

Nominal (N)	Average Load During Hold Times (N)	Picoscope (mV)
9000	8999.934	3813
8000	7999.984	3380
7000	7000.001	2940
6000	6000.000	2502
5000	4999.980	2068
4000	4000.021	1637
3000	3000.034	1212
2000	2000.027	801
1000	999.961	410
0	-0.243	-37

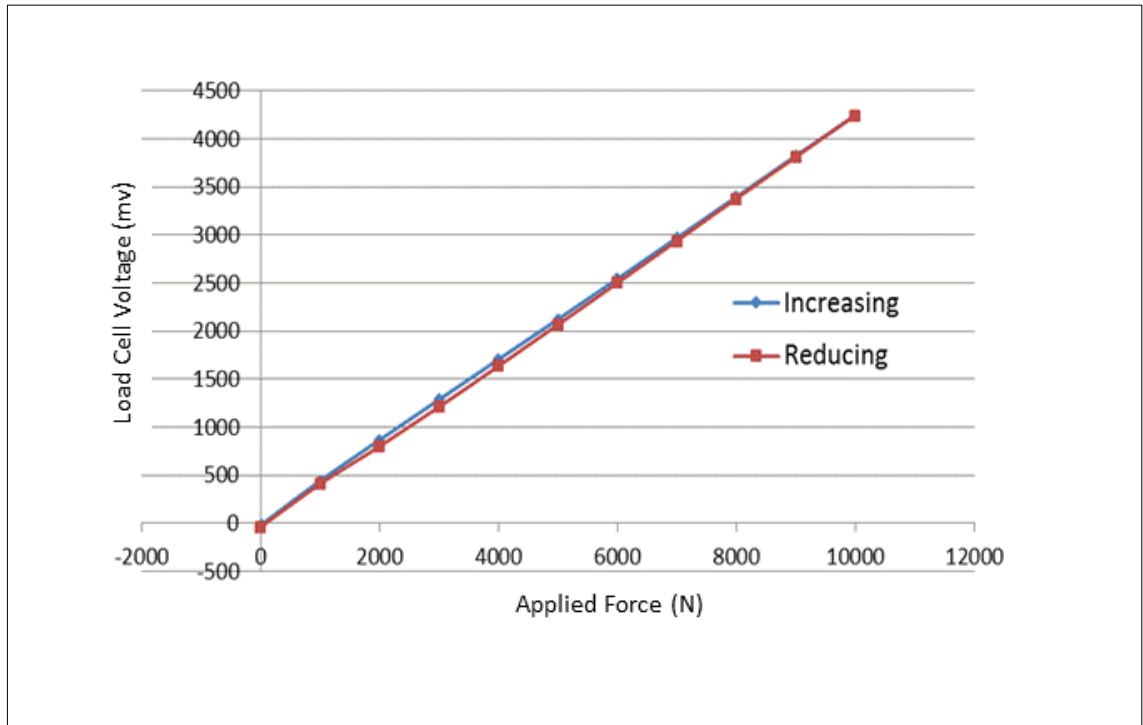


Figure 6 - 4: Omega Load Cell Calibration

### 6.5.2 Calibration of the Lever Arm Load Cell

Table 6- 2: Calibration Load of the Lever Arm Load Cell

Nominal (N)	Average Load During Hold Times (N)	Picoscope (mV)	Zero Correction
10	10.261	-40	-30
100	100.101	212	-40
200	200.072	469	212
300	300.044	724	469
400	400.072	979	724
500	500.032	1238	979
600	600.092	1492	1238
700	700.069	1749	1492
800	800.053	2004	1749
900	900.031	2261	2004
1000	1000.022	2518	2261
1100	1100.034	2773	2518
1200	1199.965	3030	2773
1300	1300.009	3284	3030
1400	1399.961	3541	3284
1500	1500.014	3798	3541
1600	1599.977	4052	3798
1700	1700.004	4309	4052
1800	1800.026	4564	4309
1900	1899.990	4821	4564

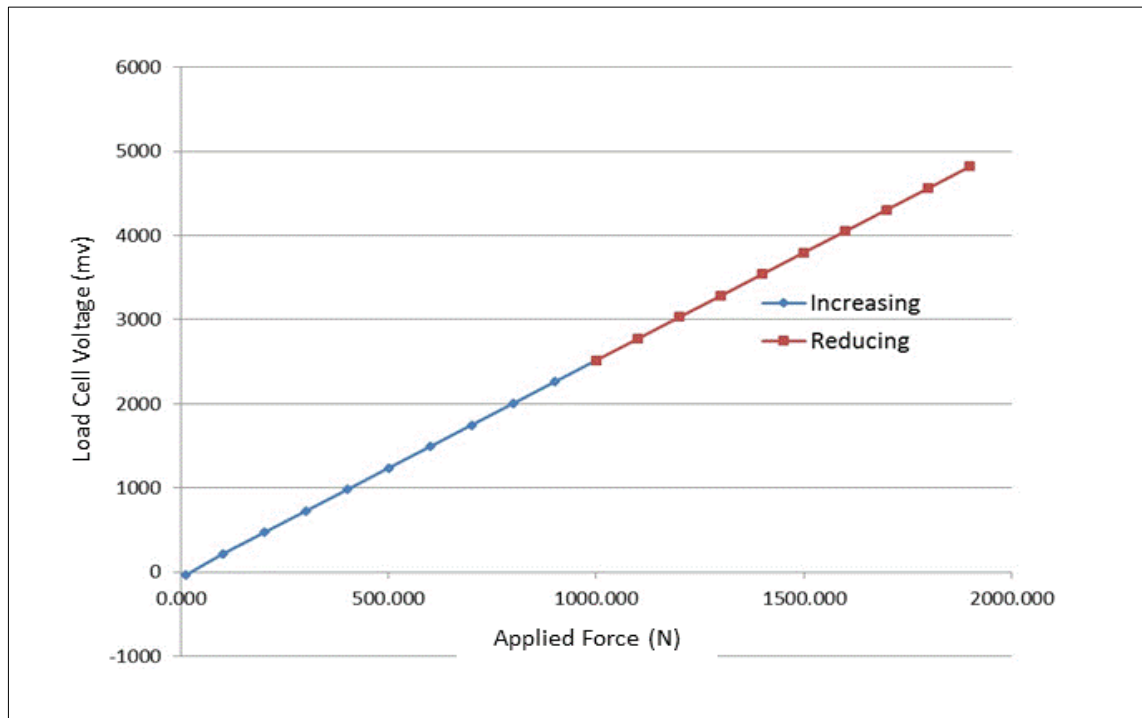


Figure 6 - 5: Lever Arm Load Cell Calibration

The data derived from calibrating a Nordic Load Cell with an INSTRON Testing System, INSTRON (2012), is given in Table 6 - 2 and plotted in Figure 6 – 9. Negative voltages were produced as the load cell was calibrated for tension and compressive load, (See Appendix K). However, testing will induce positive voltages. As the load cell is seen to be linear in both tension and compression, the voltage conversion factor can be viewed as positive.

## 6.6 Friction Effects

### 6.5.1 Definition of Friction

According to Fuller (1978), friction involves resistance due to two solid surfaces either sliding, or tending to slide, over one another. Such surfaces could be either lubricated or dry. In the latter case, relevant to the current research project,

---

such surfaces do not contain contaminating films or fluids and therefore the resistance is called dry friction.

### **6.6.2 Measurement of Friction**

Bolton (2003), uses the term 'frictional force' which describes the force arising when two bodies in contact with each other are in opposition regarding the movement of one in relation to the other. Static friction involves both bodies being at rest and refers to the frictional force needed to oppose a required movement. The measurement of frictional force and any resulting motion involves Newton's first and second laws.

According to Dorf & Kusiak (1994), for an apparatus measuring friction, two test examples are loaded against each other at a specified normal load. Then one is slid relative to the other at a specific speed of slide and a measurement made of the tangential force used to start or maintain the slide. Many different apparatuses can be used to measure friction force, but the simplest method used is the inclined-plane technique.

Friction can affect experimental results and in current research friction was measured using the mechanical classical test in the laboratory at the University of Huddersfield. This was achieved by using a 150mm section of the same material used in a V-band flat section before the process of rolling. The mechanical classical test involves a flat surface (150mm by 1000mm), which is fixed in the centre and which allows inclination around the centre. There is a large protractor attached to the flat surface that can be locked at any angle within 180 degrees. At one end of the surface a flat V-band section of around 150mm is placed. The flat surface is then manually raised to an incline position until the

---

---

V-band flat section slides off. At that point in the test, the mechanical classical test is locked and the protractor angle is read for incline.

Additionally, the flanges were measured for angle of slip and this was done for all three sizes: 114mm, 181mm and 235mm. The averages of the measurement's results were a minimum Coefficient of Friction between 0.14 - 0.15, and the maximum Coefficient of Friction was between 0.25 - 0.60, flange to flange.

## **6.7 Conclusion**

Chapter Six has presented the experimental work in the engineering laboratory of the University of Huddersfield. The chapter details the experimental setup, which used the previous configuration of the test rig, and its later development within this research project. To measure the slip point of the V-band, a technique was used involving the LVDT probe, which measured the torsional load capacity of the V-band.

Further work will need to be undertaken using the Replicates Technique Method to measure the geometrical measurements and the contact surfaces of the V-band. The same method will be employed to measure the external radius and dimensions of the contact surfaces of the flange with the V-band.

---

---

# Chapter Seven

## Comparison of the Results from Three Different Research Elements

### 7.1 Introduction

This chapter will present a comparison of the results from the Theoretical Development, the Finite Element Analysis and the Experimental Investigation. Additionally, the previous results before the development of the test rig will be included. These involved lubricated and non-lubricated flange to flange contact surfaces.

### 7.2 Experimental Investigation

Experimental results have shown the correlation between the loads applied to the lever arm against the M6 T-bolt. The following equation was used to determine the axial load predictions. The forces on a V-band clamp according to Shogi et al (2004), are given as:

$$F_{ACL} = \frac{(1 - \mu \tan \phi) F_{\beta} (\mu \cos \phi + \sin \phi)}{\mu (\mu + \tan \phi)} \left[ 1 - \exp \left( \frac{-\mu \beta}{(\mu \cos \phi + \sin \phi)} \right) \right]$$

When:

$F_{ACL}$  axial clamping load (N)

$\beta$  subtended angle of half the V-band (radius)

$F_{\beta}$  t-bolt tension (N)

$\mu_b$  flange-band coefficient of friction

$\phi$  is the half angle of the V-band clamp

---

---

This relational formula between important parameters in the experimental investigation will be valid in terms of measuring the torsional load capacity. This is described in the theoretical developments detailed in Chapter Three. The test used the Nordic Multiplication Factor. As the data points noted in the Calibration Data for Nordic Load Cell fit closely to the trend line, it can be considered to be an accurate assumption of the multiplication factor. In this case the multiplication factor was -413.34 in a compressive direction. With regard to the Novatech Multiplication Factor, the gradient of the trend line was found to be 4663.4 in a compressive direction.

Using the previous test rig configuration, at the start of V-band testing it was difficult to measure the CoF levels and to determine the theoretical axial load and the theoretical torsional load capacity. Using initial experimental work and an earlier version of the test rig, the results are shown in Figure 7 – 2. The experiment used a 180mm diameter V-band and an M6 t-bolt with unlubricated flanges. Within the graph, the t-bolt tension is plotted against torsional load.

### **7.3 Testing of the V-band Using Lubricated Flanges**

The Greased Flange Faces Test Procedure required the use of Kluber Lubrication Grease on the flange faces as well as Swarfega Jizer de-greaser to clean flange edges beforehand. The grease was spread over 235mm and 181mm flange faces with a soft cloth.

---

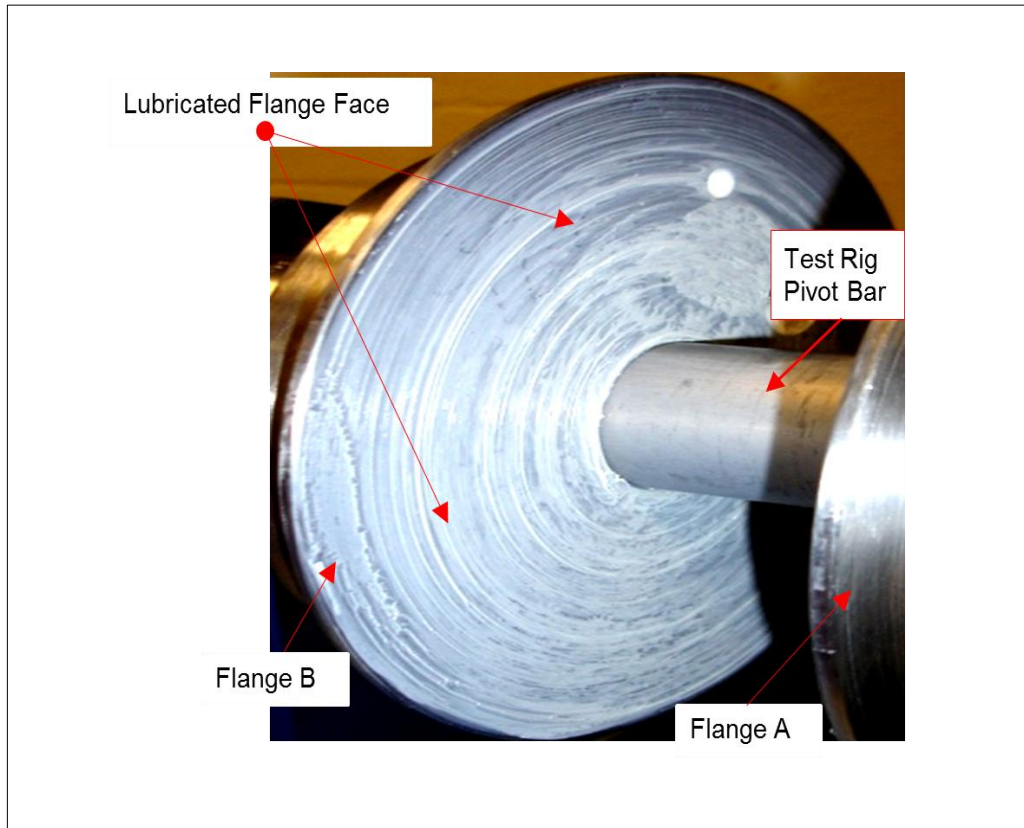


Figure 7 - 1: Lubricated Contact Surface

#### 7.4 Test Procedure for the Use of Washers Between Dry Flanges

The Dry Flanges Test Procedure was repeated but with the use of washers between the dry flange faces to reduce friction. Steel washers (approximately 0.15 & 0.2mm thick), were used and the results can be seen in Figure 7 - 3.

Recent results obtained from tests using 181mm and 235mm V-bands are detailed in Figures 7- 4 and 7 - 5. Tests used a 0.2mm washer with 10 micron tolerances, and degreased flange faces. The first results from Test 1, using a 235mm V-band and 0.2mm washer, show almost perfect linear correlation. This is with the exception of tests done at 1kN and 9kN.

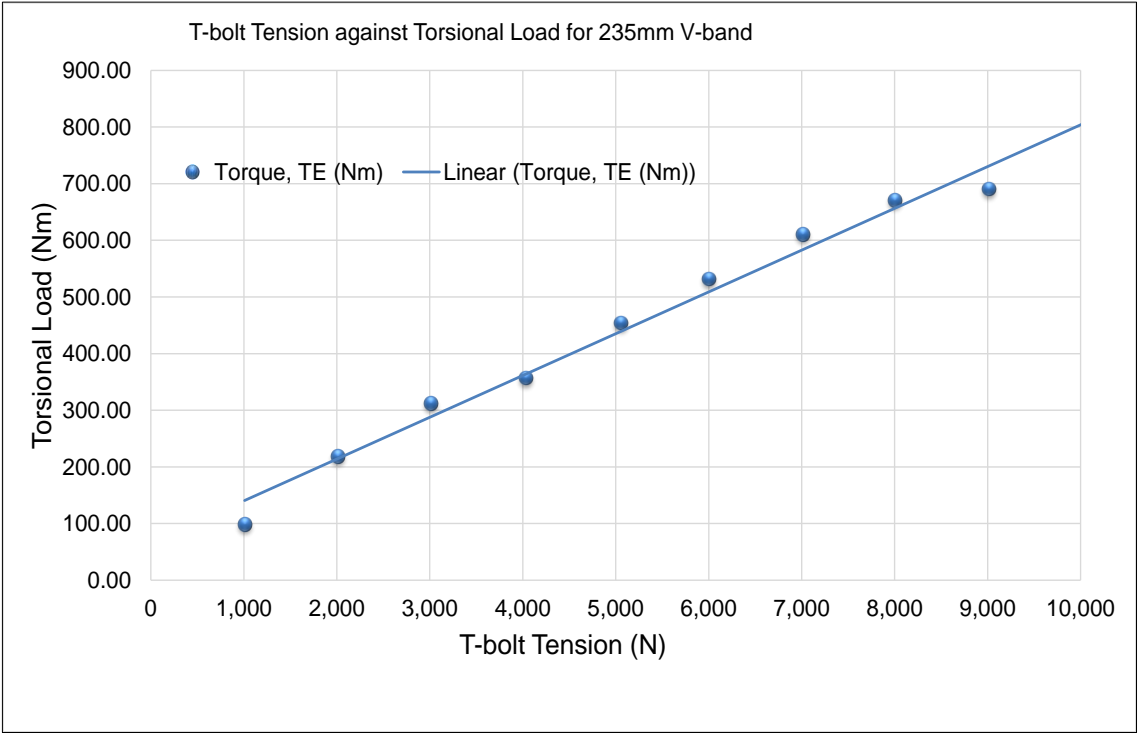


Figure 7 - 2: Test 1 - 235mm V-band

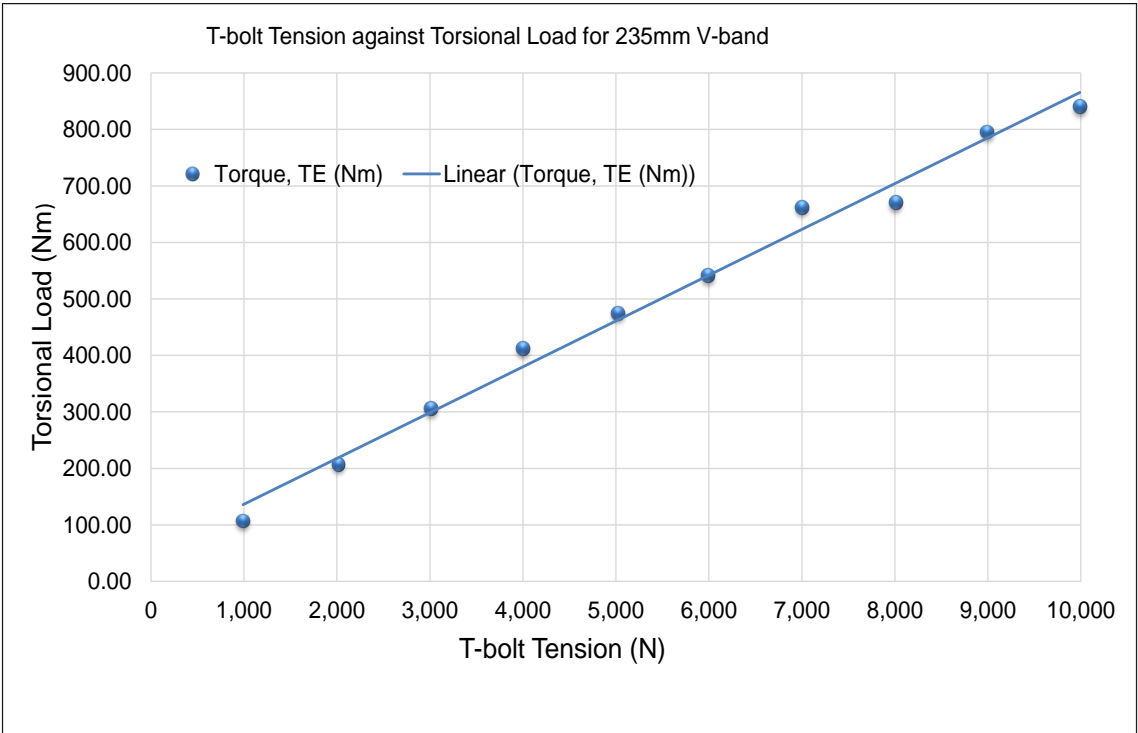


Figure 7 - 3: Test 2 - 235mm V- band

---

Data was obtained from experimental testing of a 181mm V-band using a 0.2mm washer with 10 micron tolerance between flanges. The band that was tested used an M6 t-bolt. The results can be seen in [Figure 7 – 6](#).

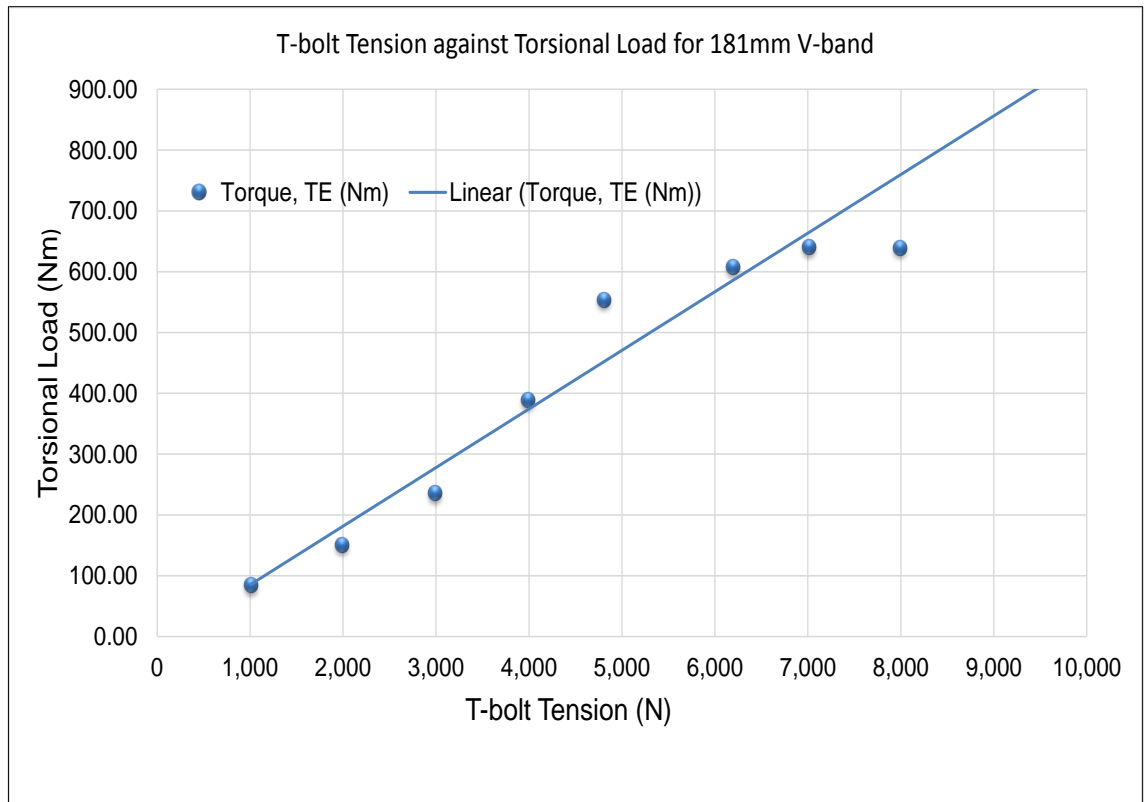


Figure 7 - 4: Test 3 - 181mm V-band

---

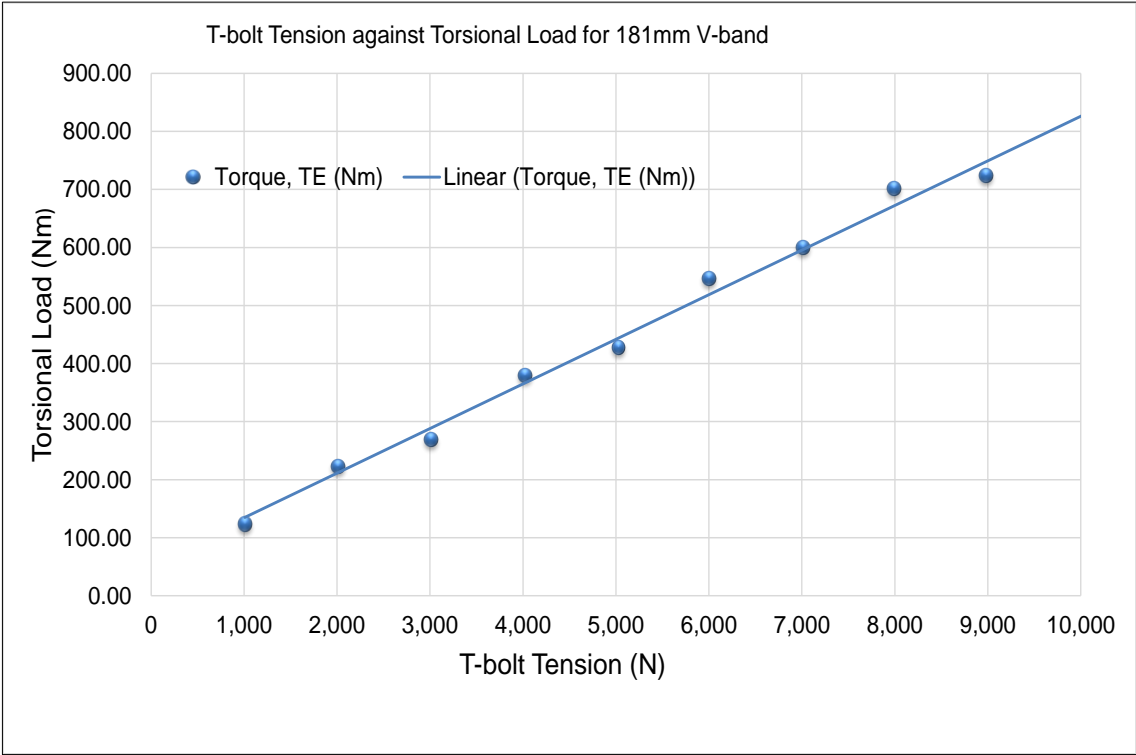


Figure 7 - 5: Test 4 -181mm V-band

As can be seen in Figure 7 – 6, the test results show an almost linear correlation. However, in Figure 7 - 7 the friction was too high. The results shown in Figures 7 - 8 and 7 – 9, detail tests of a 235mm V-band without washers between the flange faces.

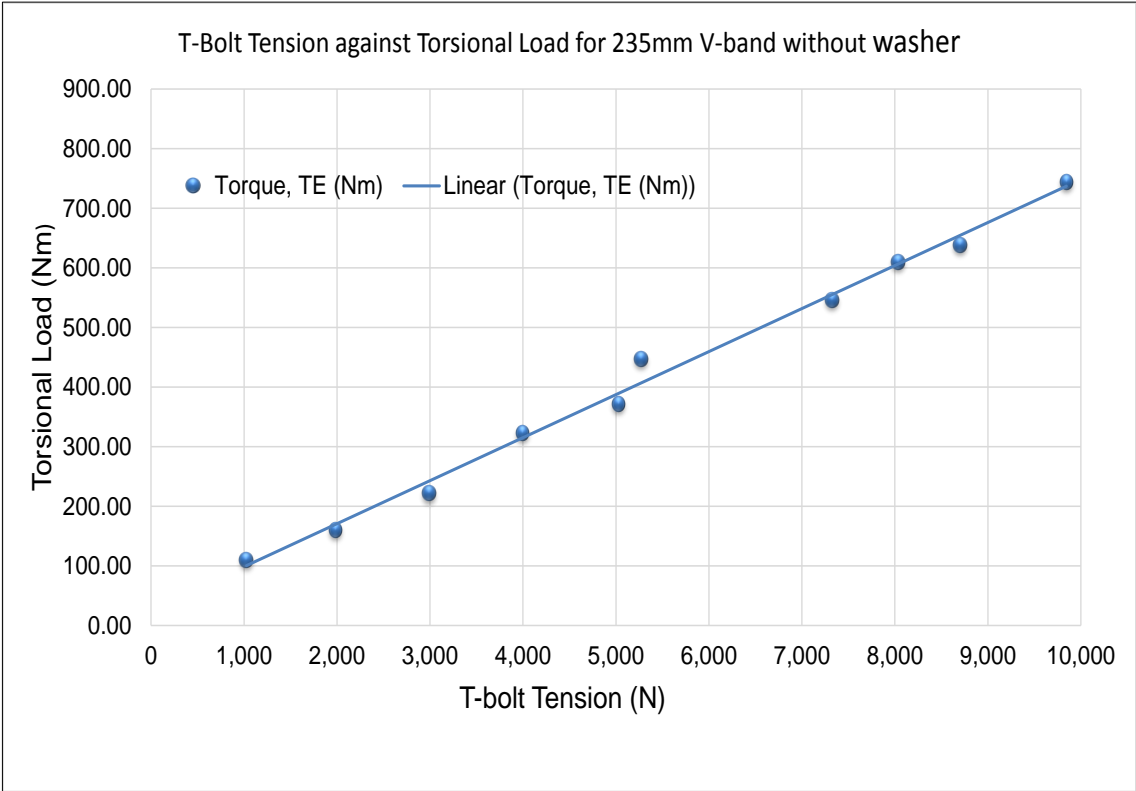


Figure 7 - 6: Test 6 - 235mm V-band Without Washer

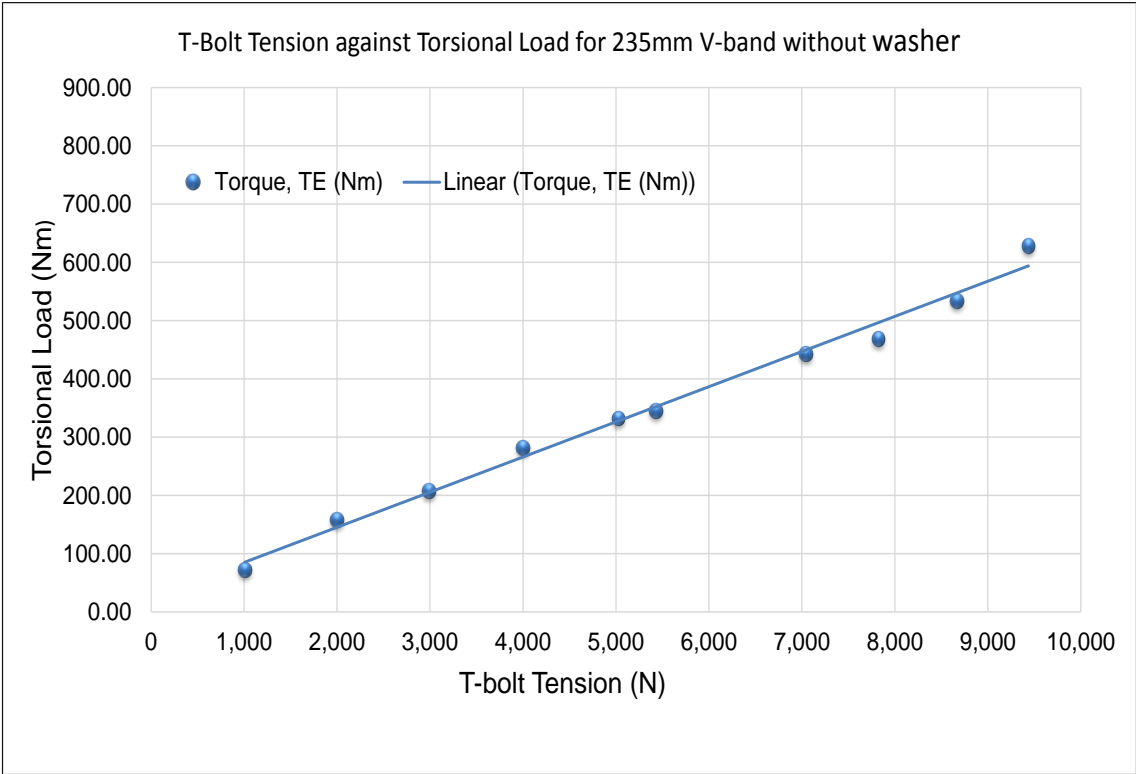


Figure 7 - 7: Test 5 - 235mm V-band Without Washer

With a 114mm V-band the test was repeated 5 times, and the results can be seen in Table 7-1. The torque applied to the t-bolt increased from 6.90 in Test 1 at 1kN to 12.47 in Test 5 at 10kN.

Table 7 - 1: Comparison of 114mm band Data Tests 1,2,3,4 and 5

Test 1	Test 2	Test 3	Test 4	Test 5
6.90	7.63	9.69	11.02	12.47
22.16	20.10	19.38	22.16	21.43
26.18	27.00	29.07	29.07	35.97
37.41	40.81	42.26	47.84	52.68
49.89	49.16	54.03	63.09	74.84
53.41	62.38	70.73	72.79	91.56
72.79	85.25	90.83	99.80	112.40
89.38	99.80	115.79	123.41	128.25
106.08	115.05	128.98	137.95	151.88
113.72	124.14	131.76	166.40	156.72

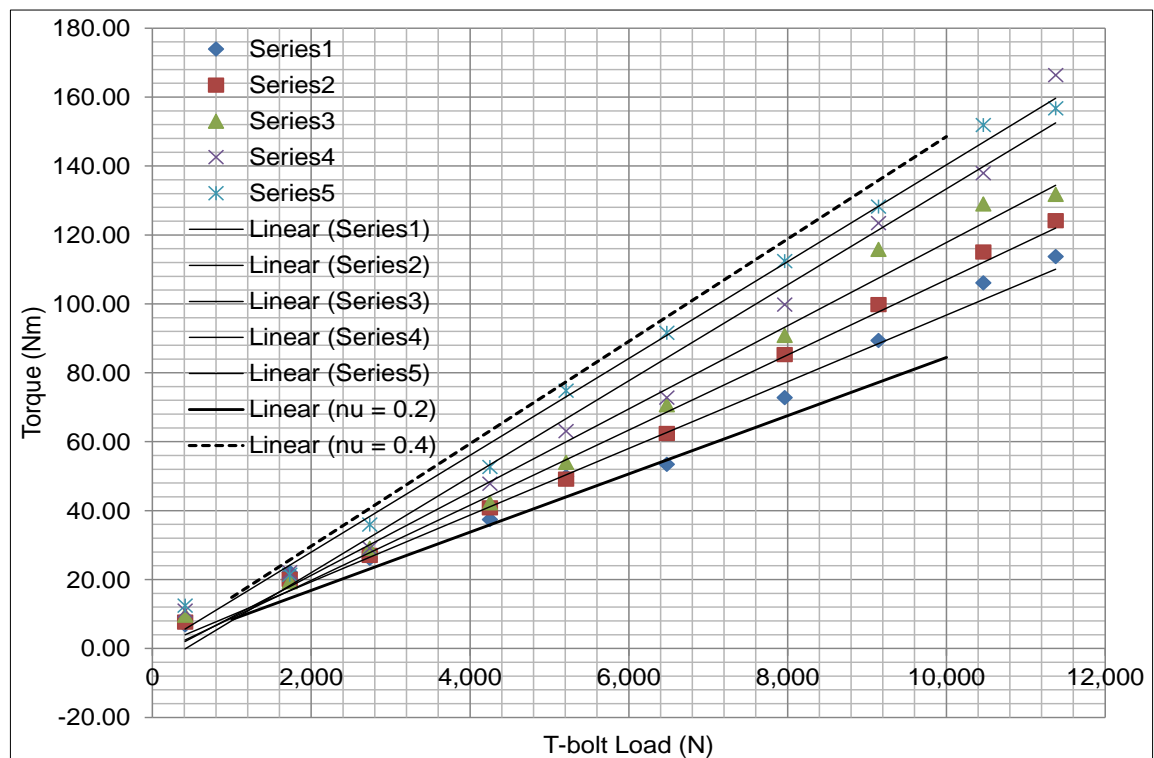


Figure 7 - 8: Results of 114mm V-band Test

## Comparison of the Finite Element Analysis and Experimental Investigation

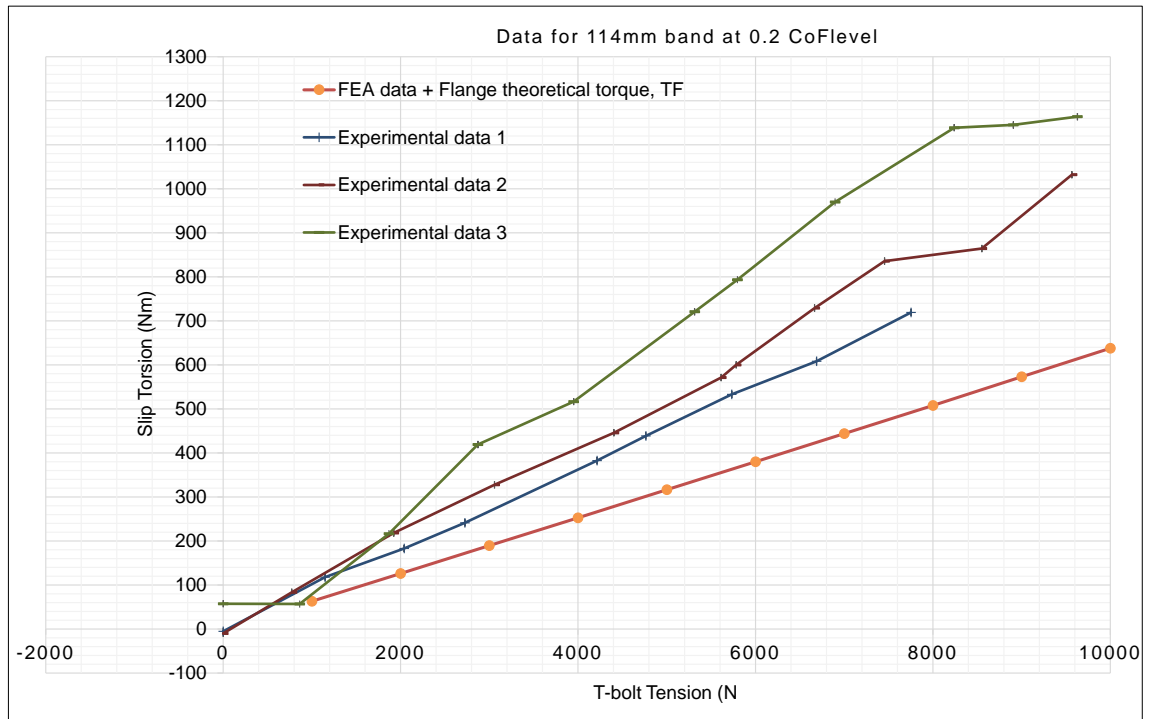


Figure 7 - 9: Data for 114mm band at 0.2 CoF Level

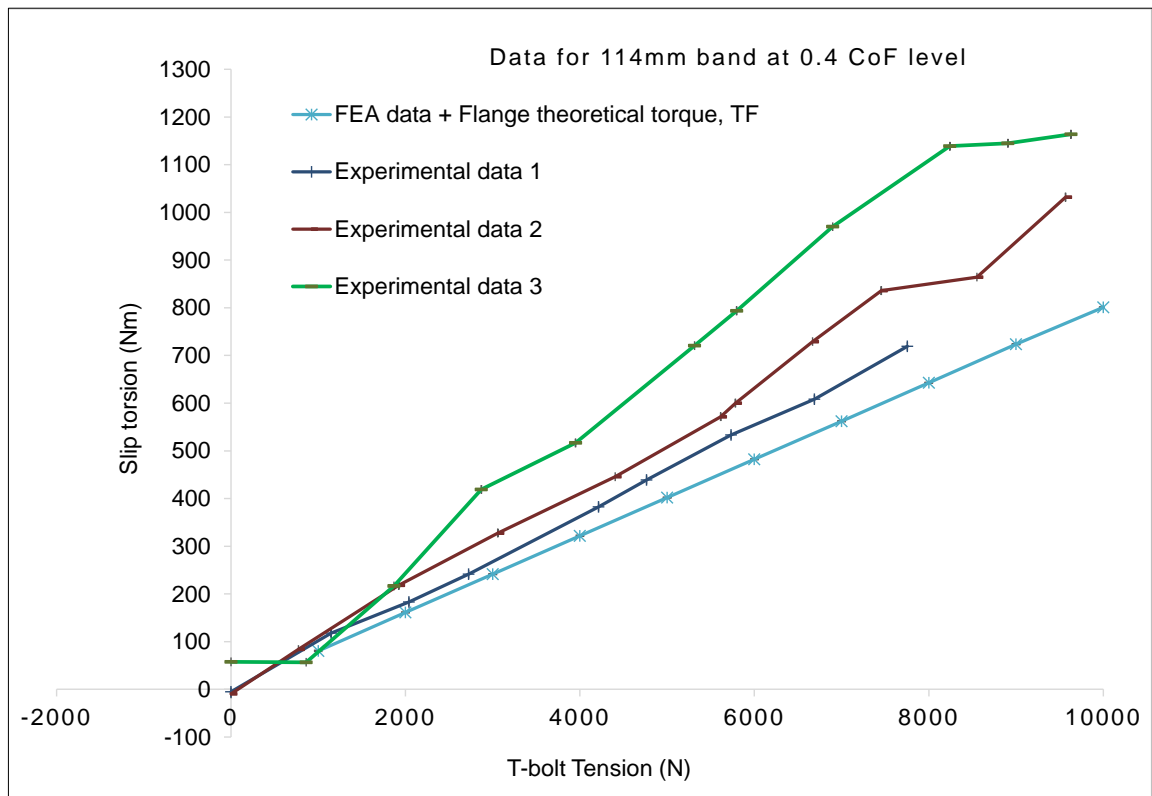


Figure 7 - 10: Data for 114mm band at 0.4 CoF Level

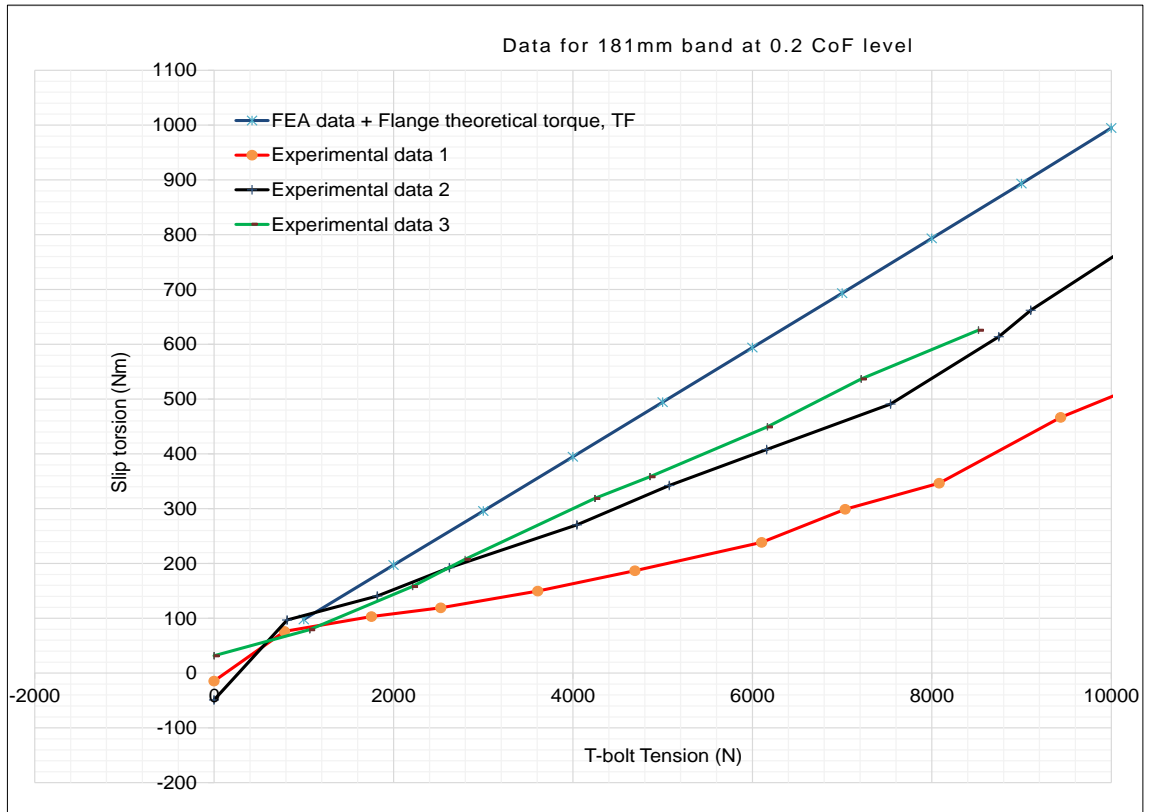


Figure 7 - 11: Data for 181mm band at 0.2 CoF Level

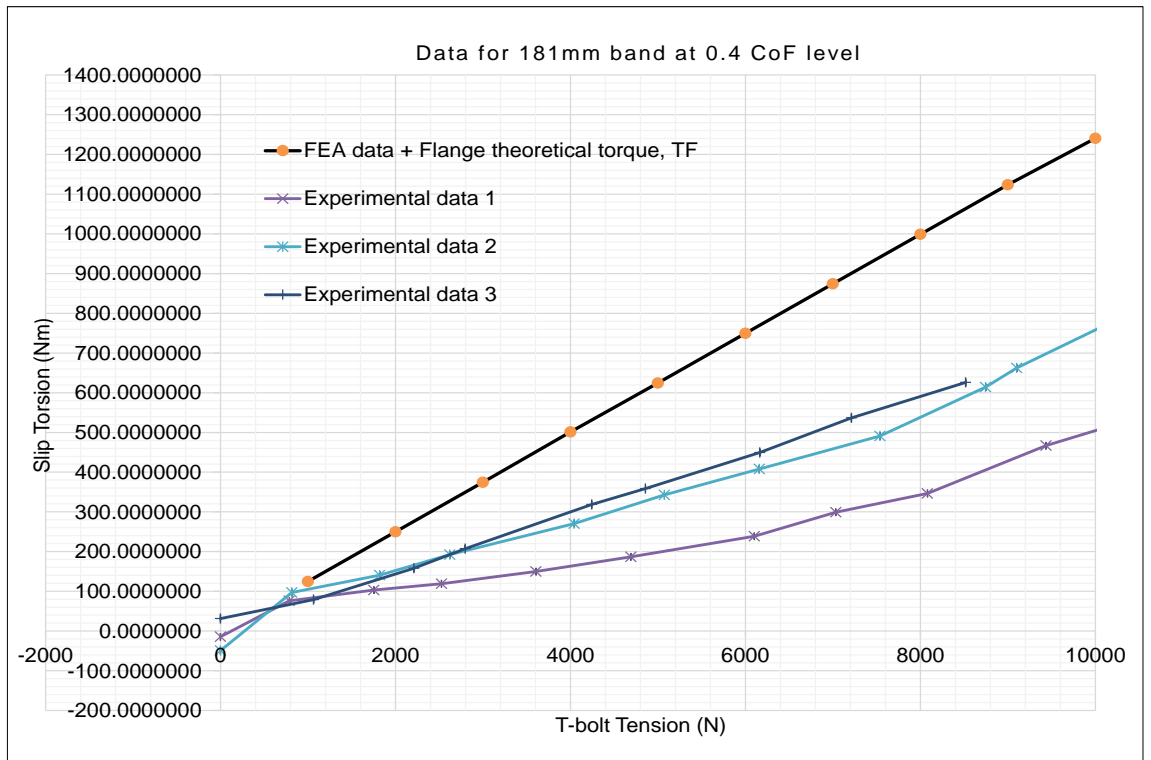


Figure 7 - 12: Data for 181mm band at 0.4 CoF Level

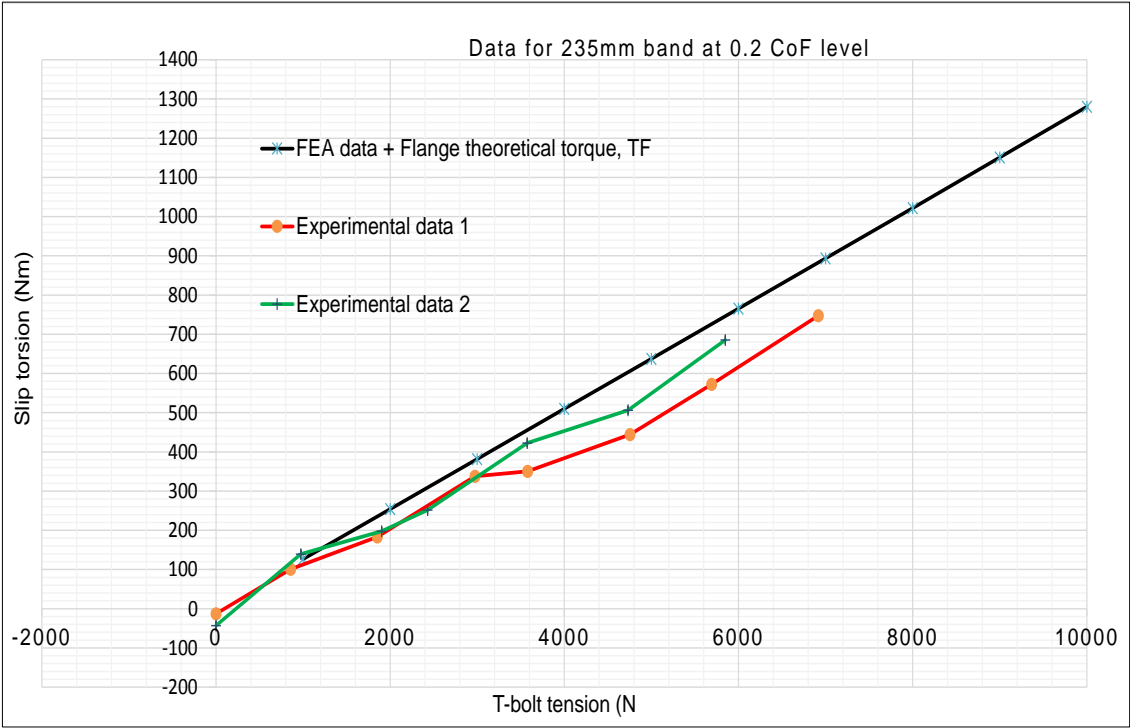


Figure 7 - 13: Data for 235mm band at 0.2 CoF Level

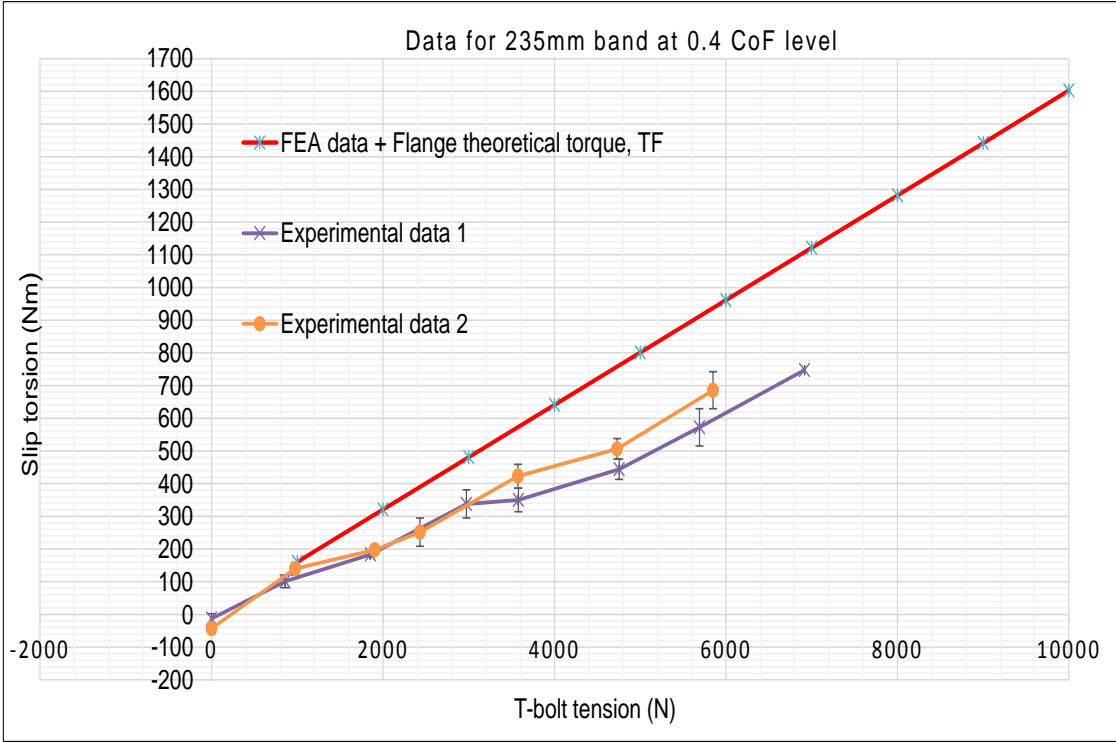


Figure 7 - 14: Data for 235mm band at 0.4 CoF Level

---

## 7.5 Experimental Investigation Results

The 114 mm V-band results with a steel washer (0.2mm with 10 micron tolerance), were not as high as expected. Additional tests and results using new bands and dry or greased flanges were required. Greased flanges were tested and the friction was greater than anticipated. When using a washer the results were also greater than anticipated, although a better indication of the friction at the interface of the washer is required. Using two spherical plain bearings would also possibly give more constant outcomes.

All the results of the experimental investigation were concerned with the theoretical total torque against the t-bolt load. Within the theoretical results, different combinations of frictional value were used with the regulation grease applied. Due to the results obtained, it is recommended that additional V-band sizes are tested as well as additional testing on previous V-band sizes. Additional testing should also include the t-bolt being placed in different positions (90, 180 and 270 degrees).

---

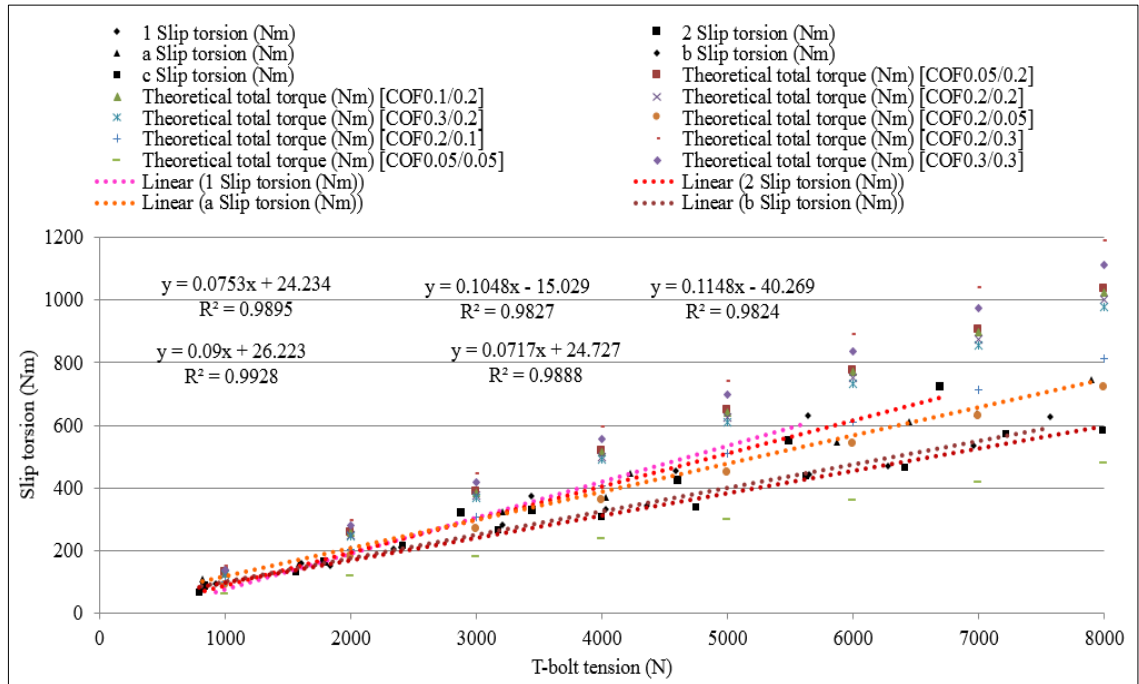


Figure 7 - 15: 181mm V-bands with Dry Flange and Dry Washer

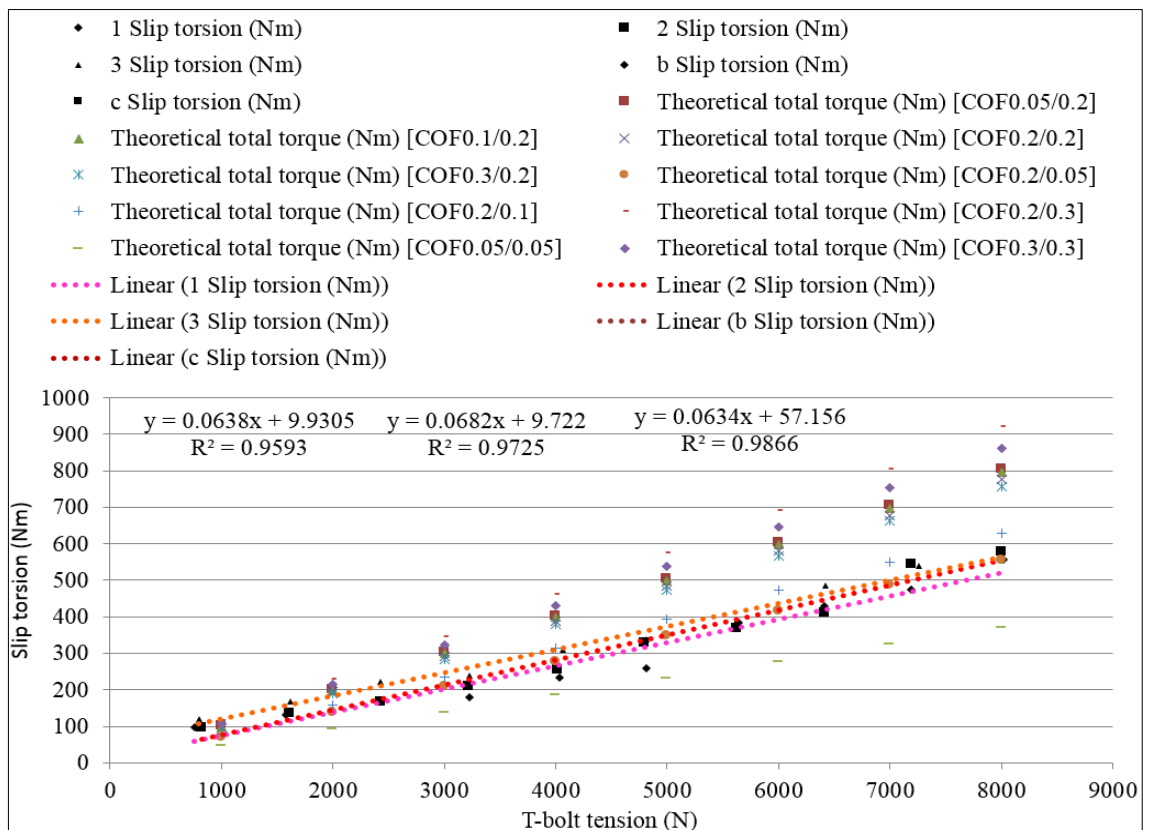


Figure 7 - 16: 235mm V-bands with Dry Flanges and No Washer

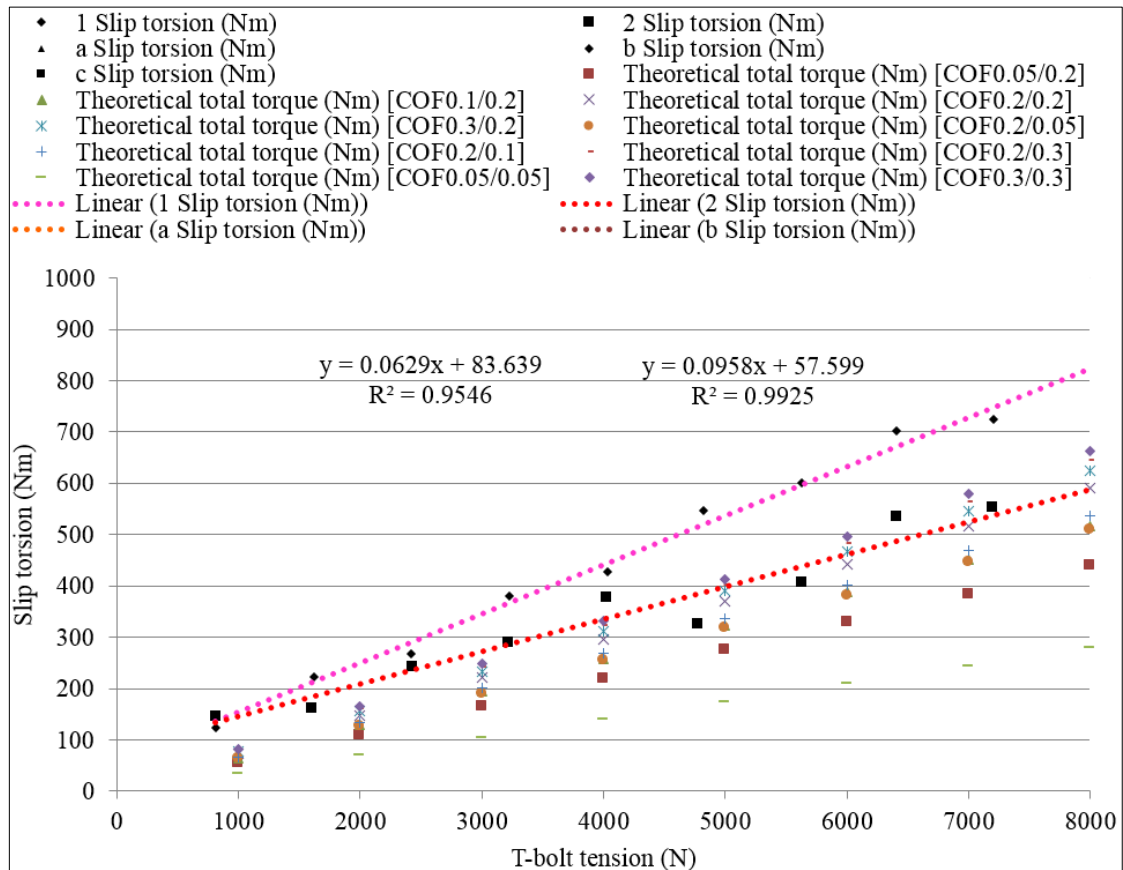


Figure 7 - 17: 235mm V-bands with Fresh Bands

A 180mm diameter V-band with M6 t-bolt was used in testing for each of the three V-band clamps. Each V-band t-bolt was tested with the torque levels referred to earlier. To give an even surface before testing, dirt was removed and the flange faces were smoothed by light sanding. The outer edges were lightly rubbed down with fine emery paper to give a consistent surface finish. This was necessary because these flanges had been used in previous testing.

One pair of dry and one pair of greased flange surface finishes were used with the same diameter flanges. This was done to ascertain how much the flange face friction affected the results and if any future testing of the flanges would lead to problems with the results. To prevent any potential oil residues signifi-

---

cantly affecting the results, all flange faces and V-bands were degreased before testing. The clamps were fitted using V-band Teconnex procedures.

The voltage output reading from the load cell reached maximum and then decreased. If the increase and decrease in the resulting data continues with a rising incline, this can be viewed as a poor result and therefore should be excluded and investigated. The expected rise and fall in the lever arm force during testing of the V-band clamps was anticipated. Yet this expected result occurred as an increasing pattern and was connected to the force used. This was seen as an erroneous result due to testing errors.

## **7.6 Procedural Comments**

Observations made during testing will be presented. Any errors will be identified and solutions will be suggested so as to ensure consistency.

A t-bolt load cell was used to measure the load applied to the t-bolt. However, because the t-bolt load cell was of a relatively large diameter, it could infringe upon the V-band and bring a torsional load upon both the V-band and t-bolt. The V-band edge pushed into the flange edge, with resulting damage to the flange as illustrated in Figure: 7 - 18.

---

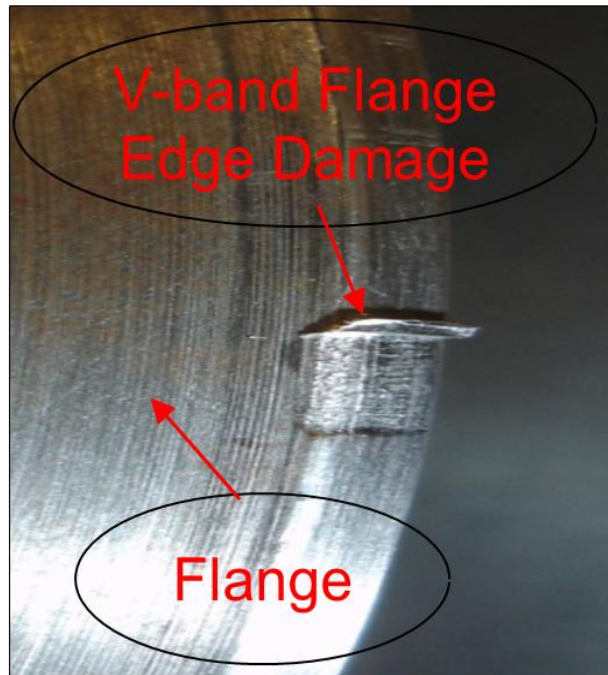


Figure 7 - 18: V-band Flange Edge Damage at a T-bolt Tension of 8kN

A t-bolt tightening of 10kN against the flange in V-band Test 3 resulted in the damage to the flange edges as illustrated in Figure: 7 - 18. This issue only happened above 5 kN. To resolve the problem of the V-band's edge impacting the flange, the edge was thinned by filing the back area of the band. This stopped the sharp edge of the V-band impacting on the flange. After this was done, all the tests were repeated.

### 7.7 V-band Test Issues

Other errors came from the issue of the flange faces sticking together during the dry flange face tests. The results are shown in Figure 7 – 15. To resolve this

---

issue, the faces were sanded down to a smooth surface finish. However, this was unsuccessful as the flanges have a matching hardness and require a Brinell hardness difference to avoid sticking. Therefore, further attention was given to the flange quality although the issue was not fully resolved.

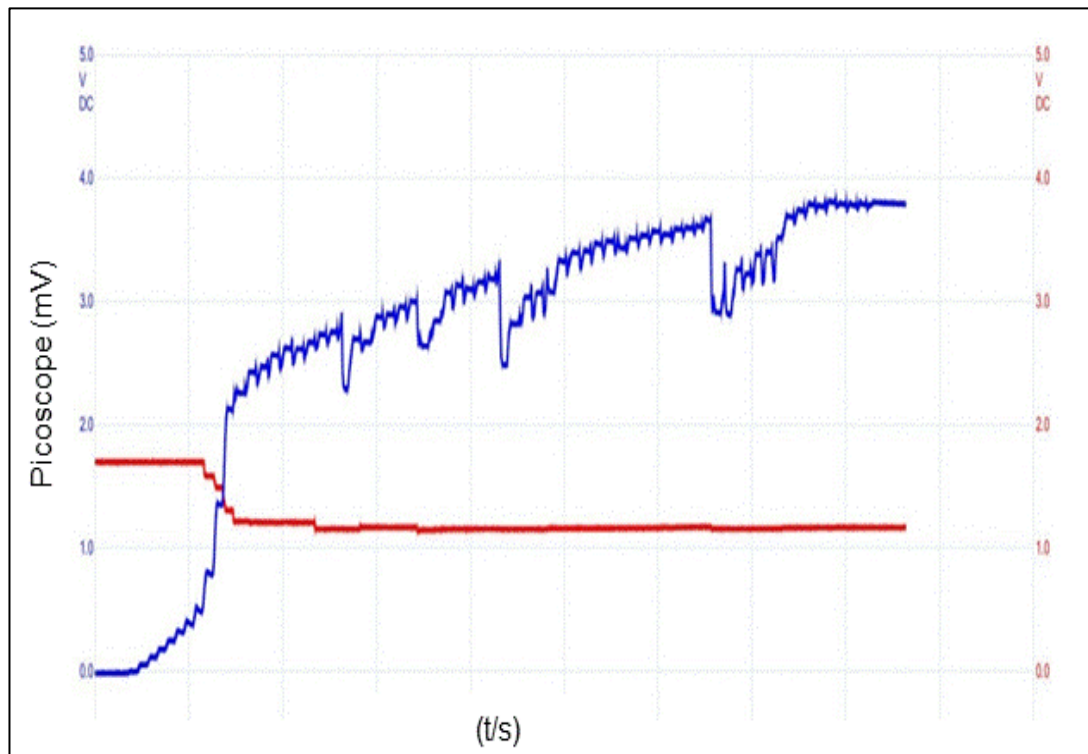


Figure 7 - 19: V-band Test Issues

## 7.8 Conclusion

Chapter Seven discusses and compares the results with regard to three different stages: Theoretical Development, Finite Element Analysis and Experimental Investigation. Theoretical Development, in comparison to Experimental Investigation, did not match with regard to the initial V-band torsional load capacity re-

---

---

sults. This was due to the CoF level being too high between flange-to-flange contact surfaces. Additionally, the load applied from the initial test rig mechanism was not applied completely to the V-band. The development and evolution of the test rig will potentially yield more stable results. As a result of the experimental outcomes, flange-to-flange contact surfaces with steel spacer washers were developed. This has been discussed in Chapter Four.

---

---

## **Chapter Eight**

### **Conclusion and Future Work**

#### **8.1 Introduction**

This research project has successfully conducted experimental work on V-bands and the measuring of their torsional load capacities. This has been through using a robust method of measurement for the torsional load capacities of V-bands. The research project has involved the successful development, construction and implementation of a new test rig. This was designed, developed and built in the engineering laboratories at the University of Huddersfield, with the generous assistance of my supervisor and mentor, Dr Simon Barrans. As noted in Chapter Four, this had led to successful initial experimental results. Some of the preliminary research results have been presented at an Aerospace Engineering Conference in 2014 in Madrid, Spain. The theoretical development with computer simulation results were presented at the International Conference on Mechanical and Aerospace Engineering (ICMAE), in Rome, Italy in July 2015. The experimental investigation and simulation results will be presented at the 7<sup>th</sup> ICMAE to be held in London in July 2016.

#### **8.2 Conclusion**

Prior to the start of current research, the focus was on improving the test rig mechanism in order to improve the quality of experimental work and subsequent results. The main research elements are:

---

- 
- To measure the torsional loading capacity of three different V-band sizes using the Huddersfield V-band test rig
  - To develop the mathematical aspects of the Theoretical model
  - To develop the features of the current test rig so as to improve on the results obtained from the previous test rig configuration
  - To use the experimental data to validate the predictive data generated by the FE model's computer simulations
  - To experiment and identify the initial slip point between the V-band and flange

Using the previous experimental test rig configuration, the results obtained did not match the Theoretical model. This was because the friction between the flange interface surfaces was too high. Consequently, the configuration was redesigned and the results were subsequently matched with the Theoretical model. Therefore, the Theoretical model was validated.

Whilst there was a moderate correlation of the experimental results with the theory regarding the 181mm and 235mm bands, the results were almost double the anticipated slip torsion for the 114mm band. Two credible reasons for the latter are suggested:

- Galling was observed in a radial direction at the flange-to-flange contact interface surfaces. This indicates an increase in the static CoF measure. However, owing to the galling marks' localised nature, the influence of friction was not assessable (see Barrans et al., 2014).
-

- 
- There is an assumption that the band creates a circular arc on contact with the flanges as the t-bolt is tightened. This is credible for larger bands, as their radial stiffness is comparatively low and they can easily conform to the flanges' circularity. However, the smaller bands with the same circumferential cross section are much stiffer. Therefore, it is likely that, for the smaller bands, only part of the V-band's circumference will be in contact with the flanges. In this case, it would be very problematic, in view of the manufacturing processes, to ensure that these smaller bands make a circular arc when tightened.

As mentioned above, for the 114mm band the results were almost double the anticipated slip torsion. This could be due to the t-bolt tension remaining constant whilst the contact area diminishes. This results in a rise in the torsional load capacity of the flange to band interface, (Barrans et al., 2014).

Especially between the flanges, the static CoF level was demonstrated to have an important effect on the theoretical torsional load capacity of V-band clamps. Of further significance in affecting theoretical torsional load capacity, is the position of the contact point between flange and band and the subsequent contact angle .

The torque band's theoretical calculations matched with the FEA simulation results. Both the theoretical calculations and the FEA showed variations in the V-band's circumferential contact pressure. There was significant correlation between the torque band within the Finite Element Analysis (FEA) and the torque band is required to slip the V-band against the flange. Contact pressure less-

---

---

ens with increasing CoF levels, but greater CoF measures increase the variation in the contact pressure along the band's circumference. Transverse and circumferential contact friction conditions will be looked at individually.

There was significant agreement between the theoretical analysis and the FE models across a wide range of band diameters and T-bolt loads. Sahboun & Barrans (2015), showed that incorporating transverse friction enables a better comparison with the FE results for lower CoF's, whilst not including this aspect gives better results for higher CoF's. In addition, torsional load capacity was demonstrated to increase with band diameter and with T-bolt tension, but to be less reliant on the CoF levels, Sahboun & Barrans (2015).

### **8.3 Recommendations for Future Work**

This thesis has presented the investigation of the torsional load capacity of the V-band clamp. The point of initial slip between flanges and the V-band has been successfully identified. Therefore, the central question of this research has been answered. However, additional areas still require further investigation. A future research strategy would need to examine the following issues:

- Experimental results were thought to be affected by the flange contact edge spacing not matching the V-band section. A Coordinate Measuring Machine (CMM) could be used to confirm the geometrical measurements of the contact surfaces of the V-band. In addition, the Replicates Technique Method could be employed to measure the circumference of the V-band.



- 
- With the current test rig configuration, friction levels between flange contact surfaces are too high. The use of a washer recess could be examined in order to resolve this issue.
  - Appropriate washer thickness is central to ensuring that the flange and washer combination gives the correct distance between the contact edges on the flanges. In the future, more accurate measurement would result from the use of a CMM and the Replicates Technique Method.
  - Small V-bands may not be circular when manufactured. A CMM and the Replicates Technique Method could be used to measure this lack of circularity. The FEA can then be employed to simulate the effect of this lack of circularity.
  - The theory developed in this thesis could be used further to investigate the effect of other V-band section geometries and so determine the optimum geometry for torsional load capacity
-



## Appendix – B: Risk Assessment

Brief description of activity: Investigation the Torsional Load Capacity of a V-Band Clamp					
Location: T4/03		Assessment by: ALL Users		Assessment date: 01/09/2012	
SPECIFIC TASK/ASPECT OF ACTIVITY: Test Rig					
Hazards identified	Risks to health and safety	People at risk	Measures to manage the risks effectively	Who	Action by: When Completed
Large in size and heavy components being assembled	Lifting risk, heavy components and/or components falling risk	Users	Lift with knees Wear appropriate footwear Ensure components are 0.5 meters from the edge of the work space	Users	Cont. N/A
Tightening bolts/nuts	Back/arm strain	Users	Ensure correct stance is taken and pressure is gradually with no 'jarring' actions	Users	Cont. N/A

SPECIFIC TASK/ASPECT OF ACTIVITY: Test Rig					
Hazards identified	Risks to health and safety	People at risk	Measures to manage the risks effectively	Who	Action by: When Completed
Large in size and heavy components being assembled	Lifting risk, heavy components and/or components falling risk	Users	Lift with knees Wear appropriate footwear Ensure components are 0.5 meters from the edge of the work space	Users	Cont. N/A
Tightening bolts/nuts	Back/arm strain	Users	Ensure correct stance is taken and pressure is gradually with no 'jarring' actions	Users	Cont. N/A

## Appendix – C: Conferences and Publications

As part of the research project, it was intended to publish and attend conferences. The following list of conferences and publications are based on this research project.

- I. Poster for the 4th Scientific Symposium for Libyan Students in the UK, 15th January 2011, Cardiff University UK.
  - II. Poster for the Research Festival (Research Poster Competition) March 2011, University of Huddersfield UK.
  - III. Attendance at the COMADEM 2012, 18th - 20th June 2012, University of Huddersfield, UK.
  - IV. Research Poster, 2012, School of Computing and Engineering, University of Huddersfield UK.
  - V. Attendance at the Annual Researchers' Conference, 2012, School of Computing and Engineering, University of Huddersfield UK.
  - VI. Attendance at the Annual Researchers' Conference 2013 , 6th December 2013, School of Computing and Engineering, University of Huddersfield UK. As part of the current research output, see the next pages regarding two Conference Papers
-

# Simulating Torsional Slip in V-band Clamp Joints

Salahaddin M Sahboun<sup>1,a</sup> and Simon M Barrans<sup>1,b</sup>

<sup>1</sup>School of Computing and Engineering, University of Huddersfield, HD1 3DH, UK

<sup>a</sup>s.sahboun@hud.ac.uk, <sup>b</sup>s.m.barrans@hud.ac.uk

**Keywords:** V-band clamp, torsional load capacity, friction, finite element analysis.

**Abstract.** In this paper a finite element technique to predict the torsional load capacity of V-band clamp joints is presented. The development of this complex, multi-step analysis is explained and the results compared with alternate theories which ignore or take account of transverse friction in the band to flange contact region. It is shown that accounting for transverse friction yields a better comparison with the finite element results for lower coefficients of friction whilst ignoring this component gives better results for higher coefficients of friction. Torsional load capacity is shown to increase with band diameter and T-bolt tension but to be less dependent on the coefficient of friction.

## Introduction

A V-band, as shown in Fig 1, is usually circular in shape with a flat bottomed, V shaped cross section. V-band clamps are used to connect circular flanges, often using a single bolt. Fig 1, shows an example of V-band commonly used to connect the main housings of a turbocharger. The V-bands discussed in this paper have the cross section dimensions shown here.

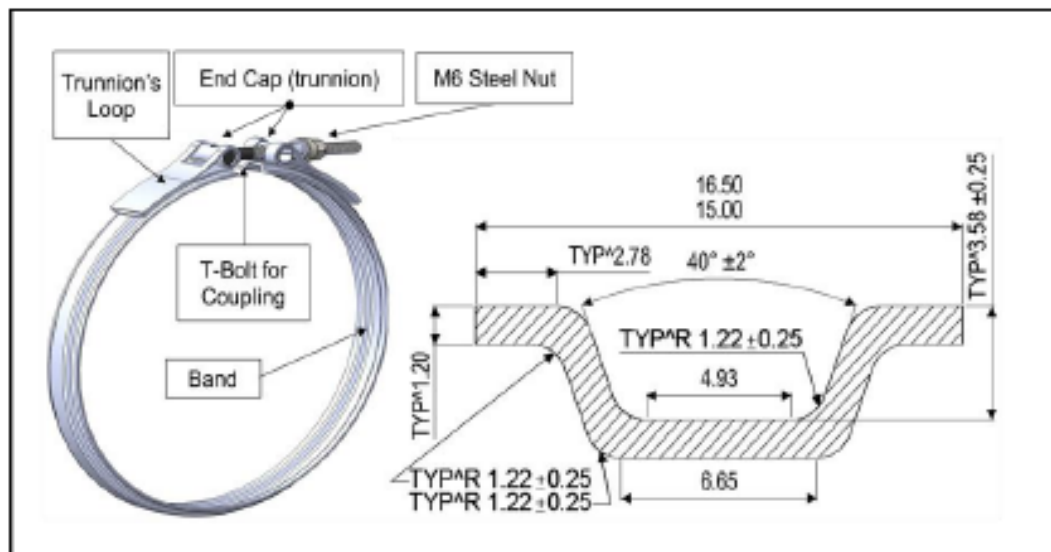


Fig 1: 181mm V-band clamp

V-band clamps are expected to perform reliably and safely under testing conditions of substantial load and temperature variation. They are used in a wide range of settings and applications, such as material handling, ducting, air conditioning systems, ground vehicles and aerospace. They can be made from a range of materials although the commonest for automotive applications is stainless steel [1,2]. A number of different types of closure mechanisms are available but considering reliability and ease of manufacture, most turbocharger manufacturers use a single T-bolt, as shown in Fig 1.

As [3] points out, there is no standard available for the design of V-band clamps and manufacturers have based their designs on experience. [1] developed a theoretical model of the internal loads generated within a V-band clamp. This work was then extended [4] to predict the axial clamping load generated by these clamps with both transverse and circumferential friction being considered. This



freedom at its reference point A further constraint in the circumferential direction was applied to the band on a line on the outside of the section, furthest from the T-bolt.

In the first loading step the band was displaced in the radial direction to bring it into contact with the flange. This initial contact region extended  $\pm 10^\circ$  either side of the back of the band. This small contact region was used to improve the stability of the analysis.

In the second load step the contact region was extended circumferentially to run all the way around the band. The band was brought into contact with the flange by applying a circumferential displacement to the ends of the band. The magnitude of this displacement was adjusted to ensure that contact was established around the full circumference but the stresses generated were small.

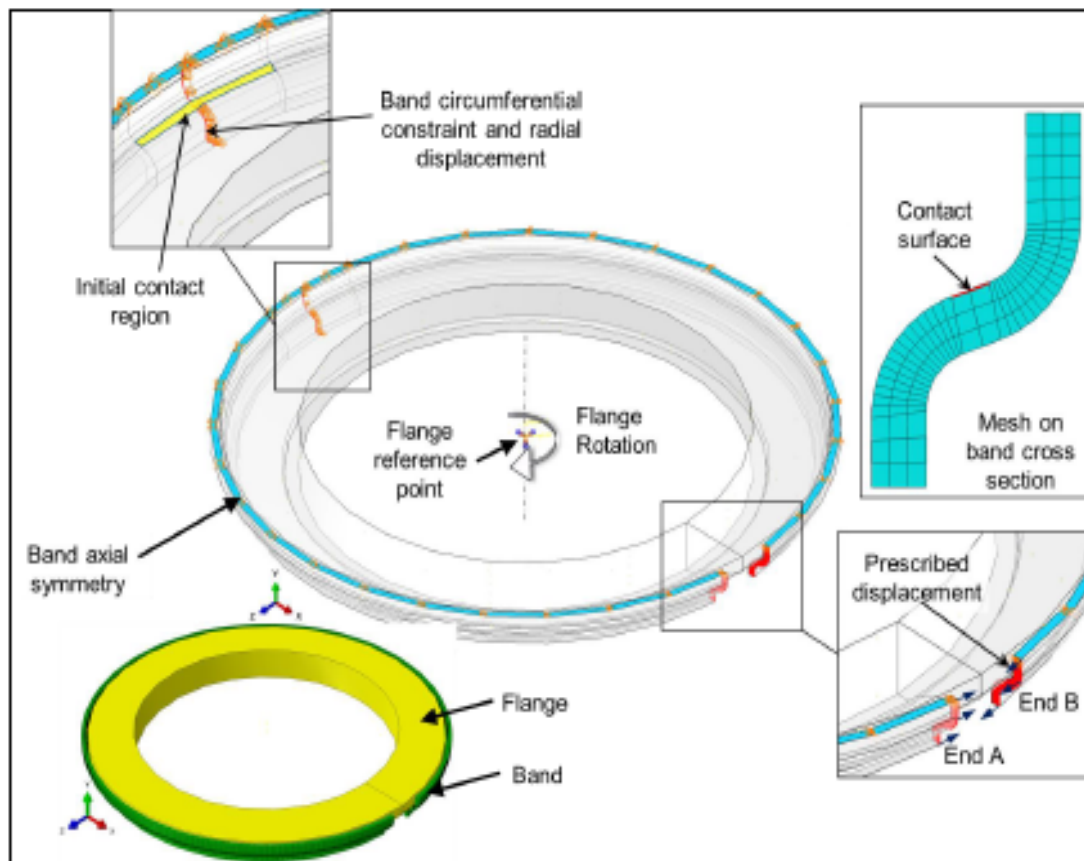


Fig 2: Summary of finite element model

In the third load step the radial and circumferential displacements defined in the 'back-contact' and 'side-contact' steps were deactivated and replaced with circumferential tractions applied to the ends of the band. The magnitude of this traction was such that when multiplied by the cross sectional area of the band, it gave a specified T-bolt load. It should be noted that the circumferential constraint on the back of the band was still present in this load step. This eliminated any potential rigid body motion due to numerical imbalance between the circumferential traction loads.

In the final load step, the circumferential constraint on the back of the band was replaced with a circumferential constraint on the symmetry plane. This constraint simulated the anti-symmetry effect resulting from the other half of the band interacting with the second flange under torsion. Also in this step, the constraint on rotation about the axis of the flange reference point was replaced with a prescribed rotation about the axis to simulate rotation of the flange.

### Resolving the Contact Problem

Within finite element analysis there are essentially two methods for dealing with contact between surfaces: the Penalty Function method and the Lagrange Multiplier method [10]. Either of these

techniques can be used to enforce both normal contact between the surfaces and the tangential stick/slip condition. However, they can introduce particular limitations and difficulties.

Table 1: Boundary condition implementation within analysis steps

Boundary condition	Step (time)				
	Initial (0)	Back-contact (1)	Side-contact (2)	Tighten (3)	Torsion (8)
Band circumferential constraint	Created	Propogated	Propogated	Propogated	Inactive
Band axial symmetry	Created	Propogated	Propogated	Propogated	Propogated
Flange reference point constraint	Created	Propogated	Propogated	Propogated	Modified
Initial contact region		Created	Propogated	Propogated	Propogated
Band radial displacement		Created	Propogated	Inactive	Inactive
Major contact region			Created	Propogated	Propogated
End A circumferential displacement			Created	Inactive	Inactive
End B circumferential displacement			Created	Inactive	Inactive
End A circumferential traction				Created	Propogated
End B circumferential traction				Created	Propogated
Band circumferential symmetry					Created
Flange rotation					Created

**Lagrange Multiplier Method.** This method introduces a strict enforcement of the contact condition. For normal contact, no penetration of the surfaces is allowed. For tangential contact, no slip is allowed until the specified friction condition is overcome. Whilst this method gives the most accurate simulation of the contact condition, it introduces additional degrees of freedom for each contacting node. This can substantially increase the size of the model. In addition, the strict enforcement of the constraint can lead to solution instability when contact and slip are imminent.

**Penalty Function Method.** This method introduces an additional, artificial stiffness into the finite element model which is dependent on the degree of surface penetration for normal contact. For tangential stick/slip, a degree of 'elastic slip' is allowed prior to friction being overcome. In both cases the technique introduces a degree of inaccuracy but also brings stability to the problems which may not be present using the Lagrange multiplier method. Solution accuracy is increased (but stability reduced) by increasing the normal stiffness and reducing the amount of elastic slip.

For the models discussed here normal contact was controlled using the Lagrange multiplier method. For smaller bands the Lagrange multiplier method was also used to enforce the tangential contact condition. However, for larger bands, use of this technique led to solution instability. It was found that using the penalty function method for tangential contact with the maximum allowable slip set to 0.001 of the characteristic surface dimension gave results that were within 1% of the Lagrange multiplier method. This slip limit was therefore used across the full range of band sizes analysed.

In Fig 2 only 2 elements are shown across the contact surface. A convergence study was carried out and determined that 16 elements were required to correctly model this contact.

### Extracting the torsional load capacity from the FEA Model

Figure 3 shows the reaction moments generated at the constrained reference point for the flange rigid body. The 'time' axis shows the stages of the analysis as indicated in Table 1. The increase in transverse bending moment, or reaction moment about the z-axis during the tightening step indicates that the axial load transmitted from the band to the flange is not uniform but is higher closer to the T-bolt. This is consistent with the findings in [6].

The torsional load capacity of the joint is shown by the reaction moment about the central axis as the rotation is applied in the torsion step. Since displacement is being applied in this step, the reaction load rises very rapidly to a peak value where slip occurs.

### Comparison with Theory

Finite element models were constructed for four different V-band sizes, diameters 114, 154, 204 and 235 mm. For each size of band the model was run 10 times in order

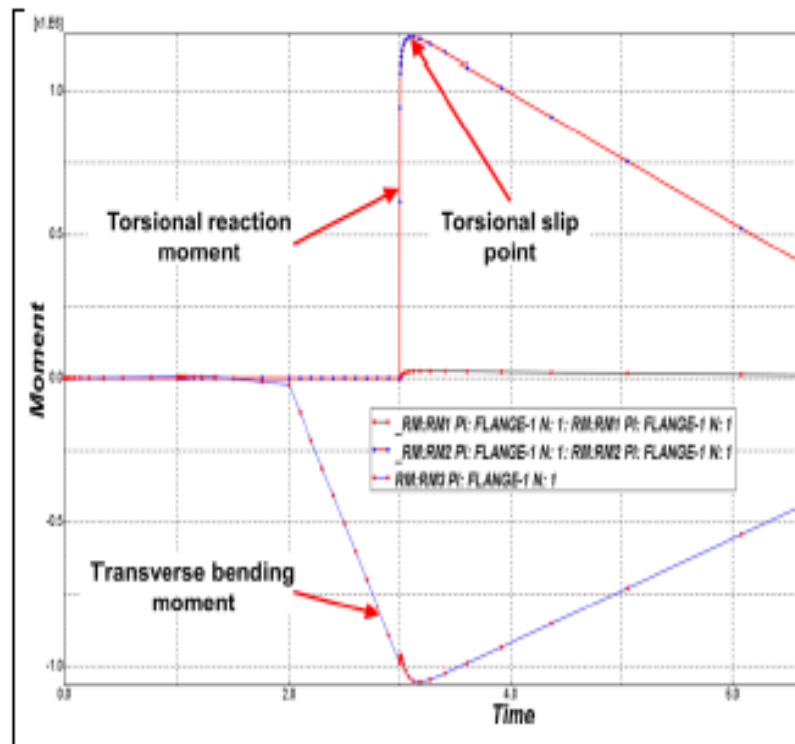


Fig 3: Reference point reaction moments (Nmm)

to generate results for 10 different T-bolt loads. The analysis was repeated for coefficients of friction of 0.2 and 0.4. The results of these analyses are shown in Fig 4. In these graphs the average of the theoretical results given by Eq 1 and Eq 2 are shown as solid lines with error bars indicating the results from the two theories. Accounting for transverse friction always gave the lower result.

For the lower coefficient of friction the FE results are slightly larger than the theoretical result accounting for transverse friction. For the higher coefficient of friction the theory ignoring transverse friction gives a better match to the FE results. It is interesting that this result was consistent over a range of V-band diameters. This suggests that the difference in the results is not due to the relative flexibility of the band as has previously been suggested [8].

For both theories and confirmed by the FE analyses, increasing the coefficient of friction increases the torsional load capacity of the joint. However, a doubling of the coefficient of friction does not lead to a doubling of the load capacity as may be expected. The principal reason for this is that, whilst the increased coefficient of friction provides greater resistance to movement in the circumferential direction during torsion, it also provides increased resistance to movement in this direction during tightening of the band. Hence, the normal force between the band and the flange is reduced, as predicted in [4].

It can also be seen that increasing the band diameter increases the torsional resistance for a given T-bolt load. Whilst [4] has shown that the axial clamping load in a V-band joint is independent of band diameter, for a larger band, this reaction between the band and the flange is transmitted at a larger diameter. Hence, the torque arm is greater. Doubling the band diameter therefore doubles the torsional resistance.

### Conclusions

Two alternate theories can be derived to predict the torsional load capacity of V-band joints, one accounting for transverse friction at the band to flange interface, the other ignoring it. Analysis of V-band joints by finite element analysis requires complex, multi-step model definition and significant run times.

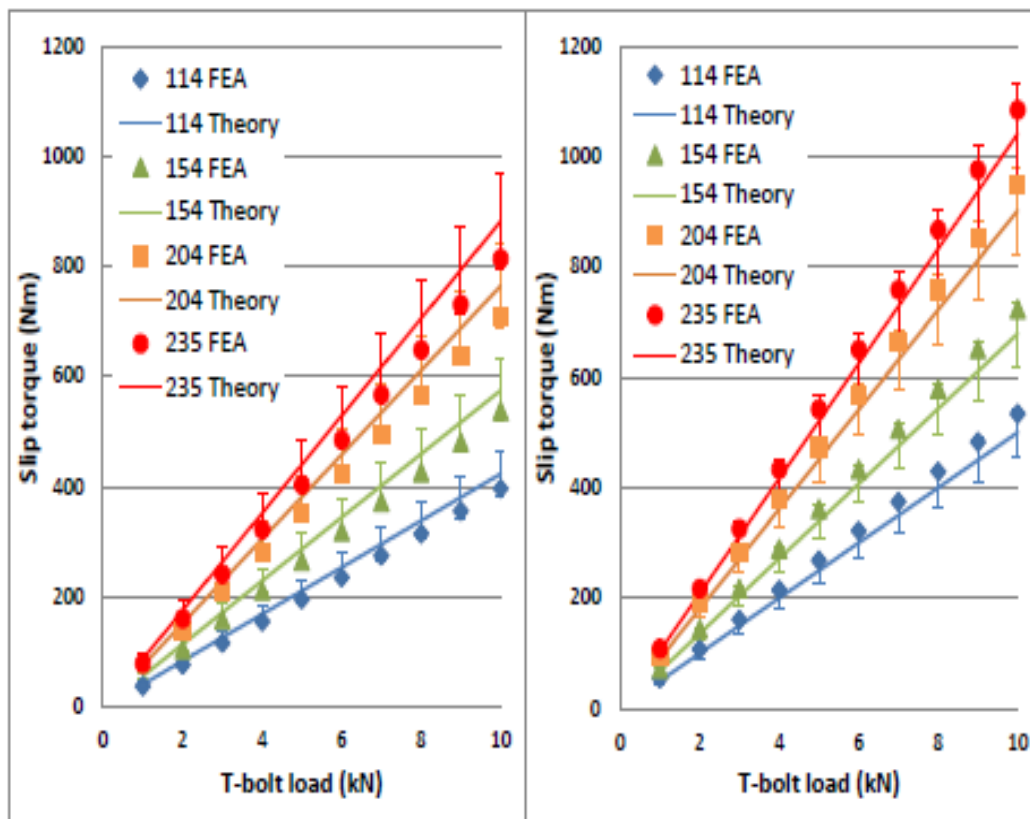


Fig 4: Comparison of FE and theoretical results with  $\mu = 0.2$  (left) and  $\mu = 0.4$  (right)

Good agreement was shown between the theoretical analysis and the finite element models over a wide range of band diameters and T-bolt loads. For lower coefficients of friction, accounting for transverse friction gave better agreement whilst for higher coefficients of friction, transverse friction should be ignored.

The torsional load capacity is directly proportional to both T-bolt load and band diameter but is less dependent on the coefficient of friction.

## References

- [1] K. Shoghi, *Stress and strain analysis of flat and V-section band clamps*, PhD thesis, University of Huddersfield (2003).
- [2] Teconnex, *High Performance Quality Clamps*, online: <http://www.teconnex.com/home/> (2010).
- [3] K. Shoghi, S.M. Barrans, H.V. Rao, *Stress in V-section band clamps*. Proc IMechE Part C, Journal of Mechanical Engineering Science, 218 (3). pp. 251-261 (2004).
- [4] K. Shoghi, S.M. Barrans, P. Ramasamy, (2005) *Axial Load Capacity of V-Section Band Clamp Joints*, 8<sup>th</sup> Int Conf Turbochargers and Turbocharging, London, pp. 273-285 (2005).
- [5] S.M. Barrans, M. Muller, *Finite element prediction of the ultimate axial load capacity of V-section band clamps*. Journal of Physics: conference series, 181. pp. 1-8 (2009).
- [6] S.M. Barrans, G. Khodabakhshi, Q. Xu, Qiang, *Contact Pressure Distribution in Joints Formed by V-Band Clamps*. Advanced Materials Research, 1016. pp 34-38 (2014).
- [7] H. Guo, D. Wang, E Liang, *A method to predict axial clamping force and anti-rotating torque for V-band joint*. Power Systems Conf. Fort Worth, USA. SAE International 2010-01-1813 (2010).
- [8] S.M. Barrans, A. Waterworth, S. Sahboun, *Analysis of the Torsional Load Capacity of V-Section Band Clamps*. Advanced Materials Research, 1016. pp. 59-64 (2014).
- [9] Dassault Systems, Abaqus user manual v6.14, (2014).
- [10] R. Weyler, J. Oliver, T. Sain, J.C. Cante, *On the contact domain method: A comparison of penalty and Lagrange multiplier implementations*, Computer Methods in Applied Mechanics and Engineering, Vol 205-208, pp 68-82 (2012).

## Analysis of the Torsional Load Capacity of V-section Band Clamps

Simon M Barrans<sup>1,a</sup>, Adelle Waterworth<sup>1,b</sup> and Salahaddin Sahboun<sup>1,c</sup>

<sup>1</sup>School of Computing and Engineering, University of Huddersfield, Queensgate, Huddersfield, West Yorkshire, HD1 3DH, UK

<sup>a</sup>s.m.barrans@hud.ac.uk, <sup>b</sup>a.waterworth@hud.ac.uk, <sup>c</sup>salahaddin.sahboun@hud.ac.uk

**Keywords:** V-section band clamp, Marman clamp, torsional load capacity, friction, turbocharger.

**Abstract.** This paper investigates the torsional load capacity of three sizes of V-section band clamps when assembled onto rigid flanges by comparing experimental data with a developed theoretical model. This mode of failure is of particular interest for turbocharger applications where, in use, they are subjected to torsional loading via thermal and vibrational effects. The theoretical model developed allows the impact on torsional load capacity of a number of joint parameters to be investigated and good correlation of the results, incorporating variations in coefficients of friction and dimensions, has been shown for the two larger band sizes. For smaller diameter bands, the experimental data suggests that as the band is tightened, contact with the flange is localised rather than being over the full circumference of the band. The coefficients of friction, in particular that between the flanges, and the position of the contact point between band and flange have been shown to have a significant impact on the theoretical torsional load capacity of V-section band clamps.

### Introduction

V-section band clamps are a derivative of Marman clamps; used for a wide range of applications, particularly in the automotive and aerospace industries. Previous work on the Marman clamp systems includes satellite separation shock [1] and dynamic behaviour [1, 2] of such clamps on spacecraft. The sealing performance [3] of V-insert clamps used on exhaust pipes has also been studied.

The V-section band clamps considered in this paper are made from a solid, flat-bottomed, V-section ring with associated trunnion loops and t-bolt fastening, Fig. 1 [4], which are the more common type used in turbocharger assemblies.



Fig. 1 V-section band clamp assembled onto a pair of stiff flanges

A theoretical model of the internal loads in V-band joints was presented in [5] extended to include axial clamping load in [6]. More recently, preliminary studies have been reported on ultimate axial load capacity [7]. However, little work has been done to analyse the torsional load capacity of such joints; a mode of failure of particular interest in turbocharger applications. A small study has been reported [8], whereby the axial clamping load predicted in [6] was used in place of the thrust load within a clutch theory based approach to predict the torsional load capacity of V-

band joints. However, the transverse friction effect reported in [6] and [9] as being significant was disregarded.

This paper will investigate the torsional load capacity of three sizes of V-section band clamps when assembled onto rigid flanges. The theoretical model developed will be based on the infinitesimal segment previously used in [6] rather than considering the V-band as a whole. The impact on torsional load capacity of a number of joint parameters including t-bolt tension, friction and the position of the contact point between band and flange will also be investigated.

### Theoretical approach

The full torsion model ( $T_{TOTAL}$ , total theoretical torque capacity) is made up of two parts, torque at the flange-to-flange interface ( $T_F$ ) and torque at the flange-to-band interface ( $T_B$ ). The first part,  $T_F$ , is calculated using single plate clutch theory, assuming a uniform pressure distribution [10]. This part of the theoretical development is similar to that presented in [8]. The transmitted torque at the flange-to-flange interface,  $T_F$ , using the definition of  $F_A$  in terms of t-bolt load,  $F_\beta$ , which is given in [6] is:

$$T_F = \frac{2}{3} \mu_F \left( \frac{r_o^3 - r_i^3}{r_o^2 - r_i^2} \right) \frac{(1 - \mu_B \tan \phi) F_\beta (\sin \phi + \mu_B \cos \phi)}{\mu_B (\tan \phi + \mu_B)} \left[ 1 - \exp \left( \frac{-\mu_B \beta}{(\mu_B \cos \phi + \sin \phi)} \right) \right] \quad (1)$$

Where  $r_o$  and  $r_i$  are the outer and inner radii of the flange contact faces,  $\phi$  is half the included angle of the V-band section and  $\beta$  is half the arc angle of the band.

In order to determine the torque capacity,  $T_B$ , of the interface between the band and the flange the theory presented in [6] is extended. Within the V-band joint, tightening the t-bolt will generate a normal force per unit length,  $q$ , between the band and the flange, which is related to the radial force per unit length,  $f_r$ , and the static coefficient of friction at the band to flange interface,  $\mu_B$ . Then, using the relationship between  $f_r$  and the circumferential force  $F_\theta$  generated in the band by tightening the t-bolt yields:

$$q = \frac{F_\theta}{2(\sin \phi + \mu_B \cos \phi)R} \quad (2)$$

Considering an infinitesimal annular segment  $d\theta$  of the band, the torque reaction between the band and one flange,  $dT_B$ , is given as

$$dT_B = \frac{F_\theta \mu_B R d\theta}{2(\sin \phi + \mu_B \cos \phi)} \quad (3)$$

where  $Rd\theta$  is the unit length over which the load  $q$  is acting and  $R$  is the radius of the torque.

Using the relationship in [6] between  $F_\theta$  and the t-bolt load,  $F_\beta$  and integrating  $dT_B$  to give the total torque reaction between the band and one flange,  $T_B$ , yields:

$$T_B = 2 \int_0^\beta dT_B = 2 \frac{\mu_B R F_\beta}{2(\sin \phi + \mu_B \cos \phi)} \int_0^\beta e^{\left[ \frac{\mu_B (\theta - \beta)}{\mu_B \cos \phi + \sin \phi} \right]} d\theta = R F_\beta \left[ 1 - e^{\left( \frac{-\mu_B \beta}{\mu_B \cos \phi + \sin \phi} \right)} \right] \quad (4)$$

The total theoretical torque capacity,  $T_{TOTAL}$  is achieved by addition of the torque at the flange-to-flange interface ( $T_F$ ), Eq. 1, and torque at the flange-to-band interface ( $T_B$ ), Eq. 4.

### Experimental work

The experimental work has been carried out on a special purpose torsional test rig, Fig. 2. The rig allows two flanges to be clamped together with a V-section band clamp on a supporting shaft. The flanges are attached to arms; one moved via a hydraulic ram (the lever arm), the other held stationary via a load cell (the fixed arm). The torsional load applied by the ram transmitted through the band-to-flange contact area and the flange-to-flange contact face and reacted by the load cell. T-bolt load is measured using a small washer load cell between the trunnion collar and the t-bolt nut. Data was recorded using a digital oscilloscope. The oscilloscope also collected data from two

LVDT probes, positioned to measure movement of the two arms. For each band a t-bolt load range of 1kN to 10kN (in approximate 1kN increments) was applied, with full face dry contact between the flanges.

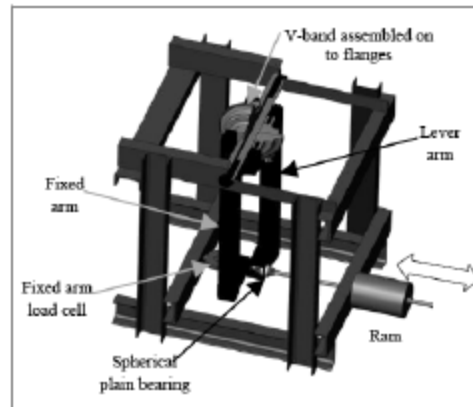


Fig. 2 V-section band clamp assembled onto a pair of rigid flanges on the torsional test frame

The point of initial torsional slip was calculated from the fixed arm load cell reading, and determined by analysing the readings from that instrument and the LVDT probe attached to the fixed arm. As joint slippage occurred, the fixed arm experienced a fast and relatively small reversal of movement as it relaxed. This slippage point was also characterised by a slight change of response from the lever arm LVDT and a small peak on the fixed arm load.

### Friction

Frictional loads affect the results in three ways. As discussed in [6], increasing the friction coefficient between the band and the flanges decreases the axial clamping load generated when tightening the T-bolt. However, increasing this coefficient of friction increases the torque resistance of the band to flange joint. The final affect is between the two flange faces where an increase in coefficient of friction also increases the theoretical torque resistance. Since the band and flanges are made of different materials and by different methods, it is assumed that the coefficients of friction will be different which further complicates the effect of friction. A preliminary theoretical investigation of the effects of friction with  $\mu$  varying between 0.05 and 0.5 for both band-to-flange and flange-to-flange contact areas showed that torsional load capacity could change by a factor greater than four.

Since these frictional effects can have such a large impact on the theoretical results, a practical test was carried out to assess the real coefficients of friction. This employed a standard inclined plane. The lowest and highest theoretical total torque values utilising a combination of minimum and maximum values (which are calculated as the average  $\pm 3$  standard deviations of the friction test results) are used in the comparison of theoretical results to the experimental results.

### Other important parameters

**Beta angle** Shoghi[5] assumed a beta angle of  $167^\circ$  in the calculation of applied axial clamping load,  $F_A$ . However, there is contact between flange and band of almost  $180^\circ$ . The stiffness of the band section and the stiffness in the circumferential direction will result in some contact pressure being generated. Using  $180^\circ$  instead of  $167^\circ$  in this theory increases the expected torsion capacity by only a small amount (i.e. approximately a 5% increase at 5kN t-bolt load).

**Band diameter.** The theoretical results have used the V-section band and flange specification nominal diameters. For the three sizes of band tested, varying the dimension of the inner and outer radii by  $\pm 1$  mm has a minimal effect, less than 3%, on the calculated torque capacity.

**Bandtoflange contact angle.** The parameter which has a significant effect on the theoretical results is the contact angle,  $\phi$ , between the outer edge of the flanges and the leg of the V-section band, see Fig.3. Nominally this angle is  $20^\circ$ , typically with a tolerance of  $\pm 1^\circ$ . However, this value can only be assumed if the flange edge contacts the band on the straight portion of its leg. Past researchers have generally assumed contact on the straight part of the V-section band leg. If the flange to band contact point moves to the radii between the end of the straight leg portion and the back of the band, the normal to the contact surface can be altered significantly. The position of contact point is determined by the flange tip width.

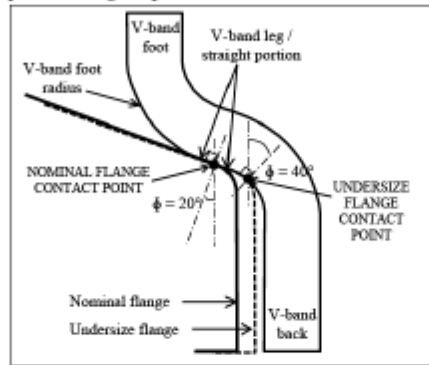


Fig. 3 Change in contact angle,  $\phi$ , with differing flange tip widths

During this research the flange tip width has been investigated using a shadow graph method. However, individual band cross section geometries were not measured. Hence, the flange tip measurements have been combined with the band specification tolerance to determine maximum and minimum contact angles as shown in Table 1 for use in the theoretical calculations.

Table 1: Contact angle,  $\phi$

Band diameter [mm]	Minimum contact angle	Maximum contact angle
114	$19^\circ$	$33^\circ$
181	$19^\circ$	$35^\circ$
235	$29^\circ$	$57^\circ$

## Results and discussion

The results are presented in Fig.4; one graph for each V-section band diameter using the various parameters discussed above to calculate an expected range drawn from the theoretical analysis. This is compared with repeated experimental tests on the same band for each size. It can be seen that for each band size, as the test is repeated, the torsional load capacity increases.

Although reasonable correlation of experimental results to the theory is seen for the two larger diameter bands, for the smaller band the average experimental results is almost twice the average expected slip torsion. There are two plausible reasons for this. Firstly, after testing of the small band, it was noted that galling had occurred on the flange-to-flange contact area in a radial direction. This effectively increases the static coefficient of friction. Due to the localized nature of the galling marks, it was not possible to assess the influence on friction using a standard inclined plane rig. A range of coefficient of friction for the flange to flange interface of 0.55 to 0.65 would correlate well with the experimental results shown.

Secondly, it is assumed that when tightening the T-bolt, the band forms a circular arc as it comes into contact with the flanges. This assumption is reasonable for large bands where the radial stiffness is relatively low and the bands will readily conform to the circular flanges. However,

smaller bands with the same cross section are much stiffer in the circumferential direction. Ensuring that these bands formed a circular arc once they were tightened to come into contact with the flanges would be extremely difficult given the manufacturing methods used (as described in [11]). Hence, it is probable that for smaller diameter bands, contact will take place over only part of the band circumference. A substantial proportion of the band tension generated by the t-bolt is absorbed by the exponentially decaying frictional circumferential reaction load. At any point on the band, this load is proportional to the contact pressure. If t-bolt tension is held constant but the contact region is reduced, the contact pressure must therefore increase. This will then lead to an increase in the torsional load capacity of the band to flange interface.

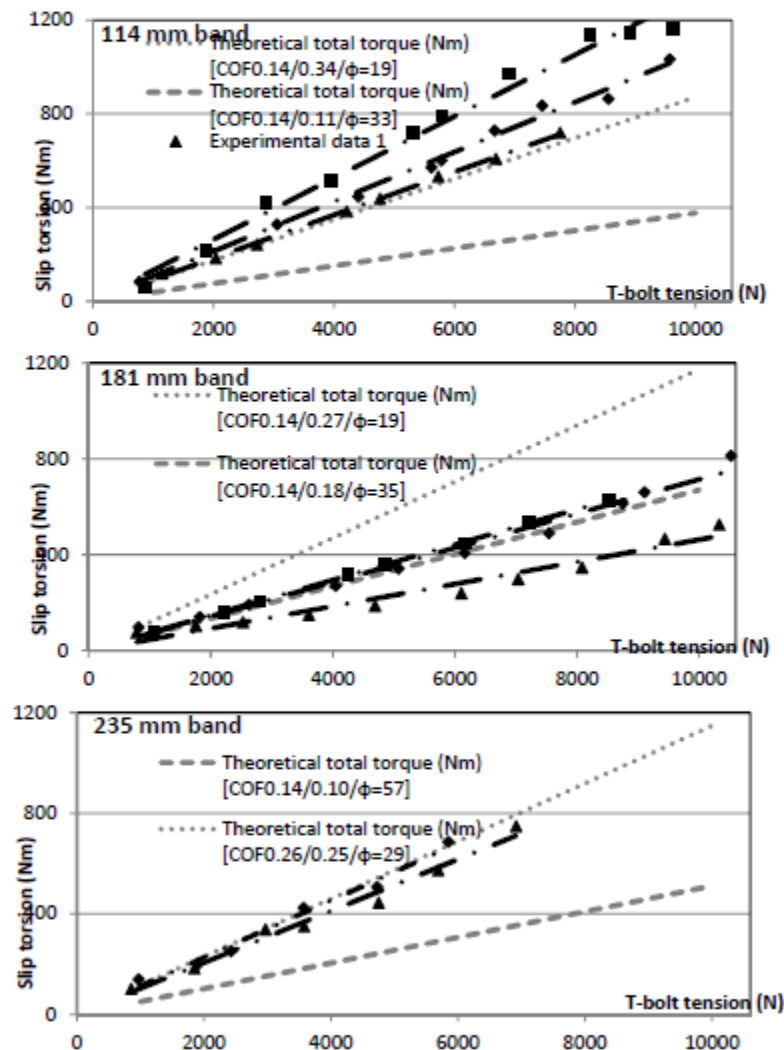


Fig. 4 Comparison of theoretical and experimental results for three band sizes

### Conclusions

This paper has investigated the torsional load capacity of three sizes of V-section band clamps when assembled onto rigid flanges. The theoretical model developed has been shown to have good correlation to the experimental results for the two larger band sizes.

The coefficients of friction, in particular that between the flanges, has been shown to have a significant impact on the theoretical torsional load capacity of V-section band clamps, warranting further investigation.

The position of the contact point between band and flange and hence contact angle,  $\phi$ , has a significant impact on the theoretical torsional load capacity.

For smaller diameter bands, the experimental data suggests that as the band is tightened, contact with the flange is localised rather than being over the full circumference of the band.

#### Further work

The test flanges have been machined to allow for the use of a greased washer during testing and hence eliminate flange to flange contact. Also, different washer thicknesses will facilitate the investigation of varying the flange tip widths to control the contact angle,  $\phi$ .

The circularity of the contact line on the bands as their nominal diameter is reduced to bring them into contact with the flanges should be measured. The impact of any lack of circularity will be investigated using numerical methods.

#### Acknowledgements

The authors gratefully acknowledge the support of Teconnex Ltd, Keighley, UK and the comments and observations made by I Brown of Teconnex Ltd and K Shoghi of Borg Warner Turbo Systems Ltd, Bradford, UK.

#### References

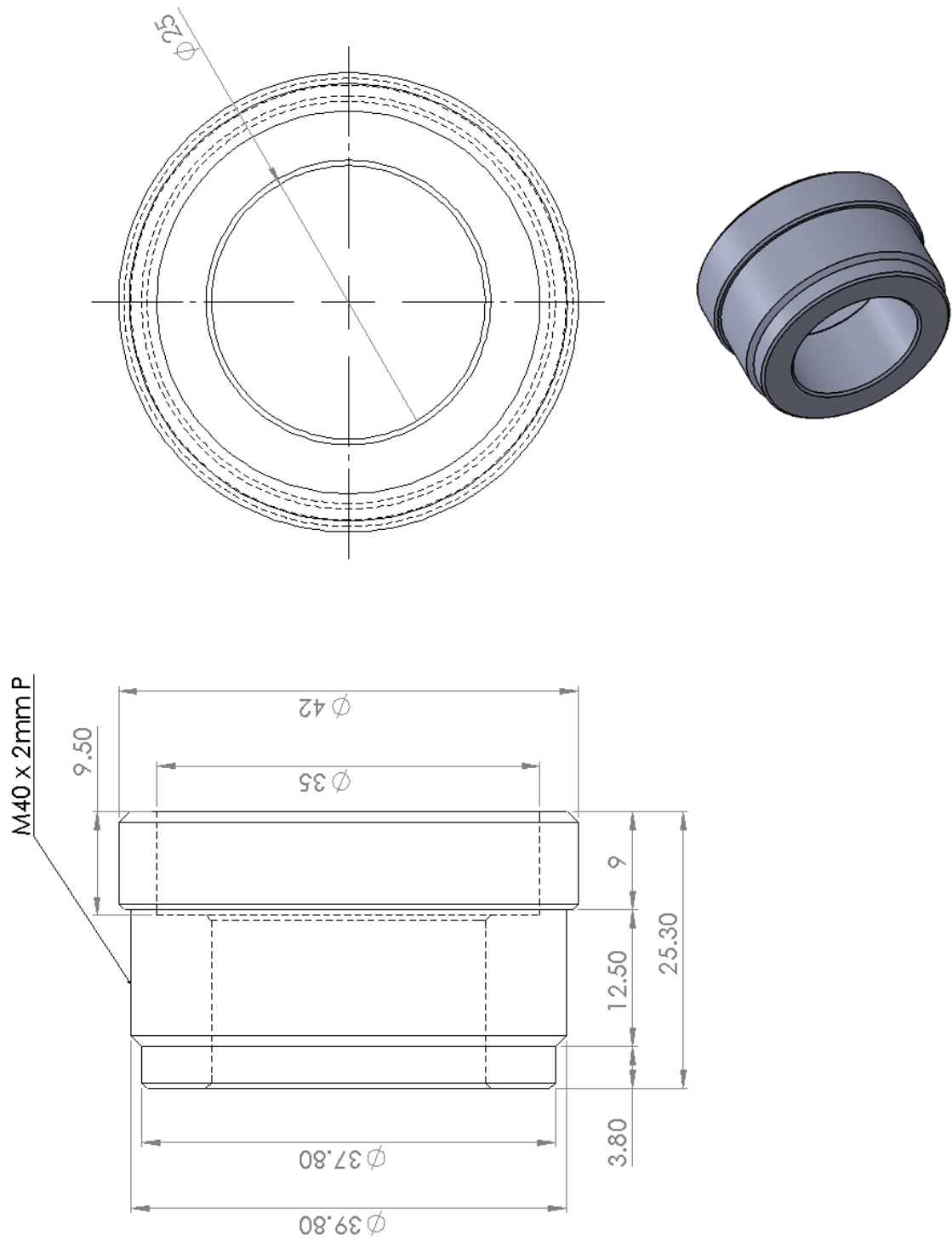
- [1]. Takeuchi S, Onoda J. Estimation of separation shock of the Marman clamp system by using a simple band-mass model. *Trans Jap Soc for Aeronautical and Space Sciences*.2002; 45: 53-60.
  - [2]. Qin ZY, Yan SZ, Chu FL. Dynamic analysis of clamp band joint system subjected to axial vibration. *Journal of Sound and Vibration*.2010; 329: 4486-500.
  - [3]. Yoon SH, Hwang YE. Sealing Performance Test for V-Insert Clamp Applicable to Automobile Exhaust Pipes.*Journal of Mechanical Engineering Science*. 2012; Part C.
  - [4]. Barrans SM, Muller M. Finite element prediction of the ultimate axial load capacity of v-section band clamps. *Journal of Physics: conference series*. 2009; 181: 1-8.
  - [5]. Shoghi K. Stress and strain analysis of flat and v-section band clamps. University of Huddersfield, UK, 2003.
  - [6]. Shoghi K, Barrans SM, Ramasamy P. Axial load capacity of v-section band clamp joints. In: 8th IntConf Turbochargers and Turbocharging. London: Woodhead Publishing, 2006, p. 273-85.
  - [7]. Muller M, Barrans SM. Impact of flange geometry on the ultimate axial load capacity of v-band clamps. IN: 9th IntConf Turbochargers and Turbocharging. London: 2010, p. 183-92.
  - [8]. Guo H, Wang D, Liang E. A Methodology to Predict Axial Clamping Force and Anti-rotating Torque for V-band Joint.*Power Systems Conference*. Fort Worth, Texas, USA: SAE International, 2010.
  - [9]. NASA. Marman clamp system design guidelines. Guideline no GD-ED-2214. 2000.
  - [10]. Hannah J, Stephens, R. C. *Mechanics of machines: elementary theory and examples*: London : Edward Arnold, 1984.
  - [11]. Muller M, Barrans SM, Blunt LA. Predicting plastic deformation and work hardening during v-band formation.*Journal of Materials Processing Technology*.2011; 211: 627-36.
-

**Mechanical and Aerospace Engineering V**  
10.4028/www.scientific.net/AMR.1016

**Analysis of the Torsional Load Capacity of V-Section Band Clamps**  
10.4028/www.scientific.net/AMR.1016.59

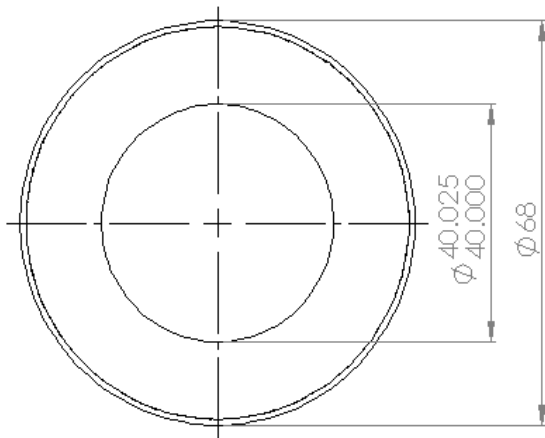
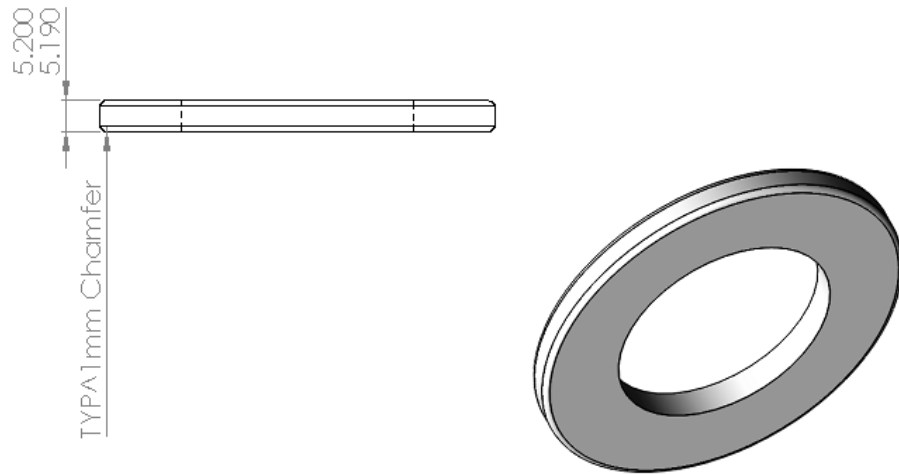


## Appendix – F : Designed Seat



## Appendix – H: Appendix H-1 Steel Washer 5.200mm

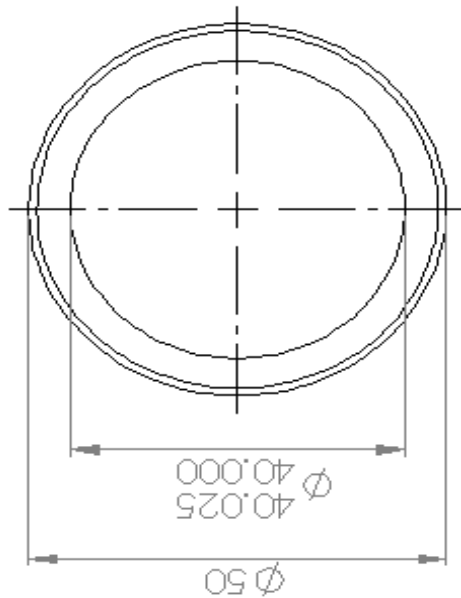
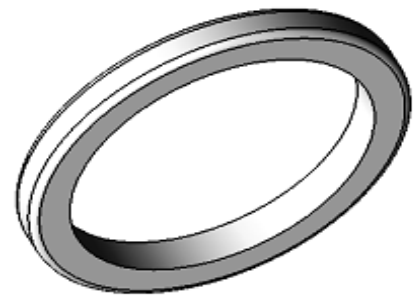
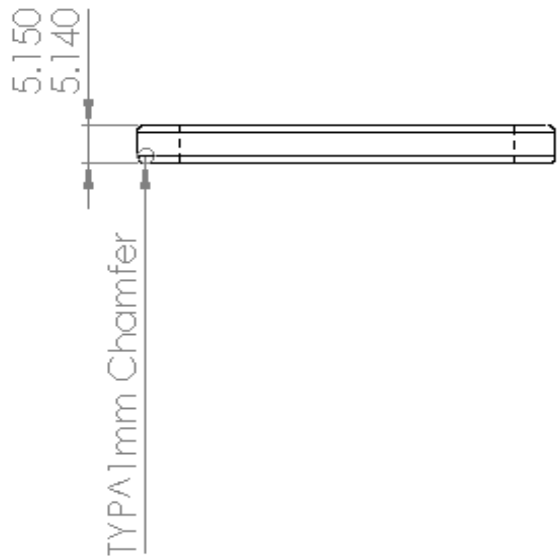
(All dimensions are in mm)



- 1mm chamfer on existing part

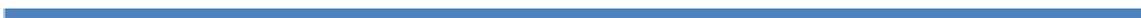
**Appendix – H: Appendix H-2 Steel Washer 5.150mm**

Appendix H-2 Steel Washer 5.150mm

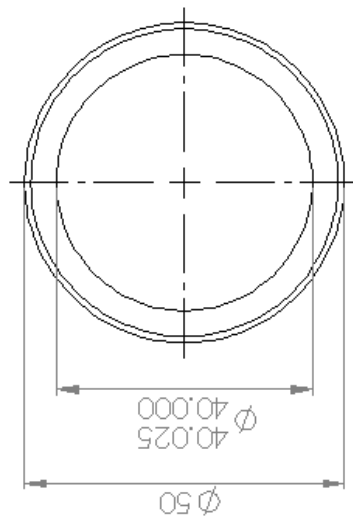
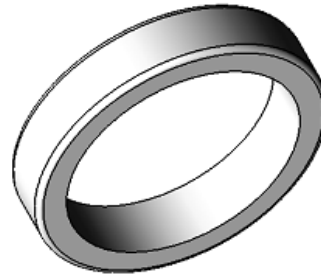
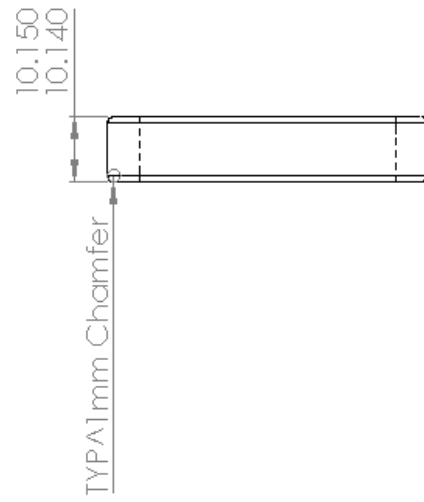


1mm chamfer on existing part

(All dimensions are in mm)



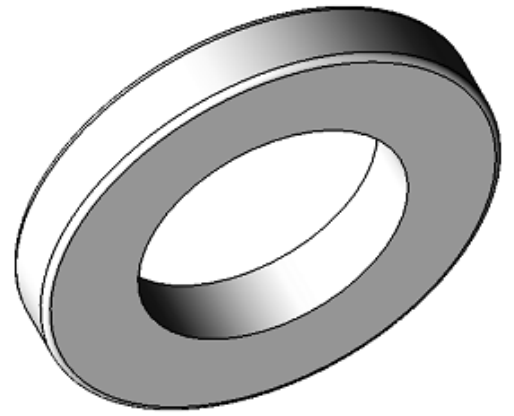
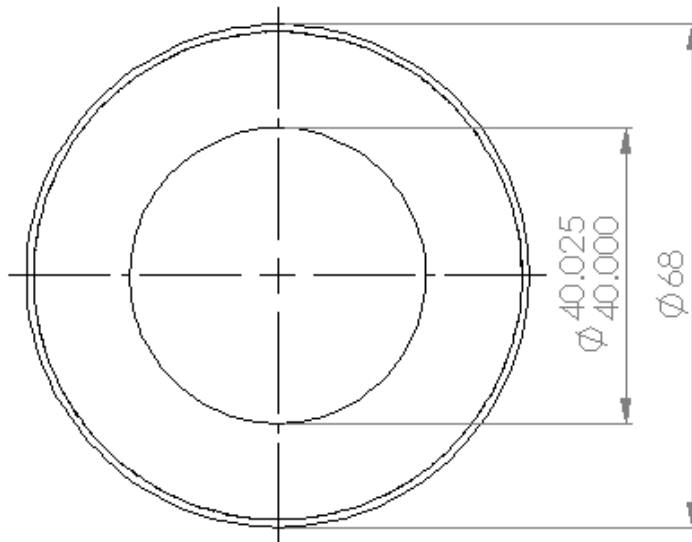
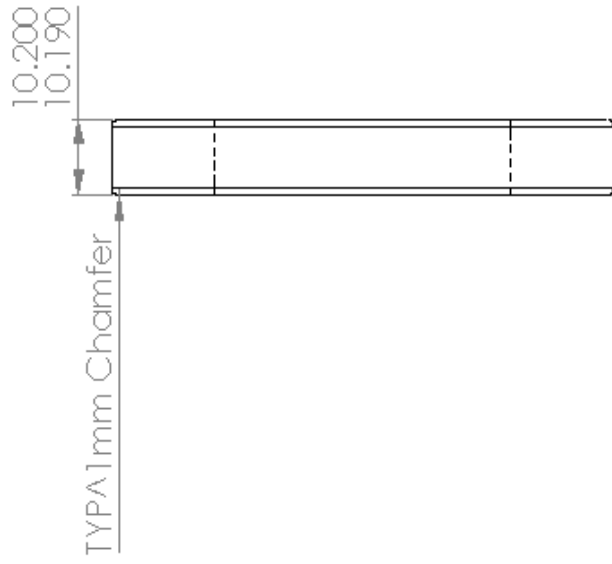
### Appendix H-3 Steel Washer 10.150mm



- Manufacturing one Steel Washer as drawing
- Material EN 24 T Steel

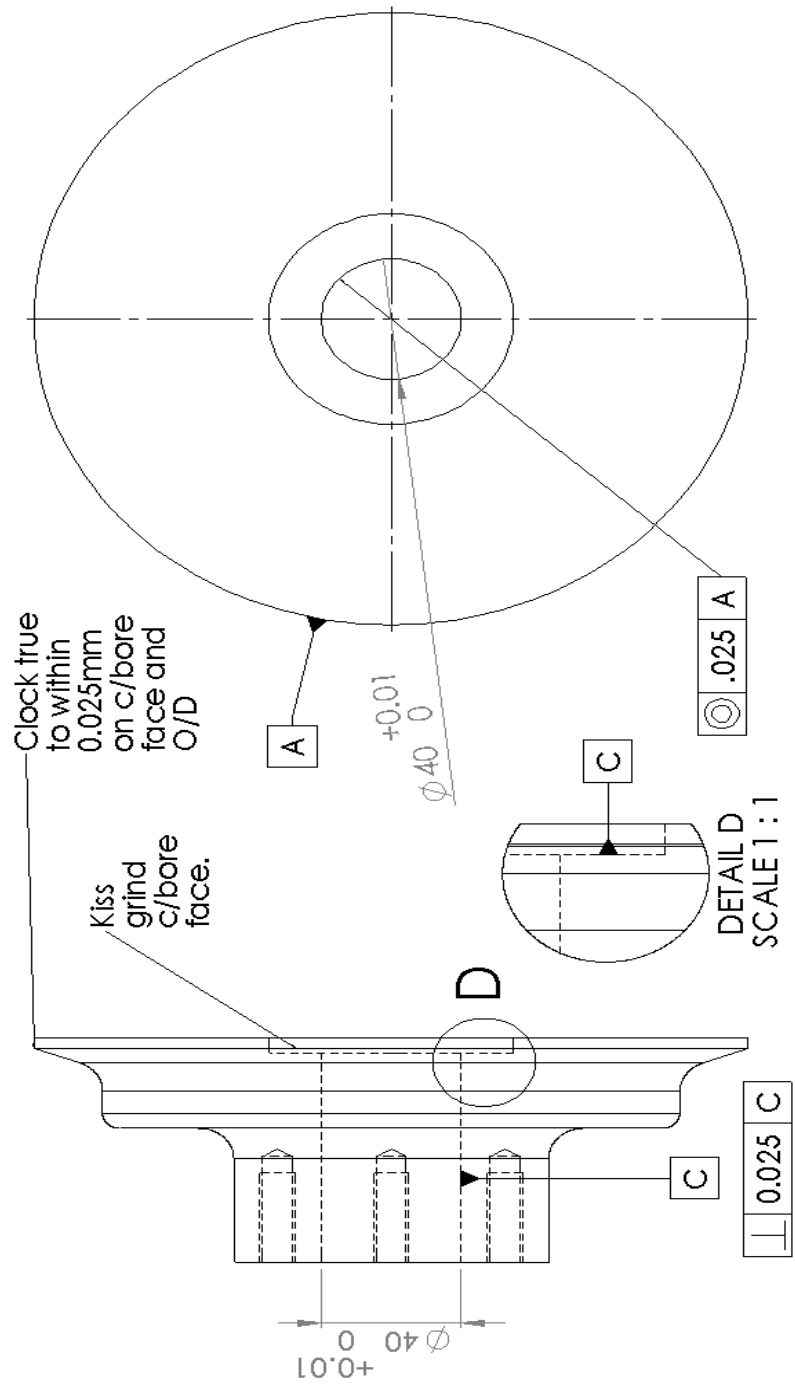


Appendix H-4 Steel Washer 10.200mm

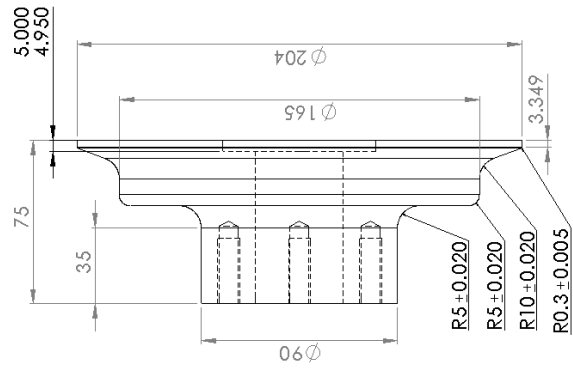


- Manufacturing one Steel Washer as drawing
- Material EN 24 T Steel

(All dimensions are in mm)

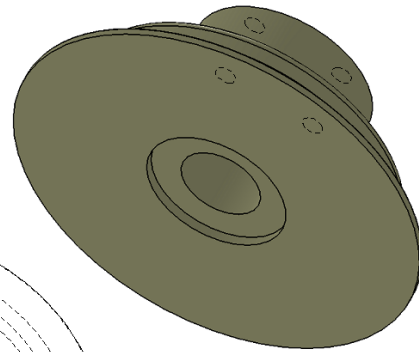
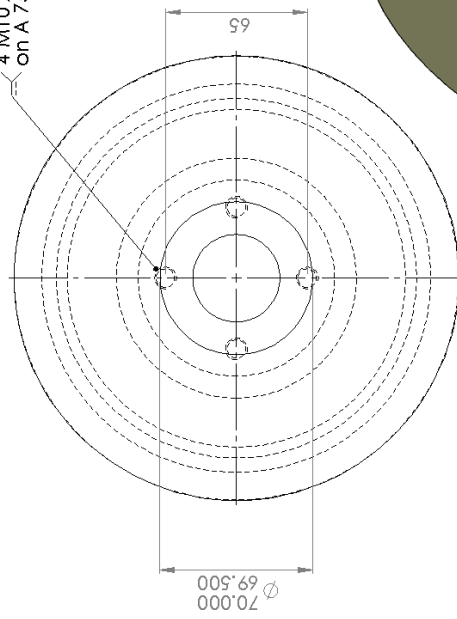


# Appendix – I: Flanges 204mm Grind



VIEW  
SCALE 1 : 2

4 M10 x 1.5 Holes  
on A 75 P.C.D



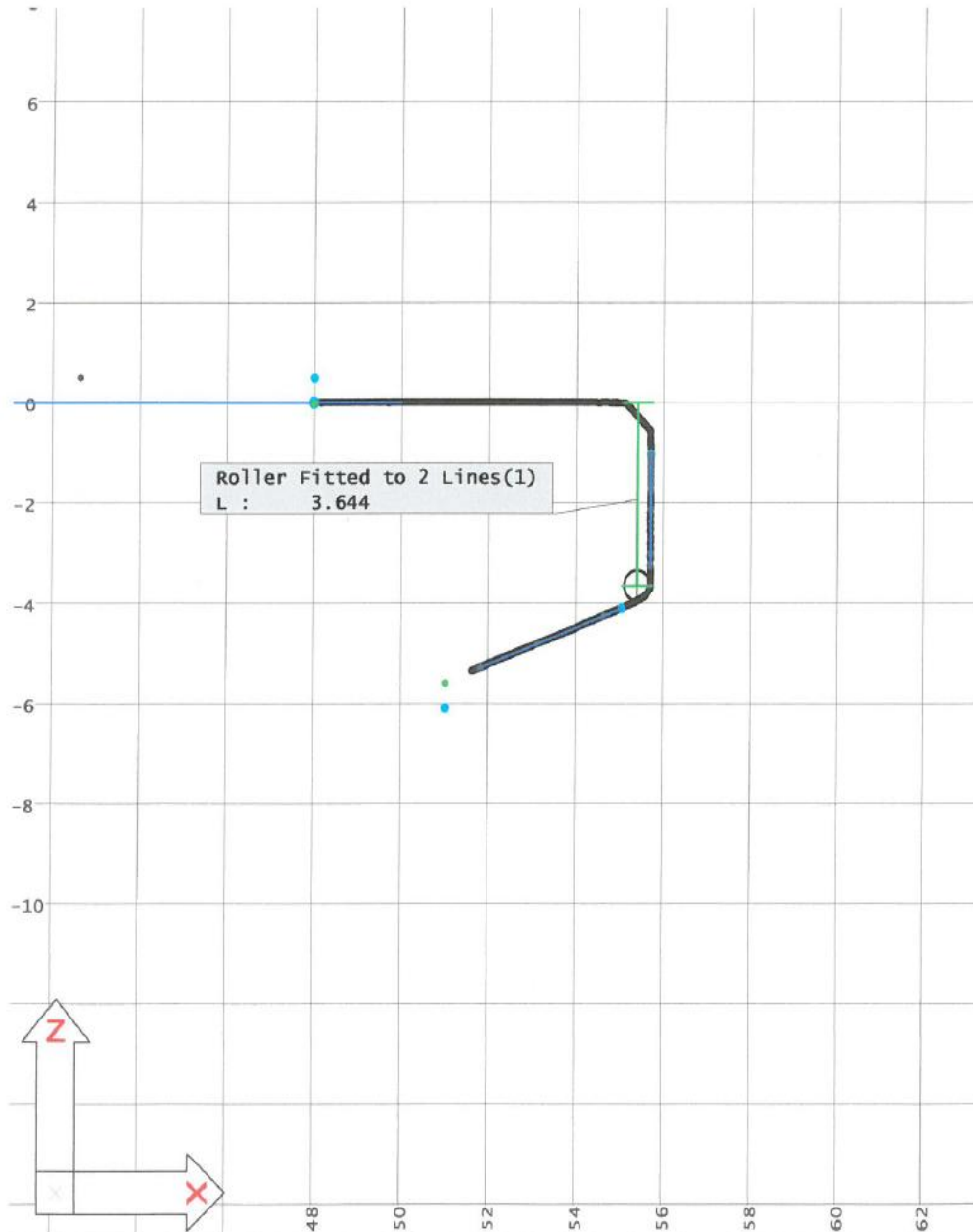
- Manufacturing two flanges
- Material EN 24 T Steel
- Only one flange have recess

# Appendix – J: Flange Measurement

ROLLER B 2 [mm]

Graphics of elements

User name SS	Date and time 27/06/2013 08:34
Drg Issue	Operator Tony
Unique Number	Part Name Flange Measurement
Drawing Number	



Scale factor = 8.24 :1  
[mm]



Protocol number (1)

User name  
SS

Part name  
ROLLER B 2

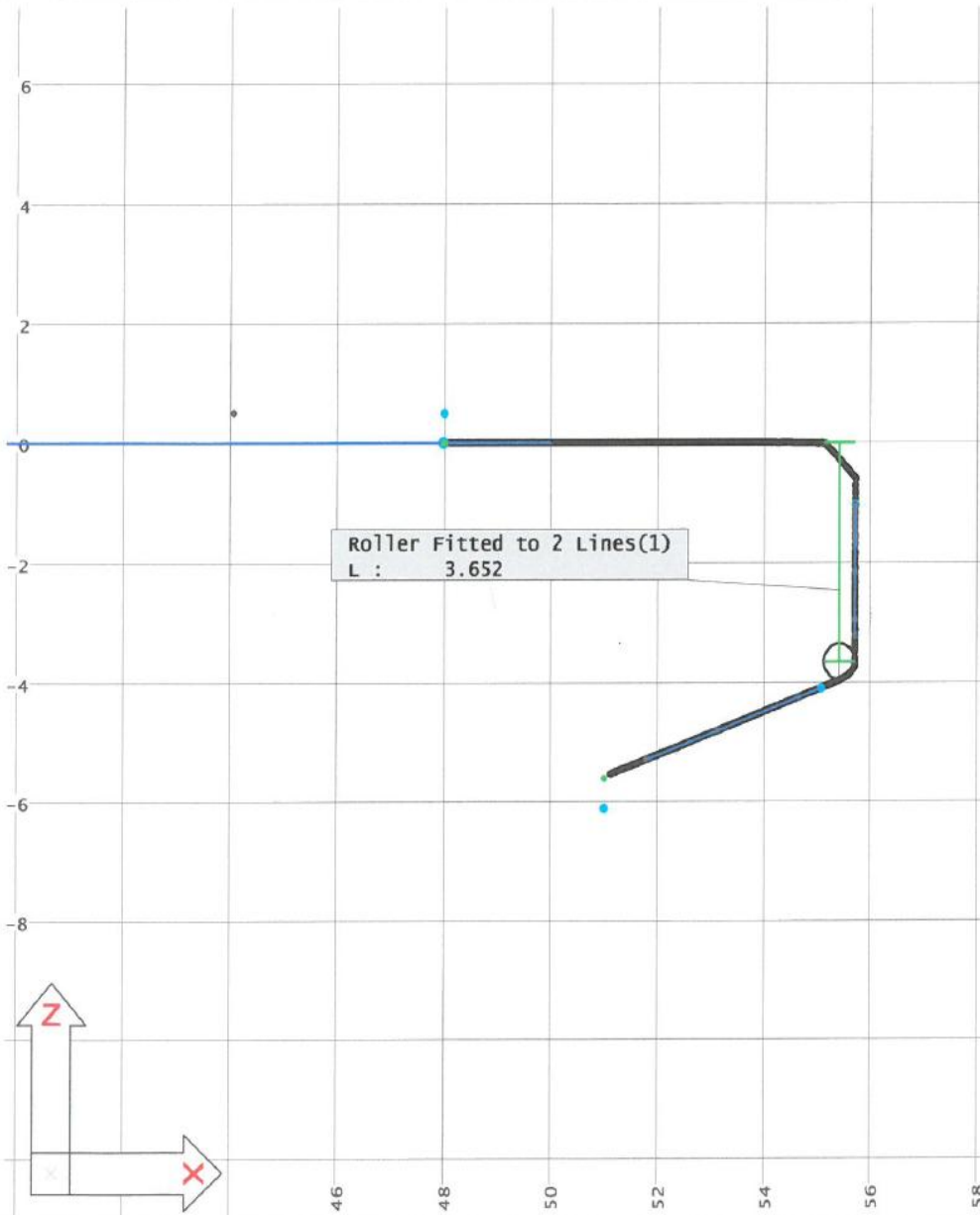
27.06.2013 08:33

Part Number	Drg Issue	Operator	Unique Number					
NA	NA	Tony	Rolle B.					
El. No.	Line No	Element	Pnt. Ref.	X-Coord. Nominal	Y-Coord. Y-Angle	Z-Coord. Z-Angle	Diameter Dist./Ang.	Variance mm
		Tolerance		Ref. Nominal	Up/Lo	Actual	Dev /Error	

1	47	Roller Fitted to 2 Lines		3.565	0.025	3.644	0.079	0.054
		Distance ZX			-0.025			----+--->>

User name	SS	Date and time	27/06/2013 08:41
Dwg Issue	NA	Operator	Tony
Unique Number	Roller B	Part Name	Flange Measurement
Drawing Number	NA		



Scale factor = 9.98 :1  
[mm]



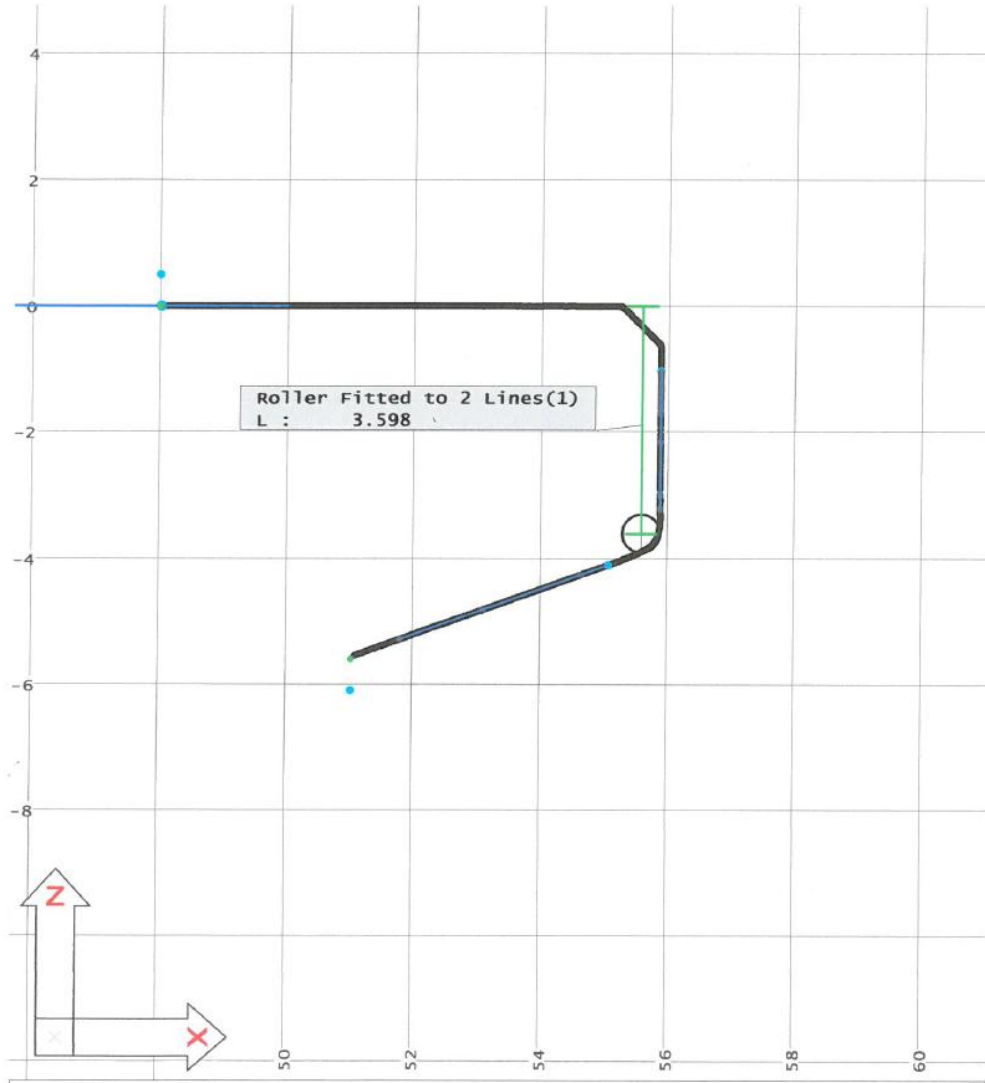
Protocol number (1)

User name  
SS  
27.06.2013 08:40

Part name  
ROLLER B 2

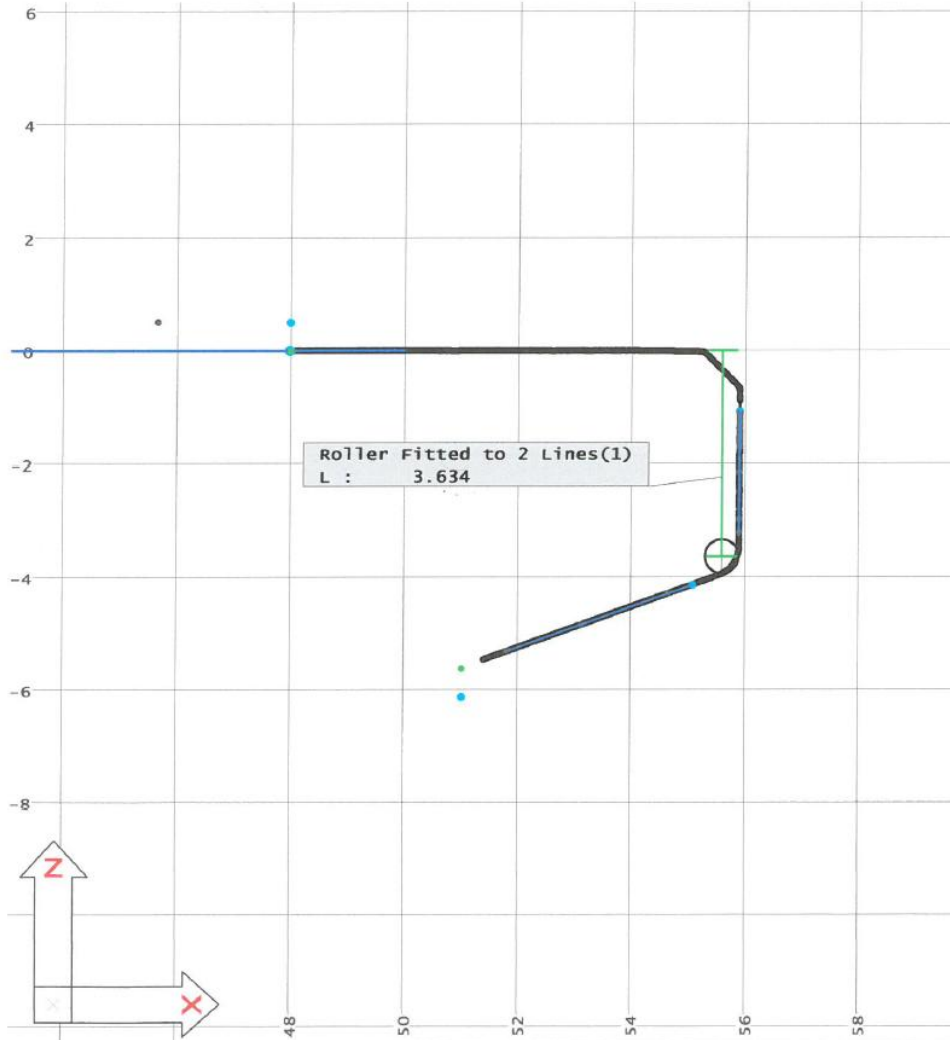
Part Number	Drq Issue	Operator	Unique Number					
NA	NA	Tony	Roller: B					
El. No.	Line No	Element	Pnt. Ref.	X-Coord. Nominal	Y-Coord. Y-Angle Up/Lo	Z-Coord. Z-Angle Actual	Diameter Dist./Error	Variance mm
1	47	Roller Fitted to 2 Lines Distance ZX		3.565	0.025 -0.025	3.652	0.087	0.062 -----+--->>

User name SS	Date and time 27/06/2013 08:19
Dwg Issue	Operator Tony
Unique Number CH	Part Name Flange Measurement
Drawing Number	



Scale factor = 11.89:1  
[mm]

User name	SS	Date and time	27/06/2013 08:27
Dwg Issue		Operator	Tony
Unique Number		Part Name	Flange Measurement
Drawing Number			



Scale factor = 10.96:1  
[mm]



Protocol number (1)

User name  
SS

Part name  
ROLLER A 2

27.06.2013 08:25

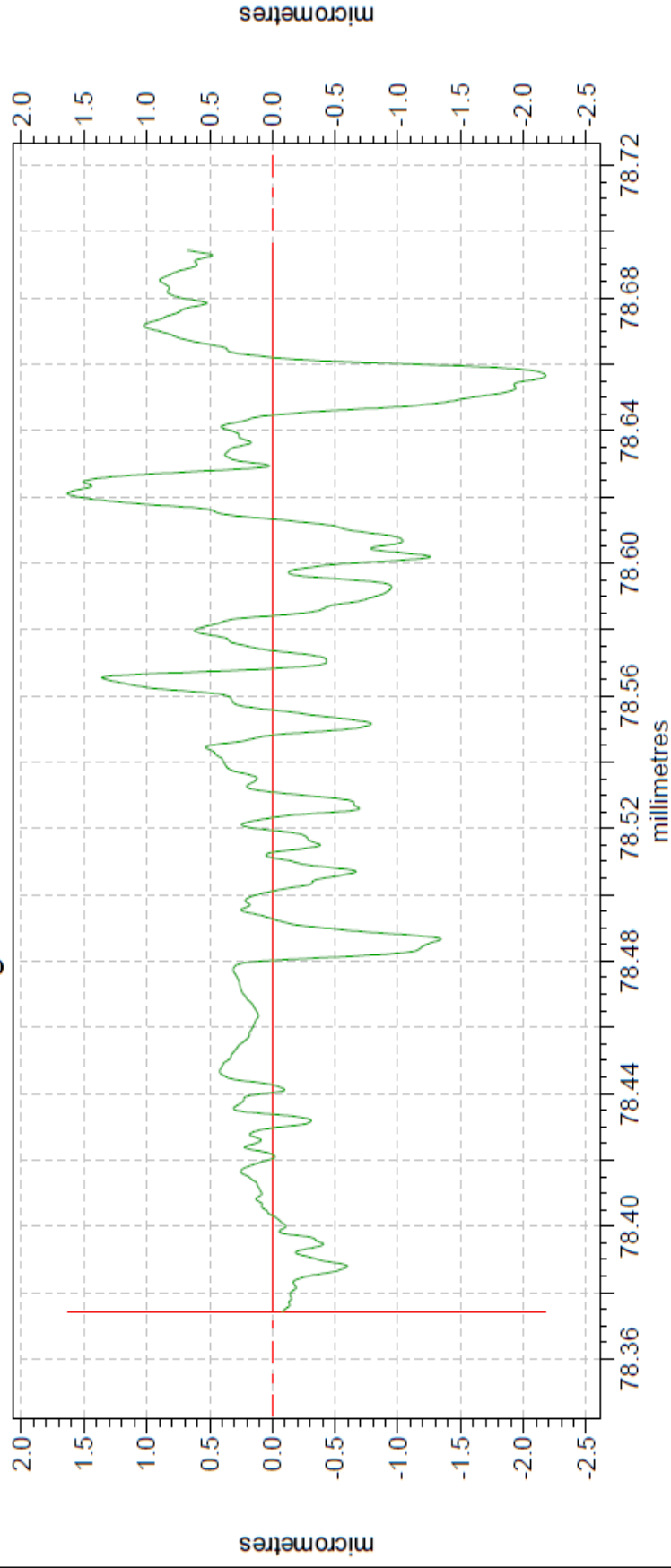
Part Number	Drig Issue	Operator	Unique Number					
NA	NA	Tony	Roller A					
El. No.	Line No	Element	Pnt. Ref.	X-Coord. Nominal	Y-Coord. Up/Lo	Z-Coord. Actual	Diameter Dist./Ang. Dev./Error	Variance mm
1	47	Roller Fitted to 2 Lines Distance ZX		3.565	0.025	3.634	0.069	0.044
					-0.025			----+---->>



Modified Profile

flange A 0 - 180 - R/4x0.08mm/G/30/LS Arc  
flange B 270 - 1.6mm/Admin/PGI

24/05/2013 07:55:05  
24/05/2013 07:54:28



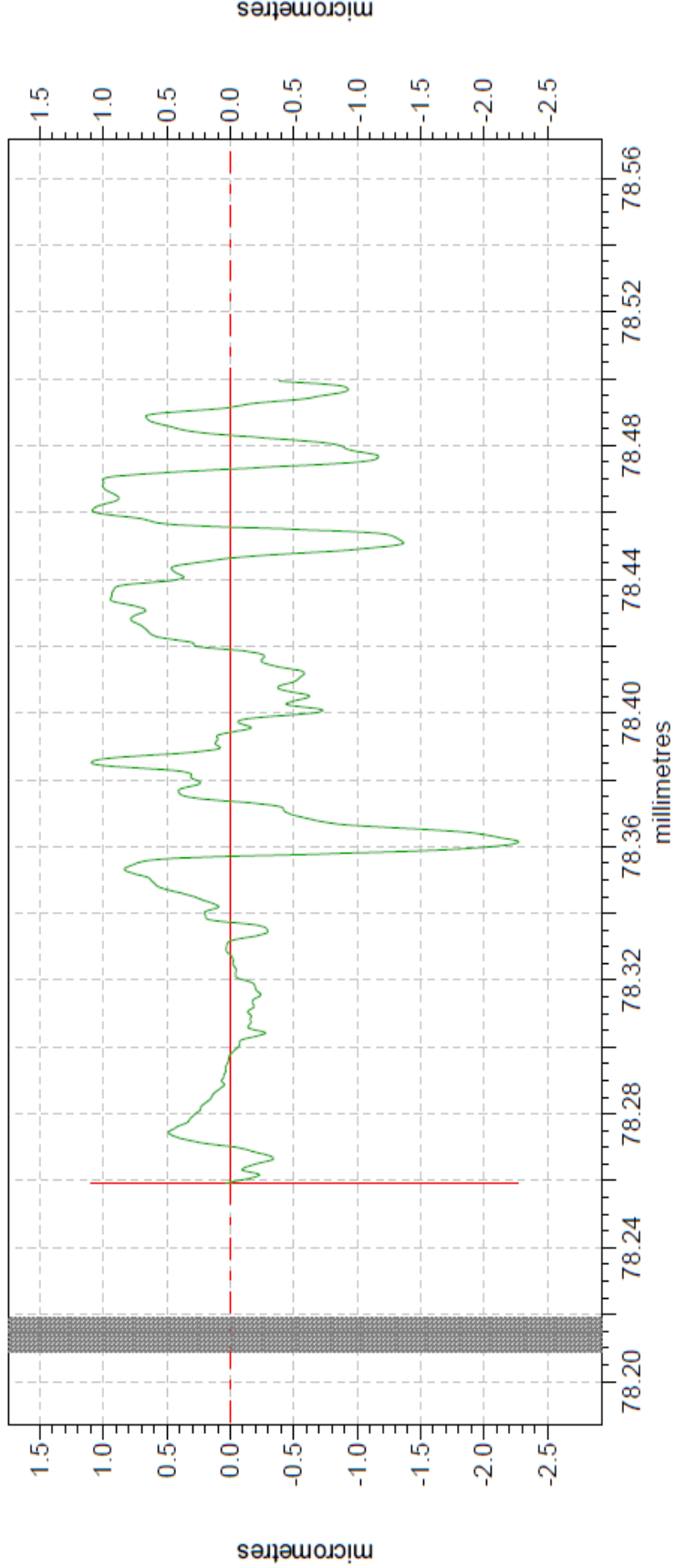
Radius	0.5674	mm	
Ra	0.4743	μm	
Rsk	-0.6770		
Rt	3.8105	μm	
Rz	2.2747	μm	



**Modified Profile**

flange A 0 - 180 - R/3x0.08mm/G/30/LS Arc  
flange B 90 - 1.6mm/Admin/PGI

24/05/2013 07:50:38  
24/05/2013 07:50:08

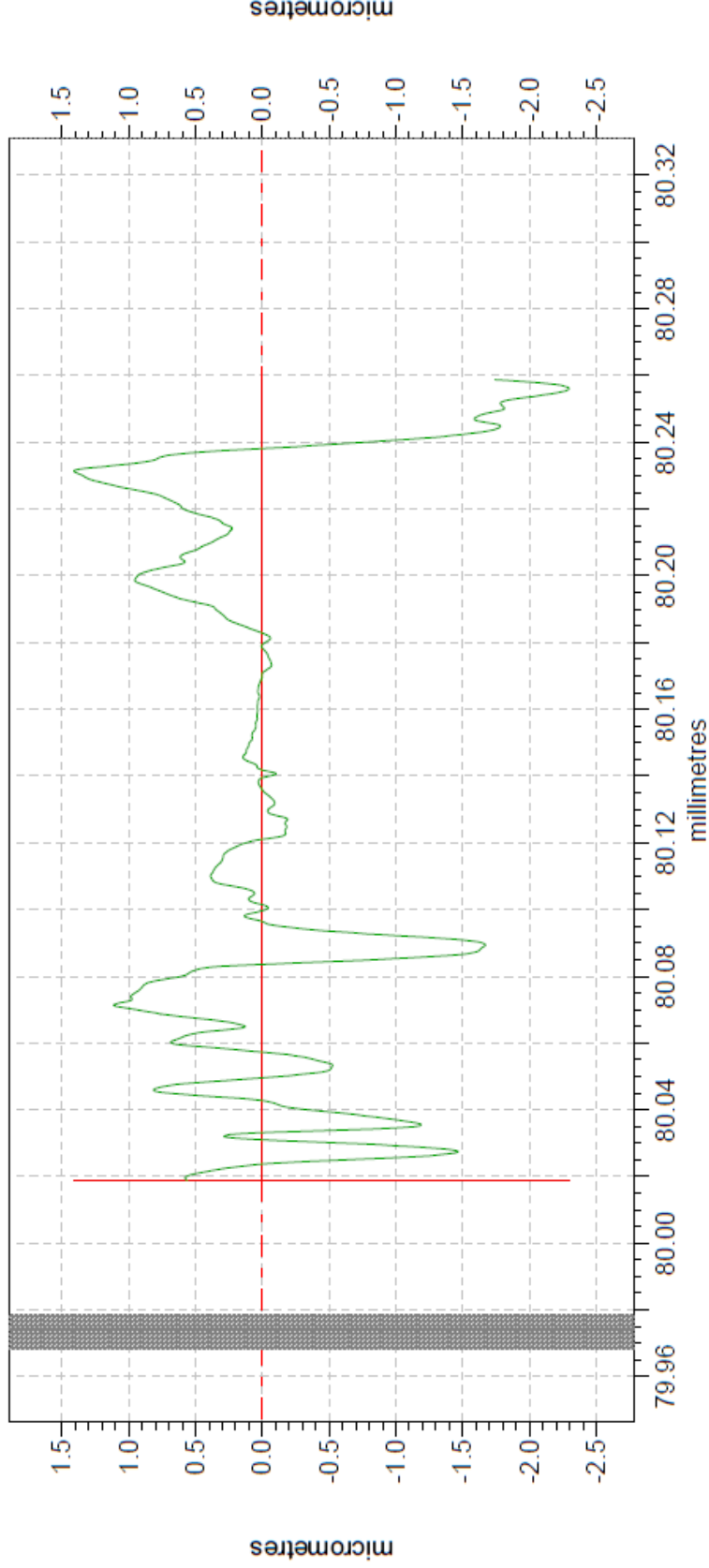


Radius	0.5684	mm	
Ra	0.4741	µm	
Rsk	-0.8639		
Rt	3.3671	µm	
Rz	2.2166	µm	

Modified Profile

flange A 0 - 180 - R/3x0.08mm/G/30/LS Arc  
flange B 0 - 1.6mm/Admin/PGI

24/05/2013 07:48:08  
24/05/2013 07:47:06



Radius 0.5634 mm

Ra 0.5351  $\mu\text{m}$

Rsk -1.0822

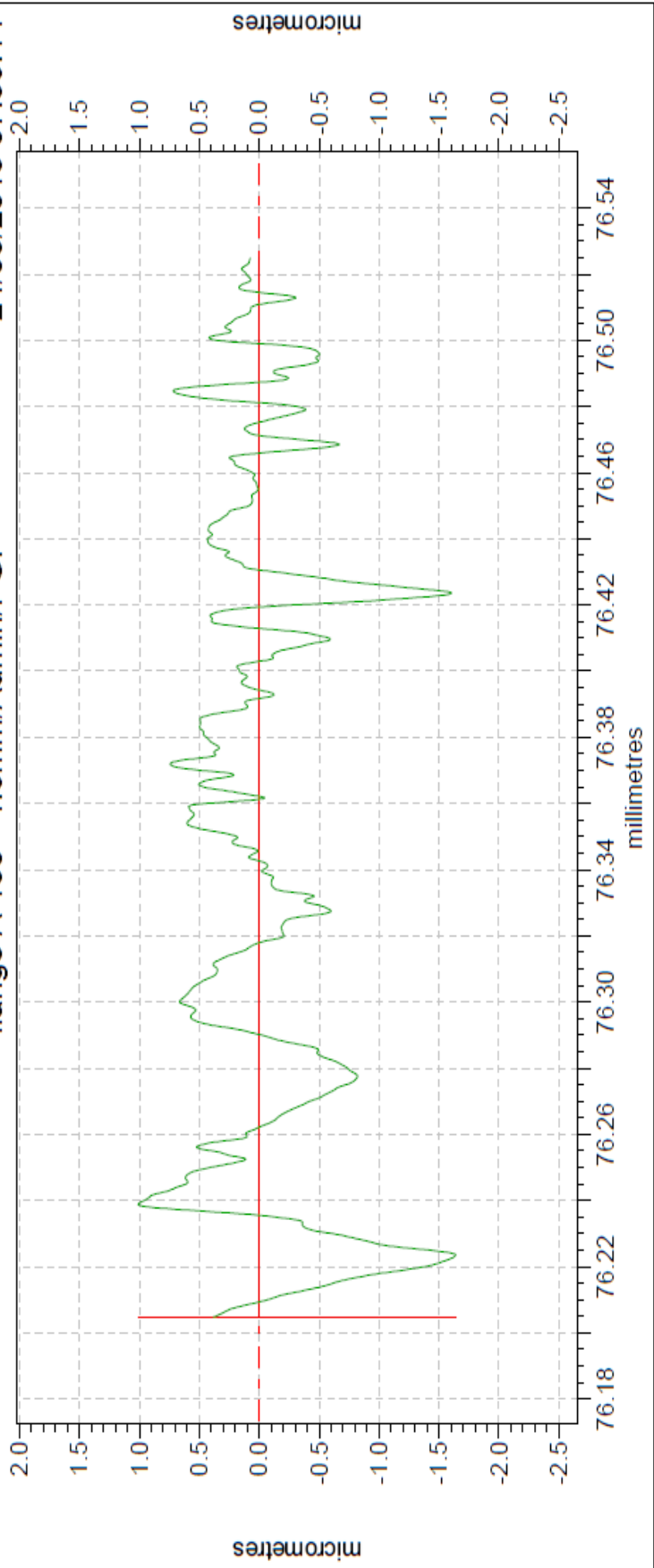
Rt

3.7053  $\mu\text{m}$

Rz

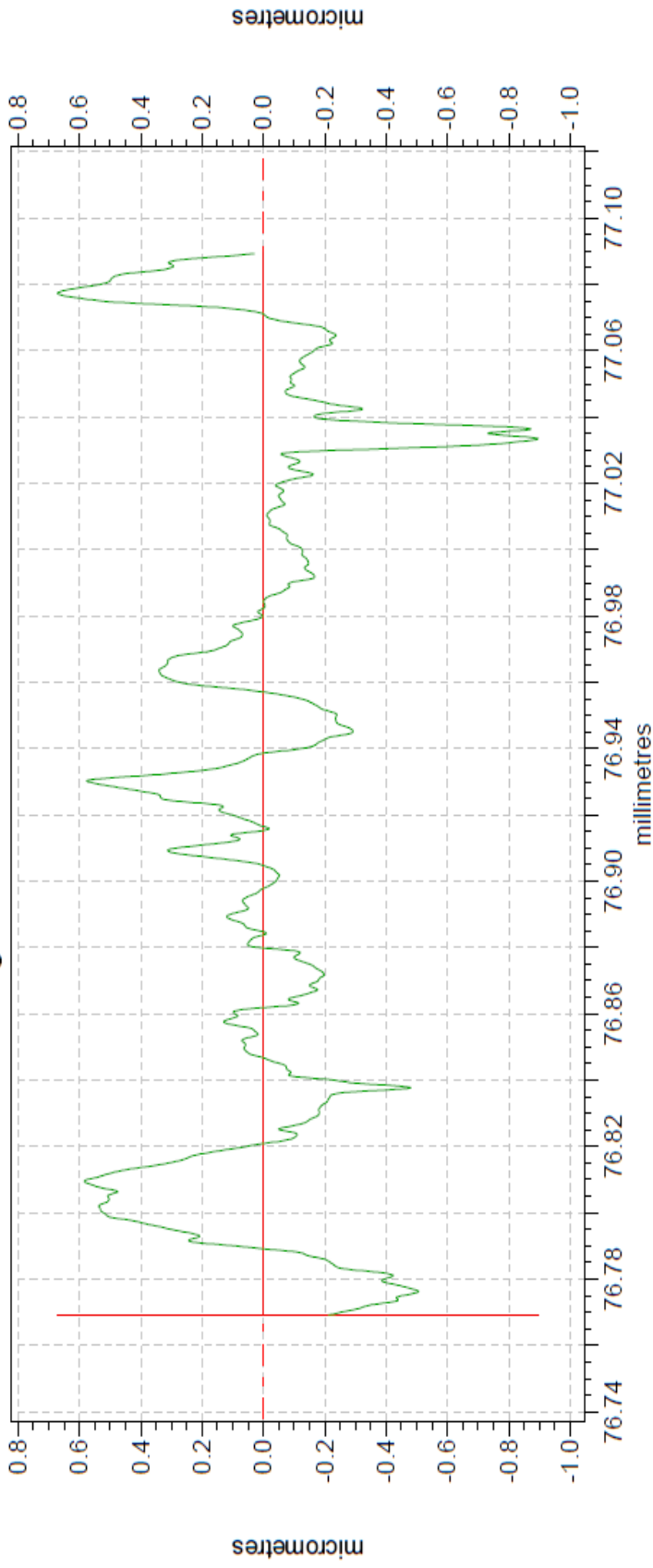
2.3555  $\mu\text{m}$

Modified Profile flange A 0 - 180 - R/4x0.08mm/G/30/LS Arc 24/05/2013 07:40:20  
 flange A 180 - 1.6mm/Admin/PGI 24/05/2013 07:39:14



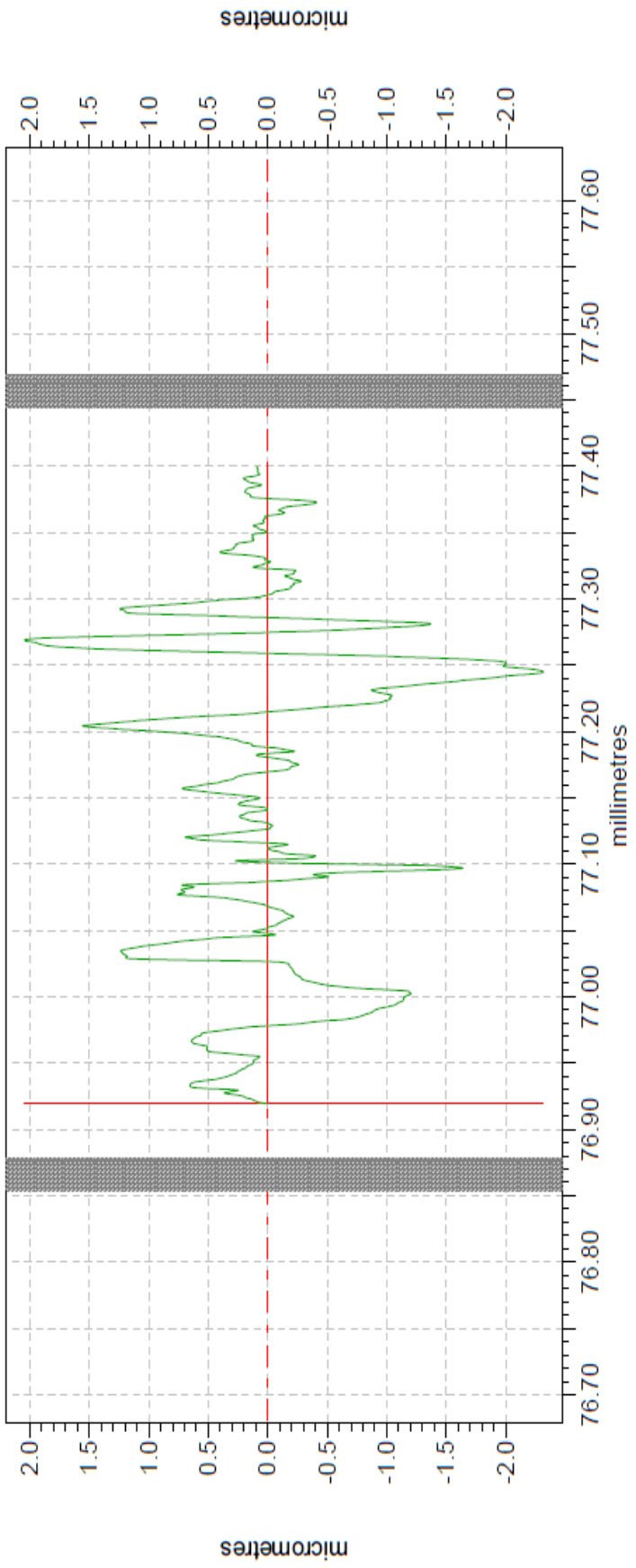
Radius	0.4267	mm	
Ra	0.3755	µm	
Rsk	-0.9464		
Rt	2.6474	µm	
Rz	1.9111	µm	

Modified Profile  
 flange A 0 - 1 - R/4x0.08mm/G/30/LS Arc  
 flange A 90 - 1.6mm/Admin/PGI  
 24/05/2013 07:36:14  
 24/05/2013 07:35:45



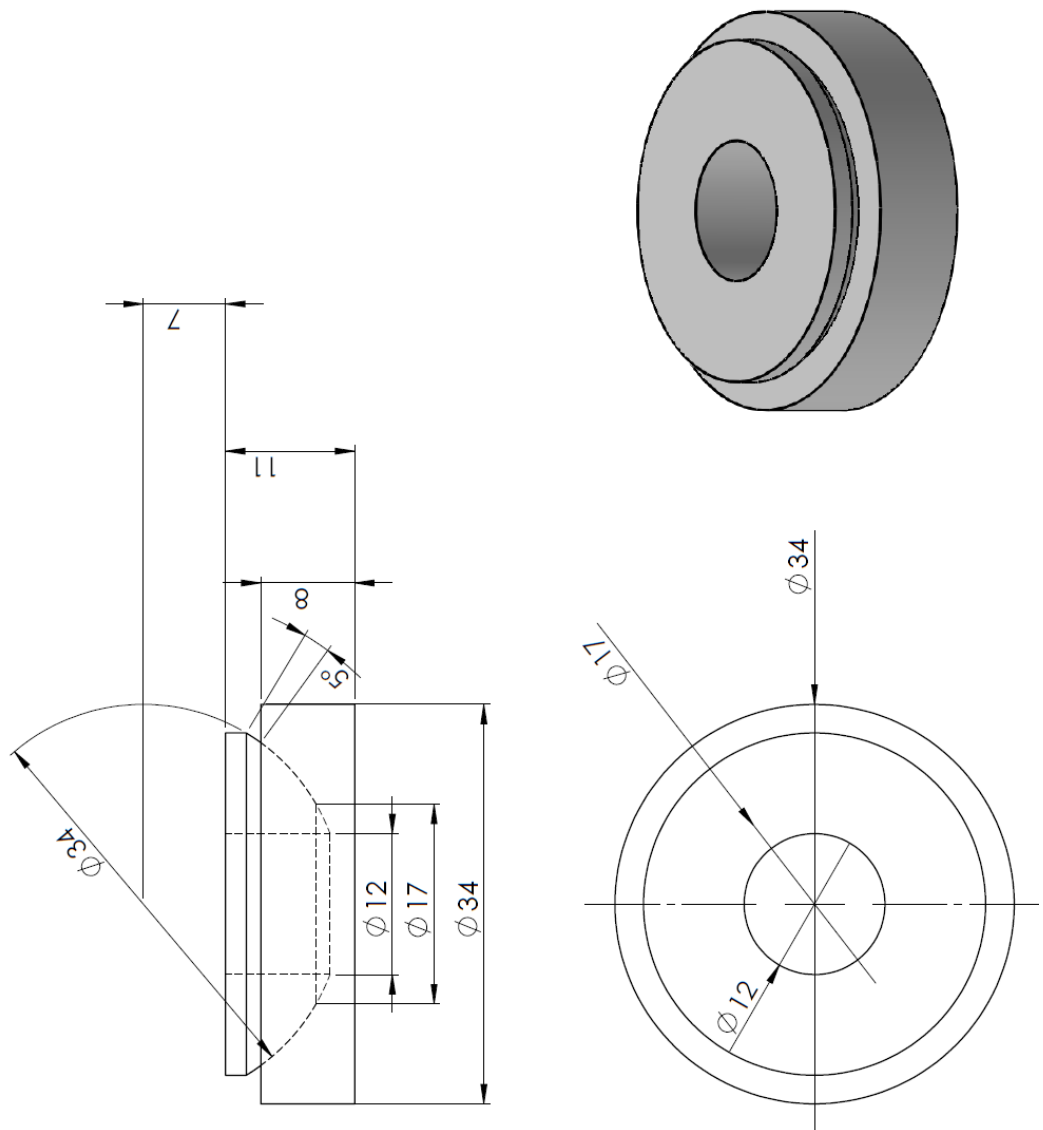
Radius	0.5243	mm	
Ra	0.1980	µm	
Rsk	0.0353		
Rt	1.5670	µm	
Rz	1.0605	µm	

Modified Profile  
 flange A 0 - 1 - R/6x0.08mm/G/30/LS Arc  
 flange A 0 - 1.6mm/Admin/PGI  
 24/05/2013 07:31:35  
 24/05/2013 07:28:34



Radius	0.5438	mm	
Ra	0.5091	µm	
Rsk	-0.4985		
	Rt	4.3605	µm
	Rz	2.5102	µm

## Appendix – J: Spherical Plain Bearings



## Appendix – K: Load Cells Calibration

### Appendix K -1 Omega Load Cell Calibration

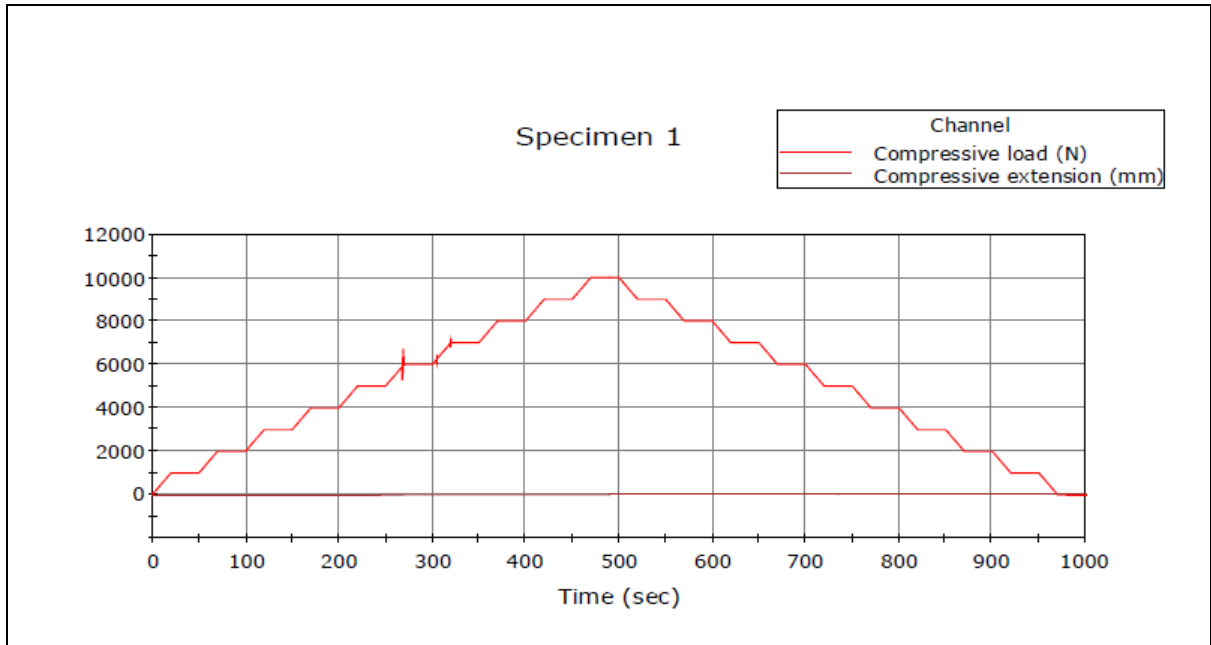
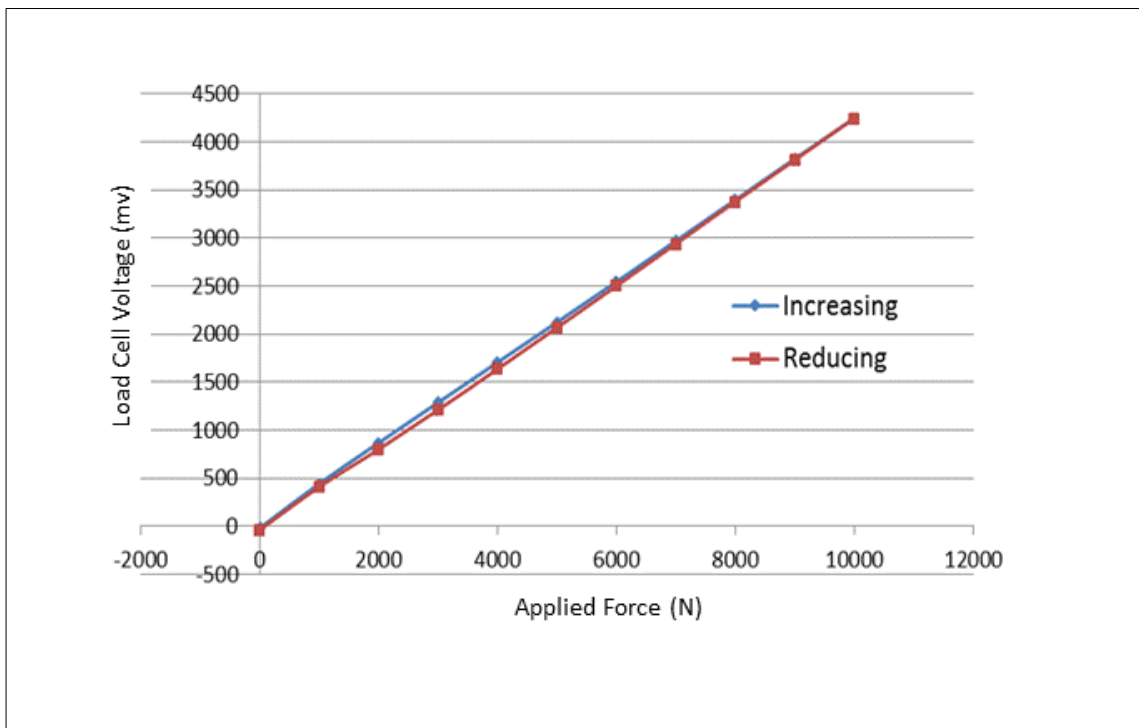


Table K Increasing the Calibration Omega Load Cell

Nominal (N)	Average Load During Hold Times (N)	Picoscope (mV)
10	10.146	-14
1000	1000.065	444
2000	2000.049	869
3000	2999.950	1289
4000	4000.023	1707
5000	4999.982	2125
6000	5999.995	2545
7000	6999.982	2971
8000	8000.043	3398
9000	9000.036	3825
10000	10000.018	4247

Table K – 1 - 2 Reducing the calibration Omega Load Cell

Nominal (N)	Average Load During Hold Times (N)	Picoscope (mV)
9000	8999.934	3813
8000	7999.984	3380
7000	7000.001	2940
6000	6000.000	2502
5000	4999.980	2068
4000	4000.021	1637
3000	3000.034	1212
2000	2000.027	801
1000	999.961	410
0	-0.243	-37



Graph plot of the Omega Load Cell calibration

## Appendix K – 2 Lever Arm Load Cell Calibration

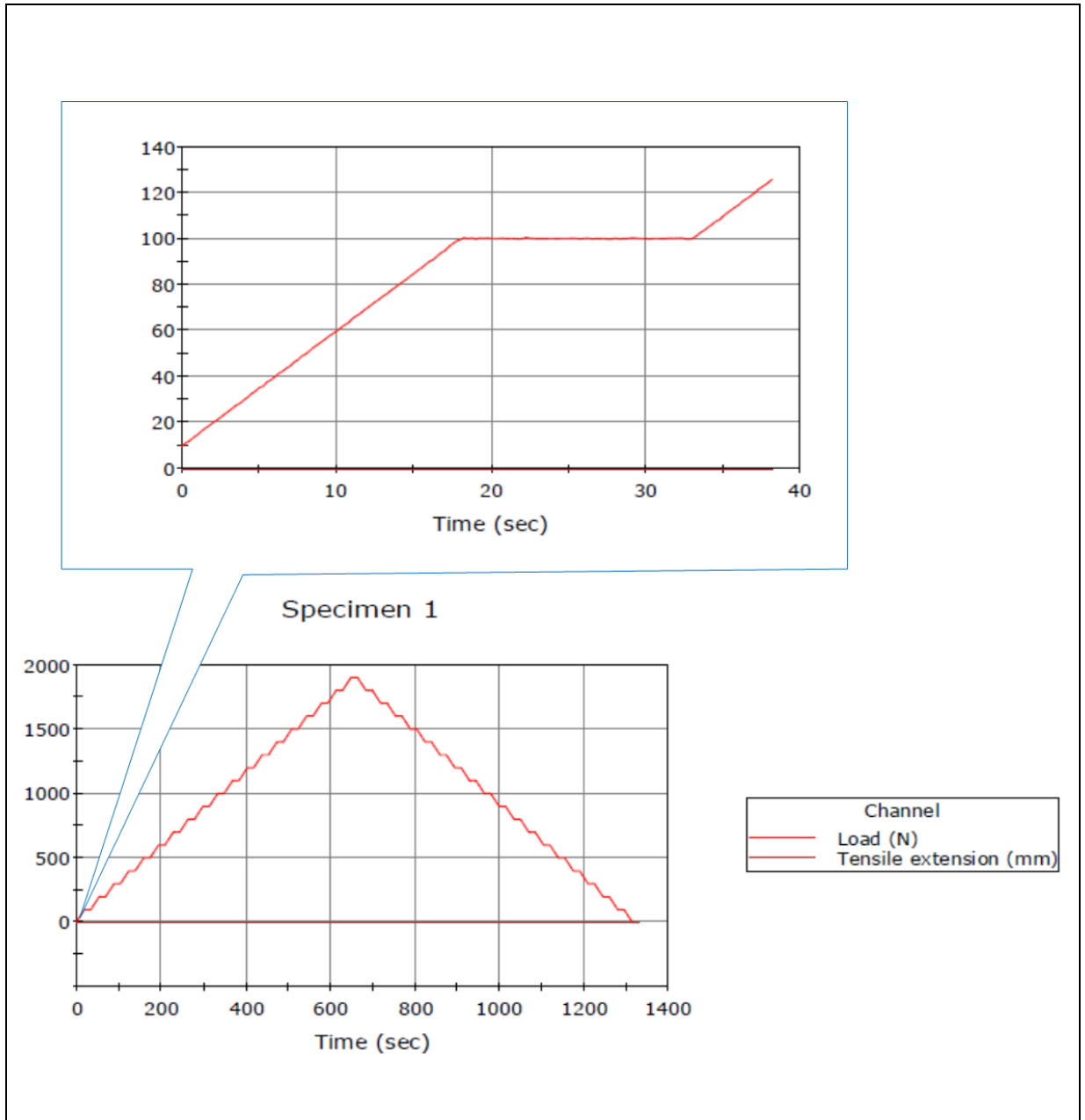
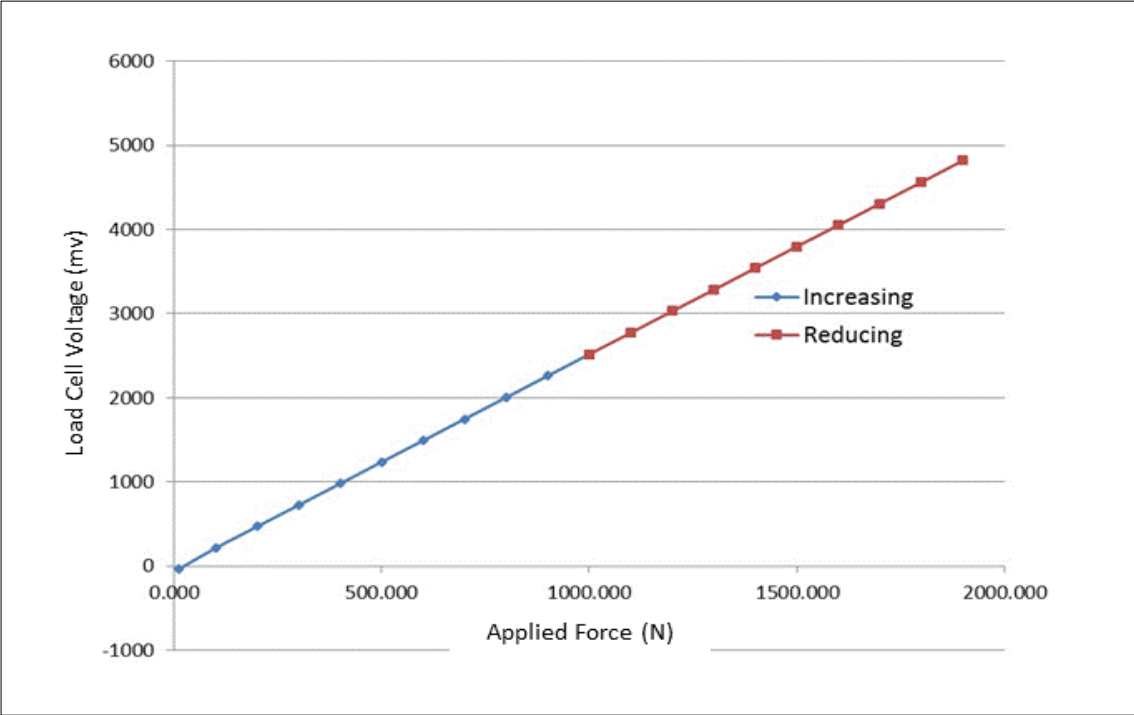


Table K – Increasing the Calibration of the Lever arm Load Cell

Nominal (N)	Average Load During Hold Times (N)	Picoscope (mV)	Zero Correction
10	10.261	-40	-30
100	100.101	212	-40
200	200.072	469	212
300	300.044	724	469
400	400.072	979	724
500	500.032	1238	979
600	600.092	1492	1238
700	700.069	1749	1492
800	800.053	2004	1749
900	900.031	2261	2004
1000	1000.022	2518	2261
1100	1100.034	2773	2518
1200	1199.965	3030	2773
1300	1300.009	3284	3030
1400	1399.961	3541	3284
1500	1500.014	3798	3541
1600	1599.977	4052	3798
1700	1700.004	4309	4052
1800	1800.026	4564	4309
1900	1899.990	4821	4564

Table K – 1 – 4 Reducing the calibration of the lever arm Load Cell

Nominal (N)	Average Load During Hold Times (N)	Picoscope (mV)	Zero Correction
1800	1799.729	4564	4821
1700	1699.841	4307	4564
1600	1599.864	4052	4307
1500	1499.889	3800	4052
1400	1399.929	3541	3800
1300	1299.877	3286	3541
1200	1199.909	3031	3286
1100	1099.863	2776	3031
1000	999.891	2519	2776
900	899.905	2264	2519
800	799.941	2007	2264
700	699.996	1752	2007
600	599.956	1494	1752
500	499.878	1240	1494
400	400.009	985	1240
300	299.953	728	985
200	199.943	473	728
100	99.926	216	473
0	-0.106	-38	216



Graph plot of the lever arm load cell calibration

